PUNCHING SHEAR STRENGTH OF CONTINUOUS POST-TENSIONED CONCRETE FLAT PLATE

BY

Mahmoud Rezai Kallage

A Thesis
presented to the University of Ottawa
in partial fulfilment of the
requirements for the degree of
Master of Applied Science
in
Civil Engineering

Supervised by : Dr. N. J. Gardner

Department of Civil Engineering
Faculty of Engineering
University of Ottawa
September, 1993

The Master of Civil Engineering Program is a joint program
with Carleton University administered by
the Ottawa-Carleton Institute for Civil Engineering

UNIVERSITÉ D'OTTAWA
UNIVERSITY OF OTTAWA

ABSTRACT

A two bay by two bay continuous, unbonded post-tensioned flat plate was constructed and loaded to failure. The slab was designed in accordance with the provisions of ACI 318-89 except that no supplementary bonded reinforcing steel was provided. The prestressing tendons were uniformly distributed in one direction and banded in span/6 column strips in the other direction. In both directions the average prestress on the concrete was 3.5 MPa. The dimensions of each bay were 2.75 m, the slab thickness was 89 mm, mean concrete cylinder strength was 44 MPa. The load was applied monotonically until punching shear occurred at an edge column on the side parallel to banded tendons. The failed column was shored and the slab reloaded until punching shear occurred at the interior column.

The lack of supplementary bonded reinforcing steel in regions of moment transfer had no apparent detrimental effects so it must be concluded that the prestress was effective right to the edge of the concrete. The use of 100% banded tendons in one direction and uniform distribution in the other direction had no adverse effects on either the flexural or punching shear behaviour.

The literature was reviewed to locate experimental results of punching shear tests for isolated prestressed concrete flat plates, continuous prestressed flat plate systems and tests of flat plate column connections under shear and moment transfer. The strength capacities calculated using the provisions of ACI 318-89, CSA A23.3-84M, BS8110-85 and the CEB Model Code 1990 were compared to the test results and those from the literature review.

ACKNOWLEDGEMENTS

The author wishes to express his sincere appreciation to his supervisor Professor N. J. Gardner for his guidance and encouragement during all phases of the author's M.A.Sc. degree program.

The financial support provided by the government of Iran is gratefully acknowledged.

The help and cooperation extended by Mr. Mongi Grira and the technical staff of the structural laboratory of the University of Ottawa during the experimental stages of this work are acknowledged.

The author's appreciation goes to all graduate students and friends who contributed their help and support.

Finally, the author wishes to thank his wife, Aliyeh, and his family for their invaluable help and encouragement during all phases of the author's study program.

To

Aliyeh and Ahrshia

TABLE OF CONTENTS

LIST OF TABLES

LIST OF FIGURES

NOTATIONS

a	Width of slab
a_1	Radius of compression zone in thick cylinder idealization
a_v	Distance from the edge of the loaded area
A	Area of shear perimeter
A_{ps}	Area of prestressing tendons
A_s	Area of bonded reinforcement
b or b_o	Perimeter of critical section
c_o	Column perimeter
c , c_1	Column side length
C	Force in concrete compression zone at ultimate
d	Average effective depth of tensile reinforcement
d_r	Effective depth to bonded reinforcement
d_{ps}	Effective depth to actual tendon profile
d_b	Reinforcing bar diameter
E_{CMA}	Compressive membrane enhancement factor
E_s	Modulus of elasticity of reinforcement
$f_c^{'}$	Characteristic compressive strength of concrete cylinders
f_{ck}	Specified compressive strength of concrete cylinders
f_{cu}	Characteristic concrete cube strength
f_{pc}	Average initial concrete prestress
f_{pcu}	Average ultimate concrete prestress prior to failure
f_{pc}^{*}	Extreme fibre compression due to prestress
f_r	Modulus of rupture
f_{se}	Effective initial prestressing force in cables
f_{ps}	Stress in prestressing steel developed at ultimate
f_{pu}	Characteristic strength of prestressing tendons

f_t	Split cylinder strength of concrete
f_y	Yield stress of the reinforcement
$f_{0.2}$	0.2% proof stress of prestressing cables
F_e	Effective prestress force per cable
F_r	Force in radial direction
F_t	Force in tangential direction
M_r	Moment in radial direction
h	Overall thickness of slab
H	Compressive membrane force per unit width
j	Ratio of internal moment arm to effective depth
J	Polar moment of inertia of the critical section
k_1	Factor relates the vertical load to slab moment per unit width
K_d	Dowel coefficient
l_s	Distance from the column face to the loaded area
L	Slab span
m	Slab moment per unit width
m_u	Ultimate moment of resisting per unit width of slab
m_{uc}	Ultimate moment of resisting per unit width of slab with considering the effect of compressive membrane action
m_o	Decompression moment per unit width of slab
n_c	Concentration factor
P_{shear}	Calculated ultimate shear load
P_{flex}	Calculated ultimate flexural load
P_c	Load carried by concrete and ordinary reinforcement
P_{pb}	Force in tendon at failure
P_{pi}	Initial force in tendon
P_s	Transverse component of prestressing force
P_u	Collapse load
P_{ur}	Ultimate punching load in reinforced slab
P_{url}	Longitudinal component of ultimate load resistance in reinforced slab

P_{urt}	Transverse component of ultimate load resistance in reinforced slab
P_o	Decompression load
P_{ol}	Decompression load in longitudinal direction
P_{ot}	Decompression load in transverse direction
P_{up}	Ultimate punching load in prestressed slab
q	Tensile reinforcement index : $\rho\frac{f_{ps}}{f_c'}$
r_o	Radius of a column or loaded area
r_p	Radius of peripheral load or reaction
r_w	Wedge or punching radius
R	Outer radius of thick cylinder
s	Cable spacing
u_d	Sum of 8 times the cover for each bar
u'	Perimeter over which v' acts
v_u	Ultimate shear stress
v'	Mean value of ultimate shear stress in compression zone
V	Column axial load or punching shear force
V_c	Shear strength of concrete
V_p	Vertical component of all prestress forces crossing the critical section
V_u	Ultimate shear force
V_d	Shear carried by dowel force
T_o	Total force in both bonded and prestress reinforcement
$\bar{x}d$ *or* x	Depth of neutral axis in a reinforced concrete slab
x_p	Depth of neutral axis in a prestressed concrete slab
α	Angle of inclination of the compressive force in the radial direction
α_c	Concrete stress-strain curve coefficient
β	Fraction of slab span
β_c	Ratio of the column sides
ϕ_o	Ratio of $\frac{P_{shear}}{P_{flex}}$
$\Delta\phi$	Small sectoral angle
ρ	Average percentage of tensile reinforcement

ρ_s	Ratio of ordinary bonded reinforcement
ρ_{ps}	Ratio of prestressed reinforcement
ρ_e	Equivalent reinforcement ratio
ρ_l	Reinforcement in the longitudinal direction
ρ_t	Reinforcement in the transverse direction
ζ	Ratio of concrete tensile to compressive strength
κ	Ratio of column size to slab thickness
ϵ_{cc}	Strain in concrete at failure
ϵ_{ct}	Strain in concrete in tangential direction
ϵ_{cr}	Strain in concrete in radial direction
ϵ_{pe}	Initial strain in tendon
ϵ_{pb}	Strain in tendon at ultimate
σ_t	Maximum tensile stress in cylinder wall
σ_b	Bearing stress
ω_e	Equivalent reinforcement index
γ_p	Level of prestressing
γ_f	Fraction of unbalanced moment transferred by flexure
γ_v	Fraction of unbalanced moment transferred by shear

CHAPTER #1

INTRODUCTION

1.1 General :

Flat-plate structures are used in many countries for the medium height multistorey commercial or residential building construction. In comparison with traditional beam-column construction, flat-slab building structures provide a comparatively new kind of skeletal structure, Fig. 1-1. The phrase "flat-plate" refers to a specific type of structures, in which the slab possesses a constant thickness, without spandrel beams or column capitals. Flat plates are widely used in many countries, because of the following reasons:

★ Simplified formwork and consequently less construction time and lower labour costs.

★ Reduction of the total height of the building by eliminating beams, drop panels or column capitals.

★ Plain bottom surfaces with minimum obstructions which make it easier for the

installation of electrical and mechanical devices.

★ Good performance from the architectural and serviceability points of views.

The simplicity associated to both the shape of such structures and the technology required in their construction is unfortunately accompanied by difficulties in analysis and design. Although regulations for the design of flat-slab structures are to be found in many countries' national building codes, there are still many issues where our knowledge is insufficient. One of the major controversial issues is to check whether a support zone without shear reinforcement fulfils the requirements for bending and punching shear. Although a great deal of research has been undertaken, there is still no simple method to determine the shear resistance of slab-column connections. This thesis will review the present knowledge of punching shear behaviour of post-tensioned flat slabs.

Flat plate structures can be constructed either of reinforced concrete or of prestressed concrete. Prestressed concrete flat slabs have some advantages which are discussed briefly. In reinforced concrete flat slabs, the thickness is usually determined by the condition of the permissible deflections. As a result, the range of spans for which reinforced concrete flat slabs are used is limited. The introduction of prestressing into slabs greatly increases the ultimate strength, and therefore enables the depth to be reduced and the range of practical spans to be enlarged. Reduction in the thickness of the slab causes the overall height and weight of the structure to be reduced. Deflection which might be excessive in reinforced concrete slabs can be minimized or even nullified by prestressing. Cracking control is an important factor in both reinforced and

prestressed concrete structures. Prestressing of slabs eliminates cracks under working loads as well as reduces the total steel consumption.

The first post-tensioned slabs in the North America were constructed in the mid. 1950's. As mentioned, post-tensioning was introduced to resolve weight, deflection and cracking problems associated with reinforced concrete flat-slabs. Since then, prestressed concrete flat plate structures have been made with bonded or unbonded tendons. The first step is to place the post-tensioning ducts in the formwork. Then after casting and curing of the concrete, the tendons are tensioned and anchored. If the design is based on bonded tendons, the ducts are then grouted and filled with concrete. In the bonded tendon, the bond between the tendon and surrounding concrete provides corrosion protection for the tendon, while in the unbonded tendon the corrosion protection is maintained by a grease-filled plastic tube and by special details at the anchorages. In the bonded tendon the basic assumption is that the change in strain in the prestressing steel is equal to the change in strain in the adjacent concrete. In the unbonded tendon the strain is constant along the length of the tendon, therefore the compatibility condition will be that the change in overall length of the tendon must be equal the total change in length of the adjacent concrete. Bonded tendons experience large stress increases in regions of high moment while unbonded tendons experience stresses which are averaged over the total length between anchorages. The parameters which are involved in choosing between bonded or unbonded tendons are the construction or economic considerations. Because of better economy, most prestressed concrete slabs are post-tensioned and unbonded.

Analysis and design of concrete slabs require simultaneous consideration of a number of different possible failure modes. These are namely **a)** overall slab failure under bending moments **b)** overall slab shear failure (beam action failure) **c)** local shear punching failure around the columns and **d)** local flexural failures around the column. Combination of these failure types may also be the cause of overall failure at loads smaller than these individual failure loads. The specific objective of this thesis is to study the local, or punching, shear failure of prestressed slabs around columns.

Local shear failures at columns can be either due to principal tension stress or diagonal tension failure or a combination of shear and flexural failures. A punching, or more appropriately, a principal tension stress failure can occur at loads smaller than that causing flexural distress if enough flexural reinforcement is provided to prevent high flexural stresses. As a result, failure occurs at the load in which the principal tension stresses in the slab concrete around a column become larger than the concrete tensile strength. The combination failure may cause the secondary punching shear failure after high reinforcement stresses, and probably some local yielding, combine with the local shear stresses developed in the vicinity of the column. Principal tension stress failures are mostly recognised as a cause of local shear failure and are characterised as a sudden, brittle failure and are difficult to predict. Principal tension stress and combination failures have commonly been prevented through use of shear head reinforcement and drop panels.

In order to achieve a rational accurate investigation of punching shear strength, it is necessary

to be able to distinguish which failure mode will be critical and what parameters influence this phenomenon. The essential parameters involved in the shear capacity of slab-column connections are the concrete strength, compressive membrane action, the ratio of the side length of loaded area to the effective depth of the slab and the relationship between shear and moment in the vicinity of the loaded area. There are some other factors which might also have marked effects on the punching shear resistance of flat slabs, namely reinforcement ratio, scale effect, column shape and rate of loading.

Many approaches towards a theoretical treatment of symmetrical punching shear failure have been presented but have met with limited success in practical applications. The complex physical nature of a cracked slab at the point of failure precludes the development of a simple procedure that can realistically evaluate actual stresses, and therefore makes a rational treatment of slab-column connections impractical. Nevertheless, in order to assess the punching shear resistance of slabs, code design procedures offer simplified empirical approaches. These procedures are based primarily on the results of slab-column tests, and therefore are reliable only over the limited range of data for which they were derived. A brief review of the differences in the design provisions for shear in the major codes of practice reveals the considerable uncertainty which exists. Totally different points of views in dealing with the shear capacity of interior and exterior slab-column connections have been proposed. This necessitates the need for more tests, with different material strengths, geometries, and boundary conditions on the shear behaviour of slabs to give more information to empirical approaches to the problem, and to yield additional hard facts to researchers who are trying to employ different rational and semi-rational approaches.

1.2 Specific Objectives :

1) Investigate the punching shear strength of prestressed flat-plate connections over the range of loading up to failure. The investigation was intended to provide more information about the distribution of cracks, the effect of unsymmetrical arrangement of prestressing tendons, the contribution of prestressing force to strength, and the adequacy of the present design methods in prediction of ultimate load capacity of slabs prestressed in both directions.

2) Review critically the existing code proposals and compare their predictions of the punching shear resistance of prestressed slabs with the present and previous test results.

1.3 Scope of The Study :

1) Review the published research on the punching shear tests of post-tensioned concrete flat plates.

2) Construct a 2 × 2 bay continuous, prestressed concrete, flat plate of banded prestressing to investigate the behaviour of such slabs through and after the elastic range.

3) Carry out a statistical analysis of data gathered from previous investigations and that recorded in the present work.

1.4 Summary of The Following Chapters :

Chapter 2 presents a literature review on symmetric and unsymmetric punching shear tests. Chapter 3 includes details of the materials used in the construction of the model slab, instrumentation, loading system and the technique used to apply the prestressing force to the slab. The testing sequences and the observed behaviour are also reported in Chapter 3. Chapter 4 discusses the overall response of the slab, such as : crack pattern, shoring the slab, ultimate load capacities and the parameters affecting the punching shear resistance of the slab. The procedures proposed by North American and European countries together with comparison of the code predictions with the experimental results are described in Chapter 5. The conclusions and recommendations are presented in Chapter 6.

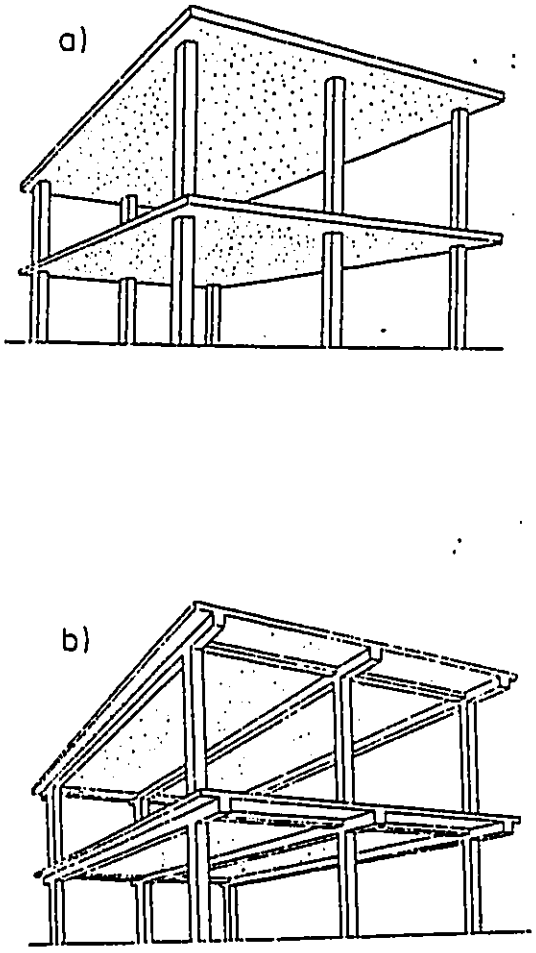

Fig. 1-1 : Skeletal building structure: **a)** flat-plate structure **b)** slab-beam-column structure

CHAPTER #2

LITERATURE REVIEW

The elastic behaviour and ultimate strength of prestressed concrete flat slabs were first investigated by Scordelis, Pister and Lin in 1956. The purpose of their study was to investigate the elastic and post-elastic behaviour of a flat concrete slab prestressed in two directions. A full scale model, having overall dimensions of 4.5 m × 4.5 m in plan, 125 mm thickness and supported at the four corners, was loaded to failure. The slab was post-tensioned with 10 six-wire cables in each direction. Each cable contained six 6.35 mm diameter steel wires with overall diameter of 19 mm (¾ in.). All cables were laid straight at mid-depth of the slab with no drape. Effective prestress in the cables after all losses was 880 N/mm² per cable, applying a total stress of 2.9 MPa to the slab. In addition to the prestressing steel, a small mesh of auxiliary flexural bonded reinforcement was placed at each corner to reduce the possibility of local failure at the supports. The following questions were intended to be answered within the limited range of the

experiment :

1) The ability of beam and elastic theory for predicting the cracking load and ultimate strength of the slab.

2) Comparison of deflections and bending moments obtained from theoretical analysis solving the Lagrangian differential equation of plate theory with the experimental results.

3) Comparison of the actual ultimate strength of such a slab with that given by yield-line theory.

The behaviour of the slab was observed and recorded for four distinct load stages. **Test 1)** Before cracking. **Test 2)** At cracking. **Test 3)** Post-cracking. **Test 4)** At ultimate. The results of the tests can be summarized as follows :

★ There was a small difference between the cracking load observed from experiment and that calculated based on concrete modulus of rupture. The difference was because the modulus of rupture obtained from beam specimens is in a state of uniaxial stress, which will not be totally valid for two-way slabs.

★ Good agreement was seen to exist between measured and theoretical values (calculated by classical elastic theory) of deflection, bending moments and load-strain relationship within the elastic range. (No Cracking)

★ The ordinary criterion for design of prestressed concrete flat slabs was based on allowing no tension in extreme fibres within the working loads condition. This concept

was found to be inappropriate as the load balanced by the prestressing was only equal to the self-weight of the slab, and hence no live load could be permitted on the slab. However, the behaviour of the slab was quite good up to a live load of 3.83 kN/m² (80 psf) with a centre deflection of about 6 mm. The maximum tensile stress recorded in the concrete was 3.45 MPa.

★ The simply supported slab developed a classic yield line crack pattern at failure even without any bonded positive moment reinforcement.

The lack of strain gauges on the prestressing steel prevented steel stress being recorded during the test. To obtain the theoretical value of the ultimate load, the value of steel stress at failure was estimated. For an unbonded cable this value was taken as 80 to 90 percent of the ultimate steel stress. The theoretical ultimate load obtained by the above assumption ranged between 10.8 kN/m² and 12.3 kN/m², which was in good agreement with the experimental ultimate load of 11.4 kN/m².

In 1958 a research investigation on the ultimate shearing stress of prestressed concrete lift slabs was undertaken by Scordelis, Lin and May. Fifteen test slabs, simulating the perimeter of the line of zero moment around an interior column in a typical lift-slab structure, were tested to collapse. All specimens were 1.8 m square, with variable thicknesses and supported along all edges. The slabs were loaded centrally through a 200 mm square column fabricated from two angles welded together to form a box section.

Prior to 1958 no design specification was available to calculate the ultimate shear strength of prestressed concrete flat slabs. The 1956 ACI (American Concrete Institute) building code recommendations were applicable only to reinforced concrete flat slabs. The ultimate shear stress of reinforced concrete flat or lift slab structures following the 1956 ACI building code was given as :

$$v_u = \frac{V_u}{bjd} \leq 0.025 f_c' \qquad (2\text{-}1)$$

b was the perimeter of vertical shear area at critical section at a distance d beyond the edges of the column, column capitals or the collar. j had a constant value of $\frac{7}{8}$. The allowable value for shear stress proposed by ACI 1956 was based on only one variable, the concrete cylinder strength, f_c' , and specified as $0.025 f_c'$.

The main objective of the experiment was to investigate the influence of the following variables on the ultimate shear strength of prestressed concrete slabs with lift-slab collars : the distribution and relative magnitude of shear and normal stresses, the amount of prestressing steel and initial prestressing force, and the amount and distribution of flexural cracking that occurred prior to failure. The following variables were the major considerations in the experimental program : **(a)** Concrete Strength (20 - 36 MPa) **(b)** Amount of prestressing steel. **(c)** Amount of initial prestress (1.7 - 3.5 MPa) **(d)** Thickness of slab (150, 200 or 250 mm) **(e)** Size of steel collars (330 and 400 mm)

The most complicated questions at that time, and may be even today, were :

1) Where is the location of critical section?

2) What is the net area available to resist shear at the critical section?

3) What criteria should be chosen for ultimate shear stress?

Undoubtedly the answers to all of these questions are dependent on the amount, location and depth of flexural cracking that occurs prior to failure. Computing the total amount of uncracked depth available to resist shear is entirely affected by the above parameters. Since in slabs, the principal stresses are generated by flexural action, the shear stress is therefore a function of shear to moment ratio. It is clear that for slabs with high shear-moment ratios, the amount of flexural cracking will be smaller than for slabs with low shear-moment ratios. In practice a fixed depth, usually equal to the effective depth of the tensile reinforcement at the critical section, is used to determine the nominal stresses. The ultimate shear stress could then be computed by applying empirical equations and by including the shear-moment ratio as a variable.

Hognestad in 1953 proposed the first empirical expression to calculate the ultimate shear strength of reinforced concrete flat slabs :

$$v_u = \frac{V_u}{\frac{7}{8}bd} = (0.035 + \frac{0.07}{\phi_0})f_c' + 130 \quad (psi) \quad where \quad \phi_0 = \frac{P_{shear}}{P_{flex}} \qquad (2\text{-}2)$$

or rewriting :

$$\frac{v_u}{f_c'} = 0.035 + \frac{130}{f_c'} + \frac{0.07}{\phi_0} \quad (psi) \tag{2-3}$$

In 1956, after performing an extensive study on the reinforced concrete flat slabs (39 specimens), Elstner and Hognestad proposed another equation for reinforced concrete flat slabs without shear reinforcement, which gave better correlation for higher concrete strengths.

$$\frac{v_u}{f_c'} = \frac{P_{shear}}{\frac{7}{8}.b.d.f_c'} = \frac{333}{f_c'} + \frac{0.046}{\phi_0} \quad (psi) \tag{2-4}$$

In 1957 Whitney derived a new equation for predicting the ultimate shear strength of reinforced concrete flat slabs :

$$v_u = 100 + 0.75 \frac{m_u}{d^2} \sqrt{\frac{d}{l_s}} \quad (psi) \tag{2-5}$$

Where m_u is the ultimate resisting moment of the slab per unit width inside the "Pyramid of Rupture" (The frustum of a cone with surfaces sloping out in all directions from the face of the loaded area at an angle of 45°). The m_u may be calculated by Eq. (2-7) for under-reinforced slabs. l_s was the distance from the face of the column to the line of support.

Elstner and Hognestad (1956) recommended that for ordinary reinforced concrete slabs the critical section (shear perimeter) can be taken at the edge of the loaded area. Whitney (1957) proposed that it be taken at a distance $\frac{d}{2}$ from the edge of the loaded area. The 1956 ACI

building code suggested that it be taken at a distance d from the edge of the loaded area.

The main problem in using Eq. (2-4) and Eq. (2-5) was the calculation of P_{flex} . When applying yield line theory for computing the ultimate flexural strength of prestressed concrete slabs with unbonded tendons, determining the developed stress in the prestressing steel at ultimate moment was difficult and had to be estimated. This estimation will be different for longer cables used in real construction, compared with the short cables used in the test slabs. Based on the test results, with approximate calculations of the cable elongation and deflection of the slab specimens, Hognestad and Elstner proposed the following expression for calculation of prestressing steel stress at ultimate :

$$f_{ps}=157{,}000+0.4f_{se} \quad (psi) \tag{2-6}$$

Once f_{ps} is established, the yield moment per unit width may be computed by means of the following :

$$m_u=f_c'.d^2.q(1-0.59q) \quad where \quad q=\rho\frac{f_{ps}}{f_c'} \tag{2-7}$$

The ultimate flexural strength, P_{flex} given by the yield line theory for a simply supported square slab loaded through a square column with the corners free to lift is :

$$P_{flex}=8m_u\left[\left(\frac{1}{1-\frac{c}{d}}\right)-(3-2\sqrt{2})\right] \tag{2-8}$$

The above expressions were applied to the prestressed concrete flat slabs to ascertain if they

would give satisfactory results. Eq. (2-4) gave values of $\frac{P_{test}}{P_{calc}}$ ranging from 0.88 to 1.20 with an average value of 1.06 and a standard deviation of 0.096 for 15 slabs, which can be interpreted as a good agreement. The range of variations for $\frac{P_{test}}{P_{shear}}$ according to Eq. (2-5) were recorded from 0.92 to 1.32 with an average value of 1.10 and a standard deviation of 0.123 for 14 slabs. The ultimate punching shear stress calculated by the Eq. (2-1) at a distance d from the edge of the collar varied between $0.058f_c'$ and $0.127f_c'$.

Even though the prediction of ultimate shear stress of Scordelis's prestressed concrete slabs from these equations was relatively good, it must be observed that none of these equations was derived for prestressed concrete slabs. There is one important parameter missing, and that is the effective prestressing force or the amount of pre-compression force applied to slab before loading. Scordelis and Lin proposed the following equation for the prediction of ultimate punching shear stress of prestressed concrete lift-slabs at the edge of the collar :

$$v_u = \frac{P_{shear}}{b.d.f_c'} = 0.175 - 0.0000242f_c' + 0.000020\frac{F_e}{s} \quad (psi) \qquad (2\text{-}9)$$

Values of $\frac{P_{test}}{P_{shear}}$ calculated by means of the above expression ranged from 0.89 to 1.2 with an average value of 1.02 and a standard deviation of 0.075 for the 12 prestressed slabs.

On the basis of Scodelis's test and analytical results the following conclusions were drawn :

1) The first visible flexural cracks were noticed at 40 to 60 percent of the ultimate load. In comparison, reinforced concrete slabs exhibited the first visible flexural cracks at 15

to 25 percent of the ultimate load.

2) Punching shear failure was the dominant mode of failure for all specimens.

3) Ultimate shear strength formulas of Hognestad, Eq. (2-4), and Whitney, Eq. (2-5), which were derived for reinforced concrete slabs, agreed quite well with the results obtained in this experiment for prestressed concrete slabs. Nevertheless the problem of calculating the ultimate flexural capacity of the slabs remained.

4) Application of the 1956 ACI building code equation applied to Scordelis's prestressed concrete lift slabs yielded a wide range of safety factors on the ultimate shear stress from 3.3 to 5.6.

One and half years later, Scordelis & Lin tested a continuous slab with four panels and supported at nine points. The purpose of their investigation was to determine the behaviour of a continuous concrete slab prestressed in two directions. The test program was designed to study the distribution of bending moments, shear forces and deflections for these type of slabs. The applicability of the available theories for predicting ultimate strength of prestressed slabs such as beam method & elastic plate method were also examined.

A 2 × 2 bay slab, measuring 4.5 m × 4.5 m in plan and 75 mm thick with supports placed at 2.13 m on centres in both directions was tested to failure. The slab was post-tensioned, using twelve ¼ in. (6.35 mm) high strength steel wires in each direction spaced 380 mm on centres. The average prestress force of 30.5 kN per cable, giving the total stress of 1.035 MPa on the slab, was applied to each cable. In order to prevent the possibility of local failure at the supports,

two layers of wire mesh were also placed over each support. The plan and elevation of the model slab and the profiles for all of the cables running in both directions are shown in Fig. 2-1.

A summary of the cases considered and the experimental and analytical studies performed is given below :

★ For the case of uniform prestressing force in both directions, there was good correlation between theoretical values using the load balancing technique, and experimental values of bending moments and deflections at all sections; indicating that beam theory is appropriate for this case.

★ The first tensile crack, as indicated by strain readings, occurred at around 40% of the ultimate load over the centre support. The first visual observation of cracks at the bottom of the slab took place at a load of 80% of the ultimate load.

★ Elastic plate theory may be used to predict satisfactorily the behaviour of a prestressed concrete slab loaded within the elastic range. Comparison of the deflection at the centre of panel, for the case of uniform load, by plate theory, approximate beam method and experimental results is shown in Fig. 2-2.

★ At sections of high moment, such as interior supports, the distribution of the experimental moments is not uniform across the section and some redistributions of the gross moment calculated by beam theory should be made. The approximate values of 75% to the column strips and 25% to the middle strips for negative moment areas and 60% to the column strips and 40% to the middle strips for positive moment areas were proposed.

There are the current ACI and CSA (Canadian Standards Association) provisions.

★ The ultimate load capacity of the slab predicted by yield line theory was in good agreement with the experimental failure load of the slab.

★ After extensive flexural cracking, ultimate failure occurred with the centre support punching through the slab. The shear angle was recorded about 45 degrees.

In 1967 Grow and Vanderbilt reported a test program undertaken to determine the effect of prestress on the shear strength of post-tensioned, lightweight aggregate concrete flat plates. The test program consisted of 10 isolated model specimens, identical except for variations in the effective prestressing force. The test specimens were 0.914 m square, 75 mm thick and had a 200 mm square stub column at the centre of panel. All specimens were made with 6 seven-wire 9.5 mm (⅜ in.) diameter cables uniformly spaced along each side of the slabs. The specimens were tested with all edges simply supported and with corners free to lift up. This type of specimen is assumed to simulate the part of slab bounded by lines of contraflexure around an interior column. The deficiencies of this assumption will be discussed latter.

The amount of prestress was the only variable investigated in the test program. All the other options, such as : column size, the amount of steel and concrete strength, were held constant for all specimens. The behaviour of the slabs can be divided into two categories : **a)** specimens with low prestress. **b)** specimens with high prestress. The typical flexural crack patterns for the specimens with low prestress and high prestress are shown in Fig. 2-3. The dotted lines represent the base of the truncated pyramid after failure occurred of which covered the major portion of

the bottom of slabs. The width of the crack propagating all around the column periphery was recorded about 1.5 mm moments before failure occurred. For specimens with high prestress, the load at which the load-deflection curves, Fig. 2-4, became non-linear increased over specimens with low prestress. This is because increasing the effective prestressing force causes the stiffness of the slabs to be increased.

The cable forces showed little increase with increase in load until serious cracks were observed in the specimens. The ultimate concrete prestress immediately prior to failure, f_{pcu} , had an average increase of 150% over the initial effective concrete prestress, f_{pc} . The ratio of $\frac{f_{pcu}}{f_{pc}}$ recorded from 1.17 to 2.70. The higher values belong to the specimens with low prestress indicating that as the initial effective prestress increased the ultimate concrete prestress tended to decrease.

All specimens failed in shear, exhibiting a sudden punching through of the column stub. A plug of concrete which had the form of a truncated pyramid made an angle of about 22° with the top surface of the slab was forced out.

The shear stress of the test specimens were calculated using the empirical equations developed for reinforced concrete slabs by previous researchers and the equation that had been developed for prestressed slabs by Scordelis. The equation derived by Moe (1961) which formed the basis for the ACI standard building code, ACI 318 - 63, was :

$$\frac{V_u}{b.d.\sqrt{f_c'}} = \frac{15(1-0.075\frac{c}{d})}{1+\frac{5.25b.d.\sqrt{f_c'}}{P_{flex}}} \qquad (psi) \qquad (2\text{-}10)$$

The above equation was revised by Hognestad, Elstner and Hanson for lightweight aggregate concrete :

$$\frac{V_u}{b.d.f_t} = \frac{2.24(1-0.075\frac{c}{d})}{1+\frac{0.784b.d.f_t}{P_{flex}}} \qquad (psi) \qquad (2\text{-}11)$$

Yitzhaki developed the following equation :

$$V_u = 8(1-0.5q)d^2(149.3+0.164\rho.f_y)(1+0.5\frac{c}{d}) \qquad (2\text{-}12)$$

Surprisingly, considering that the above equations were derived for normally reinforced concrete slabs, the test strengths were reasonably well predicted by all of the equations.

Two equations relating shear stress to effective and ultimate prestressing force based on Vanderbilt's observations from the test program were derived.

$$V_u = (360+0.30f_{pc})b.d \qquad (lb) \qquad (2\text{-}13)$$

$$V_u = (190+0.53f_{pcu})b.d \qquad (lb) \qquad (2\text{-}14)$$

Vanderbilt's results showed that there is a linear relationship between shear strength and initial prestress or ultimate cable force, Fig. 2-5.

Vanderbilt concluded any equation derived on the basis of the isolated simply supported model tests may be used with good accuracy in computing the strength of any other similar test programs. However, Vanderbilt noted :

★ The lines of contraflexure around the columns in continuous slabs do not coincide with those of isolated specimens.

★ Shears and deflections at the edges of isolated specimens are completely different from those of prototype structures.

★ The in-plane forces (membrane action) that may exist in real structures are generally ignored in the test specimens.

In 1970 Burns and Gerber conducted a series of tests to study the ultimate strength of post-tensioned flat plates. Ten isolated models 175 mm thick and 3.6 m square, normal weight concrete slab specimens with 250 mm column stubs were tested. All of the specimens were post-tensioned with six tendons, each composed of six wires having a diameter of 6.35 mm, in both directions. The final force, after losses, was 187 kN per tendon which resulted an average compression of 1.725 MPa in the concrete. Four of the specimens simulated cast-in-place concrete slabs and the rest simulated lift-slab construction. Various types of supplementary reinforcing steels were placed in the specimens over the supports to investigate their contribution to the behaviour of such slabs.

Primary failure in each specimen occurred as a combination of flexure and shear but shear

capacity was reached before the flexural capacity in all cases. After shear failure occurred the surface of failure spread conically from the face of the column stub at the bottom surface of the slab to a diameter of roughly 1.8 m at the top surface of the slab. In each specimen after primary failure occurred the capacity of slab to resist post-failure "reserve" loads was also examined. The reserve load was defined as the load which individual wires in the post-tensioning tendons commenced to break.

According to the ACI 318-63 the value of principal tension at failure, f_t , around the support (lifting collar, column or column capital) in a flat slab structure was limited to $0.03 f_c'$ or a maximum of 120 psi under working load condition. The ratio of f_t / f_c' determined in this experimental program varied between 0.068 and 0.109 representing a factor of safety between 2.27 and 3.63. The ratio was higher for cast-in-place specimens than lift-slab specimens. The average stress on the shear area ($\frac{d}{2}$ from the edge of the column) varied from $0.38\sqrt{f_c'}$ to $0.51\sqrt{f_c'}$. The highest value belonged to the specimen with added shear reinforcement. The authors concluded that the current design procedure was sufficiently conservative. The empirical equation developed by Scordelis *et al* at the University of California, Eq. (2-9), predicted the ultimate shear capacity below the test results by about 40 percent. It could be because the only variables in the equation were due to concrete strength and prestressing force. In this case, the prestress force was kept the same for all specimens and had no contribution to the change in shear strength. On the other hand, the presence of supplementary reinforcing steel around the support had a great contribution to the failure load.

Specimens with supplementary bonded reinforcement carried more load before failure than those without added bonded reinforcement. That could be because the supplementary reinforcing steel helps control cracking, increases ductility of the structure and greatly improves transmission of loads to columns. Adding supplementary reinforcement also increased the reserve capacity of the specimens. The strain measurements on the post-tensioning tendons revealed only a small stress increase in the tendons up to primary failure. The stress increase in the tendons passing over the column stub and near the centre of the specimens was approximately twice of the tendons near the edges. Also after primary failure, by increasing the load the centremost tendons were strained into the plastic range, as was expected, while the side tendons revealed rather minimal increases in stress.

In 1974 the first phase of a continuing research program on post-tensioned flat slabs at the University of Texas at Astin was published by Smith and Burns. Three isolated column-slab model were tested to investigate the behaviour and strength of post-tensioned flat plates in the critical column area and to give a better understanding of the influence of supplementary bonded reinforcement placed over the column stub.

Each specimen was made of normal weight concrete, 2.75 m square, 70 mm thick, with a 200 mm square column stub in the centre of the panel. Load was applied as a line load around the column located at a distance away from the stub-column. This type of loading was selected to simulate the zero moment requirement at the location of contraflexure lines, Fig. 2-6. The tendons were distributed 70 percent in the column strip and 30 percent in the middle strip. The average

concrete prestress was 2.25 MPa in each direction. The main variable in all three specimens was the amount of bonded reinforcement. The first specimen contained no supplementary bonded reinforcement, the second contained the minimum requirement recommended by ACI-ASCE committee 423, 0.15 percent of the cross-sectional area of the column strip, and the third specimen the amount of non-prestressed reinforcing steel was increased by 60% over that in the second specimen to 0.24 percent.

The behaviour of all three specimens was identical in the elastic range up to first cracking load. After reaching the first cracking load, the extra stiffness and ductility provided by non-prestressed bonded reinforcement became important in the response of each specimen including deflections, crack patterns, crack width, and mode of failure. All three specimens failed in a combination of shear and flexure, with the dominant failure mode occurring as punching shear. The specimen without any bonded reinforcement exhibited very large flexural cracks which opened suddenly under an applied load of around 90 percent of the ultimate load. The other two specimens behaved in a ductile manner with an improved crack distribution and maintained applied load even after serious cracks. Almost no stress increases were recorded in prestressing tendons for all three specimens up to near the failure load. The maximum stress increases were observed in the tendons passing through the column stub and recorded at about 10 percent of the initial prestressing force.

Cracking loads for all three specimens were found to be below the cracking loads calculated by ACI 318-71. This could be because the modulus of rupture was computed using the ACI

equation, $f_r = 7.5\sqrt{f_c'}$. This requirement refers to a cracking moment based on beam action, which arises questions regarding its validity when applied to two-way prestressed flat plates.

Based on the predicted ultimate moment capacity according to ACI 318-71 all three specimens should have failed in flexure. The values of $P_{u(test)}$ were higher than $P_{u(calc)}$ for ultimate moment capacity. But the large flexural cracks and deformation of each specimen near the failure load could indicate that flexural failure was almost reached and had a significant contribution to the punching shear failure. The nominal ultimate shear stress equation recommended by the ACI-ASCE committee 423, Eq. (2-15), yielded unconservative values compared to the test results.

$$v_{cw} = 3.5\sqrt{f_c'} + 0.3f_{pc} + \frac{V_p}{b_o \cdot d} \quad (psi) \qquad (2\text{-}15)$$

The low values of the shear stress from Eq. (2-15) could be attributed to the severe flexural cracking occurred at loads near failure. Widespread cracking in the critical section area around the column reduced the shear strength of the specimens in this region, resulting in early shear failure. As the amount of bonded reinforcement increased the shear stress values increased, because the bonded reinforcement improved the crack distribution and reduced the maximum crack width.

The disadvantage of the ACI-ASCE Committee 423 equation is that it makes no attempt to include effects of supplementary reinforcing steel around the column region in the punching shear strength.

In 1974 ACI-ASCE Committee 423 presented a report as a guide to the design of prestressed concrete flat plates. The main idea of the report was to supplement the applicable clauses of ACI 318-71 building code with additional recommendations. The outline of the report was about analysis and design methods, allowable stresses for concrete in flexure and shear, tendon distribution and spacing, auxiliary bonded reinforcement, the ratios of span to depth for deflection control, seismic design provisions, fire resistance and construction procedures.

The load balancing technique, together with the equivalent frame method were recommended as a widely used approach to analysis of post-tensioned flat plates. In applying the load balancing method on a prestressed concrete slab the effects of concave downward portion of the tendon profile can generally be neglected, since the reversed curvature acting near the column line has only a little influence on the elastic moments. However, it is necessary to consider the vertical component of the convex segment over the support in order to evaluate the shear carried by the tendons inside the critical section. The committee recommended the following allowable stresses at service loads when the equivalent frame (or beam) method is utilized for analysis of post-tensioned flat plates. The maximum allowable compressive stress in the concrete was limited to $0.30f_c'$ in negative moment areas. The maximum permissible tensile stress was recommended $0.5\sqrt{f_c'}$ for both positive and negative regions with addition of non-prestressed bonded reinforcement. The distribution of tendons in continuous spans was proposed as 65 to 75 percent in the column strip with the rest in the middle strip.

The use of non-prestressed bonded reinforcement to control cracking, increase ductility of the structure and improve the deflection response in slabs with unbonded cables was strongly recommended. The minimum amount of bonded reinforcement required in the top of column areas was defined as 0.15 percent of the cross-sectional area of the column strip in each direction.

The shear strength of post-tensioned flat plates was considered to be governed either by two-way action with diagonal cracking extending along the surface of a truncated cone or pyramid around the column or by beam action with a potential diagonal crack extending across the entire width. The critical section for slab action was defined as a periphery outside the column at $\frac{d}{2}$, which was presumed to control over the shear design based on beam action. The ACI 318-71 limit of $0.33\sqrt{f_c'}$ as the allowable shear stress for both ordinary reinforced and prestressed flat plates was believed to be too restrictive for prestressed concrete flat plates, Fig. 2-7. The committee recommended the use of design method considering shear as a two-way action which may result higher permissible shear stresses for prestressed flat plates.

In 1977 Burns and Hemakom reported the results of the test on a multi-panel model slab, slab 1, from their continuing study on the behaviour of prestressed flat plate structures. The model slab was a one-third scale model of a nine panel slab with overall dimensions of 10 m × 10 m in plan and average thickness of 74 mm with cantilever overhangs on two sides. Columns 200 mm × 200 mm × 345 mm high were spaced 3.0 m apart on centre in both directions. The slab was post-tensioned with 6 mm seven-wire strands in each direction. The average concrete compressive stress was 1.725 MPa. The distribution of tendons was 70% in the column strip and 30% in the

middle strip. The minimum amount of bonded reinforcement recommended by ACI-ASCE committee 423 was also added as top steel in the immediate column vicinity. The plan and elevation of the test slab as well as tendon arrangement and profile and location of bonded reinforcement are shown in Fig. 2-8.

The behaviour of the slab was entirely elastic until the load approached service loads, (D + L). No sign of cracking nor yielding of reinforcement was observed. The first crack was observed at the face of the interior columns at a load slightly above service load. Above this load, the load-deflection curves started to become nonlinear as the slab lost stiffness in the column areas. Under the ACI factored load, (1.4D + 1.7L), there were extensive cracks around the interior columns. The tendon stresses up to this stage, had not changed significantly, and there was no yielding of bonded reinforcement. With increasing load, very large deflections occurred, which could be observed visually in the middle of panels. Top and bottom flexural cracks lengthened and widened until at a load 30% above the factored load the interior column failed in punching shear. The crack pattern on the top surface of the slab immediately before failure is shown in Fig. 2-9.

The comparison between the moments calculated from the measured strains and those computed by the equivalent frame method and elastic plate theory showed fairly good agreement in both the column strip and middle strip. The yield line theory for predicting the ultimate flexural load was found to be quite satisfactory.

The failure mechanism at each column-slab connection was a combination of flexure and shear, in which the primary failure occurred as flexure. Punching shear failure was the second mode of failure. All the columns exhibited a sudden and complete punching failure with extensive cracks all around them. A plug of concrete having the shape of a truncated pyramid was formed with inclined surfaces made an angle of about 20° with the top surface of the slab. The comparison of the test results with the equation recommended by the ACI-ASCE Committee 423 (Eq. 2-15) showed that the prediction of the slab shear strength was reasonably safe.

From the analysis of this model slab, the following conclusions were made by the authors :

★ The bonded reinforcement in the prestressed concrete slab effectively controlled the distribution of flexural cracks and contributed to the ultimate load capacity of the slab.

★ The slab carried the ACI factored load without severe flexural cracking or distress. The ultimate flexural strength was well predicted by yield line analysis.

★ The steel stress in the tendons did not increase until the load approached the failure load and large deflections developed in the panels. At ultimate load, the maximum stress increase was recorded at about 10% of the initial prestressing force. The ACI 318-71 equation for calculation of the ultimate stress in the tendons predicted the tendon stresses at ultimate 2 to 13 percent above the measured values. The relationship between the increase in stress in unbonded tendons and applied load is shown in Fig. 2-10.

★ Concrete compressive strength, amount and location of supplementary bonded reinforcement, tendon arrangement and the average effective prestress in the slab were

found to be the main parameters influencing the shear capacity of prestressed concrete flat plates.

In 1977 a brief review regarding the current analytical methods for treating the flexural behaviour, shear strength and distribution of the tendons of prestressed concrete flat slabs was presented by Marti, Ritz and Thürlimann.

The application of the ordinary methods of the elastic or plastic theory for thin plates with small deflection was recommended for the analysis of the internal force resultants of post-tensioned slabs with bonded tendons. Application of the above methods for unbonded post-tensioned slabs was found to be unsatisfactory, because there are no frictional forces between the concrete and tendons, so the strain in an unbonded tendon is almost constant over its whole length. In unbonded structures after cracking, a compressed shell or arch action (concrete in compression) and a tension membrane action (tendon force) are formed as shown in Fig. 2-11. The analysis of such slabs should corporate these two actions. A more realistic model, including the effect of membrane forces along with tied-arch action, shown in Fig. 2-12, was proposed to provide a better understanding of the real behaviour of unbonded prestressed concrete slabs. In this model the restraining effect against lateral movements (membrane forces) was idealized by a horizontal spring. The whole idea was based on subdividing the strength of an unbonded prestressed slab into different parts : the upward transverse component of the prestressing force, concrete acting as a compressed arch or shell and tendons as a tension membrane and finally the extra bending action provided by bonded reinforcement and flexural rigidity of concrete.

However, the authors mentioned that in practice simple approximate methods like beam method, equivalent frame method, finite differences or finite elements may be used for both type of slabs without noticeable errors.

Using the above concept, the ultimate load of laterally restrained slabs was found to be greater than slabs without lateral restraint, Fig. 2-13. Marti concluded that the influence of membrane forces on crack pattern and crack width is an important factor which should be included in the design process.

Prevention of shear failure at slab-column connections is one of the critical problems for flat slab systems. Shear forces are assumed to be carried by arch action, aggregate interlock and by dowel action of the reinforcing bars. The results of slab-column tests have clearly shown that the value of nominal shear stress at the critical section around the column is dependent on concrete strength, ratio of flexural reinforcement and the ratio of column diameter to the effective slab depth. The collapse load P, Fig. 2-14. when there is no shear reinforcement and also no lateral movements is allowed was derived as :

$$P_u = \pi.\kappa.d^2.f_c'\left(\frac{\sqrt{\zeta}}{2}+\frac{1-\zeta}{4\kappa}\right) \qquad (2\text{-}16)$$

Where ζ denotes the ratio of concrete tensile to compressive strength

κ is the ratio of column size to slab thickness

A brief survey by Marti *et al* on the load carrying system in prestressed concrete flat slabs

recognized the influence of prestress on enhancing the load-deflection capacity as shown in Fig. 2-15. Part of the load is transmitted to the column by transverse component of the prestressing force, P_s. The remaining part, P_c , is carried similar, although not identical, to that of an ordinary reinforced flat slab, i.e. after cracking by aggregate interlock, dowel and arch action and possible shear reinforcement. The value of $(P_s - P_b)$ relates to the tendon force increase and depends on the flexural behaviour of the slab system. If the amount of prestressed and non-prestressed reinforcement supplied over the column regions is enough, then a satisfactory behaviour for large deflections will be provided for the slab. If not, shear failure will be more vigorous than for a reinforced concrete slab because failure will occur without warning by flexural cracking.

Marti *et al* concluded that, placing of tendons in the column lines (at least 50%) improves the factor of safety in slabs with regard to punching failure. Also the use of properly arranged non-prestressed reinforcement over the column area was strongly suggested.

In 1978 Clark proposed a load carrying mechanism for shear resistance of slabs mainly based on Regan's work. He assumed that the ultimate shear resistance of a slab is represented by the sum of shear carried by the concrete in compression zone near the column and the dowel action of the reinforcing steel within the area inside the inclination of the shear crack.

The shear carried by the compression zone, V_c , was defined as :

$$V_c = v' . u' . \bar{x}d \qquad (2\text{-}17)$$

Where v' is the mean value of ultimate shear stress in the compression zone and according to Regan (1971) was given as, $v' = 0.27 f_{cu}^{(2/3)}$, $\bar{x}d$ is the depth of neutral axis, Fig. 2-16, and u' is the shear failure perimeter. The shear stress $0.27 f_{cu}^{(2/3)}$ is based on beam action and it may be higher for slabs due to the confined nature of compression zone. The perimeter on which compression zone in concrete fails was taken as $\frac{d}{4}$ from the face of the column giving :

$$V_c = 0.27 f_{cu}^{(2/3)} (c_o + \frac{\pi d}{2}) \bar{x}d \qquad (2\text{-}18)$$

The shear carried by dowel force was taken as :

$$V_d = k_d . f_{cu}^{1/3} . d_b . u_d \qquad (2\text{-}19)$$

Where k_d is a coefficient depending on the type of bar (1.5 for deformed bar and 1.0 for plane bars). u_d is the sum of 8 times the cover for each bar crossing a perimeter 2d from the column face but not more than $c_o + 4\pi d$.

Finding the neutral axis depth, $\bar{x}d$, is difficult as it depends on the compatibility of all deformations in the reinforcement and the concrete over the projected length of shear crack. By referring to the strain diagram, Fig. 2-16, and assuming that concrete reaches its maximum load capacity in flexure while tensile reinforcement remains elastic, the depth of neutral axis was calculated as follows:

$$\frac{\bar{x}}{1-\bar{x}}=\frac{\epsilon_{cc}}{\epsilon_{pb}-\epsilon_{pe}} \qquad (2\text{-}20)$$

Where ϵ_{pb} and ϵ_{cc} are the strain in the tendons and concrete at failure and ϵ_{pe} is the initial strain in tendons.

$$\epsilon_{pb}-\epsilon_{pe}=\frac{(p_{pb}-p_{pe})}{A_{ps}.E_s} \qquad (2\text{-}21)$$

According to CP110 (1972) the compressive concrete force at failure was defined as,

$P_{pb}=C=\alpha_c.f_{cu}.b.\bar{x}d$ so :

$$\frac{\bar{x}^2}{1-\bar{x}}=\frac{\epsilon_{cc}E_s}{\alpha_c f_{cu}}\rho_{ps}\frac{1}{1-\frac{P_{pe}}{P_{pb}}} \qquad (2\text{-}22)$$

The same equation can also be derived for reinforced concrete slabs :

$$\frac{\bar{x}^2}{1-\bar{x}}=\frac{\epsilon_{cc}E_s}{\alpha_c f_{cu}}\rho_s \qquad (2\text{-}23)$$

If an equivalent steel ratio equal to $\rho_s=\rho_{ps}(\frac{f_{pu}}{410})$ is substituted in Eq. (2-23) then the two equations give the same value of $\bar{x}d$ when $\frac{P_{pb}}{P_{pe}}=1.3$. This ratio is rather unlikely to happen for unbonded tendons, but by assuming the ratio of tendon force at failure to initial tendon force after losses for each particular case, it should be possible to find the depth of neutral axis by iteration and then determine V_c .

The combined steel ratio, ρ_e , for both prestressed and reinforcing steel was defined as : (This value was recommended not to be taken more than 0.03)

$$\rho_e=\frac{f_{pu}}{410}.\rho_{ps}+\rho_s \quad \text{where} \quad \rho_{ps}=\frac{A_{ps}}{b_o h} \quad , \quad \rho_s=\frac{A_s}{b_o h} \tag{2-24}$$

In 1982 Franklin, Cleland and Long proposed a method for predicting the ultimate punching capacity of post-tensioned slabs at internal connections. They believed that flexural stresses have a significant effect on the punching stress, because the slab-column connection is the location of both maximum shear and bending moment. There is strong experimental evidence to demonstrate that the slab moment at the column face is the critical moment for punching failure. They assumed that by increasing the load, the initial flexural crack at the slab-column interface propagates towards the neutral surface and eventually failure occurs by crushing of the highly stressed compression zone. The failure criterion was based on the assumption that the concrete extreme fibre strain reaches a limiting value of 0.0038. This is reasonable for slabs with bonded reinforcement and high prestress level, because failure of the concrete compression zone can occur prior to yielding of the bonded steel.

The relationship between the two important factors in punching strength, the vertical load V and the slab moment per unit width m , at the critical section was given by :

$$V=k_1.m \tag{2-25}$$

The factor k_1 is dependent on the ratio of column side length to slab span $\frac{c}{L}$ and the slab boundary conditions. The ultimate moment of resistance of post-tensioned slabs according to Cleland's work was taken as :

$$m_u = \rho_e . f_{pb} . d^2 (1 - 0.60 \frac{\rho_e . f_{pb}}{f_{cu}}) \qquad (2\text{-}26)$$

Where ρ_e is the equivalent reinforcement ratio given by :

$$\rho_e = \rho_s + \rho_{ps} \frac{f_{pb}}{f_y} . \frac{d_{ps}}{d} \qquad (2\text{-}27)$$

In using the above equations, the tensile stress in prestressing tendons at slab failure, f_{pb} was estimated on the basis of the values recorded in previous tests. Combining Eqs. (2-26) and (2-25) the punching strength capacity can be obtained. A comparison between this method and experimental results, Fig. 2-17, showed that their method underestimates the failure load by about 40% in some cases. This was attributed to dowel action of the reinforcement. A factor 1.3 was proposed in Eq. (2-22) to take into account the contribution of dowel force. Any additional increase in the failure load was related to the effect of membrane forces. In the case of post-tensioned unbonded slabs it was considered improbable that dowel action could be effective to such an extent. Therefore they assumed that any increase in failure load in prestressed concrete flat slabs is solely due to compressive membrane action and tried to evaluate the influence of compressive membrane action on the ultimate strength of flat slabs.

The development of compressive membrane action around a simply supported single slab-column connection is concisely explained by Fig. 2-18. As the load is applied, the slab regions adjacent to the stub column deflect and circumferential cracks form at the column junction, Fig. 2-18(b). However, the regions further away from the column and close to the outside boundaries undergo almost no deflection or cracks; as opposed to the regions nearer the centre which have

no desire to expand. If there is no lateral restraint, the slab tries to deform the shape shown in Fig. 2-18(c). If the slab is not free to move laterally, the centre areas are subjected to a compressive in-plane force resulting from the outer regions of the slab resisting against lateral movement by tension force, Fig 2-18(d). The existence of this tension ring and compressive membrane forces has been verified by Smith and Burns, Fig. 2-19, and Franklin (1982).

Long *et al* believed that the creation of compressive in-plane action in a test model is analogous to the problem of a thick hollow cylinder subjected to a uniform internal pressure, Fig. 2-20. The compressive membrane force at internal column using thick cylinder theory was given by :

$$\frac{H}{h}=\frac{R^2-a_1^2}{R^2+a_1^2}\sigma_t \qquad (2\text{-}28)$$

Where H is the compressive membrane force per unit width.

When the pressure inside the compression zone is big enough to create radial cracking of the tension ring, the contribution of compressive membrane action in punching failure is considered to have finished and punching failure occurs. For a reinforced concrete section, cracking of the tension ring does occur, when the tensile strength of concrete is attained. In the case of post-tensioned slabs the amount of tangential stress, σ_t , in the above equation is due to pre-compression force, because of prestress, and the tensile strength of concrete :

$$\sigma_t = f_t + f_{pc} \tag{2-29}$$

It is obvious that the ultimate moment of resistance will be increased by considering the compressive membrane force. According to Long, referenced from Wood's work, when a slab section of unit width is subject to a total compression H with the tension steel having been yielded, then the stress diagram over the effective depth can be established as shown in Fig. 2-21. By assuming that the lever arm does not change with the presence of compressive force, the increase in moment over the normal ultimate moment to a first approximation can be written as:

$$E_{CMA} = \frac{m_{uc}}{m_u} = 1 + \frac{H}{2T_o} \tag{2-30}$$

Where T_o is the total force in both bonded and prestress reinforcement.

The radii of the compression zone, a_1, based on the limited data on unbonded flat slabs was assumed equal to 0.125L. Based on the above information, the following equation was proposed for punching shear strength of prestressed unbonded flat slabs.

$$V = (1 + \frac{H}{2T_0}) k_1 . m_u \tag{2-31}$$

$$\textit{in which} \qquad H = \frac{R^2 - (0.125L)^2}{R^2 + (0.125L)^2} . (f_t + f_{pc}) h \quad , \quad T_o = \rho_e . f_y . d \tag{2-32}$$

considering the effective depth d as $0.8h$ and tensile strength of concrete as $0.44\sqrt{f_{cu}}$, the punching shear force in SI units becomes :

$$V=k_1.d^2.f_{cu}.\omega_e(1-0.60\omega_e)\left[1+\frac{0.279\lambda}{\omega_e\sqrt{f_{cu}}}(1+2.24\frac{f_{cp}}{\sqrt{f_{cu}}})\right] \qquad (2\text{-}33)$$

Where ω_e is the equivalent reinforcement index $\omega_e=\rho_e\frac{f_y}{f_{cu}}$ and $\lambda=\frac{R^2-(0.125L)^2}{R^2+(0.125L)^2}$

For slabs extending to the line of zero moment, $R=0.2L$ and $\lambda=0.438$ while for slabs extending to mid-span, $\lambda=0.882$. The comparison of this approach and test results is demonstrated in Fig. 2-22.

The above equation consists of two important parts. One is the equivalent reinforcement index, ω_e and the other is the concrete strength and the effective concrete prestress. The influence of each of these terms in the proposed method is illustrated in Figs. 2-23. It is evident that the equivalent reinforcement index has the most significant effect on the ultimate moment resistance and therefore punching shear capacity. Long concluded that the influence of the membrane action decreases as the reinforcement level increases. Concrete strength and effective concrete prestress show a minor effect on the ultimate moment resistance. This conclusion was confirmed by the previous results (Grow & Vanderbilt) in which two similar specimens with different levels of prestressing failed at almost identical loads.

In order to simplify the application of equation (2-33) to practical slab situations a simplified design method was also developed by the authors.

The relationship between critical slab moment and vertical load according to Masterson was

found to be largely dependent on the $\frac{c}{L}$ ratio and this relationship was expressed as :

$$\frac{m}{V}=0.046\left(\frac{L}{c}\right)^{0.5} \qquad (2\text{-}34)$$

Combining Eqs. (2-33) and (2-34) and assuming that the average prestress normally lies between 1 N/mm² and 3 N/mm², while the reinforcement index $\omega_e=\rho_e\frac{f_y}{f_{cu}}$ lies between 0.075 and 0.25, yielded the following equation for the punching shear capacity of prestressed concrete flat slabs extending to mid-span :

$$V=10\left(\omega_e\frac{c}{L}\right)^{0.5}.f_{cp}^{0.133}.f_{cu}.d^2 \qquad (2\text{-}35)$$

The same procedure was followed for derivation of similar equation for slabs extending to the line of contraflexure :

$$V=20\left(\omega_e\frac{c}{L}\right)^{0.67}.f_{cp}^{0.08}.f_{cu}.d^2 \qquad (2\text{-}36)$$

The term ω_e is more pronounced in the second equation. This is due to the smaller contribution of membrane forces in the slabs extending to the contraflexure line. The use of the above equations was not recommended for ω_e greater than 0.3 as the critical section was presumed to be over-reinforced and the value of m_u might be underestimated. In using Eqs. (2-35) and (2-36) for calculation of ultimate capacity of a post-tensioned slab, the portion of the load balanced by prestress was not included in the equations. The load associated with the generation of secondary reactions and moments in a multi-panel slab due to prestressing and eccentricities of tendons should be calculated and added to the ultimate load obtained from the proposed method.

In 1982 a series of tests on unbonded flat slabs using scaled models was carried out by Franklin and Long at Queen's University, Belfast. The main parameters involving the test program were the level of eccentricity of applied load and the slab boundary conditions. All models (except one) tested were subject to both shear and moment transfer.

Seven one-third scale models with different eccentricities and support conditions were chosen for the test program. The models were extended to mid-span between column centres in order to give displacements and load-deflection relationships similar to those of a real structure. Three of the models had carefully controlled edge restraint system (models type M) to demonstrate the effect of boundary conditions on the ultimate strength of slabs, where as the remainder had free edges (models type B). The slabs were post-tensioned using 5 mm dia. high tensile wires, providing average slab stresses between 2.43 MPa and 3.09 MPa. Ordinary bonded reinforcement was also used over the column region in order to control cracking and transit the load to the column. In the models with free edges, external loading was applied by means of 16 point loads along the ring approximately corresponding to the line of contraflexure. For models type M a uniformly distributed load was effected by 16 point loads distributed all over the slab as shown in Figs. 2-24 and 2-25.

The general behaviour of the models with moment transfer (unequal spans) can be described as development of circumferential cracks at the moment transfer face , followed by radial tension cracks propagating from the corners of the column stub. At the design ultimate load (1.4D.L. + 1.6L.L.) a few radial cracks localized near the column region were observed. With further

increase in applied load the radial cracks spread across the full width of the models. Just prior to failure in all specimens, there was significant opening of the flexural cracks across the moment transfer side of the columns. The specimen with maximum eccentricity in the test series exhibited least extensive failure surface. The specimen with zero eccentricity had an elliptical shape after failure with major axis parallel to the banded tendons. Inspection of the slabs lower surface revealed severe crushing of the concrete compression zone at the slab-column connection. This is not usually the case for reinforced concrete slabs.

The variations of tendon forces with applied load was insignificant until severe flexural cracking occurred around the slab-column connection. The maximum stress increase in all specimens occurred in the banded direction and measured about 10% of the initial prestressing force. The measured increases were compared to the predictions of the Concrete Society report (1974). The ratio of experimental tendon stress increases to predicted values varied between 0.93 and 1.44. The ACI 318-77 method was criticized for not taking into account the span to depth ratio $\frac{L}{d}$ in the equation predicting the stress in prestressed tendons at nominal strength.

The ultimate capacity of each model was calculated using ACI 1977 and Concrete Society 1974 methods. The predicted capacities by both methods were very conservative and both methods showed poor agreement with the test results.

In 1985 Regan reported fifteen tests of flat slabs post-tensioned in one direction and provided with light supplementary reinforcement of deformed bars in the transverse direction. The test

program was undertaken to provide experimental data on the punching shear resistance of the regions around intermediate column supports of prestressed slab bridges. The model slabs were mainly constructed as 225 mm thick slabs with widths of 1.5 m and lengths equal to 3 m. The slabs were fully prestressed by twelve 18 mm Dyform strands in the longitudinal direction with an average concrete compression stress of 8.9 MPa. Two specimens were made with low prestress (2.2 & 2.8 MPa) to investigate the influence of prestress on the ultimate strength of slabs. In most of the specimens the tendon ducts were grouted except one which simulated an unbonded post-tensioned flat slab. The model slabs were loaded through a 150 mm square plate.

Three specimens failed in flexure and the rest failed by punching. For the case of punching failure a truncated cone of concrete with an angle of about 30 degree to the slab plane in a polar-symmetric surface was formed. The influence of the prestressing force on the ultimate load of the slabs was important. Two specimens similar in all respects except their prestress, one with 2.8 MPa and the other with 8.9 MPa, showed an increase in ultimate load from 715 kN to 832 kN. Also in specimens with low prestress the main direction of cracking was in the transverse direction with cracks almost parallel and extended over a large part of the span, while with full prestress, the crack pattern was roughly radial in the specimens with restricted transverse cracking and some tendency towards longitudinal direction as shown in Fig. 2-26. The lack of bond in one of the specimens reduced its resistance by only about 10%.

Strain gauges placed inside the specimens to detect the internal diagonal cracking indicated the initiation of these cracks at about 70% of the ultimate punching strength. The strand strain

measurements were found to be relatively uniform over the width of slabs. The arrangement of the bonded steel and the longitudinal prestress had a considerable effect on the steel stresses in the transverse direction. The midspan strains in the specimens with bars spaced uniformly over the entire length were almost twice as the specimens with heavily banded reinforcement. The low prestress reduced the longitudinal stiffness of the slabs and caused the transverse flexure to be concentrated near the loading point. In fully prestressed specimens the distribution of transverse steel strains was almost uniform along the length of specimens.

In developing a design equation for prestressed concrete slabs, Regan introduced the idea of treating prestressed slabs as a reinforced slab having the same ratio of flexural reinforcement after the load at which the extreme fibre stress reaches zero. In this method the influence of prestress on punching strength was to add the decompression load to the punching resistance of geometrically similar slabs without prestress. Hence,

$$P_{up}=P_{ur}+P_o \quad or \quad P_{up}=P_{ur}\left(\frac{1}{1-\frac{P_o}{P_{up}}}\right) \tag{2-37}$$

And for slabs prestressed in both directions :

$$P_{up}=P_{ur}+P_{url}\left(\frac{1}{1-\frac{P_{ol}}{P_{up}}}\right)+P_{urt}\left(\frac{1}{1-\frac{P_{ot}}{P_{up}}}\right) \tag{2-38}$$

The above equation was found inconvenient as it contained P_{up} on both sides. So a simple approximation was taken as :

$$P_{up}=P_{ur}+P_{ol}(\frac{P_{url}}{P_{ur}})+P_{ol}(\frac{P_{urt}}{P_{ur}}) \qquad (2\text{-}39)$$

The nominal ultimate shear stress of a reinforced slab was given as in the draft version of CP110 (1982) :

$$v_u=0.27\sqrt[4]{(\frac{500}{d})}\sqrt[3]{(100\rho.f_{cu})} \qquad (2\text{-}40)$$

The effective width of the slab to be used for calculation of ρ was not well-defined in the codes. In CP110 (1982), ρ was computed over a width $(c+6d)$. CEB determined the reinforcement ratio at $1.5d$ to either side of column breadth. Regan's tests demonstrated no sign of enhancement in the ultimate load with increasing concentration of transverse reinforcement toward the load. Therefore, Regan proposed that ρ would be best calculated for the full width of slabs supported on a single central column. The definition of ρ for the case of longitudinal tendons accompanied by supplementary longitudinal bars was given as :

$$\rho=\frac{(A_s+A_{sp})}{bd} \quad in\ which \quad d=\frac{A_s.f_y.d_r+A_{sp}.f_{0.2}.d_{ps}}{A_s.f_y+A_{sp}.f_{0.2}} \qquad (2\text{-}41)$$

The control perimeter around the column was taken at a distance $1.5d$ from the edge of the loaded area. Thus :

$$P_{url}=0.27\sqrt[4]{\frac{500}{d}}\sqrt[3]{(100\rho_l.f_{cu})}(2(b_l+3d_l)d_l) \qquad (2\text{-}42)$$

$$P_{urt}=0.27\sqrt[4]{\frac{500}{d}}\sqrt[3]{(100\rho_t.f_{cu})}(2(b_t+3d_t)d_t) \qquad (2\text{-}43)$$

$$P_{ur}=P_{url}+P_{urt} \tag{2-44}$$

The only additional step was to estimate the load corresponding to zero stress at the extreme fibre applied by the external loading. This estimation was based on the relationships between P_o and decompression moment per unit width of slab, m_o :

$$m_o=(\frac{h^2}{6})f_{pc}^* \tag{2-45}$$

Where f_{pc}^* is the extreme fibre compression due to prestress. For slabs prestressed in only one direction, the moment equation for a full slab width affected by a concentrated load at the centre of a span of length L is :

$$P_o=\frac{4m_o a}{L} \tag{2-46}$$

For slabs prestressed in two directions, all that needs to be considered is an equation of moments for a line across the full width of slab, Fig 2-27.

In some cases where the test slabs were continuously supported at all edges, P_o was taken as $2\pi m_o$ with m_o calculated based on the average eccentricity of the cable forces at the yield lines, Fig. 2-28. That's because the decompression load is influenced by the parabolic shape of the prestressing tendons crossing the ultimate crack lines.

The comparison between calculated and experimental results was seen to be generally good even though most cases were with unbonded tendons, Fig. 2-29. It should be mentioned that

Regan developed his theory for bonded post-tensioned slabs.

At the end of the report some important aspects of the behaviour of prestressed slabs in the vicinity of concentrated supports were reviewed :

★ Where the tendons are continuous over multiple spans in a real structure the increments of strand stresses when loading is applied to only one region would be much smaller than in test conditions.

★ If the ultimate stresses in tendons were known, the value of ρ in Eq. (2-42) could be calculated with complete accuracy. Therefore the lack of bond could be allowed by reducing the value of ρ .

★ In a multi-panel slab a surrounding area with minor cracking will produce significant in-plane forces.

★ Concentration of the tendons over the support with maximum eccentricity at the column will increase the resistance load of the slab in a great deal.

In 1985 two consecutive papers were published by Burns *et al* reporting load tests of two different prestressed model slabs. Both slabs were one-half scale models with banded arrangement of unbonded tendons; one consisted of a nine panel flat plate and the other a four panel flat plate. The experiments were performed to study the behaviour and strength of a continuous prestressed slab with a banded tendon arrangement. The first slab (nine panel) was designed as a building floor with overall dimensions of 10 m in plan and 70 mm thick with sixteen 200 × 200 mm

columns spaced at 3.048 m on centre in both directions. Fig. 2-30 shows the details of the half-scale model. The slab was post-tensioned with 24-6.35 mm diameter tendons in each direction. The total compressive stress on the slab was 0.932 MPa. The minimum bonded reinforcement (0.15% of the cross-sectional area of the column strip) was added as top steel near column regions to increase the ductility and the ultimate strength of the slab.

The slab was loaded with various patterns of loading. The first load stage was a test with all panels loaded to check the instrumentation. At the second load stage the slab was loaded to design live load (D + L). Cracks formed along the face of some edge and inner columns. When the slab was unloaded the deflection recovered completely and the cracks closed. At load stage 6 all panels were loaded corresponded to the ACI factored load (1.4D + 1.7L). The slab carried the load without severe cracking. The cracks were described as very fine cracks extending radially outward from the column faces. At a load 20% above the ACI factored load the slab failed. The primary failure was flexural with a secondary punching shear at the middle column. The slab behaved in a ductile manner so that very large deflections occurred at the centre of panels before failure. The maximum increase in tendon stress was recorded at about 12% of the initial prestressing force in the banded direction. After punching shear failure had occurred at the first interior column, that column was shored and slab was reloaded again to determine the shear capacity of individual column-stub connections. The slab behaved nonlinearly from the beginning of loading because of the previous cracking. In all punching shear tests, the slab failed first in flexural mode with large rotations developed at the negative moment areas followed by the punching shear failure.

The typical shape of shear cone at punching shear failures can be described as a plug of concrete with unsymmetric surface making an angle of about 34° with the slab plane in the direction of uniformly spaced tendons and 19° with the direction of banded tendons, Fig. 2-31. The shear stresses calculated from the test results ranged from $0.23\sqrt{f_c'}$ to $0.32\sqrt{f_c'}$ and appeared to be much lower than those found by the previous investigators or computed according to the equation of ACI-ASCE committee 423, Eq. (2-15). The explanation was given that because of very large rotations at the negative moment area, it was unable to increase the load. Also maintaining the flexural failure load on the slab resulted in large deflections and curvatures in the slab-column connection areas. The curvature of the slab seemed to be an important factor for the shear capacity and it was concluded that punching shear is always recognised as a secondary mode if the curvature of the slab at the column junction increases indefinitely.

The second slab (four panel) was designed following the recommendations of ACI-ASCE committee 423 (1974). The model slab, shown in Fig. 2-32, was 6.1 m square, 70 mm thick and supported on nine 200 mm square columns placed 3.048 m on centre in each direction. The cables were uniformly distributed in one direction and banded through the column strip in the other direction. The total compressive stress for the slab was 1.27 MPa. Ordinary bonded reinforcement was placed over the column region in order to control the cracks giving more ductility and higher shear capacity. At several locations No. 2 deformed bar stirrups were provided to investigate their behaviour throughout the test.

The overall behaviour of the slab was elastic and symmetric up to service load. At a load slightly above service load, the first visual cracks appeared on the top surface of the slab, spreading radially from the corners of the intermediate column. At design ultimate load further cracks developed around the interior column. As load was applied beyond the design ultimate load the cracks widened and lengthened, new cracks developed until at a load 15% above the design ultimate load, a punching shear failure occurred at the edge column. The damage was so bad that much of the prestress force was lost in the banded tendons running through the column. The angle that the inclined surfaces of shear failure made with the top surface of the slab was about 26° along the banded direction and 19° along the uniform tendon spacing direction. The relationship between the tendon-strain gauges and applied load revealed that the increase in tendons stress was quite small until very near to ultimate load. The measured tendon-stress increase was found to be around 8% of the effective stress immediately after transfer. The ACI code 318-77 equation predicted the ultimate stress 10-16% higher than measured values. The following equation was suggested for predicting the ultimate stress in unbonded tendons.

For $\frac{L}{h}$ ratios less than 28 :

$$f_{ps}=f_{se}+\frac{10{,}000f_c'}{100\rho_p} \qquad (2\text{-}47)$$

For $\frac{L}{h}$ higher than 28 :

$$f_{ps}=(1.265-9.375\times10^{-3}\frac{L}{h})(f_{se}+10{,}000+\frac{f_c'}{100\rho_{ps}}) \qquad (2\text{-}48)$$

The ultimate flexural load was well predicted by yield-line analysis. The yield line pattern is

shown in Fig. 2-33. The very small difference between measured and calculated ultimate loads was attributed to the effect of membrane action of the slab.

In each column connection shear failure occurred by sudden punching of the column stub through the slab with little warning of failure. The use of stirrups along the banded direction of the edge column prevented a violent failure and concrete spalling, but had no contribution to the load-carrying capacity of the slab-column connection. The shear strength of the slab-column connections tested were safely predicted by the equation recommended by ACI-ASCE committee 423, Eq. (2-15).

In 1989 the results of tests to failure on six full-size statically determinate unbonded post-tensioned slab-edge column specimens simulating parts of a two-way unbonded post-tensioned multi-panel slab were reported by Dilger and Shatila. The effect of stud shear reinforcement on the strength and behaviour of this type of connections was the main objective of the investigation. Slab-edge column connections are considered more susceptible to brittle shear failure because of smaller resisting section combined with a large bending moment.

The test specimens were 150 mm thick, varied in size and supported on 250 mm square columns. The average prestress in both banded and uniformly distributed directions was 1.2 MPa. Bonded non-prestressed reinforcement was also placed in the vicinity of columns in both directions as required by CSA (1984) and ACI (1983) codes. Three of the specimens were provided with shear reinforcement.

All the specimens showed the same load-deflection pattern, with a decrease in the slab stiffness after cracking of the concrete had occurred. A further decrease occurred when the bonded reinforcement started yielding. At loads close to the failure load large deflections and rotations were generated resulting in a sudden drop in the stiffness of the connections. Cracking developed at the column periphery with formation of radial cracks at a load of approximately 40% of the ultimate. As the load increased radial cracks extended from the column corners towards the slab free edges and more flexural and torsional cracks developed. Close to failure the width of the flexural cracks increased and circumferential cracks connecting the radial cracks also developed. The tendon stresses remained almost constant until the load approached the ultimate. The maximum measured tendon stresses recorded at failure were of the same magnitude as obtained by Burns (about 12% of the initial prestress). It was found that ACI code (1983) equation predicts the tendon stresses roughly 5% higher than experimental results while CSA code (1984) predicts 3% lower. Immediately prior to failure all bonded reinforcement passing through the column and perpendicular to the free edge yielded. Yield-line theory provided an excellent prediction of the flexural resistance of slab-edge column connections.

Shear stresses were calculated along the critical section $\frac{d}{2}$ from the face of the column according to the ACI and CSA codes. The nominal stresses predicted by ACI code were considerably lower than the observed values. This indicated that the ACI code equation for shear strength of reinforced concrete slabs can be safely applied to prestressed slab-column connections. The ACI code approach in modelling the behaviour of exterior slab-column connections, Fig. 2-34, was shown to be unsatisfactory. According to this code, the shear stress is supposed to reach

the zero value at point c between a and b, Fig. 2-34, However, the highest value of stud forces was observed at this point. The measurements of the forces in the studs confirmed the failure model established by Hawkins (1977) shown in Fig. 2-35. According to this model, where the failure surface intersects the stud, the forces in studs should be highest. The same conclusions were made for the CSA provisions for shear resistance of slabs.

Based on the test observations and numerical analysis, Regan and Shehata (1989) proposed a rational approach to model the behaviour of slabs failing by punching. The slab was considered as rigid segments, each bounded by two radial crack lines, the circumferential crack around the column periphery and the contraflexure lines, Fig. 2-36. Each radial segment is assumed to rotate around the root of shear crack at the face of the column. The following assumptions were implied by the proposed model :

1) Bonded reinforcement crossing the tangential crack at the column yields.

2) Near the failure the small wedge shape element bounded by the internal shear crack and the initial circumferential crack is separated and rotates independently.

3) The inclination angle of the internal shear crack was taken as 20°.

4) The concrete in compression zone is considered to be in the plastic range.

In order to establish a relationship between all forces involved in the analysis of each radial segment, Fig. 2-36, the three equilibrium conditions $\left(\sum F_r=0\ ,\ \sum F_t=0\ ,\ \sum M_r=0\right)$ in a radial plane are written:

$$dF_{cr}.\cos\alpha + F_{ct}.\Delta\phi = (dF_{sr} + dF_{srp}) + (F_{st}.\Delta\phi + F_{stp}.\Delta\phi) \qquad (2\text{-}49)$$

$$P\frac{\Delta\phi}{2\pi} = \xi\, dF_{cr}.\sin\alpha + dD \quad , \quad \xi = \sqrt[3]{\frac{500}{d(mm)}} \qquad (2\text{-}50)$$

$$P\frac{\Delta\phi}{2\pi}(r_p - r_o) = (dF_{sr} + dF_{srp} + F_{st}.\Delta\phi + F_{stp}.\Delta\phi)z + dD(r_w - r_o) \qquad (2\text{-}51)$$

$$z = lever\ arm = (d - 0.45x)$$

In slabs with unbonded cables, steel stress changes insignificantly due to the slab deformation, so F_{st} and dF_{cr} can be taken as zero. Because of no bond between the cables and concrete, and flexibility of the tendons dD can also be considered equal to zero. dD can also be ignored when the steel reaches its yield strength at the time of punching failure.

For these three non-linear equations, for a certain value of ψ the values of neutral axis x, the inclination of the bearing force α and the load P can be found. This iteration continues until one of the following critical states is achieved :

1) The inclination of the compressive force at the column face α reaches 20°. Failure occurs by splitting of concrete due to principal tensile stresses.

2) The radial strain on the bearing stress face reaches a value of 0.0035 in the plastic length. According to the experimental ultimate rotation, the plastic length was assumed to be 150 mm measured from the face of the column. Thus, $\epsilon_{cr} = 0.0035 = \psi\left[\frac{x(mm)}{150 + r_o}\right]$ Failure occurs by radial crushing of concrete.

3) The tangential strain of the compressive face at a distance x from the column periphery reaches a characteristic value of 0.0035, $\epsilon_{ct} = 0.0035 = \psi\left[\frac{x}{r_o + x}\right]$. Failure occurs by tangential crushing of concrete.

Regan compared his results of the proposed model with the theory of Kinnunen and Nylander (1960), with ACI 318 (Building Code 1983), BS8110 (Structural Use of concrete 1985) and with test data collected from previous experiments.

The improvements of the model over Kinnunen and Nylander were stated to be :

1) The value of dowel forces are calculated based on equilibrium. (Kinnunen presumed a constant value of 30% of the ultimate load as the effect of dowel forces.)

2) The definition of failure is more complete.

3) The bearing strength of concrete acting in the radial direction is calculated on the basis of longitudinal stress gradient, Fig. 2-37. This value was determined based on the bearing area of concrete normal to the inclined force dF_{cr} and the area of the section at a distance x from the bearing area as shown in Fig. 2-36. Kinnunen assumed an established value of $2.35 f_c^{'}$ for bearing strength based on a discussion of triaxial stress behaviour.

A parametric study of the proposed model with respect to code approaches showed that the effect of concrete strength on the ultimate punching load is very similar to BS 8110-85. BS8110

takes into consideration the influence of the steel ratio very close to the theory, while ACI method ignores it. From the comparison between the proposed method and test data, it was concluded that the proposed model represent the true structural behaviour of slabs subjected to symmetric central loadings. The results of 27 slabs tested by previous researchers were examined. The average $\frac{P_{test}}{P_{calc}}$ was 1.02 with an standard deviation of 0.08.

In 1990 Shehata derived a simpler rational model over the model he and Regan had previously proposed. The characteristic of this new method was essentially the same as the previous, but was easier for designers or to be adopted by codes. The slab was divided into radial sectors which could rotate independently around a centre of rotation located at the face of the column and on the level of neutral axis. The internal diagonal crack was taken at an angle of approximately 20° with the slab plane, and the equations of equilibrium were derived. The first step of simplifying the former model was to calculate the neutral axis depth on the basis of a semi-rational equation derived by the author :

For ordinary reinforced slabs : $$\frac{x}{d}=0.8(n\rho_s)^{\frac{1}{2}}\left(\frac{35}{f_c'}\right)^{\frac{1}{3}} \qquad (2\text{-}52)$$

In prestressed slabs, the level of prestressing $\gamma_p=\frac{\sigma_{sp}}{f_{0.2}}$ is a paramount factor in punching shear resistance of slabs. After the decompression load, a prestressed slab and ordinary reinforced slab are assumed to behave in reasonably similar manner. The only difference is the precompression force which causes the depth of the neutral axis to be smaller compared to a reinforced slab. Shehata based on his observations on the punching strength of the two types of slabs, as demonstrated in Fig. 2-38, suggested the following equation for prestressed slabs with

unbonded tendons.

for prestressed slabs with unbonded cables : $\frac{x_p}{d}=\frac{x}{d}(0.35+0.85\frac{\gamma_p}{0.9})$ (2-53)

ρ_e is the reinforcement ratio defined as : $\rho_e=\rho_{ps}(\frac{f_{0.2}}{500})$

Because of the confined nature of concrete around the column face, the stress concentration factor that expresses the concrete strength under a multi-axial state of stress was calculated on the basis of simplified approximate function obtained as :

$$\sigma_b=n_c.f_c^{'} \quad \textit{Where} \quad n_c=1.4(\frac{2d}{r_o})^{\frac{1}{2}}\geq 1.25 \tag{2-54}$$

Including size effect, the estimated punching load equation proposed by Shehata was established as :

$$P=2\pi.r_o.x.n_c.f_c^{'}.\tan 10^{\circ}(\frac{500}{d})^{\frac{1}{3}} \tag{2-55}$$

The comparison of the presented method equation and 107 test results of conventionally reinforced slabs and prestressed ones gave the average $\frac{P_u}{P_{calc}}$ values between 0.98 and 1.02 with standard deviations of 0.11 and 0.10, respectively.

In 1990 the results of tests of four two-thirds scale isolated slab-edge connections were presented by Foutch, Gamble and Sunidja. The effect of compressive strength of concrete, precompression in the concrete and moment-to-shear ratio on enhancing the shear strength of an

exterior column-slab connection were the specific objectives of the investigation. The layout of the models was selected as 1.5 m square, 100 mm thick and supported on 250 mm square stub columns. Two of the models were constructed with eleven 9.5 mm diameter tendons banded over the column line in one direction with an average stress of about 4.55 MPa. Tendons in the orthogonal direction were five and uniformly distributed over the cross sectional-area of the specimens with an average stress of about 1.72 MPa. The other two specimens were made with six and four 9.5 mm dia. tendons respectively in banded and uniformly distributed directions. Non-prestressed deformed bars were also provided in the vicinity of columns to control cracking.

The first two specimens were identical in the amounts and distribution of reinforcement, column size, concrete strength and prestressing force. The only variable was the location of the loading points which changed the moment-shear ratio. The moment deflection behaviour was linear to the cracking point of concrete. Then the stiffness of the slab decreased gradually to the point of yielding of bonded reinforcing steel. After this point the responses of the two specimens (S1 & S2) differed significantly. The specimen with the lower moment-shear ratio failed in shear with a sudden collapse of compression zone. The other one failed in flexure with considerable rotation occurred at the face of the column, Fig. 2-39.

The second group of specimens had a different reinforcement pattern and a lower initial prestressing force, since the banded tendons were parallel to the free edge. The overall behaviour was similar to that of the first type of specimens. The moment capacity was reduced 25% . The total increase in tendons stress was less than predicted by ACI building code (1983). Larger

increases in tendon stress occurred for tendons running through the column at the expense of large deflection. On the other hand, the change in tendon stress in the transverse direction tendons was very small.

The ACI building code recommends the use of shear stress equation, $v_c=0.33\sqrt{f_c'}$, derived for reinforced concrete slabs, for prestressed concrete slabs at exterior columns. This limit was found to be unsatisfactory because of significant differences between the amount of ultimate moments and shear forces measured from the test and predicted by the ACI equation. In fact there was a considerable improvement in the predicted strength by taking into account prestress. ACI limiting shear stress equation for interior columns, Eq. (2-15), was recommended to be used to exterior columns. The ACI code 318-83 limitations on compressive concrete strength, f_c' , and precompression force, f_{pc} , were found to be unnecessary. In this experimental program the values of f_c' and f_{pc} were considerably greater than 34.5 MPa and 3.45 MPa.

In 1992 a preliminary study on the effect of corrosion of ordinary reinforcement and unbonded prestressed tendons on the punching shear strength of concrete slabs was performed by Rahman. Four full-scale specimens octagon-shaped isolated slab-column connections with column stubs representing a region around an interior column of a multiple panel slab were tested, Fig. 2-40. The outside boundaries of the specimens were bounded by a 1.2 m radius circle about the centre of the stub c olumns. Each specimen was made with normal weight concrete, 165 mm thick with a 300 mm square column stub in the centre of the panel. The main variable in the test was the loss of area of tendons, simulating the effects of corrosion, and consequently the effective

prestressing force to the slab. The arrangement of tendons was banded in one direction and uniformly distributed in the orthogonal direction. The effective concrete prestress varied between 0.6 MPa and 2.87 MPa.

All specimens failed in punching shear indicated by a sudden drop in load. As prestress decreased, the ultimate load necessary for punching shear also decreased. Losses of prestress equal to 50% and 100% reduced the punching capacity by 26% and 55% respectively. The load-deflection behaviour of the specimens is illustrated in Fig. 2-41. With the reduction in the effective concrete prestress, the specimens failed in an increasingly ductile manner. This was expected, as increasing the precompression load effectively reduces the rotational capacity of the slab-column connections. As a result, the ductility prior to failure will generally decrease. The punching shear capacities computed using the CSA (1984) design code equation were found to be quite conservative. The amount of prestress was demonstated to be a factor on the punching shear strength of post-tensioned slabs.

In 1993 an experimental study of the behaviour of post-tensioned unbonded concrete flat slabs at the edge-column was published by Long and Cleland. The effects of the level of average prestress, the distribution of prestressing within the panel and the tendon profile on the behaviour of edge panels in post-tensioned unbonded slabs were examined. The test program consisted of five ¼-scale model specimens with the dimensions shown in Fig. 2-42. The model slabs were extended to the mid-panel strip of the prototype structure and are therefore directly comparable to the section used in the equivalent frame analysis. The simulation of the slab deformations at

the edges was in a manner similar as those in the real structure. Redistribution of moments from the positive to negative moment regions as a result of cracking and yielding can occur as in a prototype structure. The model slabs were 45 mm thick and were supported on 162.5 mm square columns which were restrained against horizontal movements at approximately 600 mm above and below the slabs. Prestressing wires, of 5 mm diameter, applying average prestresses ranging from 1.17 MPa to 3.5 MPa were used. The minimum amount of non-prestressed bonded reinforcement required by ACI 318-89 was also added over the columns. One specimen was provided with a 50% increase in the amount of bonded reinforcement recommended by the ACI code.

The behaviour of all specimens within the application of the design live load was elastic. Cracking first appeared at corners of the columns at a value of live load between 50% and 100% above the design value. By increasing the load, more cracks developed, torsion and radial cracks extended toward the free edge and inner region of the slabs, respectively. At ultimate, the specimens failed in a punching mode. The failure surface in the direction of moment transfer extended to about 1/6th of the span. The rate of increase of stress in the tendons was quite small up to failure. The maximum increase of 10% was recorded in the wires passing through the columns in the moment transfer direction. The increase in the transverse direction was relatively small. Variation in the level of prestress was found to be more or less effective on the ultimate punching capacity. Increasing the prestress by a factor of 3, only increased the failure load by about 37%. Banding the tendons in one specimen appeared to have a little influence (only 6% increase) on the ultimate load, when compared to the specimen with uniformly tendon distribution

but with 50% increase in the amount of bonded reinforcement. This indicates that the presence of non-tensioned bonded reinforcement has a significant effect on the punching shear strength of prestressed slabs.

The comparison between the results from the experiment and ACI-ASCE committee 423 design equation for interior columns, Eq. (2-15), indicated very conservative predictions of the punching shear capacities of edge columns, Fig. 2-43. A factor of safety about 2 was given by ACI-ASCE equation for the failure load in the specimens. It was recommended that the concrete prestress at slab failure, instead of initial average concrete prestress, be used in the ACI-ASCE equation. The result, Fig. 2-44, shows improved agreement between the test results and modified design equation. The specimens which contained larger amounts of bonded reinforcement, specimen E1 in this series and those reported by Smith and Burns, showed less agreement with the equation. This could be the effect of bonded steel which is known to contribute to the punching capacity, but it is not a variable in the equation recommended by ACI-ASCE committee 423.

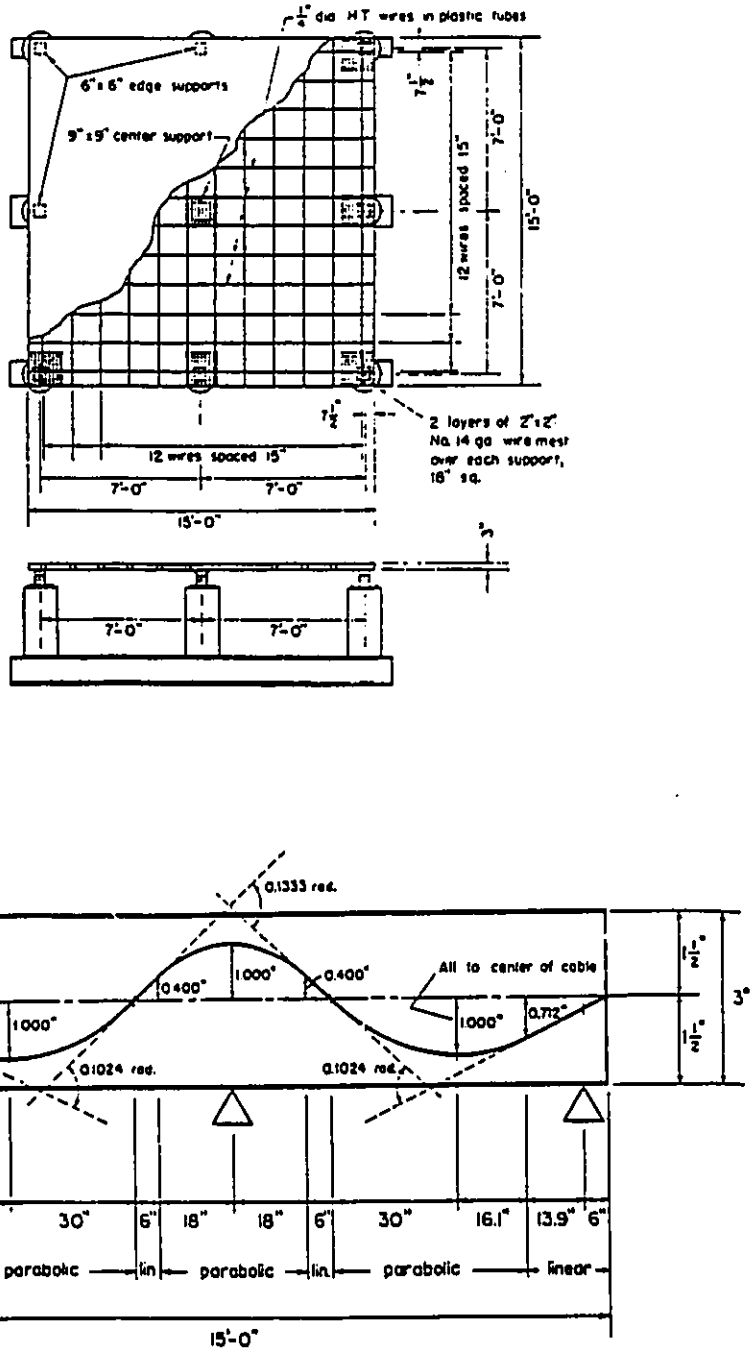

Fig. 2-1 : Plan, elevation and typical cable profile of Scordelis's test slab (1959)

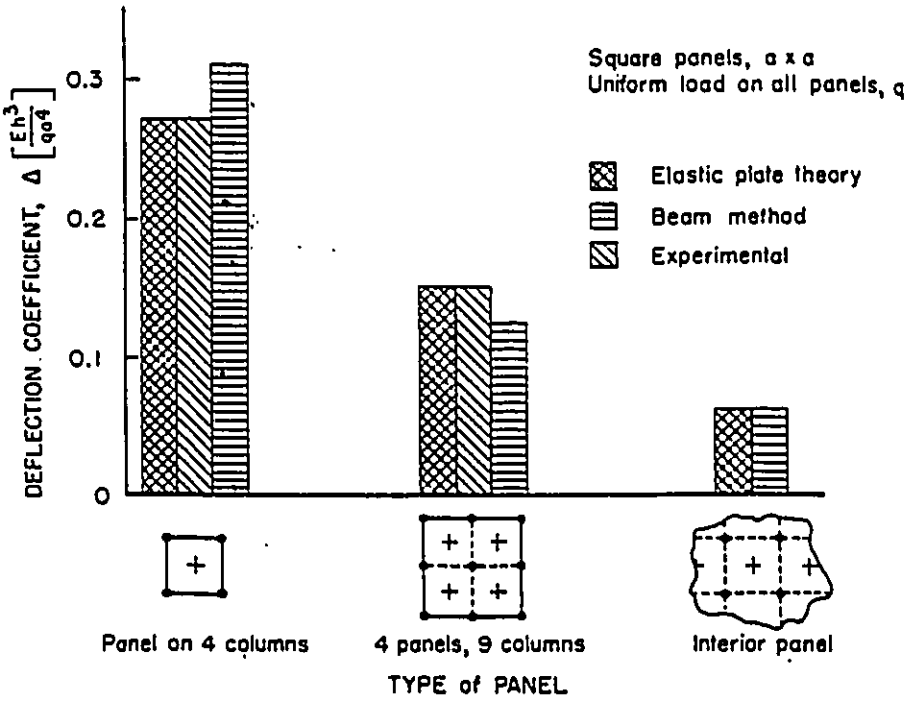

Fig. 2-2 : Comparison of deflections at centre of panel by plate theory and approximate beam method for uniform load

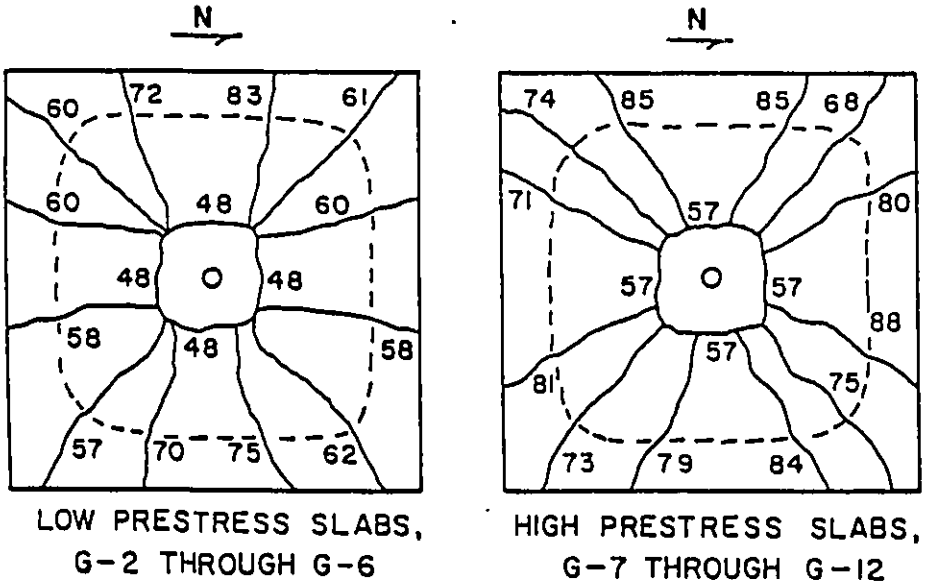

Fig. 2-3 : Typical crack pattern of Vanderbilts's specimens (1967)

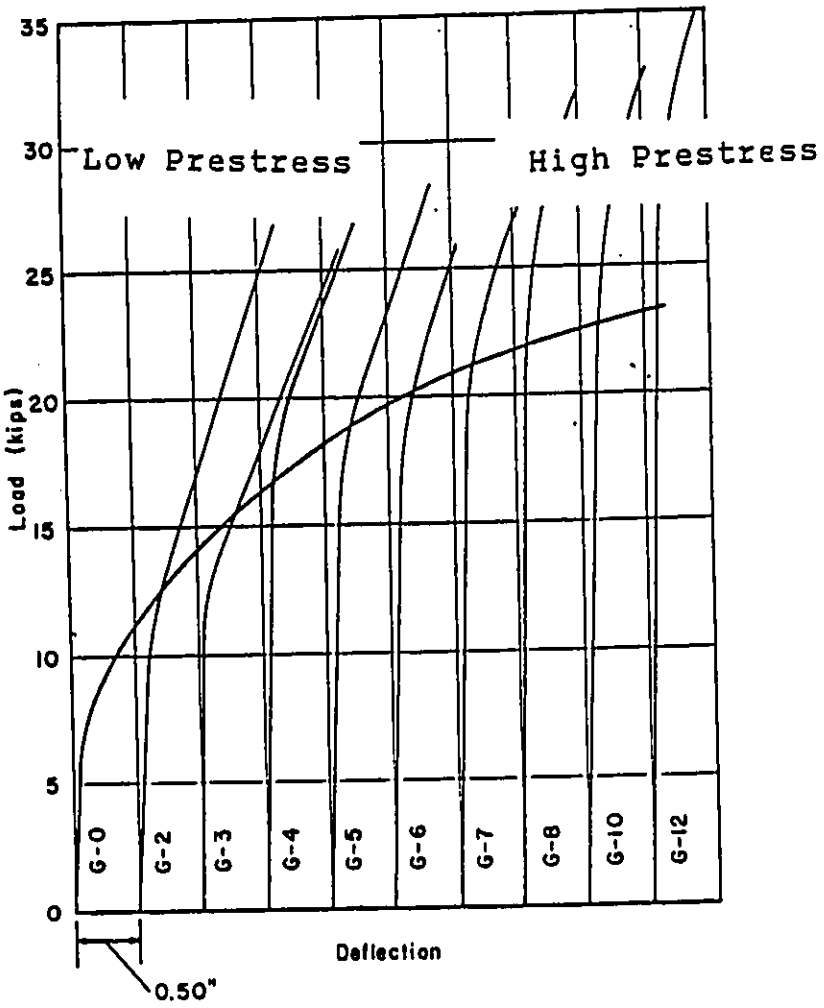

Fig. 2-4 : Comparison of load-deflection curves for Vanderbilt's specimens (1967)

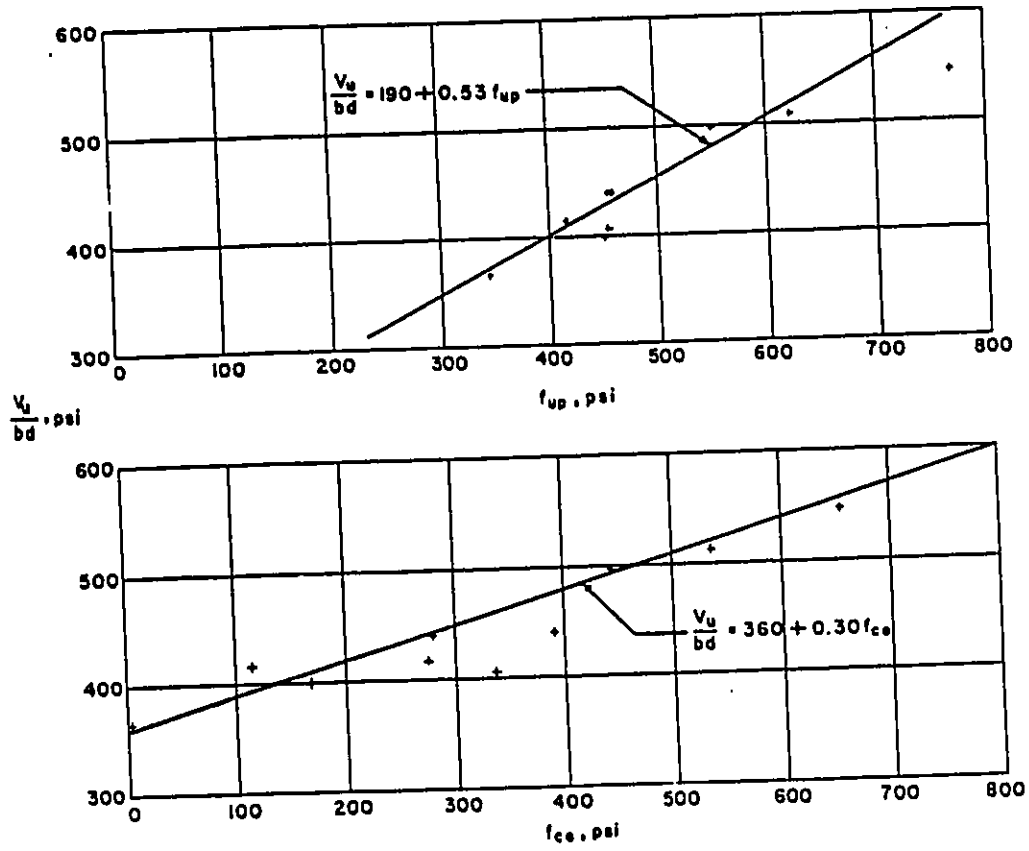

Fig. 2-5 : Plot of Vanderbilt's ultimate shear stress equations 2-13 and 2-14

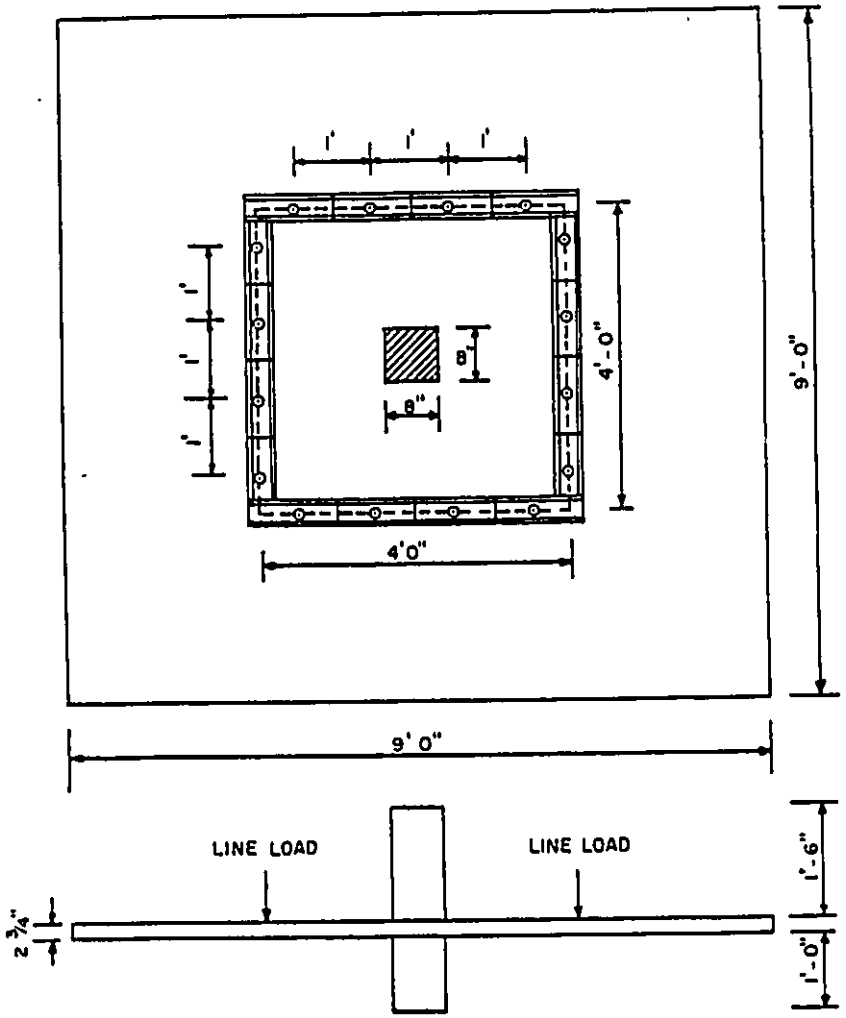

Fig. 2-6 : Loading scheme in Burns's experiment (1974)

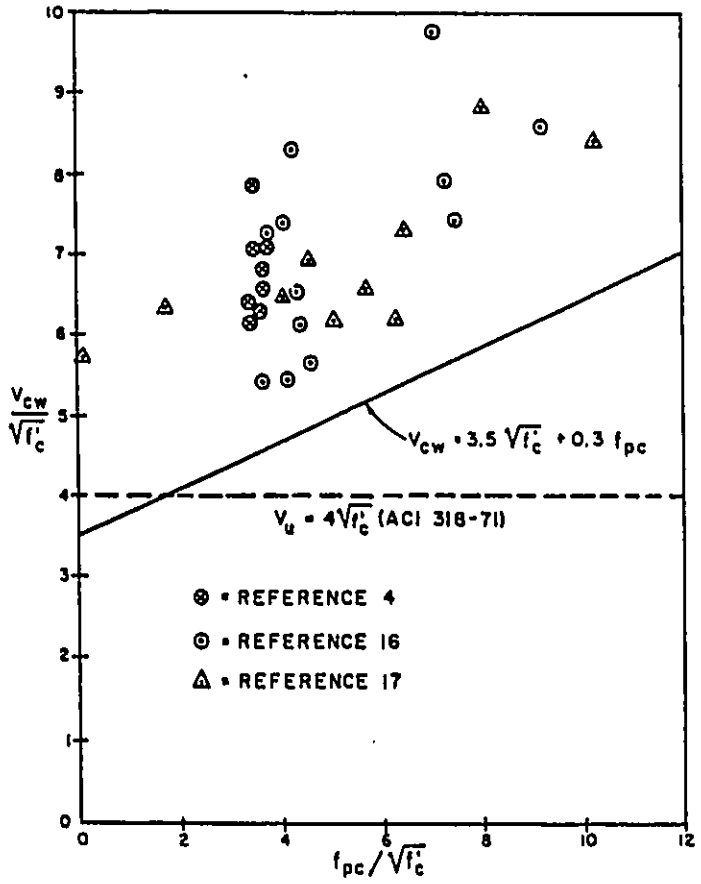

Fig 2-7 : ACI-ASCE committee 423 equation versus shear test data (1974)

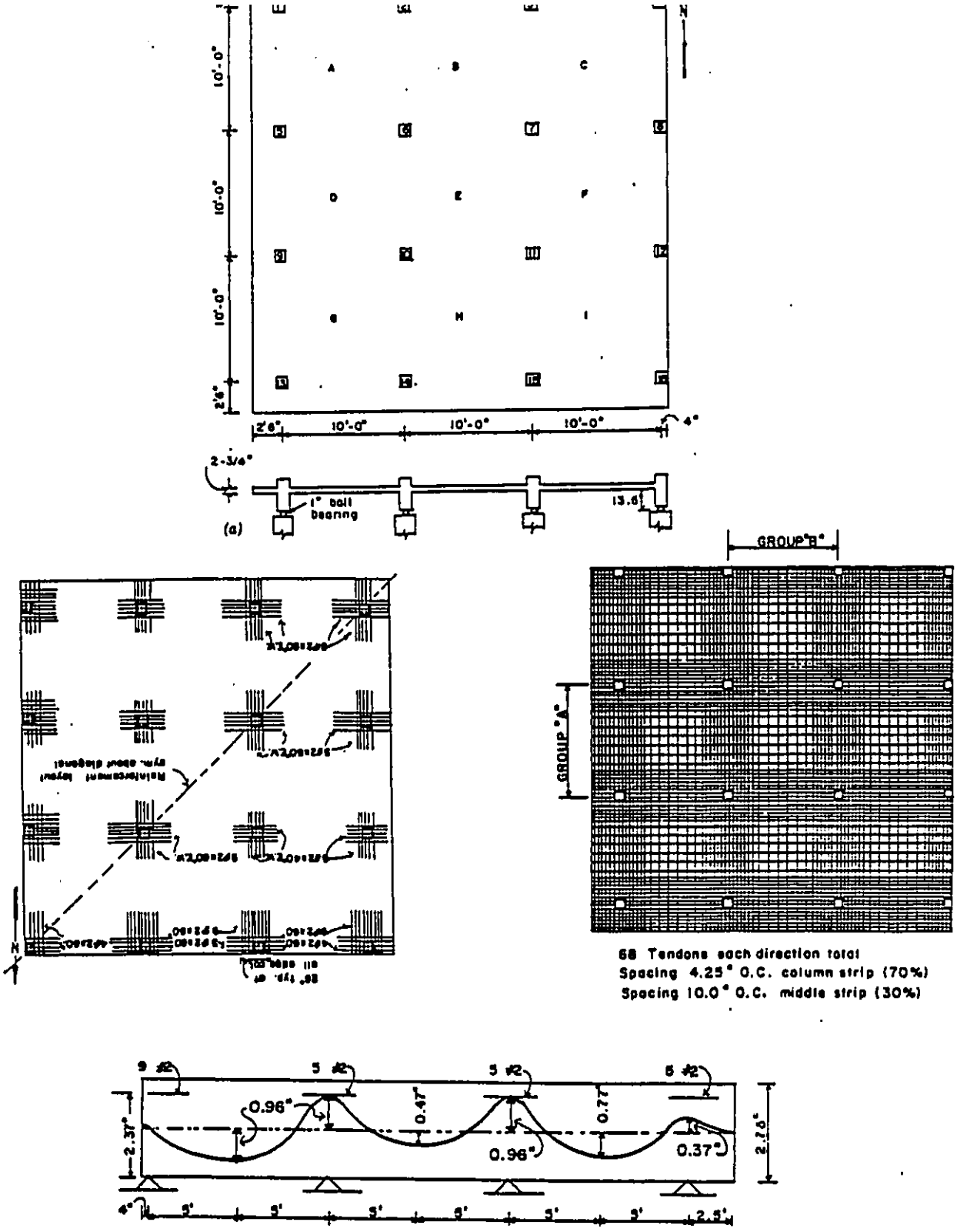

Fig. 2-8 : Details of the nine-panel slab tested by Burns (1977)

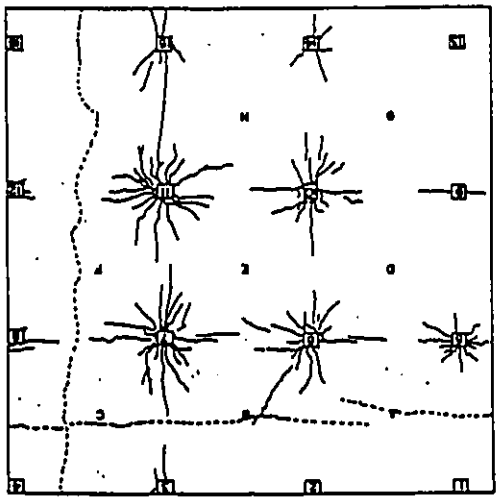

Fig. 2-9 : Crack pattern on Burns's test slab immediately before failure (1977)

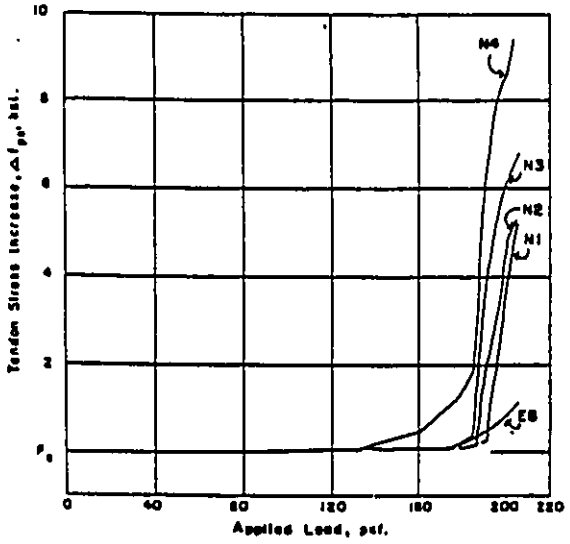

Fig. 2-10 : Relationship between the applied load and increase in stress in unbonded tendons (Burns's nine-panel model slab 1977)

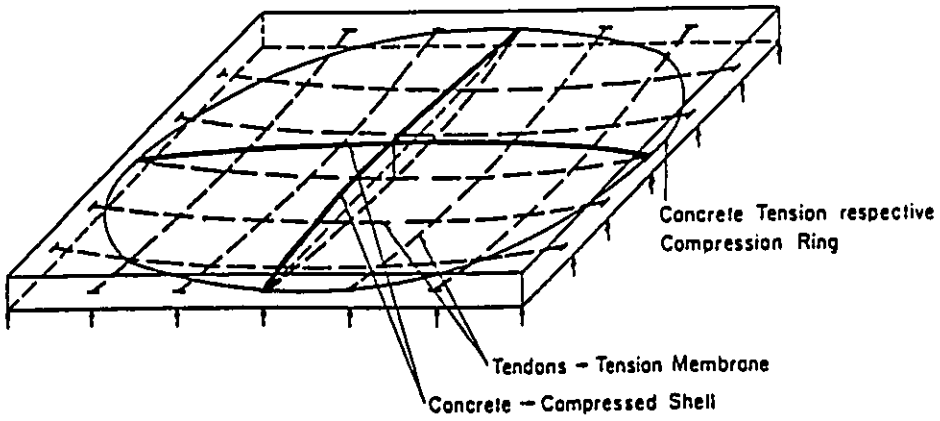

Fig. 2-11 : Formation of static forces in a simply supported unbonded post-tensioned slab (Marti 1977)

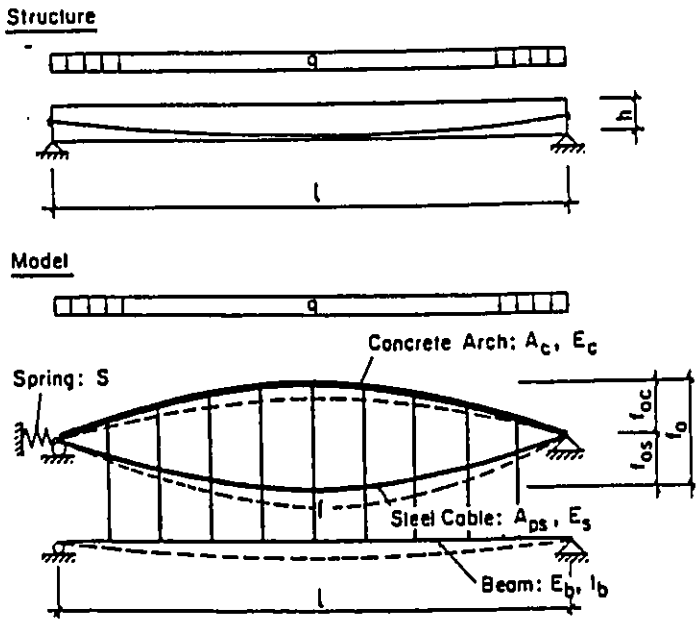

Fig. 2-12 : Tied-Arch model for slab strip proposed by Marti (1977)

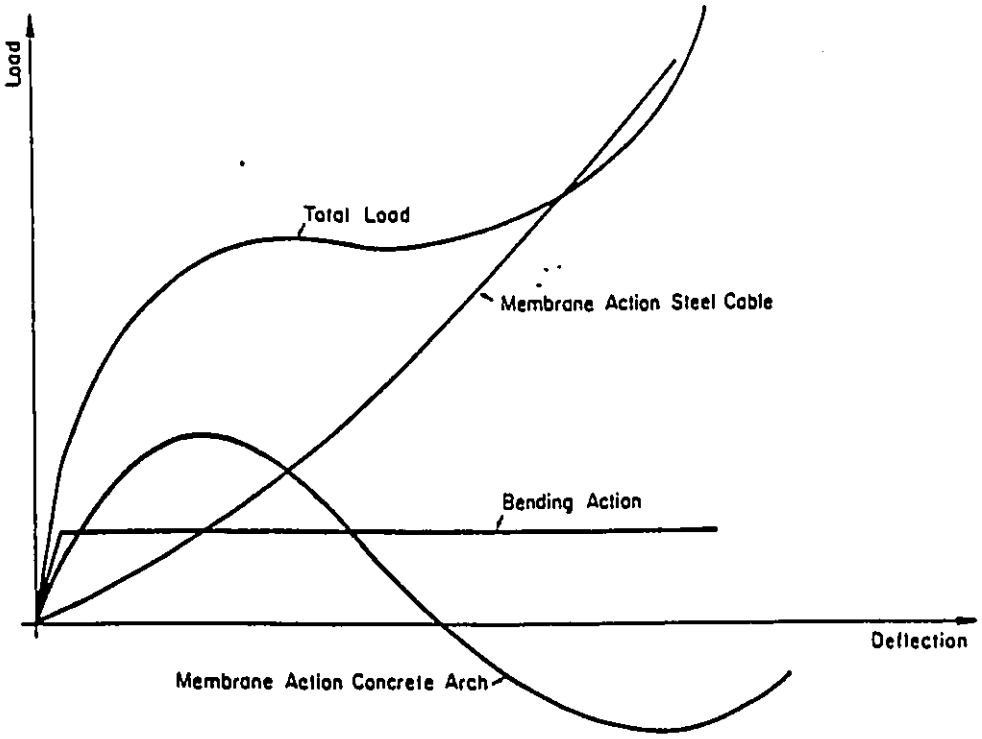

Fig. 2-13 : The effect of different actions in laterally restrained slab strip (Marti 1977)

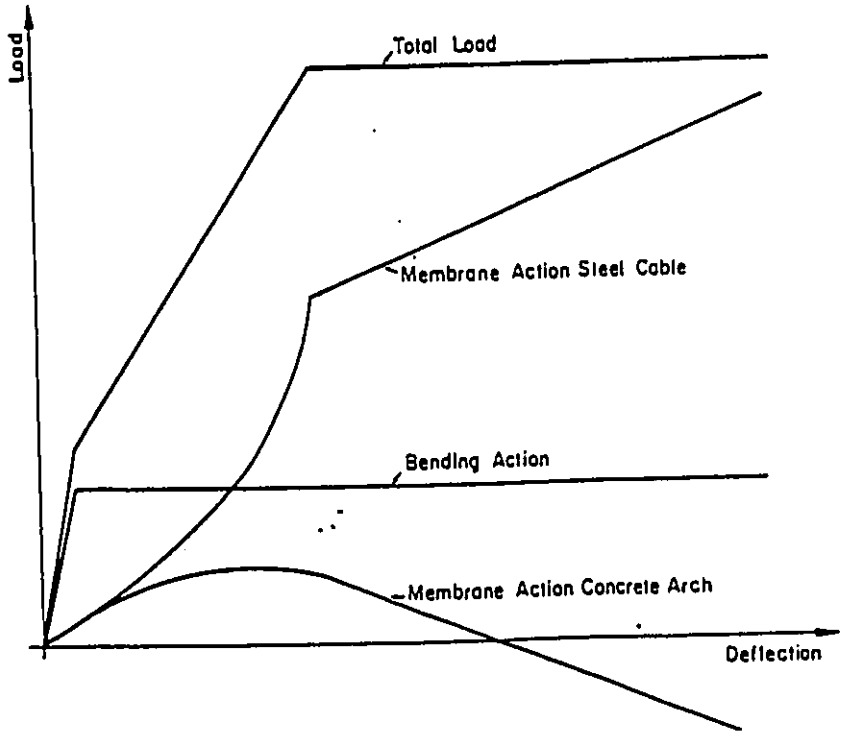

Fig. 2-13 : The effect of different actions in laterally unrestrained slab strip (Marti 1977)

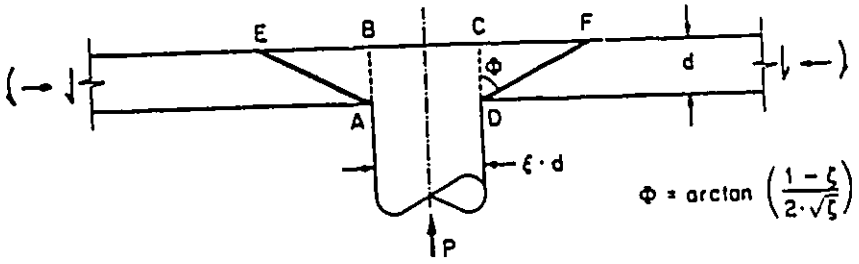

Fig. 2-14 : Punching shear mechanism at interior column (Marti 1977)

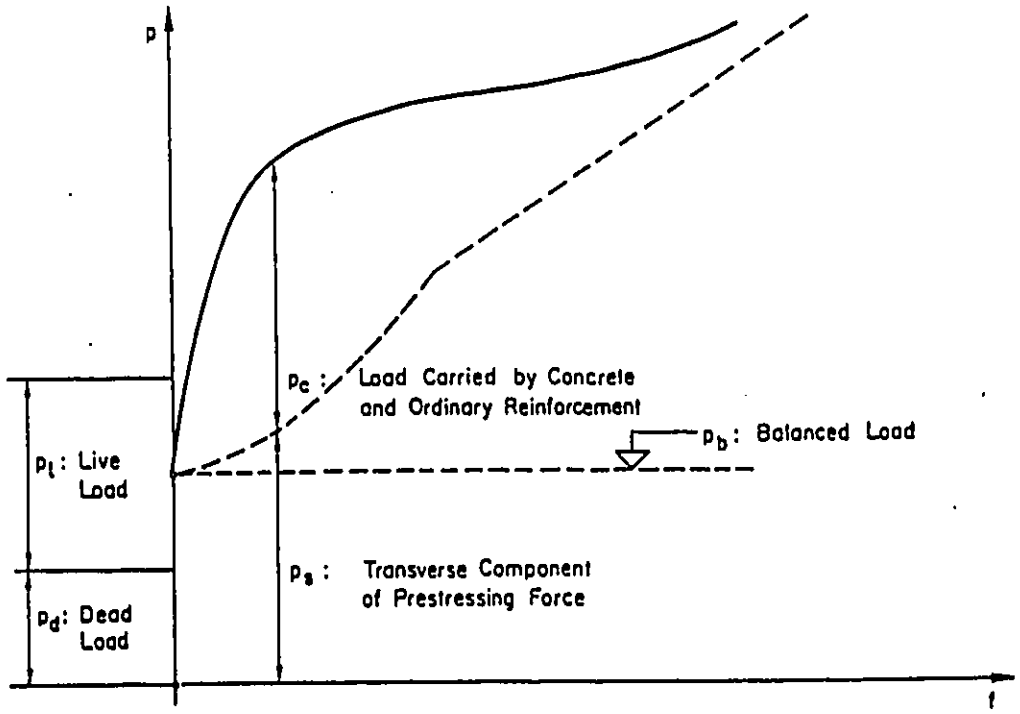

Fig. 2-15 : Schematic load-deflection curve for a prestressed flat slab (Marti 1977)

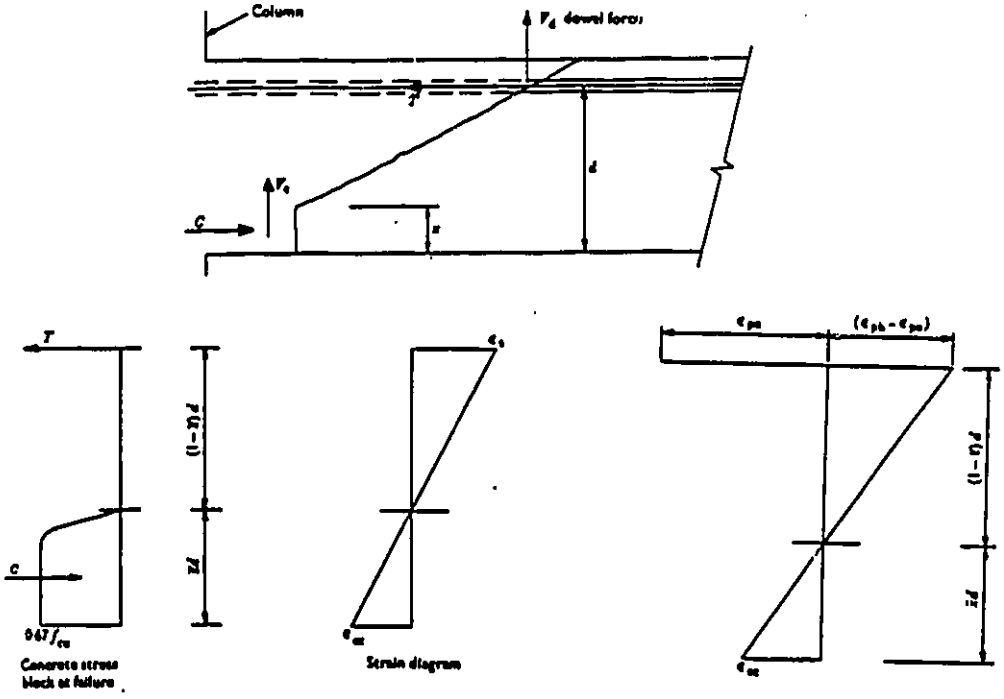

Fig. 2-16 : Stress, strain diagrams for reinforced and prestressed slabs (Clark 1978)

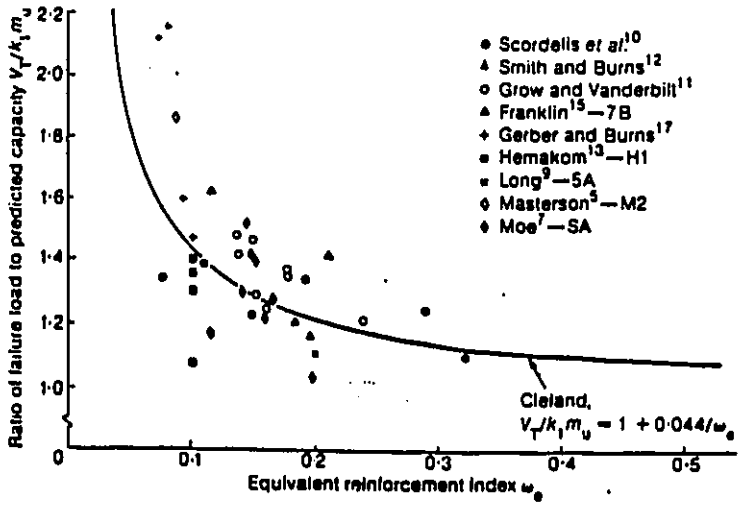

Fig. 2-17 : Comparison of punching shear test results with Long's method (1982)

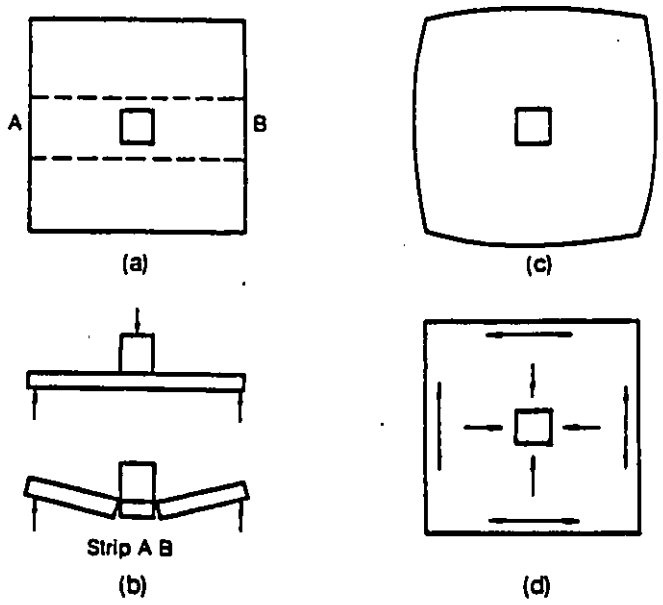

Fig. 2-18 : Development of compressive membrane action in a simply supported slab (Long 1982)

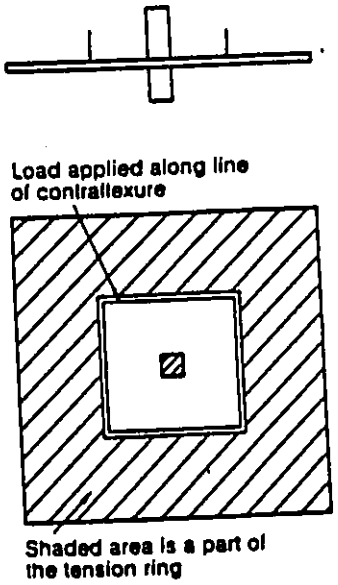

Fig. 2-19 : The tension ring in models used by Smith and Burns (1974)

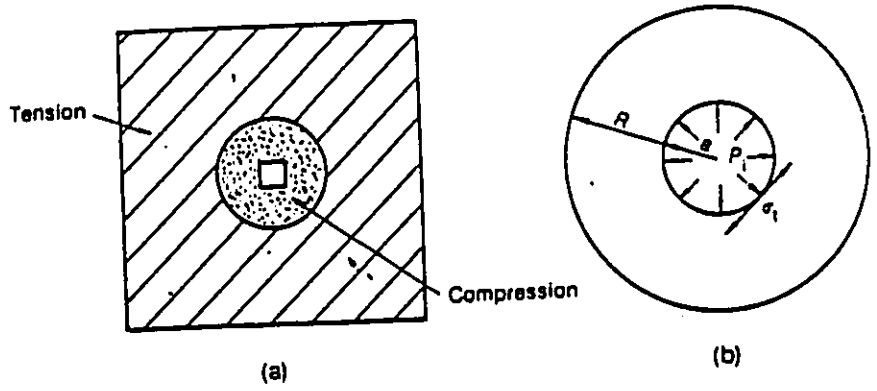

Fig. 2-20 : Derivation of compressive membrane force at internal connections : (Long 1982)

(a) Zones of in-plane tension and compression in test models

(b) Thick cylinder model of stresses in system

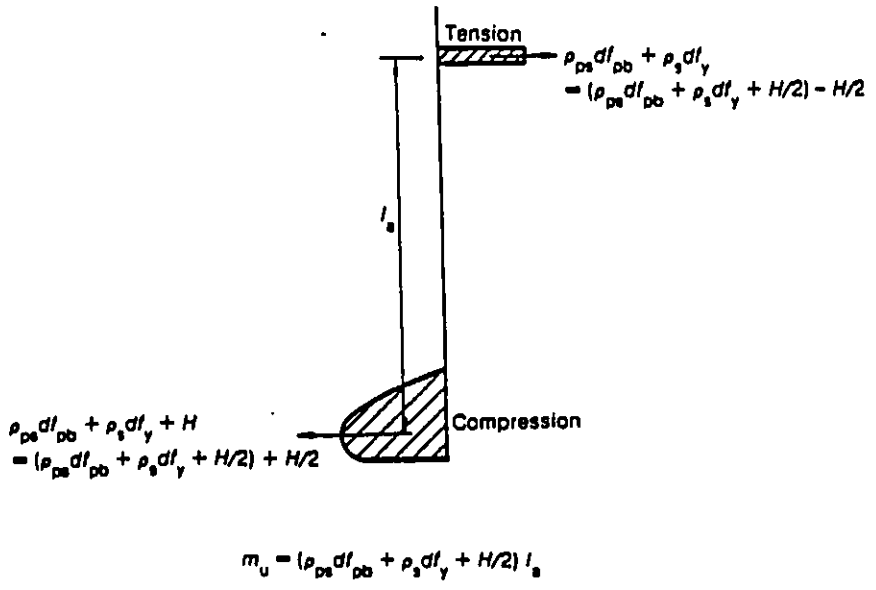

Fig. 2-21 : Ultimate moment of a slab section subject to an overall compression H (Long 1982)

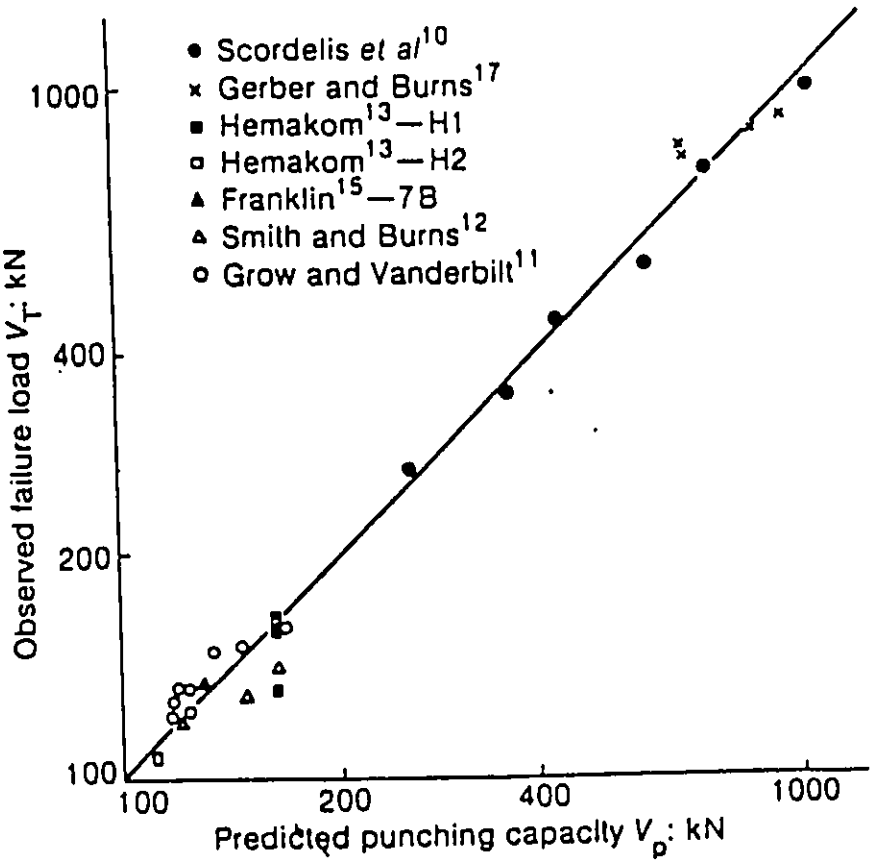

Fig. 2-22 : Comparison of Long's proposed method with test results (1982)

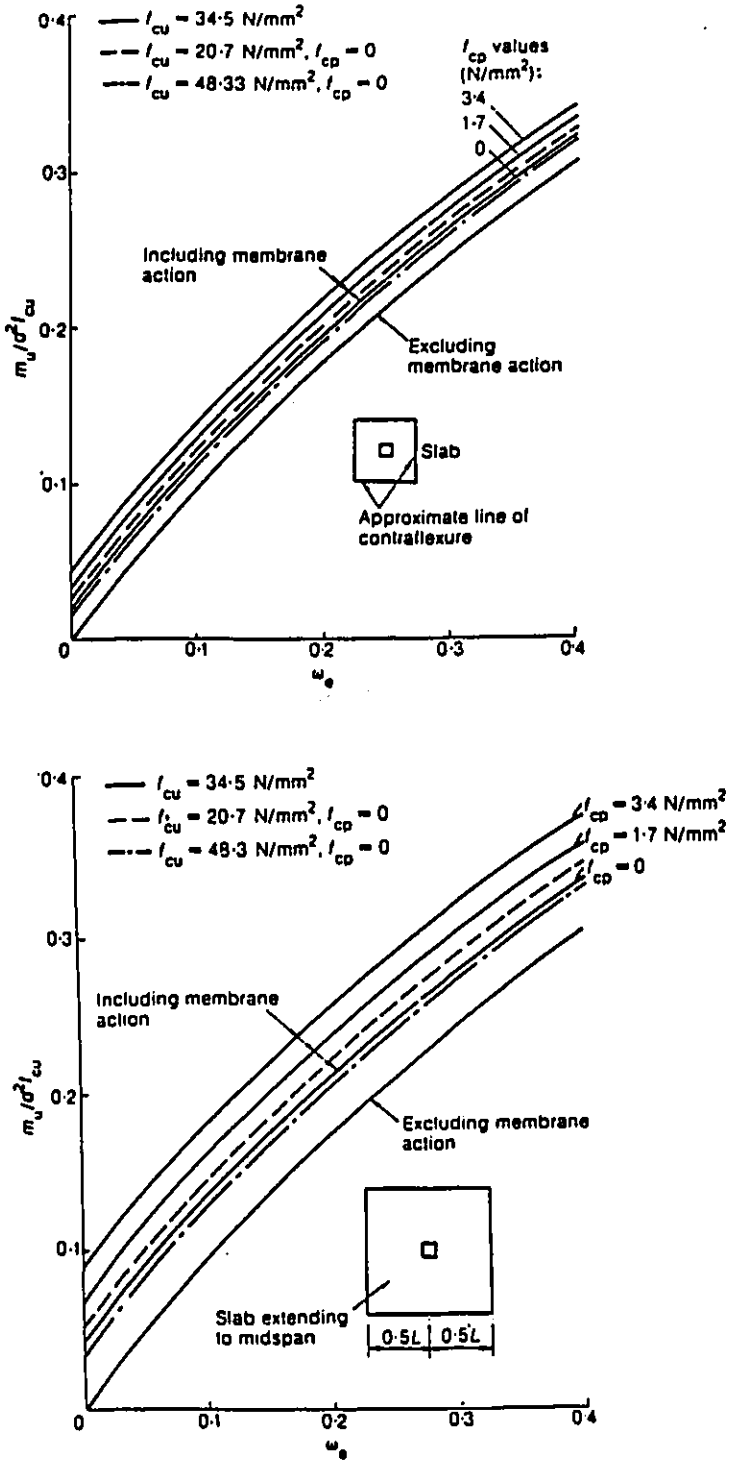

Fig. 2-23 : Variation of Long's ultimate moment of resistance with equivalent reinforcement index (1982)

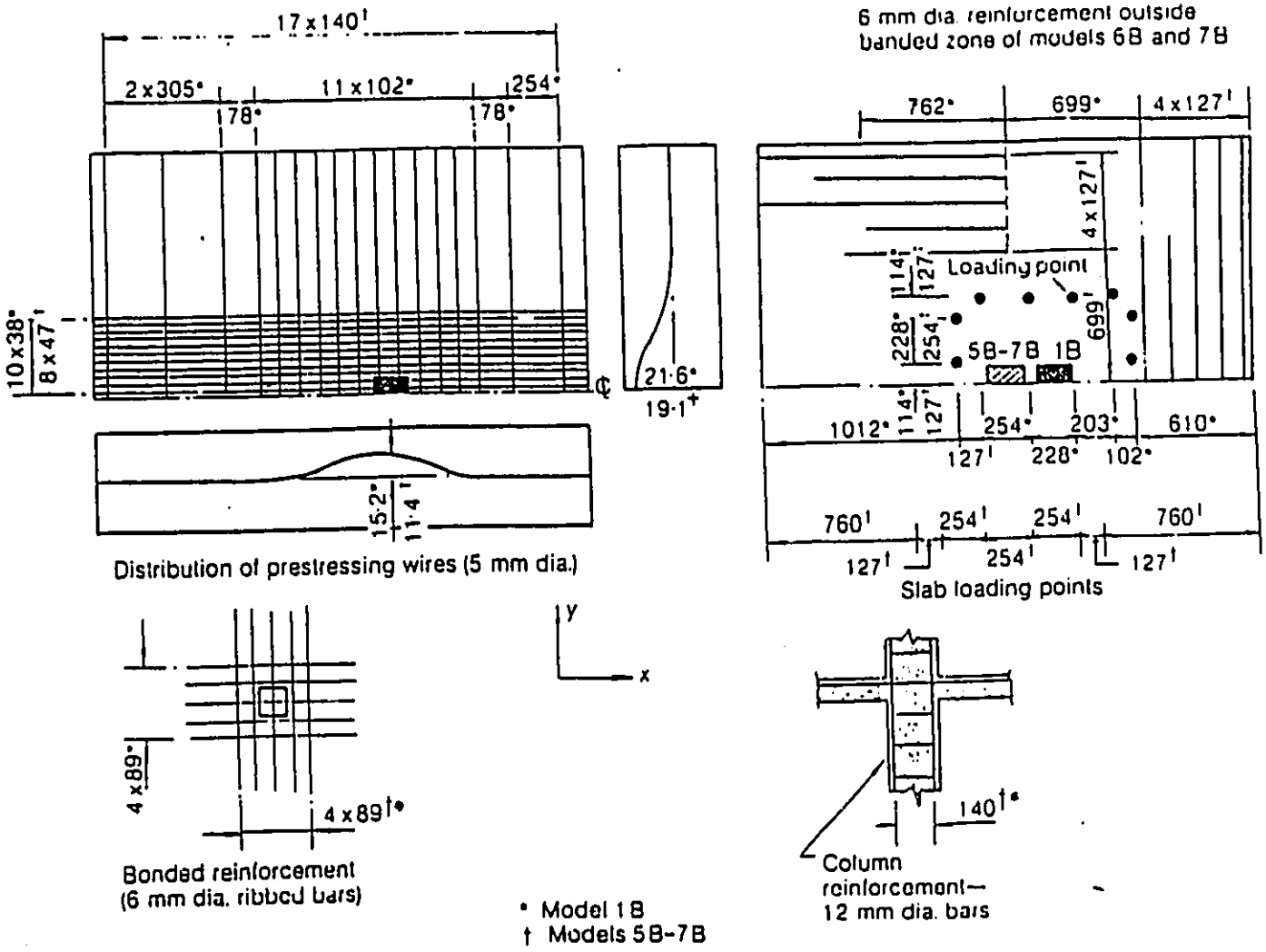

Fig. 2-24 : Details of Franklin's test models (1982)

(models type B)

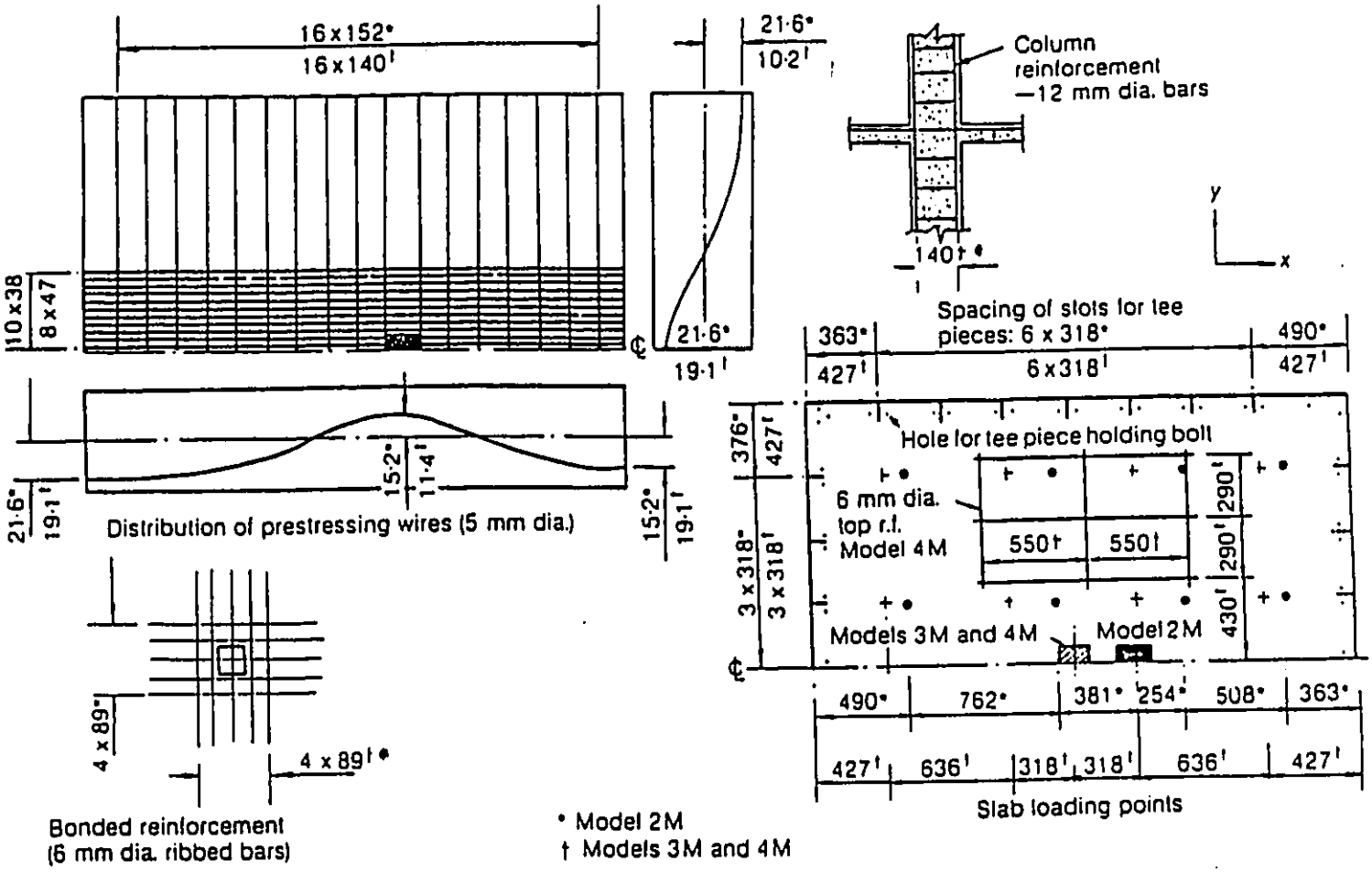

Fig. 2-25 : Details of Franklin's test models (1982)

(models type M)

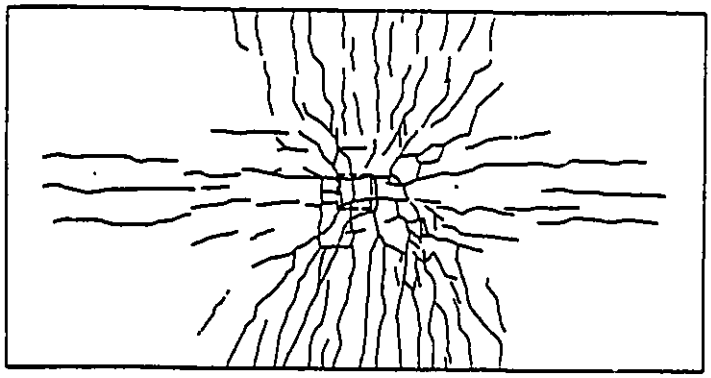

Slab OT7

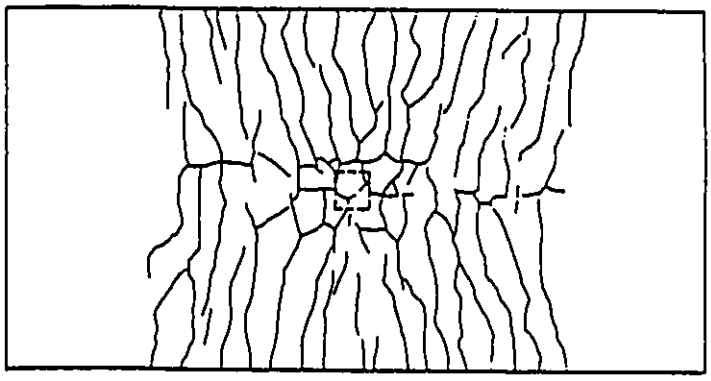

Slab OT8

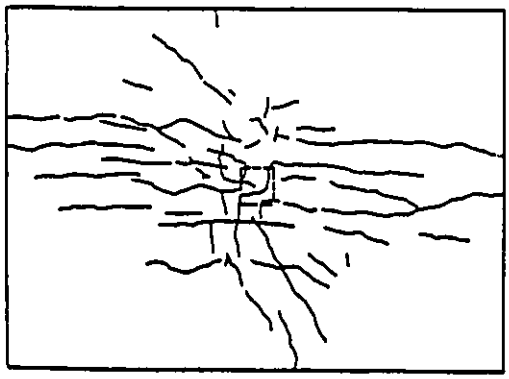

Slab OT10

Fig. 2-26 : Crack patterns immediately before failure in models tested by Regan (1985)

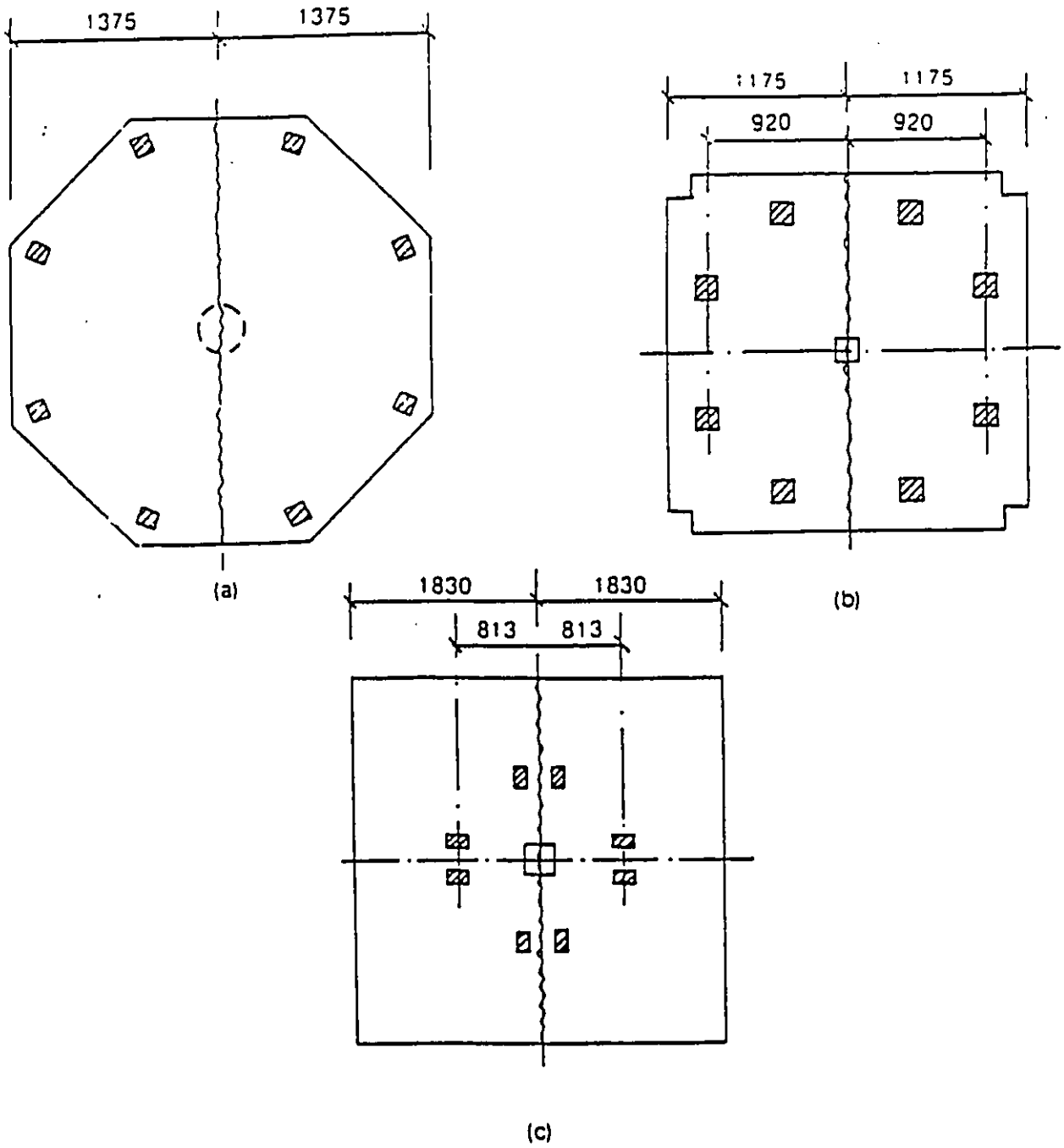

Fig. 2-27 : Load and support systems for two-way prestressed slabs (Regan 1985)

(a) Pralong *et al* (180 mm thick slabs)

(b) Shehata (175 mm thick slabs)

(c) Gerber and Burns (178 mm thick slabs)

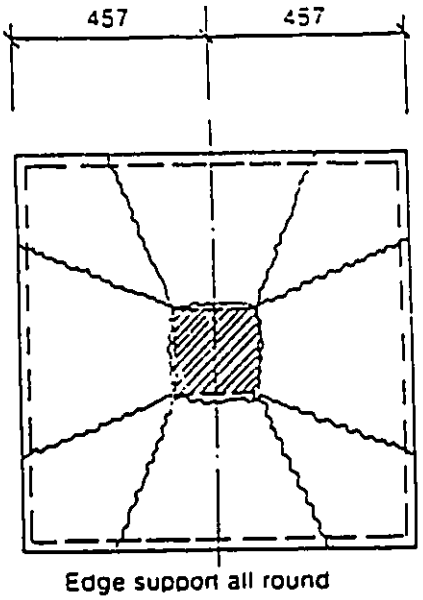

Fig. 2-28 : Plan and support condition of Vanderbilt's model specimens (Regan 1985)

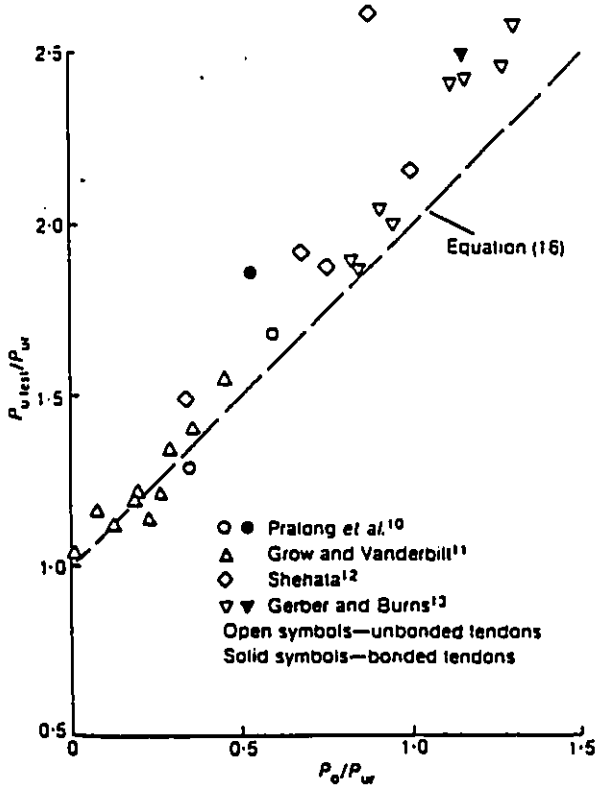

Fig. 2-29 : Comparison of calculated, based on decompression method, and experimental strengths for slabs with two-way prestress (Regan 1985)

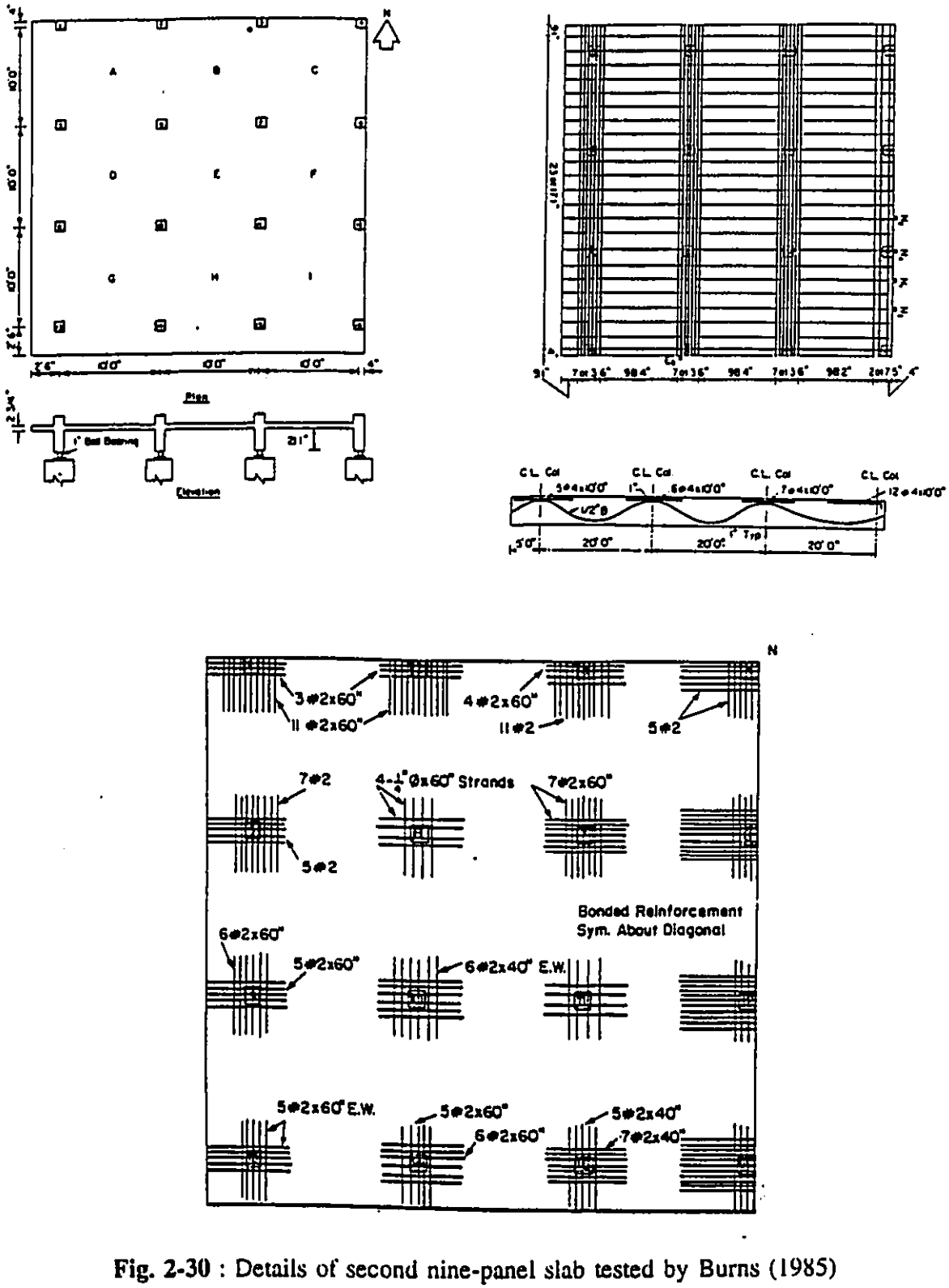

Fig. 2-30 : Details of second nine-panel slab tested by Burns (1985)

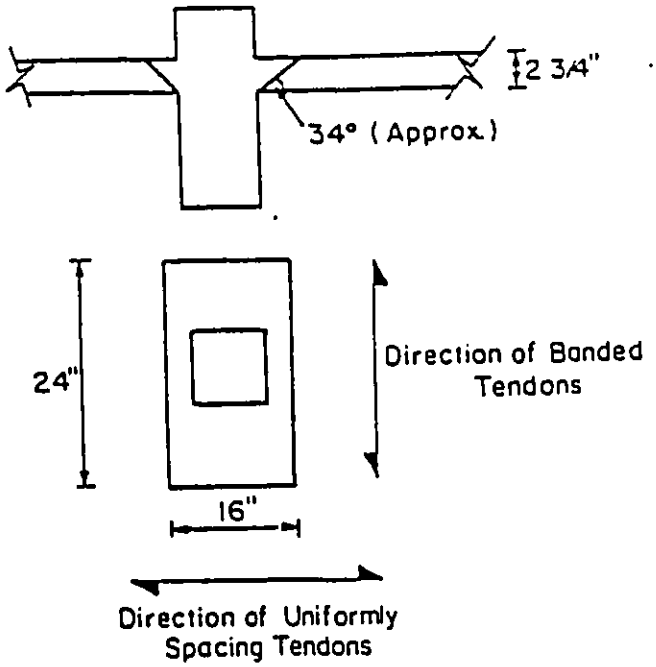

Fig. 2-31 : Typical size of punching shear cone (Burns 1985)

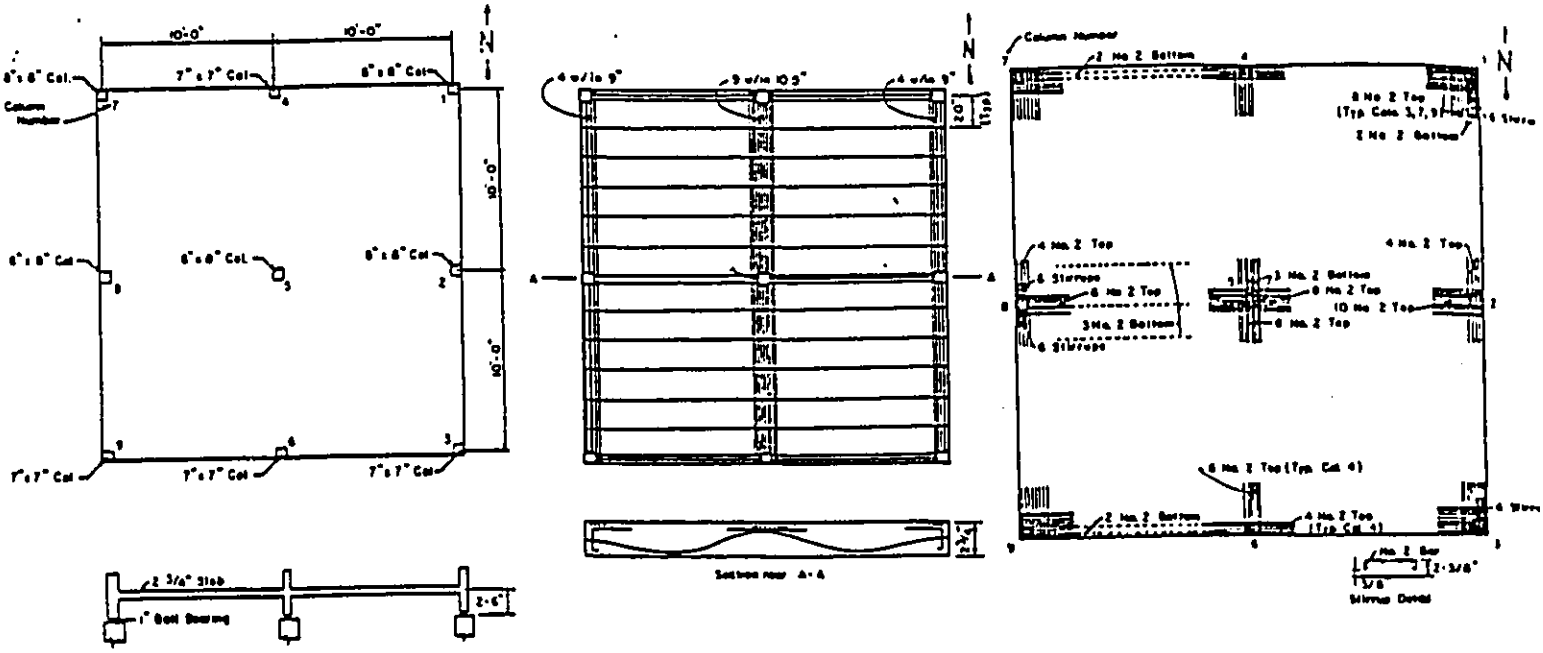

Fig. 2-32 : Details of four-panel slab tested by Burns (1985)

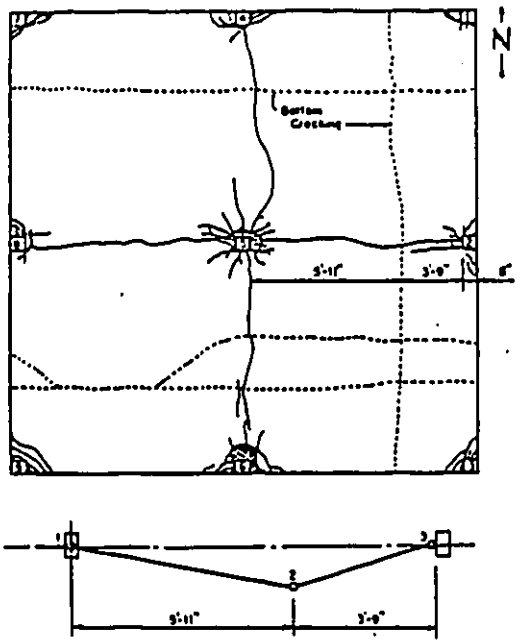

Fig. 2-33 : Yield line pattern at ultimate : (Burns 1985)

(a) Cracking pattern (b) Collapse mechanism

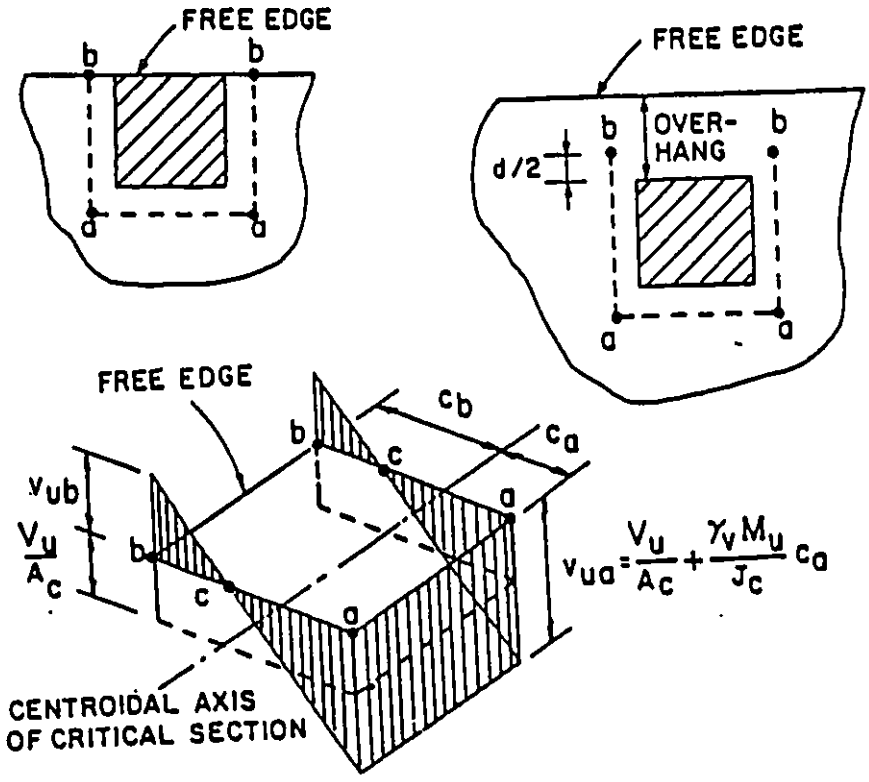

Fig. 2-34 : ACI definition of critical section at edge columns

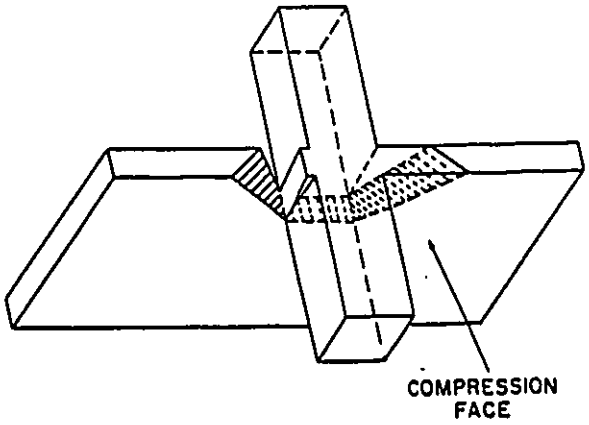

Fig. 2-35 : Failure surface around edge columns proposed by Hawkins (Dilger 1989)

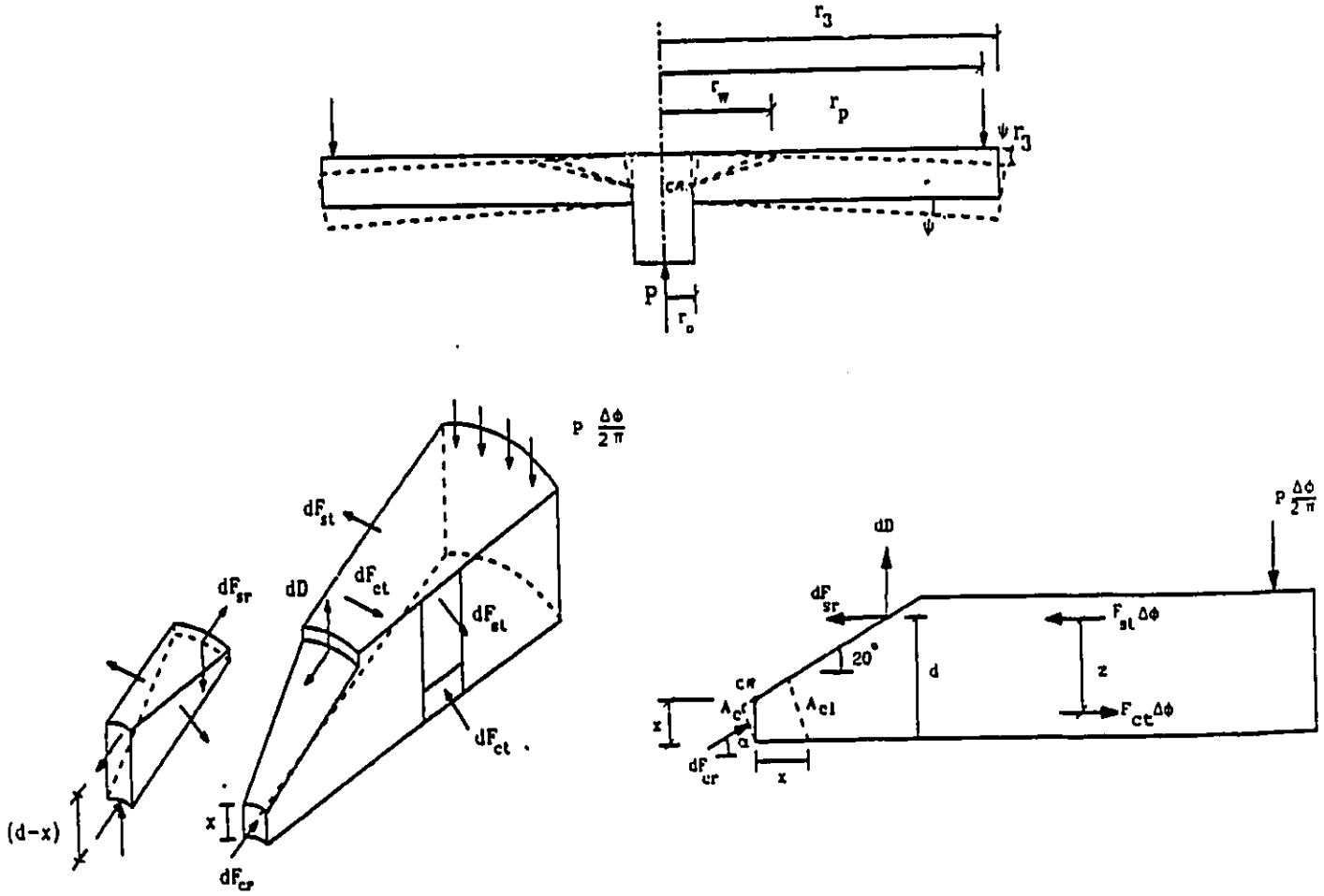

Fig. 2-36 : Punching shear model and forces involved (Regan 1989)

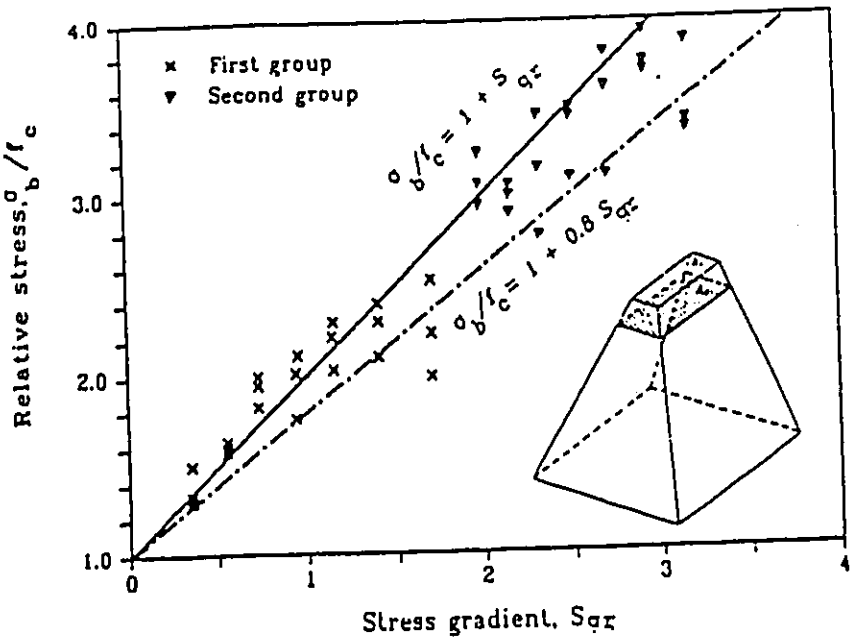

Fig. 2-37 : Influence of the longitudinal stress gradient

on bearing strength of concrete (Regan 1989)

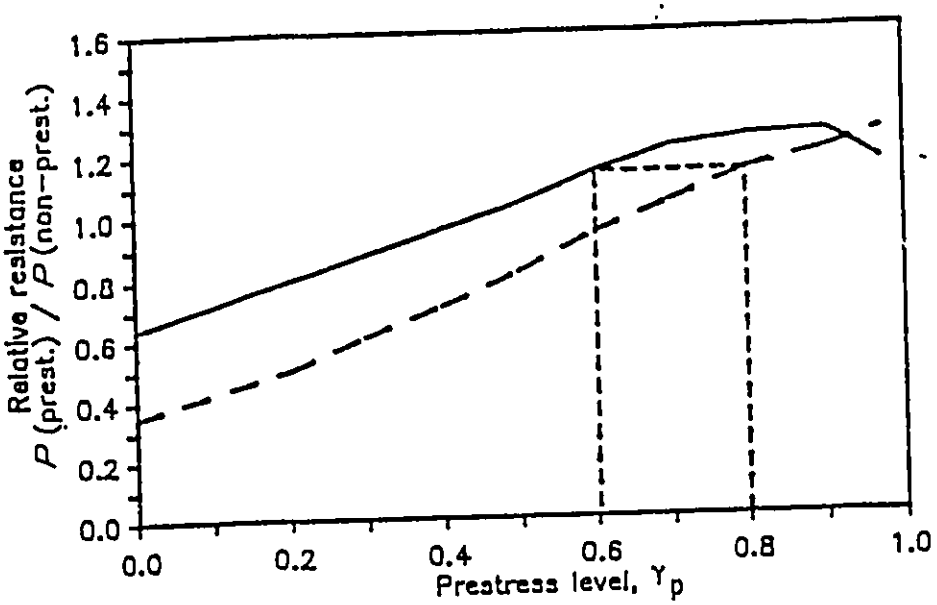

Fig. 2-38 : Effect of the prestressing level on punching strength : (Shehata 1990)

(---) unbonded, (—) bonded

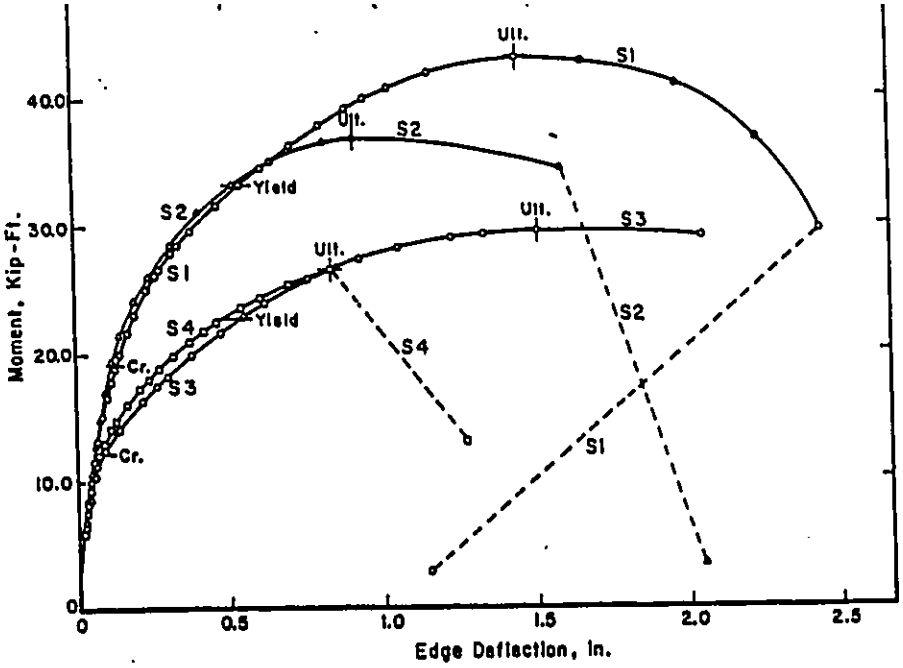

Fig. 2-39 : Moment-deflection relationships for all specimens (Gamble 1990)

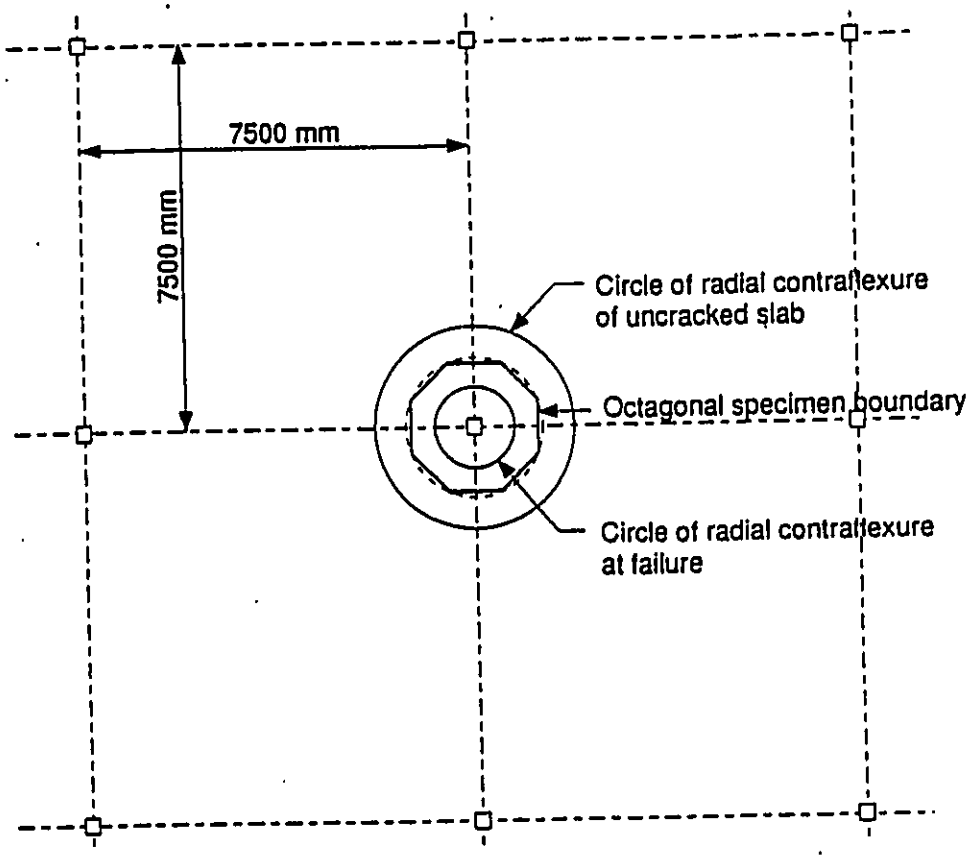

Fig. 2-40 : Plan of slab showing specimen location (Rahman 1991)

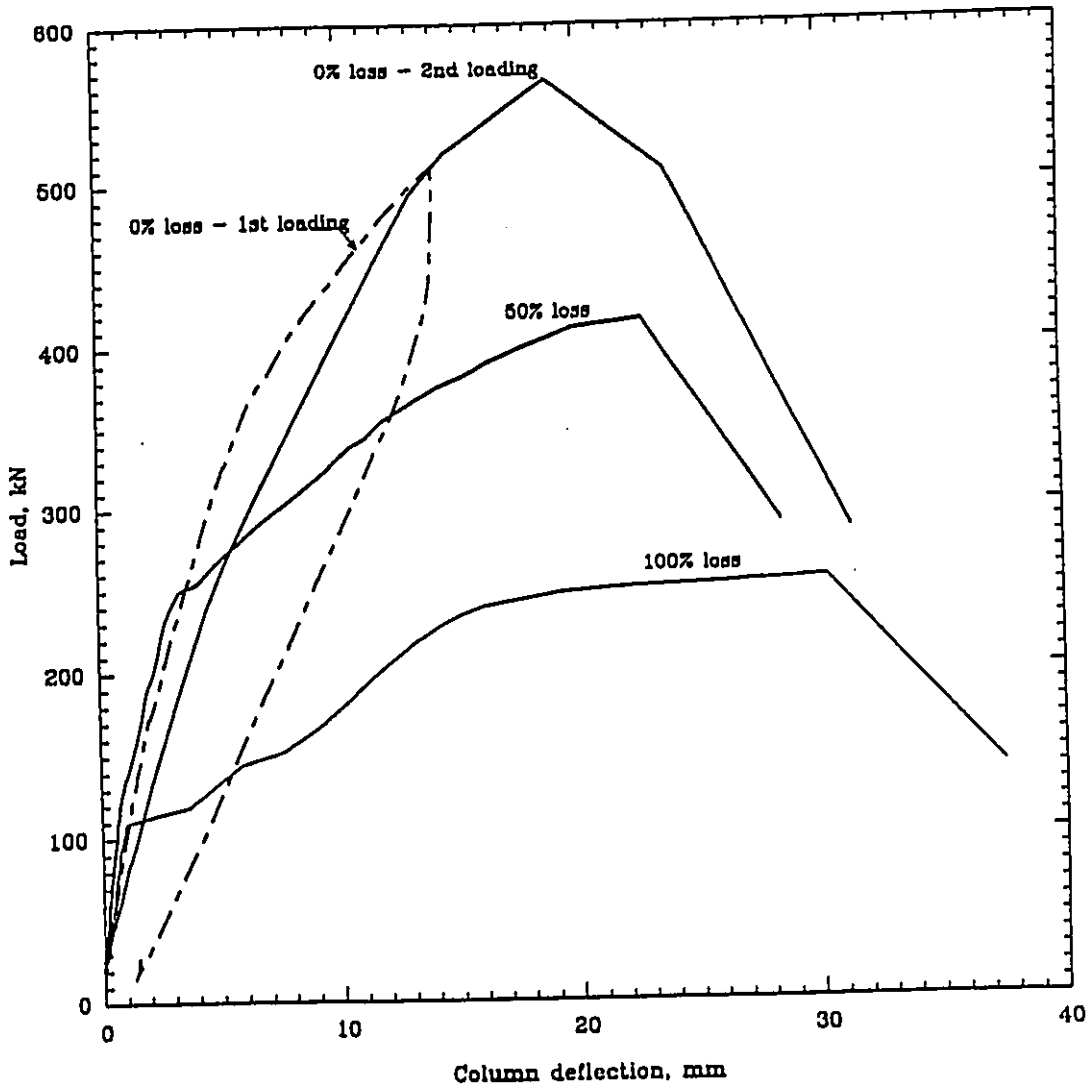

Fig. 2-41 : Effect of loss of tendons on load-deflection behaviour (Rahman 1991)

Fig. 2-42 : Details of structural models (Long 1993)

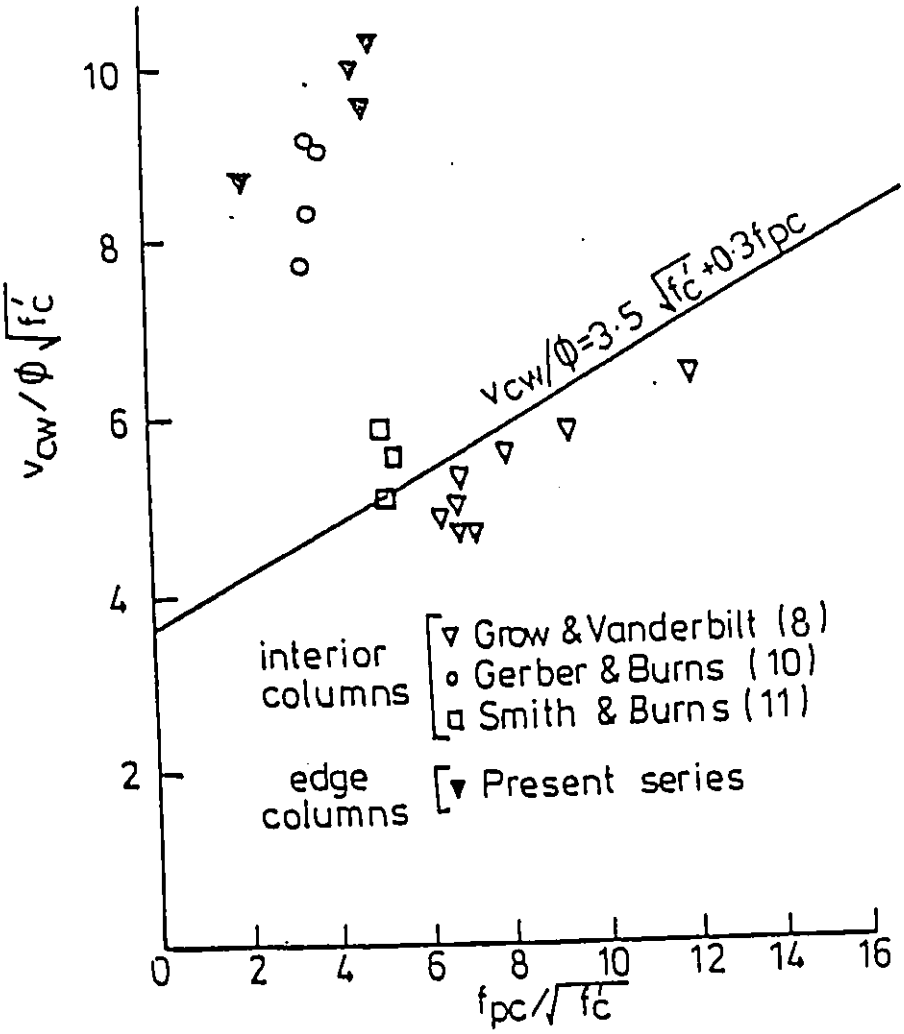

Fig. 2-43 : Comparison of test results with ACI-ASCE committee 423 equation (Long 1993)

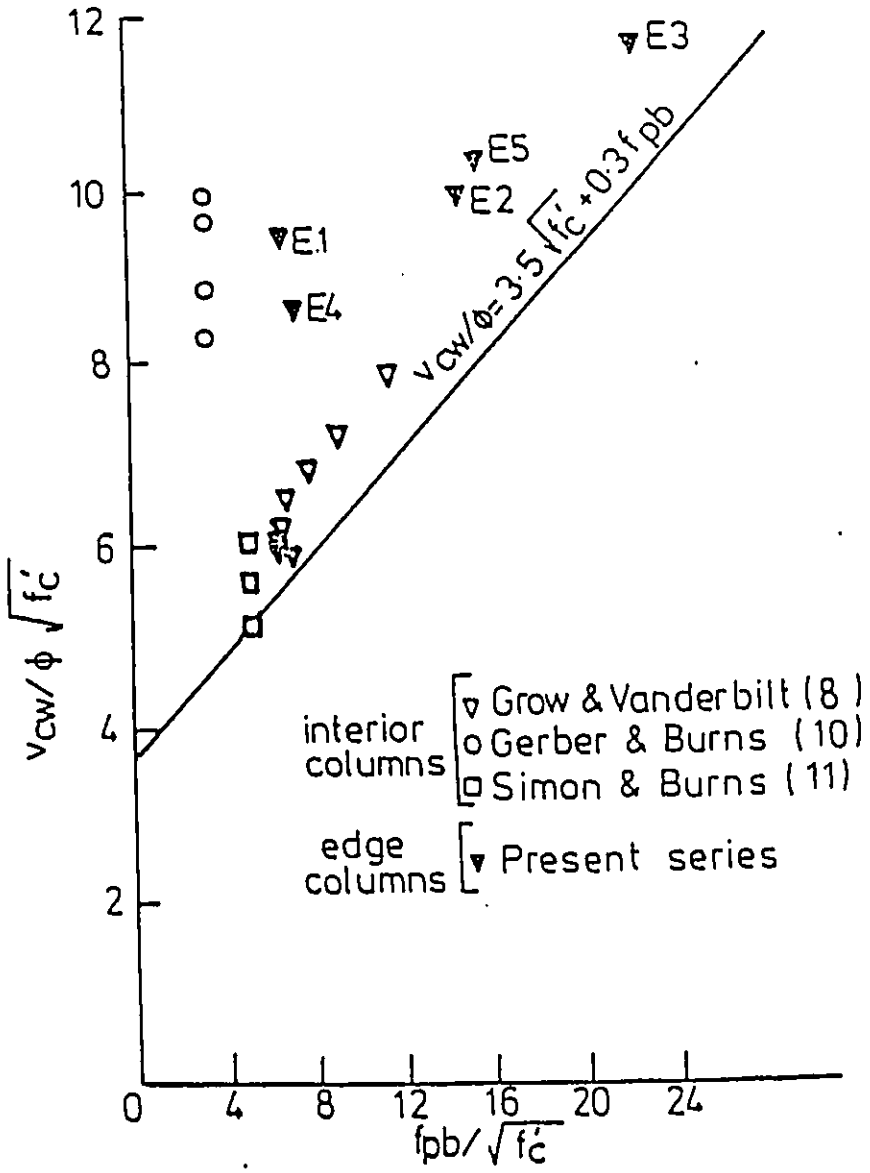

Fig. 2-44 : Comparison of test results with ACI-ASCE committee 423 equation using local value of prestress at slab failure (Long 1993)

CHAPTER #3

EXPERIMENTAL PROGRAMME AND TEST OBSERVATIONS

3.1 Introduction :

One of the most undesirable failure modes of flat plate structures is known as punching or two-way shear failure. Flat plate structures collapsing during, or even after, construction have clearly demonstrated the disastrous consequences of this phenomenon. While there have been some theoretical approaches providing reasonable explanations of the actual behaviour, most of the research efforts on the shear strength of slabs have been concerned with the generation of experimental data. The majority of current code provisions and design practice are based primarily on the results of slab-column tests. The usual way of modelling a flat slab structure has isolated the portion of slab bounded by contraflexure lines and applying load through a short column stub. The external boundary of the model slab is simply supported with the corners free to lift up. However, with regard to continuous structures, this way of modelling a real slab-

column connection will affect the actual behaviour of such connections in a number of important respects : redistribution of moments does occur in a multi-panel floor, so none of the selected lines of contraflexure matches with real lines, which move inwards as steel around the column yields; the equilibrium and the compatibility conditions at the edges of the model are quite different from those of the prototype structure. In a continuous slab panel, lateral movement of the edges of interior panels is prevented, hence large compressive membrane forces can be developed, which in turn increase the collapse load of the interior panel. This condition does not occur in isolated model test specimens. In the case of unbonded post-tensioned slabs, isolated models have more disadvantages : secondary moments and shears due to prestressing which increase the magnitude of column reactions are neglected in isolated models; because of stress increase within the entire length of the tendons between anchorages, considering a single column slab junction with short cables will result higher stress increases in tendons than those in multi-panel systems.

An experimental program performed in the structural laboratory at the University of Ottawa involved constructing and loading to failure a 2 × 2 bay continuous slab prestressed in both directions. The test slab, Fig. 3.1, was 5.69 m × 5.69 m in plan and 90 mm thick. The slab was supported by 9 columns placed 2.74 m on centres in each direction. The primary objective of the experiment was to determine the overall behaviour of a continuous prestressed concrete slab through the elastic and inelastic ranges with particular attention to punching shear. The major attention was focused on the interior column-slab connection and then the edge column-slab connections.

3.2 Description of the Test Slab :

The test slab was designed and constructed to ensure a punching shear failure prior to flexural failure. The experimental slab model, shown in Fig. 3.1, was 5.69 m square, nominally 90 mm thick, supported on six 200 mm square columns and three 200 mm dia. circular columns spaced 2.74 m on centre. The stub columns supporting the test slab were 580 mm in length. The analysis and design of the slab was accomplished for the interior column frame of the slab using the provisions of section 13.7 of ACI 318-89. The exterior frame was treated as a half-strip of the interior frame. The equivalent frame method, together with the load balancing concept, was employed for the determination of moments and shears in the slab. The internal forces were also compared with the theoretical values gained based on the solution of the Lagrangian differential equation for plate structures using a finite element technique. The procedure carried out for analysis and design of the model slab is presented in Appendix A.

The model slab was prestressed with 20 cables in each direction. Tendon layout was symmetrical in each direction with respect to numbers, length, drape and forces. Fig 3-2 shows the plan view and the arrangement of tendons for the test slab. The tendons were uniformly distributed in one direction, spaced 340 mm on centres, and banded within the column strip in the orthogonal direction. In the direction with uniformly spaced tendons over the entire width of the slab, there were two tendons running through the centre line of a row of columns. In the banded direction, all tendons passed together in a narrow band within the column strip and no tendons were placed in the middle strip regions of the slab. Each tendon was a 13 mm dia. high

strength steel, seven-wire strand greased and placed in a plastic tube to eliminate bond. The chosen profile for all of the cables lying in both directions is shown in Fig. 3-3. All tendons were stressed to a force of 96 kN or 973 MPa, with the final force after all losses being 89 kN or 901 MPa per tendon. The average design compressive stress of the slab was 3.5 MPa in both the banded and uniformly distributed directions. The model slab was constructed without any supplementary bonded reinforcing steel in the negative moment regions over the columns. This is not in accordance with the ACI code recommendations, but the experimental work concentrated on the influence of prestressing steel on the punching shear capacity of two-way slabs.

3.3 Construction of the test slab :

The formwork was made of 19 mm (¾ in.) plywood sheets. The plywood sheets were supported by 90 mm × 150 mm 'Aluma' aluminium beams, crossing each other in both directions and resting on 90 mm × 90 mm wooden supports. The forms were covered by polyethylene plastic sheets to fill the gaps between the plywood sheets and for water tightness. Great care was taken to align the column forms and level the slab form.

Column cages were made and placed in the formwork first. Then tendons in the banded direction were placed on the support chairs located at designated points to assure the desired tendon layout. Tendons in the uniform direction passed over the tendons in the banded direction, except over the centre columns, where tendons in the banded direction were placed above the tendons running in the uniform direction. All tendons close to the column cages were tied to the

vertical steel of the column cage. Also all tendons crossing each other were tied together. Special care was taken to prevent any movement of the tendons during casting. Threaded load rods, which passed through the slab were encased in plastic tubes to prevent them bonding with concrete.

The purpose of casting the stub columns monolithically with the slab was to provide the relative flexural stiffness to the slab equivalent to that provided by the columns of the real slab structure. The length of the stub columns was chosen to avoid any possibility of buckling of the columns, and to obtain easy access to the top surface of the slab in order to install the mechanical and electrical instruments and to observe the crack patterns in the negative moment regions around the columns. The column stubs above the slab were only 300 mm long and did not supply any flexural stiffness, but provided the development length required for reinforcing bars inside the columns and caused a stress concentration around the slab-column connections. The reinforcement details for columns are illustrated in Fig. 3-4. Five column bases were supported on load cells allowing for any necessary rotations in all directions. Loads on the other columns could be obtained by symmetry. Two steel plates with bearing areas of 200 × 200 mm were placed at each support, one between the load cells and column stubs and the other beneath the load cells. The remaining four columns sat on the structural laboratory floor. Horizontal movement at the base of the stub columns was prevented by embedding 15 mm diameter threaded rods inside the columns and passing them through the structural lab floor. All the rods were tightened with nuts and plates underneath the strong floor, as shown in Fig. 3-5.

3.4 Materials :

A normal weight concrete, with a specified strength of 30 MPa at 28 days and 19 mm maximum size aggregate, was ordered from a local supplier and delivered by a ready-mix truck. Slump was 75 mm and placing the concrete took approximately 3 hours. The slab was cast-in-place on the forms, moist cured with damp burlap covering for two weeks, and then air-cured until the day of testing. Twelve standard concrete cylinders (150 mm × 300 mm) were also cast in order to determine the compressive strength of the concrete slab. and were cured with the slab. At the day of test, concrete cylinder tests indicated an average strength of $f_c' = 44\ MPa$, which was almost 50% higher than the specified strength of 30 MPa. This increase in the concrete strength not only had no serious effect on the design of the slab but gave the opportunity to investigate the validity of the code expressions when the concrete strength is above their limit.

The prestressing tendons were seven-wire stabilized 13 mm diameter strand with an average breaking stress of 1930 MPa; they met the requirements of A.S.T.M - A416 - 88b and CSA - G279 specifications. Samples of the prestressing tendons tested by the manufacturer, Fig. 3-6, gave the following average values : Yield point as measured by the 0.2 percent offset method, 1790 MPa; Ultimate strength, 1930 MPa; Modulus of elasticity, 204,300 MPa and ultimate elongation, 3.4 percent.

The steel reinforcement used in the columns consisted of #10 and #15 deformed bars. The specified yield strength of the bars was 400 MPa.

3.5 Method of Loading :

3.5.1 Prestressing Load :

The tendons were post-tensioned approximately 60 days after the date of casting the slab. The equipment used for tensioning were two hydraulic rams, a steel trestle, pump, pressure gauge and load cells. The tendons were stressed individually using a combination of the two hydraulic rams, 15-ton and 5-ton capacities with centre holes, together with the steel trestle placed behind the anchorage and bearing plate as shown in Fig. 3-7. The outward length of the tendons had to be long enough to allow them to pass through the prestressing system. Once everything was set up, the tendon was tensioned by the 15-ton jack to an average force of 96 kN. Then the smaller jack was used to push the wedge-type anchor grips into the anchorage against the bearing plate and the pressure from the system was then released. To achieve the force desired for each cable, the tendons were over-tensioned by the estimated loss due to elastic shortening, friction losses and anchorage take-up or slip at the grips. For each tendon, the hydraulic pressure was measured with a calibrated pressure gauge. Aluminum load cells were also used on some selected cables to measure the force in the tendons. However, the elastic shortening and friction losses were found to be negligible.

At first, half the strands were stressed at each side of the slab to load the concrete under uniform pressure from both directions. Tensioning was started from the interior column strip and finished with the exterior column strips. At each side, tendons were tensioned alternatively to prevent the concentration of compression force to the slab. Tensioning the second group of

tendons was carried out with more caution. The concrete behind and around the bearing plate was inspected after tensioning each tendon to see if there was any sign of distress or cracking in the concrete. When all tendons were stressed to the desired value, the average compressive force on each face of the slab reached about 1800 kN or 3.5 MPa. The schematic of variation of prestressing force within the slab in the banded direction is presented in Fig. 3-8.

3.5.2 External Loading :

It was desired to have a method of loading on the slab which would approximate a uniform load over the entire slab. A plan was developed by which the slab was loaded by pulling downward with 40 load points, Fig. 3-9. At each load point the load was applied through a 15 mm dia. high strength steel threaded rod. The rods were spaced 0.914 m from each other in both directions. Every two rods were tied to a box-section steel beam located underneath the slab and structural lab floor. Each box-section beam was 1.0 m long. A 10-ton hydraulic jack was installed on top of each box-section steel beam, between the lower surface of strong floor and the beam to load the model slab through the high tension rods. In order to prevent each box-section beam from lateral buckling and acting individually, lateral supports were provided to connect all loading points together by small box-section steel beams.

Because different tributary areas were attributed to each threaded rod, different forces had to be applied to the loading points in the experiment. The applied load was dependent only on the hydraulic pressure exerted on the jacks. The applied load on each loading point is the result of the measured hydraulic pressure multiplied by the ram area. All the calculations presented in this

and the following Chapter are based on the loads measured by the hydraulic pressure gauges only. For simplicity all threaded rods inside the slab were attached to two pumps while all the edge rods were connected to the third pump. The load pattern may be different from a uniform loading pattern, but it was verified using a finite element program that the discrepancy is less than 3 percent.

3.6 Instrumentation :

The instrumentation was placed to measure the following quantities :

1 - Strains in concrete on top and bottom surfaces of the slab

2 - Forces in prestressing tendons by aluminum load cells at the remote end of some selected tendons

3 - Reactions at some selected support points

4 - Deflections at various locations

5 - Pressure at the pump at each load stage

A total of forty six strain gauges on concrete, each 30 mm long, were used to measure concrete strains on the top and bottom surfaces of the slab. The gauges were placed near the column regions and at the centre spans of the panels. The location of these gauges is indicated in Fig. 3-10. At each location, gauges were mounted in both x and y directions. Because of symmetry it was only necessary to instrument a quarter of the slab to obtain all of the required strain data. In some cases it was possible to obtain readings at two or more gauge locations

which could be averaged to give a more precise value for strain at a particular point in the slab.

The initial prestress force at the jacking end of the prestressing tendons was measured with a pressure gauge attached to the hydraulic pump. In addition, 19 aluminum load cells were placed between the anchorage plates and the end grips at the anchorage ends of some selected strands. Fig. 3-11 shows the location of these load cells.

Reactions at some selected support point were measured by load cells, placed between the columns and bearing plates. The load cells were calibrated in a testing machine before being used in the experiment and were able to measure a maximum load of 180 kN.

The vertical deflection was measured at various points, Fig. 3-12, on the top surface of the slab at 25 locations with mechanical dial gauges. These dial gauges, which have an accuracy of 0.01 mm, were used until the load approached its ultimate value. Deflections were obtained at the centre of each panel and on the column lines to check for symmetry. The deflections measured were the increase in deflection in the slab during the test and did not include the dead load of the slab.

The lead wires from strain gauges, aluminum load cells and load cells placed beneath the columns were connected to the strain connection boxes, and then all boxes were wired to a strain indicator unit which displayed the results on the screen. At the end of each load stage, all of the data was recorded from the strain indicator.

3.7 Test Results and Observations :

The test program consisted of two separate loading sequences. The first loading was due to prestressing in which the slab was subjected to relatively very high in-plane compressive force. The general response of the slab was quite good. No flexural distress or cracking was detected anywhere in the slab. Then the slab was subjected to external loading in five distinct load cycles. In the following, the details of the slab behaviour and test observations in each of the loading sequences are described concisely. Data recorded after the application of each load increment included deflections, cracking, strains in concrete and the force in each cable.

3.7.1 Prestressing :

Fig. 3-3 shows the idealized tendon layout for the model slab structure. The tendons were carefully draped in three series of parabolic segments with points of inflection 180 mm from column centre line in each direction. After the prestressing was completed, with regard to the load-balancing technique the slab was subjected to upward and downward forces. These forces provided by prestressing are a function of the tendon force, the tendon drape and the span length. The moments and shears created in the test slab due to prestressing were calculated by the load balancing method. Because of the applied prestress on the slab (3.5 MPa) the intensity of the upward and downward forces could be expected to be high. Upon completion of prestressing, all corner columns, when released from underneath the slab, lifted up, which clearly demonstrated that the upward forces had overcome the slab self-weight load. For the edge and middle columns, the concave downward portion of the tendon profile will apply a more intense downward force,

Fig. 3-13, resulting in a considerable amount of shear force over the column. In this experiment the maximum upward deflection recorded due to prestressing was 0.85 mm which occurred at the centre of panels. There was no sign of cracking nor any problem with concrete crushing anywhere in the slab.

3.7.2 Slab Loading :

Test 1 was a test with all panels loaded to the live load (50 psf or 2.4 kN/m^2) to check the instrumentation. After readings were taken from all strain indicators and dial gauges the load was increased to 4.8 kN/m^2. Again all data were recorded to be compared with the previous results. Most of the responses were doubled which showed a complete linear elastic behaviour throughout this test. The only discrepancy was that the deflections at centre panels were not identical, one panel was only 70% of the others. The load was released to check if there might be any malfunctioning in the loading system. After checking the pumps, jacks, hoses and connections everything was found to be working properly. The deflections recovered completely when the slab was unloaded. The answer to this problem at this stage was considered to be the thickness of the slab, which might be larger in the low deflection region than the other areas in the slab.

Test 2 was the test in which the structure was intended to be loaded to failure. At each load stage all readings were recorded from a strain indicator unit and deflection gauges and the slab was examined for possible cracks. The load on the slab was increased in increments of 2.8 kN/m^2 (58.4 psf) until the first crack was observed. As the area around the column would experience the largest negative moment, the appearance of the first cracks at this location was

expected. The first crack was observed at a load of 8.7 kN/m² around the perimeter of an interior column. The first crack was a tangential crack, at the column periphery very close to the column face, accompanied by radial cracks extending outward from the column and more pronounced from the column corners. Both the tangential and radial cracks could be described as very fine cracks. The load-deflection curves for the middle of panels deflections were still linear. The maximum deflection was 2.97 mm at the centre of panel C. Almost no significant changes in tendon stresses were observed. The load on the slab was increased to 11.2 kN/m² and the radial cracks extended further from the column corners. A few small cracks appeared in the N-S direction around the circular south-edge column. The slab started to exhibit a non-linear load-deflection behaviour due to loss of stiffness of the slab in the column areas. The maximum deflection was 4.41 mm observed at panel C. The load was increased to 13.99 kN/m² (290 psf), which was almost six times live load . The top cracks near the middle column lengthened slightly and widened under the load. There was no sign of bottom cracking. Deflection at the centre of panel C reached 5.89 mm. Torsional cracks at the north and south edge columns of the slab were found together with the flexural cracks on the slab around the columns. The cracks can be described as very fine radial cracks extending about 100 mm from the column face in various directions. With a further increase in load, to 16.78 kN/m², the first bottom crack appeared and many more cracks were formed around the columns. Two cracks in the N-S and E-W directions along the lines of prestressing tendons from the middle column extended gradually to meet those initiating at the edge columns. The tangential cracks were still limited to the column vicinity. The maximum deflection was 7.44 mm at the centre of panel C. The load was increased to 19.6 kN/m². Torsional cracks extended further from the initial cracks to the free edge, making an angle

of about 45° with the free edge. The maximum deflection achieved was about 10 mm in panel C. The widths of the cracks were easily observed. The aluminum load cell measurements indicated very small increases in tendon stress. The deflection-load response became less linear due to loss of slab stiffness at the column areas. As load was increased to 22.38 kN/m², the bottom crack noticed in the previous load stage ran along the entire width of the slab parallel to the banded direction. As cracking increased, the stiffness of the slab decreased rapidly. The maximum deflection recorded was 12.58 mm. The change in tendon stress at this stage was again found to be minor. Further cracking developed around the interior and exterior edge columns and some cracking became more pronounced near the centre column. At this loading stage a small leakage problem at the pump connection was observed. To maintain the desirable pressure on the system, it was necessary to turn the pump on and off frequently to compensate for the amount of the spilled oil. It was decided to increase the load one more step to see if the leakage would stop by increasing the pressure. When the load reached 25.17 kN/m² the leakage of the oil was excessive and it was very difficult to maintain the pressure on the system. Readings were taken as quickly as possible. The middle deflection reached the highest value of 16 mm at the centre of panel C. Then the slab was unloaded to allow fixing the damaged hose and connection. After releasing the pressure, neither the deflection dial gauges nor strain gauges nor load cells came back to the same point they were started. That was expected, because the load was well beyond the load at which cracking occurred. The maximum residual deflection was 4.0 mm from the dial gauge mounted over the centre of panel A. The divergence between the initial readings and the readings taken after unloading the slab can be attributed to the cracking of concrete. Centre deflections of panels A and C are plotted in Fig. 3-14, giving the typical load-deflection

relationship for a complete cycle of loading and unloading. At the end of the test the damaged hose and connection were replaced and all the other hoses were inspected and tested to 7,000 psi, 10 MPa.

In test 3, first all the strain indicator readings and the deflection dial gauges were zeroed, and then the slab was loaded to the same point as in the previous test with increments twice those used previously. The overall behaviour of the slab was similar to test 2 and reloading did not change the existed crack pattern on the slab. The deflections at the centre of panels moved back relatively very close to the unloading curve. As it can be seen from Fig. 3-15 by reaching the load to 25.17 kN/m^2 on the slab the deflections in the middle of panels A and C were greater than the previous values recorded in test 2. The discrepancies were due to the residual deflections in the slab because of the previous loading and unloading cycle. The flexural cracks on the top of the slab near edge columns together with torsional cracks at the sides propagated longer and deeper as the applied load increased. The nonlinearity of the load-deflection curves was more pronounced than in previous loading stages. In spite of excessive cracks developed on the top and bottom surfaces of the slab, it was still capable of carrying more load. As the load was maintained on the slab to allow for recording the data and examining the slab for possible cracks, it was realized that the rotation of the west-edge column, and the adjacent slab, was larger than the east-edge column of the slab. The rotation of the column was clearly observable. It was evident that the top portion of the column had moved inward. The stiffness required for the base of the columns to be restrained against horizontal displacement was provided by the shear resistance of threaded rods passed through the column stubs and fixed from underneath the

structural lab floor, Fig. 3-5. It was concluded that the slab was behaving with zero restraint at this edge. As the load was applied beyond the 25.17 kN/m² level, bottom cracks developed at an almost similar rate across all panels perpendicular and parallel to the uniformly spaced tendons direction. The deflections increased rapidly. As the load approached 28 kN/m² the centre-of-panel A deflection recorded was 24.5 mm. The west edge column rotation due to the smaller thickness of the slab around this region was large, so that a relatively wide local bottom crack formed along the north-south direction of the slab at a distance 0.8 m from the column centre. This crack was accompanied by minor crushing of concrete on the top surface of the slab at the same location. The layer of concrete near the top surface of the slab spalled into flakes. The length of the crack was measured as 0.6 m. As a result, the test slab was susceptible to local flexural failure, and it was expected that the slab might fold down and break at this location. While, this problem might have had some effects on the overall flexural behaviour and bending moment distribution of the slab, its influence on the shear forces would be negligible. Therefore, it was decided to increase the load on the slab with more caution. As the load was increased to 30.8 kN/m², a punching shear failure occurred at the south edge slab-column connection. Nothing further was observed in the crushing area of concrete near the west-edge column. It seemed that redistribution of the moment from negative region, edge column, to the positive region, middle of span, had occurred. The maximum deflection at the interface of panels A and C, deflection gauge No. 20, was 17.84 mm, approximately 90% higher than comparable point. The slab failed in a rather brittle fashion due to punching shear failure with no warning and with pieces of concrete being thrown away from the failure zone. The slab failed along a surface formed by inclined cracks and made a shape of a truncated cone with the base at the top of the slab. The

angle of inclination in the direction of moment transfer (uniformly spaced tendons) was about 16.5°. This angle increased to 20° for the banded direction. Fig. 3-16 illustrates the size and appearance of the shear cone at punching shear failure. The relationship between unbonded tendon-stress increase and applied load is shown in Fig. 3-17. As indicated by the curves, a significant increase in the prestressing tendon stress occurred at a load very close to ultimate. The tendons passing over or very near to the support demonstrated the larger increases. As expected, very little change in stress occurred in the tendons away from the failure zone. The maximum stress increase was of the order of 25%, and was recorded for the two tendons placed over the column and running in the north-south direction. Fig. 3-18 shows the crack pattern on the slab, moments before the occurrence of punching shear failure. As soon as the south-edge column punched through the slab, the pressure in the hydraulic system was relieved and the load dropped to about 23.5 kN/m² for the southern panels and 29 kN/m² for the northern panels. Deflections increased markedly in the southern panels due to the shear displacement even though the load had decreased. The crack pattern and failure surface of the failed edge-column is shown in Fig. 3-19.

To obtain more information regarding the shear strength of interior columns, the next test was carried out to fail the interior column.

In test 4, in order to eliminate the possibility of punching shear failure to occur at any other edge-columns, all of them were shored and load was reapplied to the slab. The shoring was provided at three faces of the columns to prevent additional settlements and to increase the

perimeter of critical section around them. This would result a higher shear resistance for the edge columns. The shoring consisted of four (90 mm × 90 mm) timber struts placed two on the inside face and one on each outside opposite face of the columns, Fig. 3-20. All wooden supplementary supports were placed underneath the slab at a distance of 500 mm from each column face. Shoring had to be provided for south and west-edge columns, because of the existing punching shear failure surface of the south edge column, and at the west edge column because of the local bottom crack. To avoid applying any unbalanced moment to the intermediate column, the north and east-edge columns were also supported at the same distance. The slab was loaded in test 4 at 5.58 kN/m² increments until a total load of 28 kN/m² was reached. The increments were then reduced to 2.79 kN/m². The behaviour of the slab was totally different from the previous tests. For instance, when the load reached 28 kN/m², the maximum deflection at the middle of all panels was almost identical and about 5.6 mm. This is only one quarter of that recorded at the same load stage and at the same location for test 3. The behaviour of the slab changed surprisingly relative to the previous tests by simply adding wooden supplementary supports around edge columns. The crack pattern was entirely similar to the preceding tests with one important difference. The width and visuality of the cracks were much less pronounced in test 4. All these events implied that the stiffness of the shored slab was relatively high. When the load was increased to 39.16 kN/m² on the slab, there was still no sign of any large deflection or opening crack width on the slab. The maximum deflection attained was about 11.72 mm at the centre of panel B. At this load stage a sudden flexural crack around the perimeter of the north-edge column appeared on the top surface of the slab. The crack can be described as a fine crack surrounding the column and wooden supplementary supports, located at a radius of approximately

0.7 m from the centre of column as shown in Fig. 3-21 with solid lines. The occurrence of the crack was attributed to the negative bending moment generated over the additional supports placed in front of the north-edge column and underneath the slab. There was no bonded reinforcement in the slab around this region to resist the tension generated by negative bending moment. Continuing the test was considered unnecessary as there was a risk of failing the edge column by exposing the concrete to pure tension. The pressure was removed from the hydraulic system. The deflections recovered completely as shown in Fig. 3-22. The behaviour of the slab was elastic even though the applied load was 27% higher than the load on the slab in test 3.

In test 5 all the temporary supplementary supports were removed from the edge-column connections, except for the south-edge column which had failed in punching shear. Also to increase the flexural rigidity of the slab near the west-edge column, two 90 mm × 90 mm timber struts were placed in front of the inside column face as close as possible to reduce the probability of breaking the slab. The slab was loaded to 11.2 kN/m² and then to 22.38 kN/m². The deflections recorded at the middle of panel C were 4.72 mm and 13.65 mm respectively. These deflections were reasonably close to those recorded at the similar load stage in test 3. Little increase of the tendon-stress occurred up to this load stage. In the next load increment, it was decided to increase the load to 28 kN/m². When the pressure gauge showed the desired value, readings of the response gauges commenced. The load was not thoroughly stable on the slab. To keep the pressure constant in the hydraulic system, the pump's on and off button was frequently turned on and off several times. All of a sudden, punching shear failure occurred in the interior column. Punching was sudden and accompanied by a loud noise and a considerable release of

energy. The total stress-increase in all tendons crossing the failure area was recorded at about 12-15 percent. The tendon-stress increase in the north-south direction was slightly larger than in the east-west direction, Fig. 2-23. It is noteworthy to mention that test 3 and 5 were identical in loading arrangement, and the crack patterns were similar. In test 3 the applied load on the slab reached 30.8 kN/m^2 while the middle column was still capable of carrying the load. In test 5 the same column failed at a load 10% below the final load in test 3. The difference could be related to the nature of shear cracks developed inside the thickness of the slab. The discussion of this effect is presented in Chapter 4.

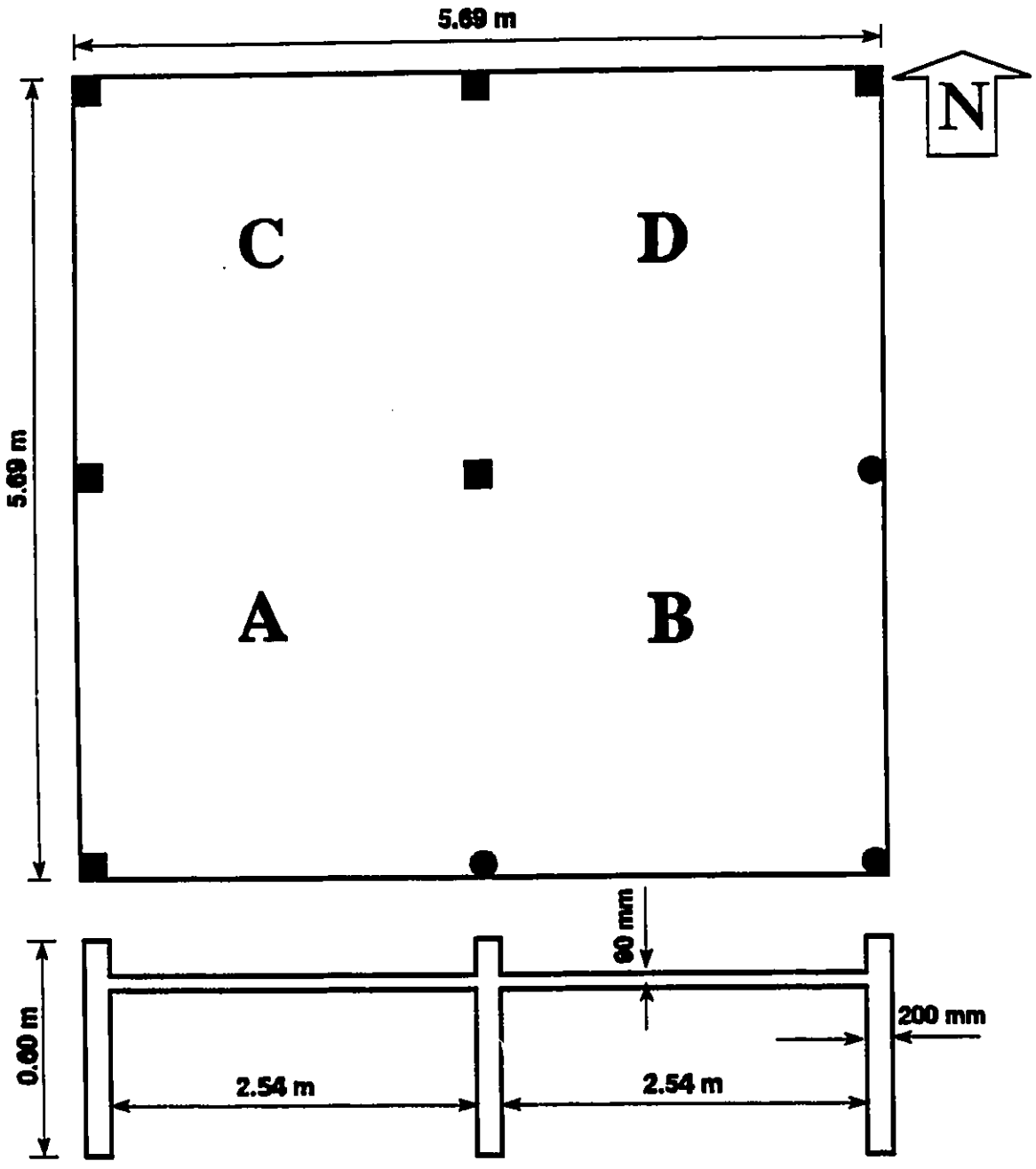

Fig. 3-1 : Plan and elevation of test slab

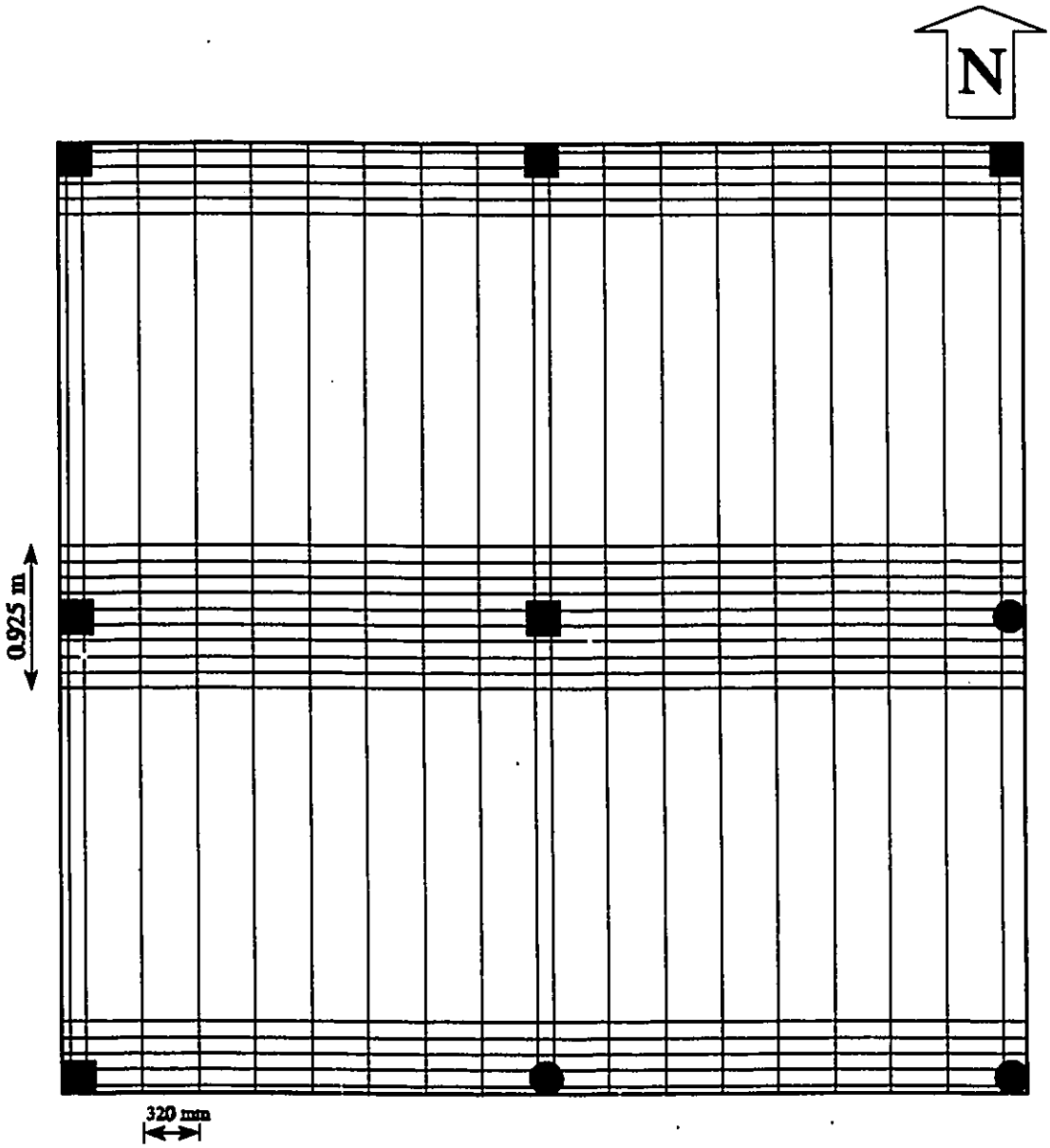

Fig 3-2 : Tendon arrangement of test slab

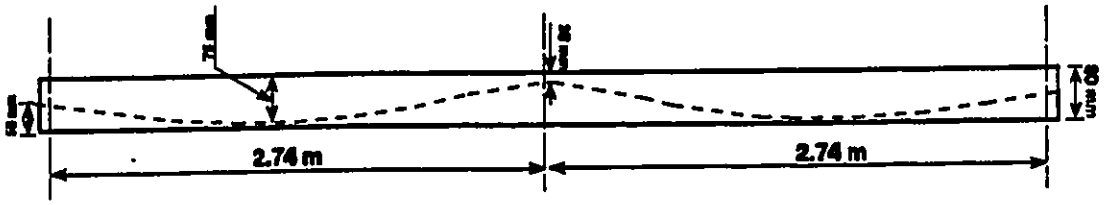

Fig. 3-3 : Typical tendon profile through the slab width

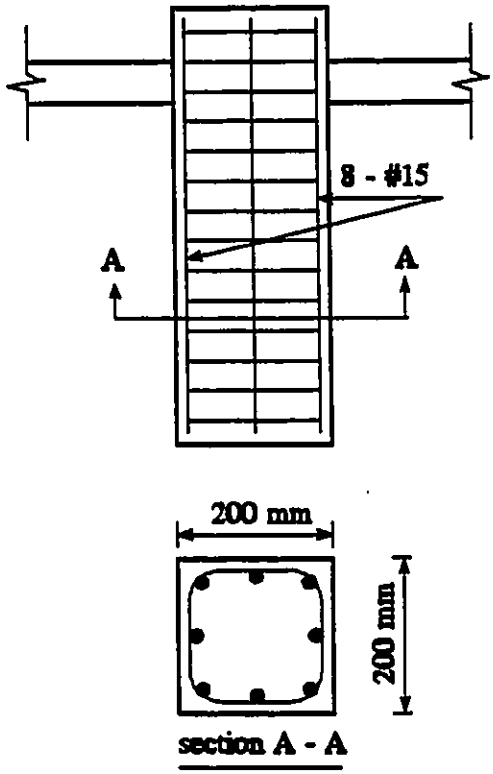

Fig. 3-4 : Typical column reinforcement for test slab

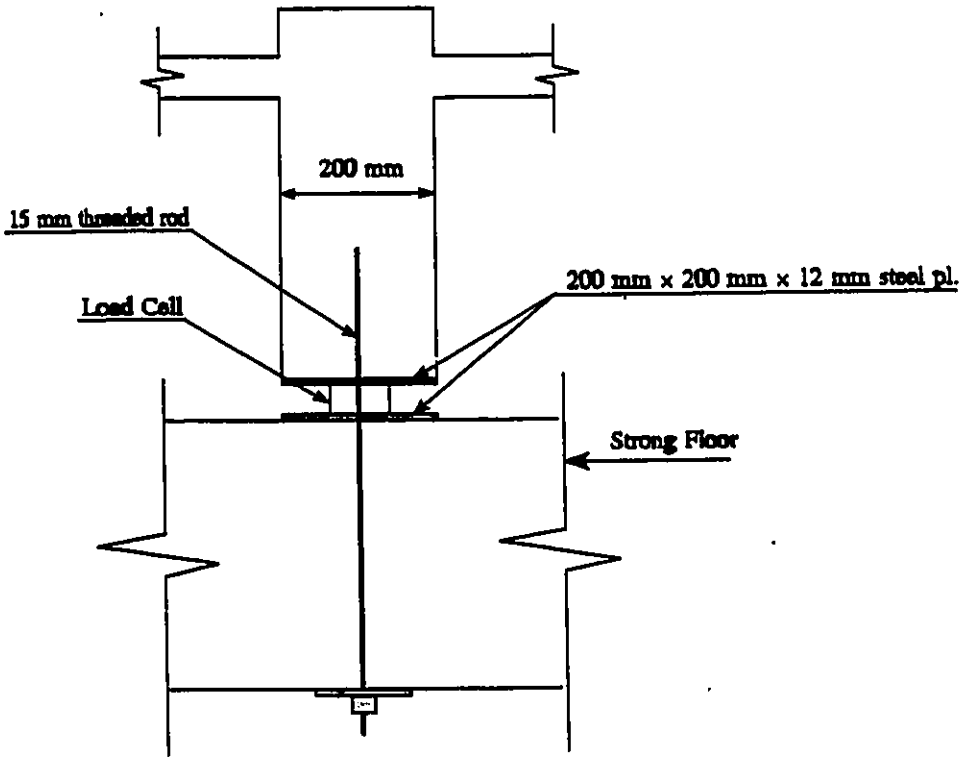

Fig. 3-5 : Typical column base arrangement with load cells

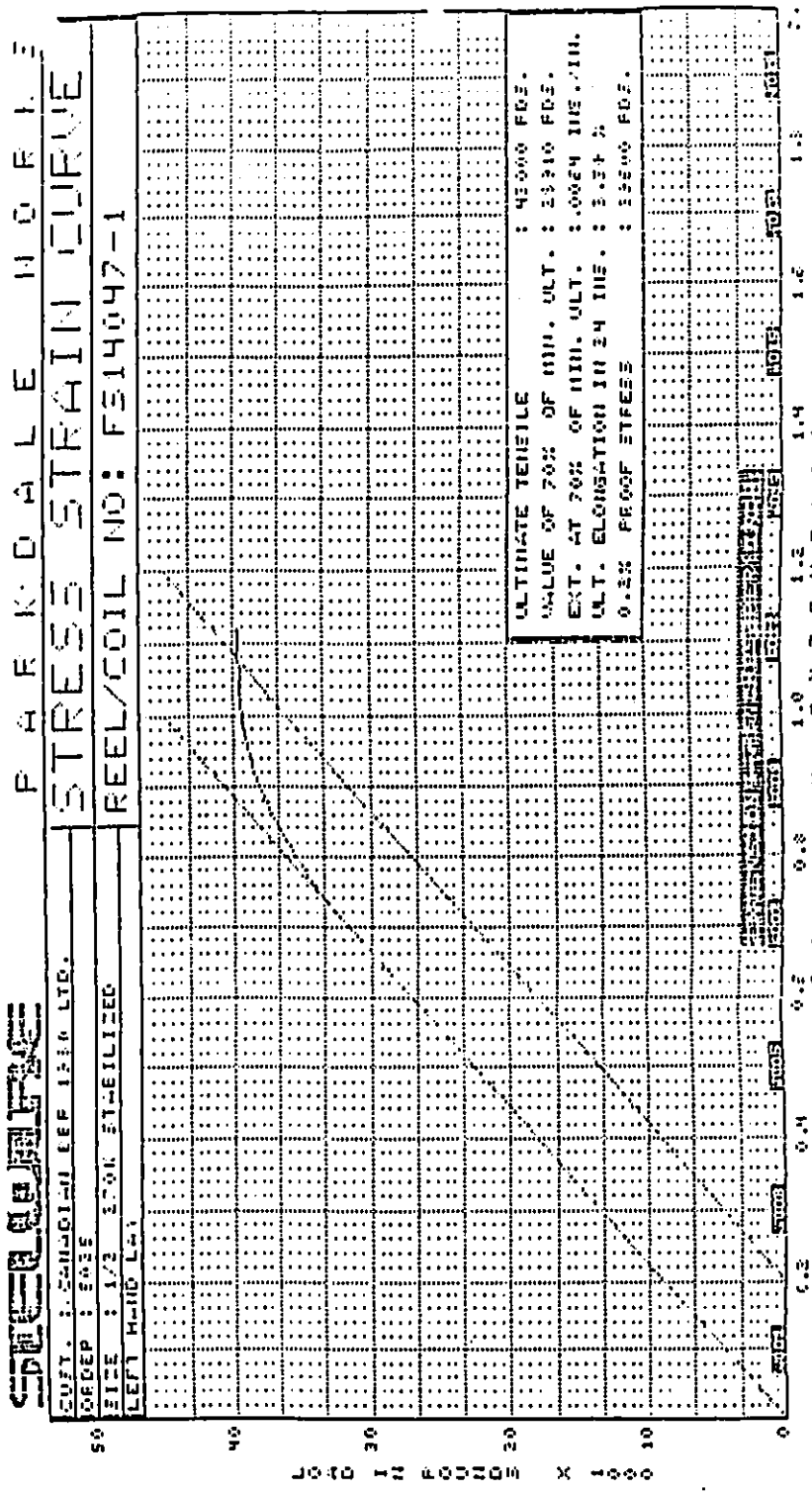

Fig. 3-6 : Typical stress-strain curve for 13 mm dia. seven-wire strand

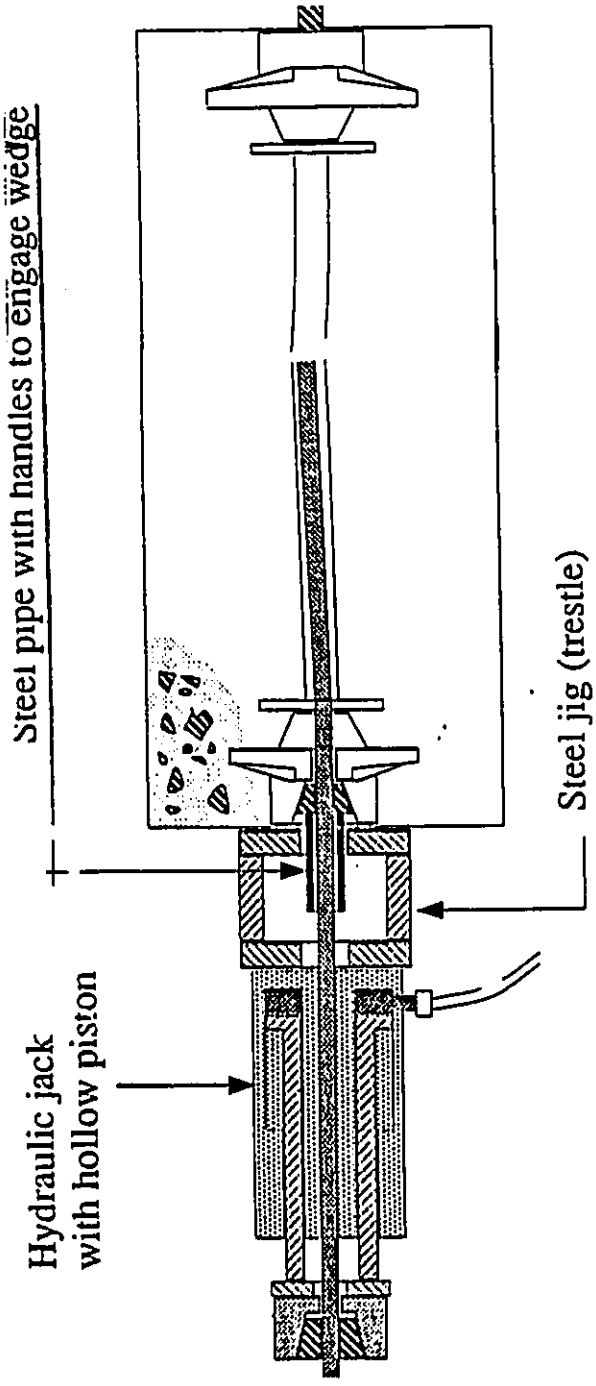

Fig. 3-7 : Schematic of prestressing device employed for test slab

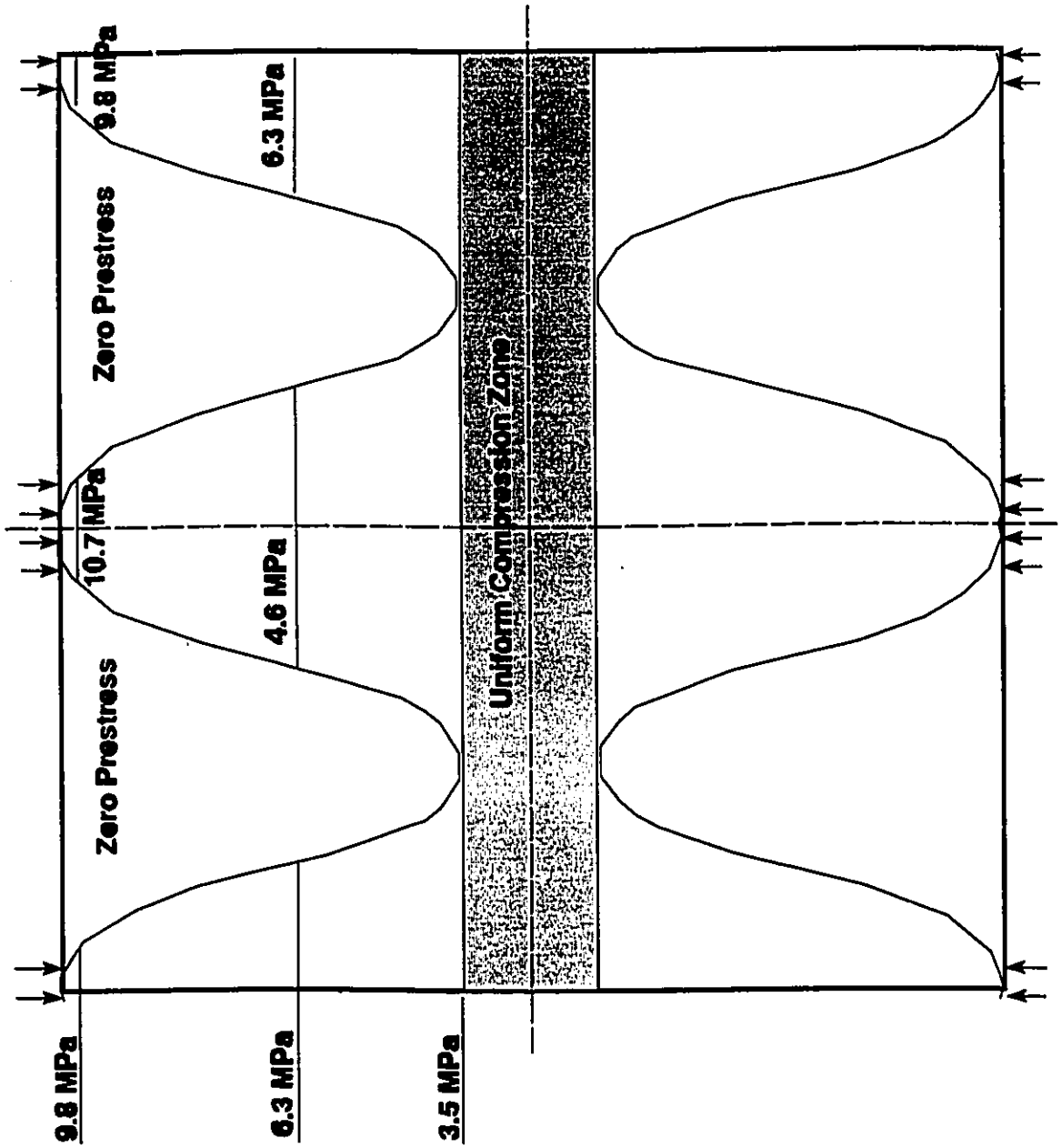

Fig. 3-8 : Variation of the prestressing force in the banded direction within the slab

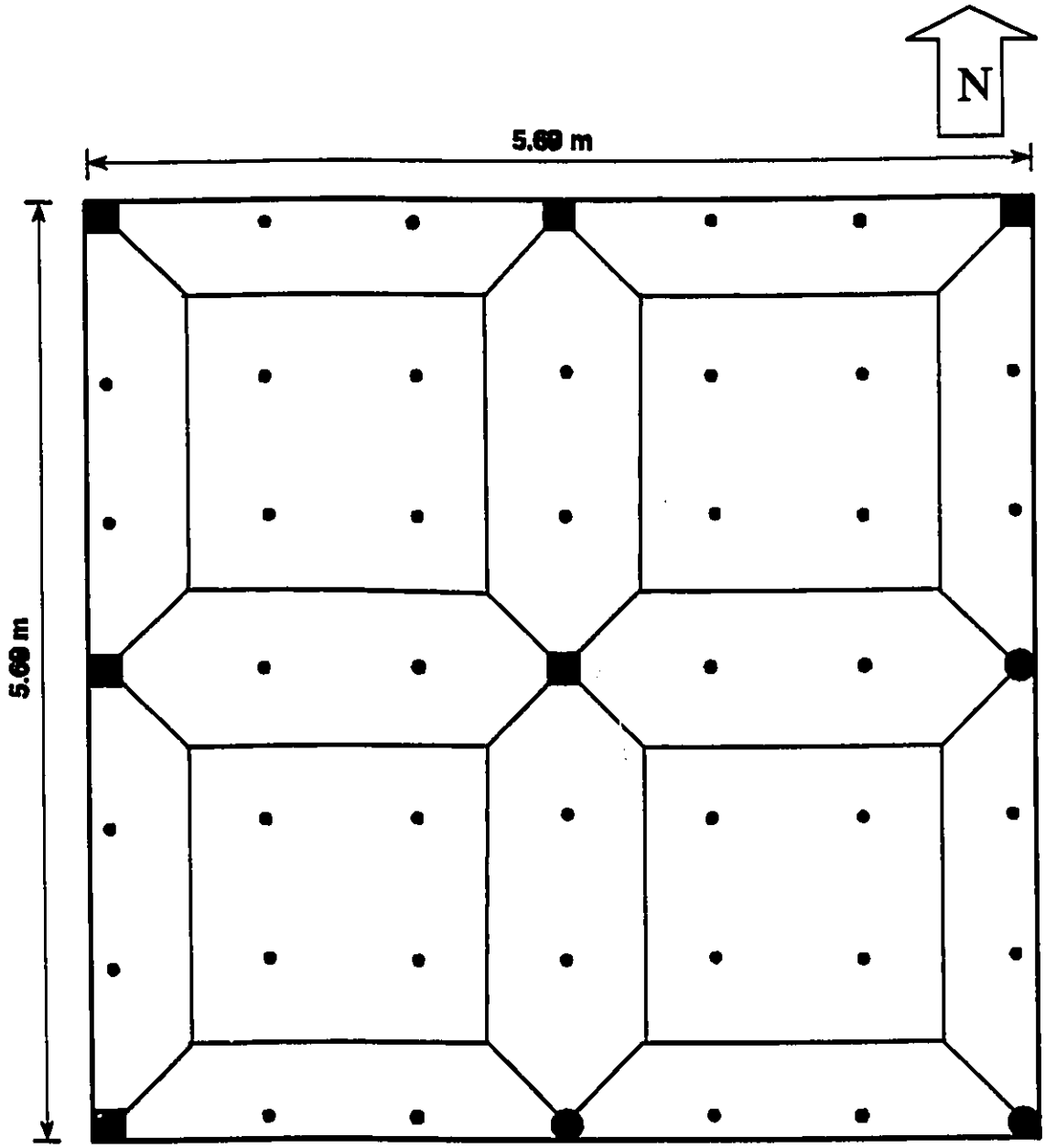

Fig. 3-9 : Schematic of test slab loading points with associated tributary areas

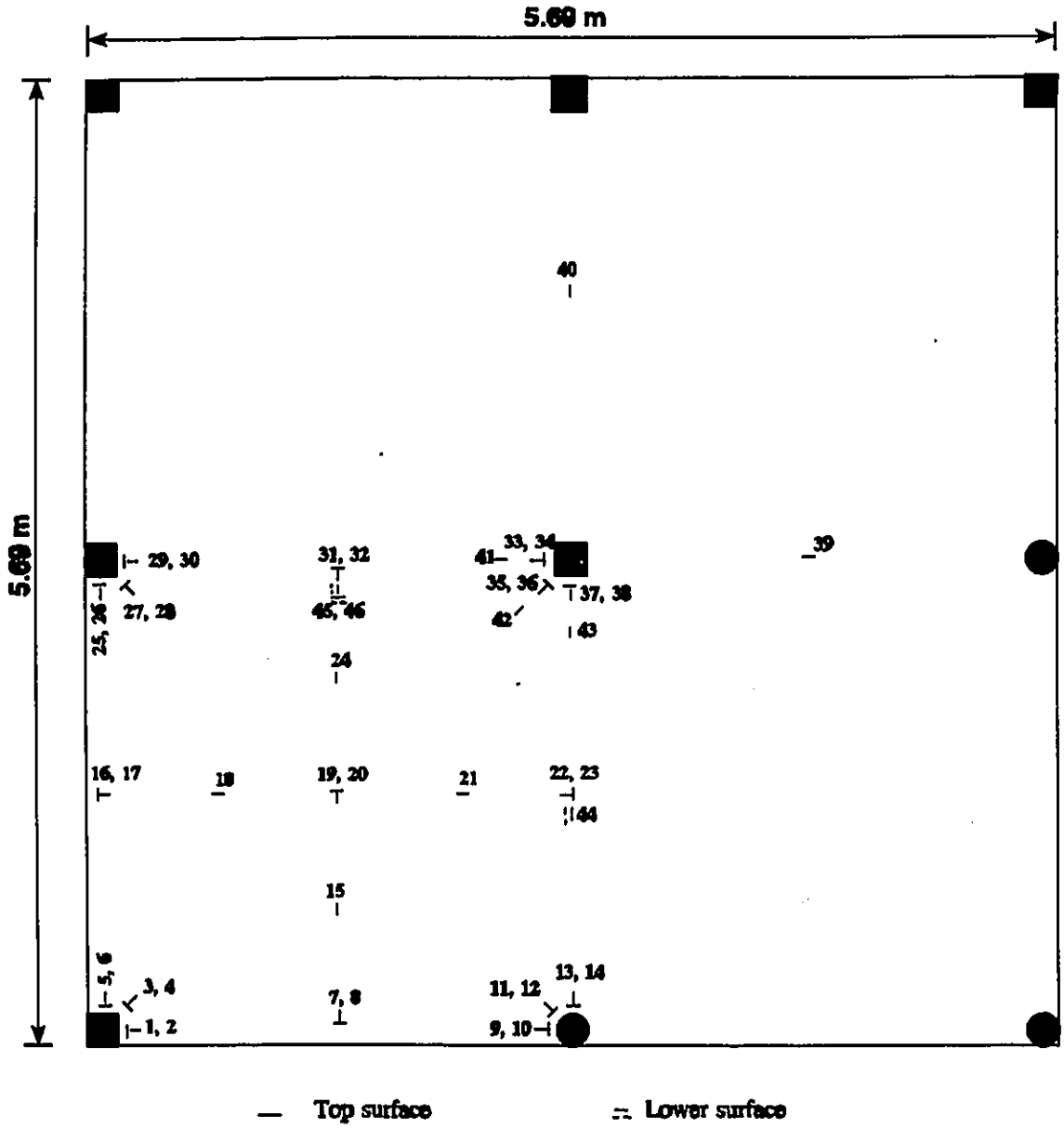

Fig. 3-10 : Location and designation of strain gauges

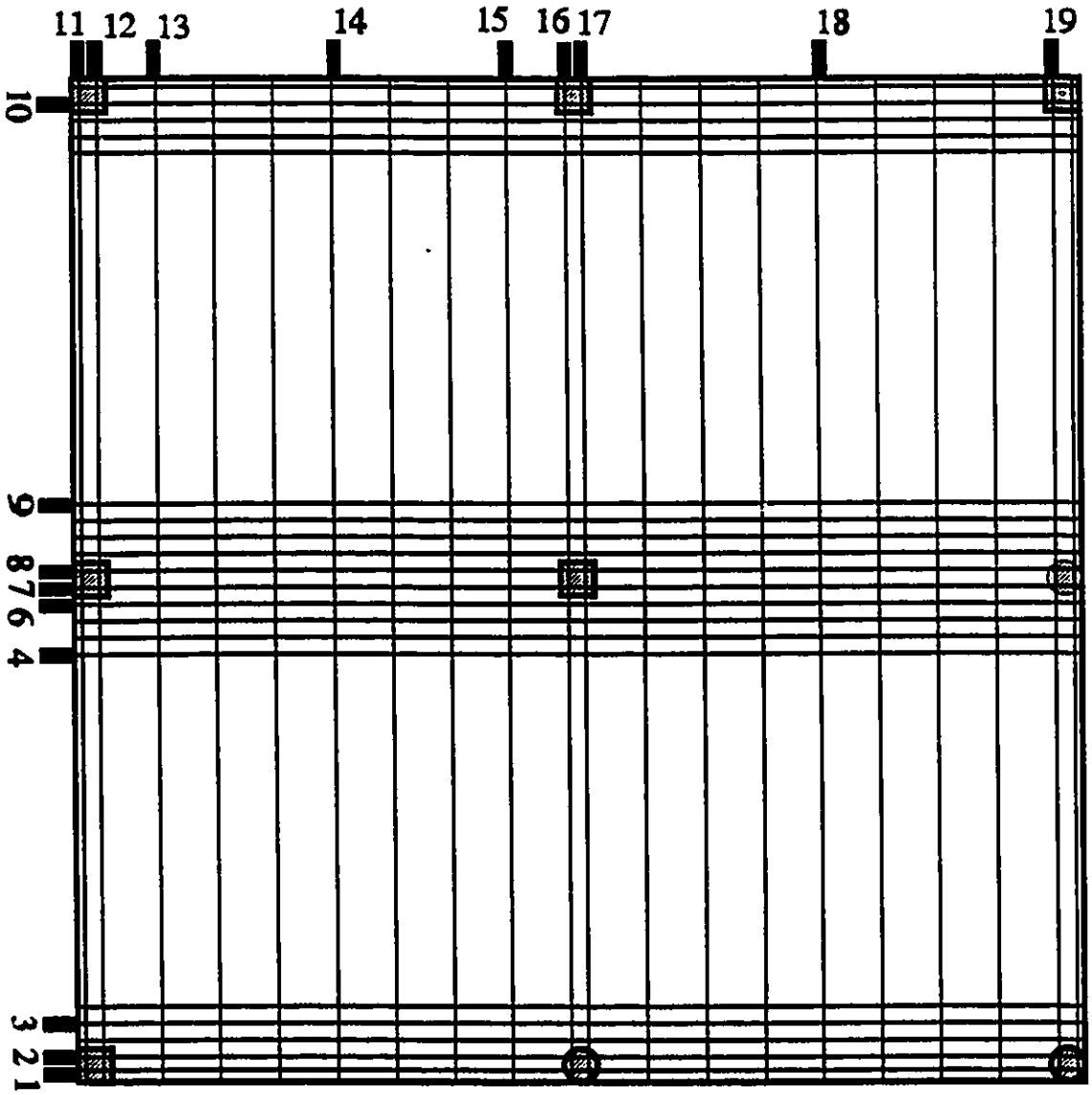

Fig. 3-11 : Location of aluminum load cells at the holding end of the tendons

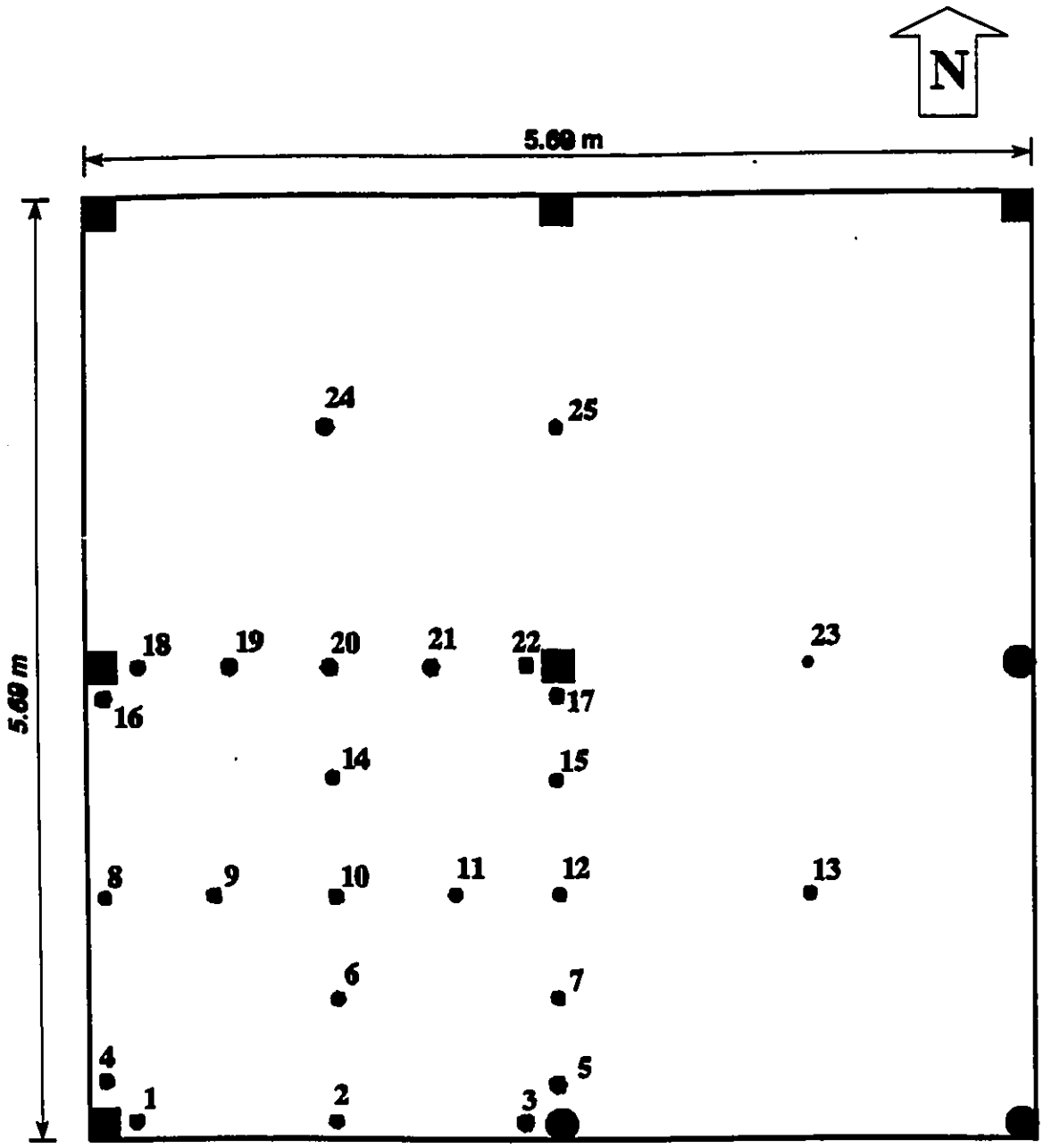

Fig. 3-12 : Location of deflection dial gauges

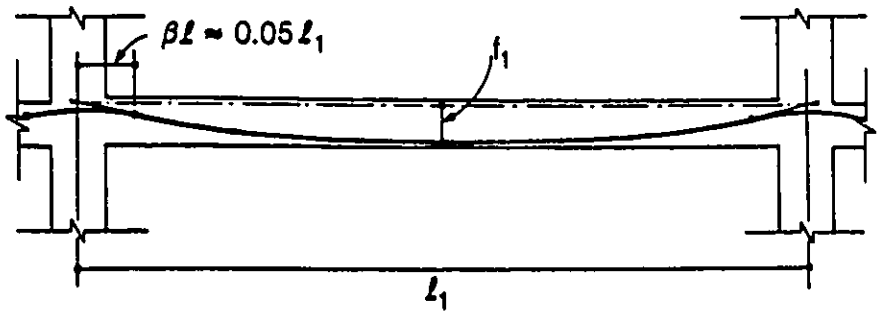

(a) Tendon profile

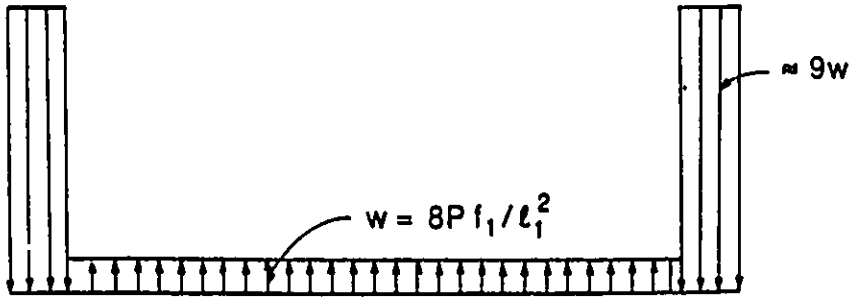

(b) Radial forces

Fig. 3-13 : Typical tendon profile with radial forces (Collins 1989)

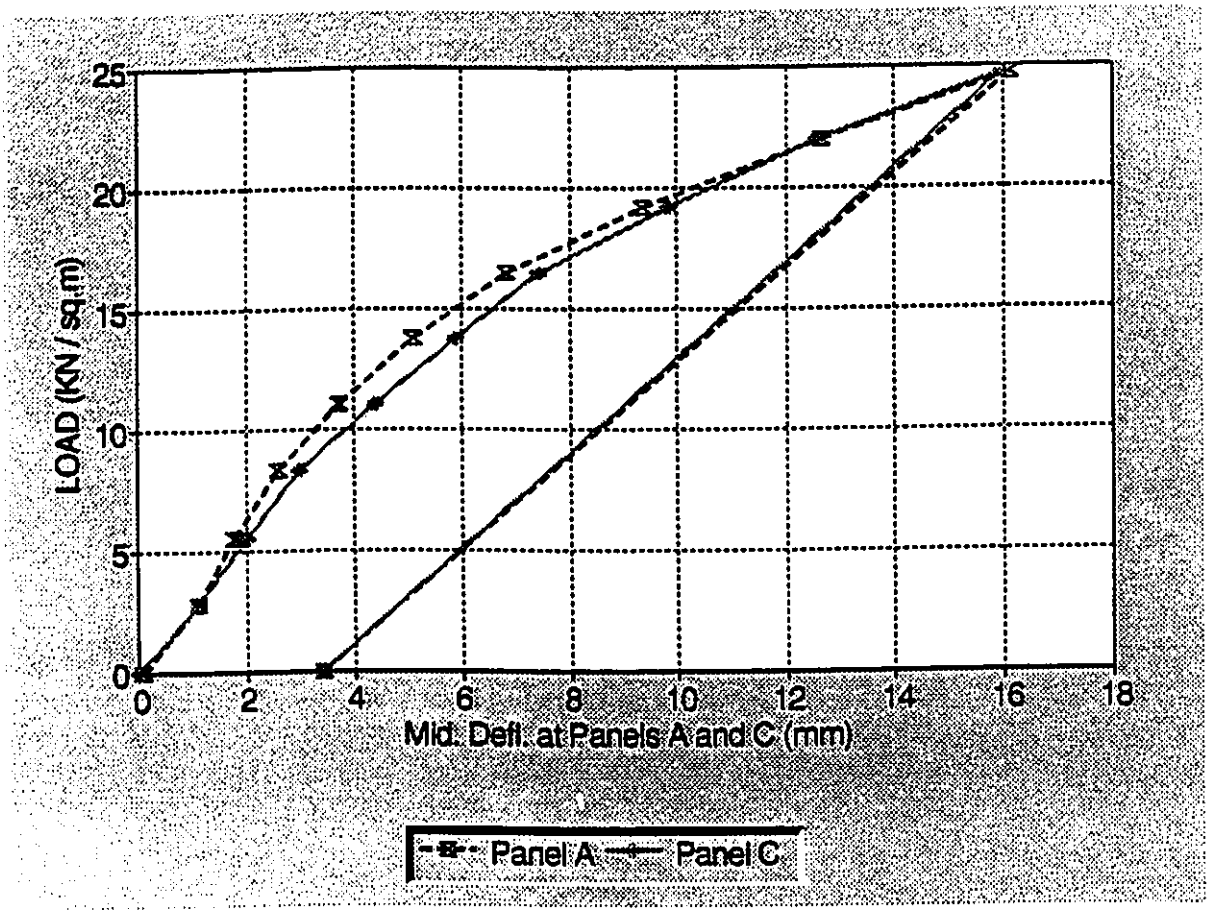

Fig. 3-14 : Load-centre deflection curve for one cycle of loading and unloading (test 2)

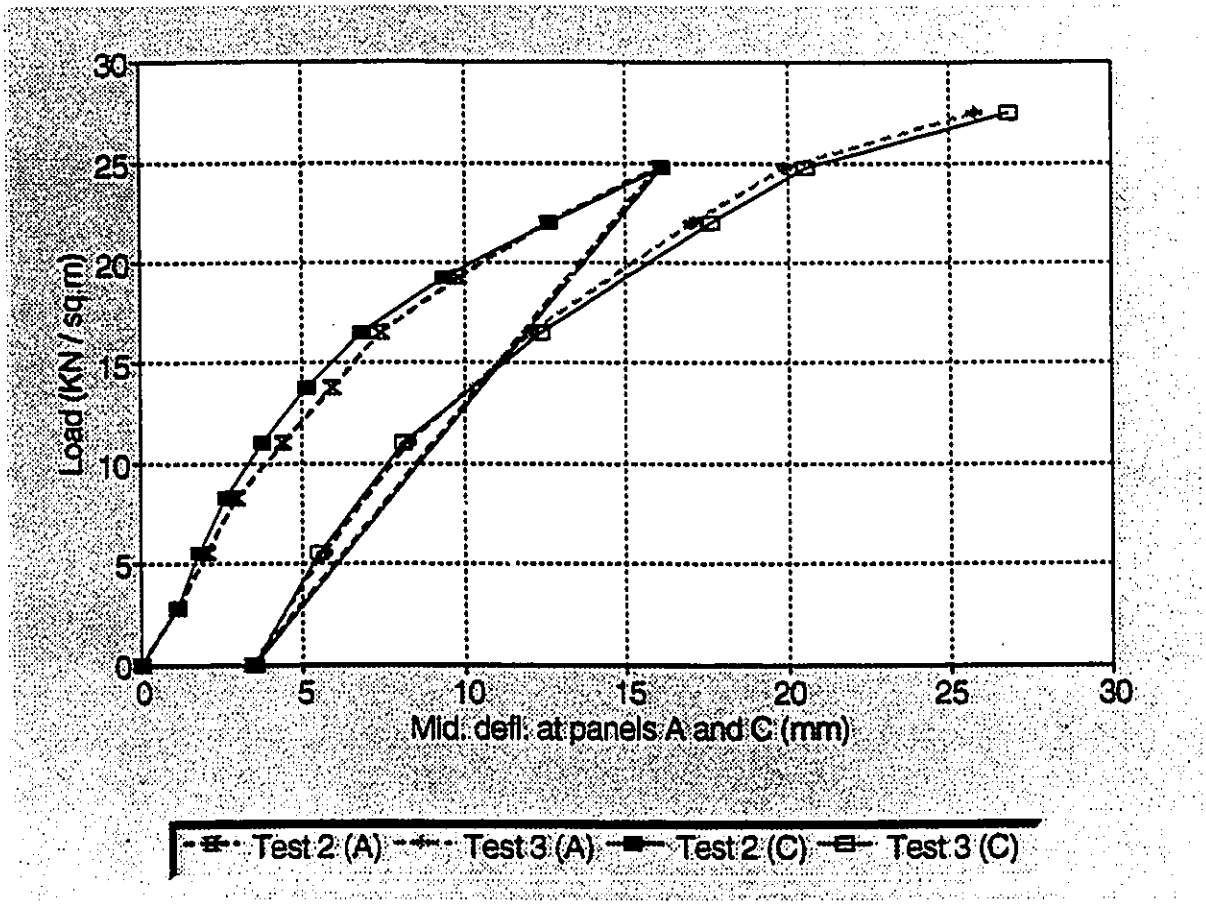

Fig. 3-15 : Load-centre deflection curve (test 2 and 3)

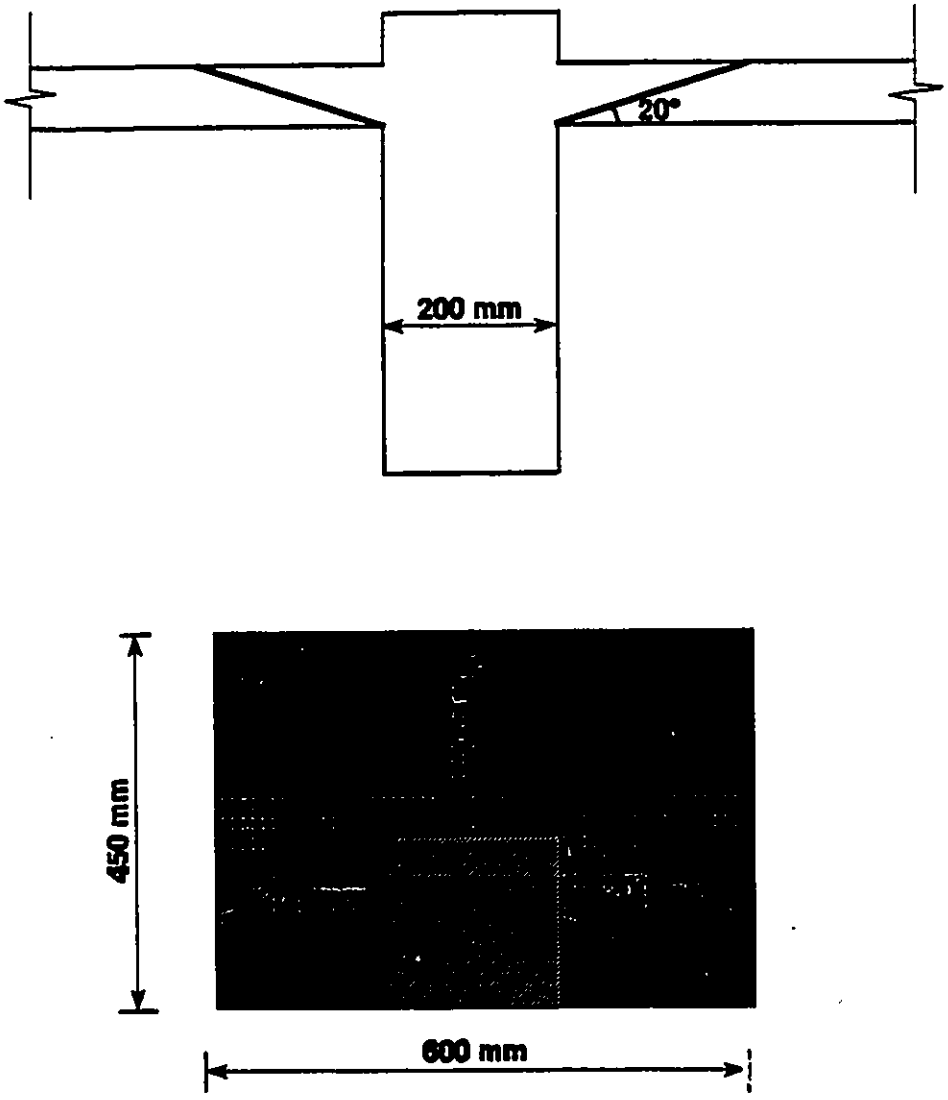

Fig. 3-16 : Size of shear cone at punching shear failure for the south-edge column (test 3)

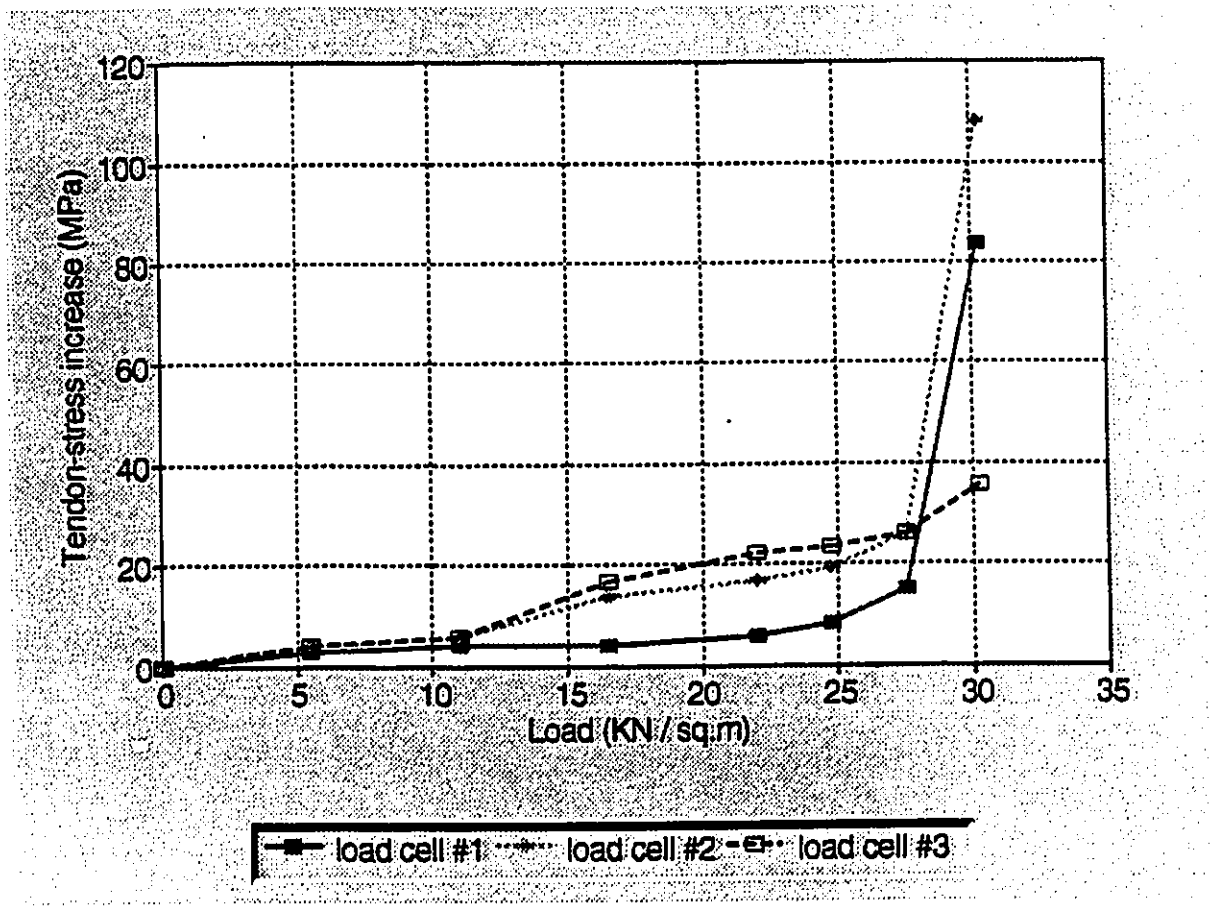

Fig. 3-17a : Variation in tendon force with applied load (test 3)

(Banded-tendon direction)

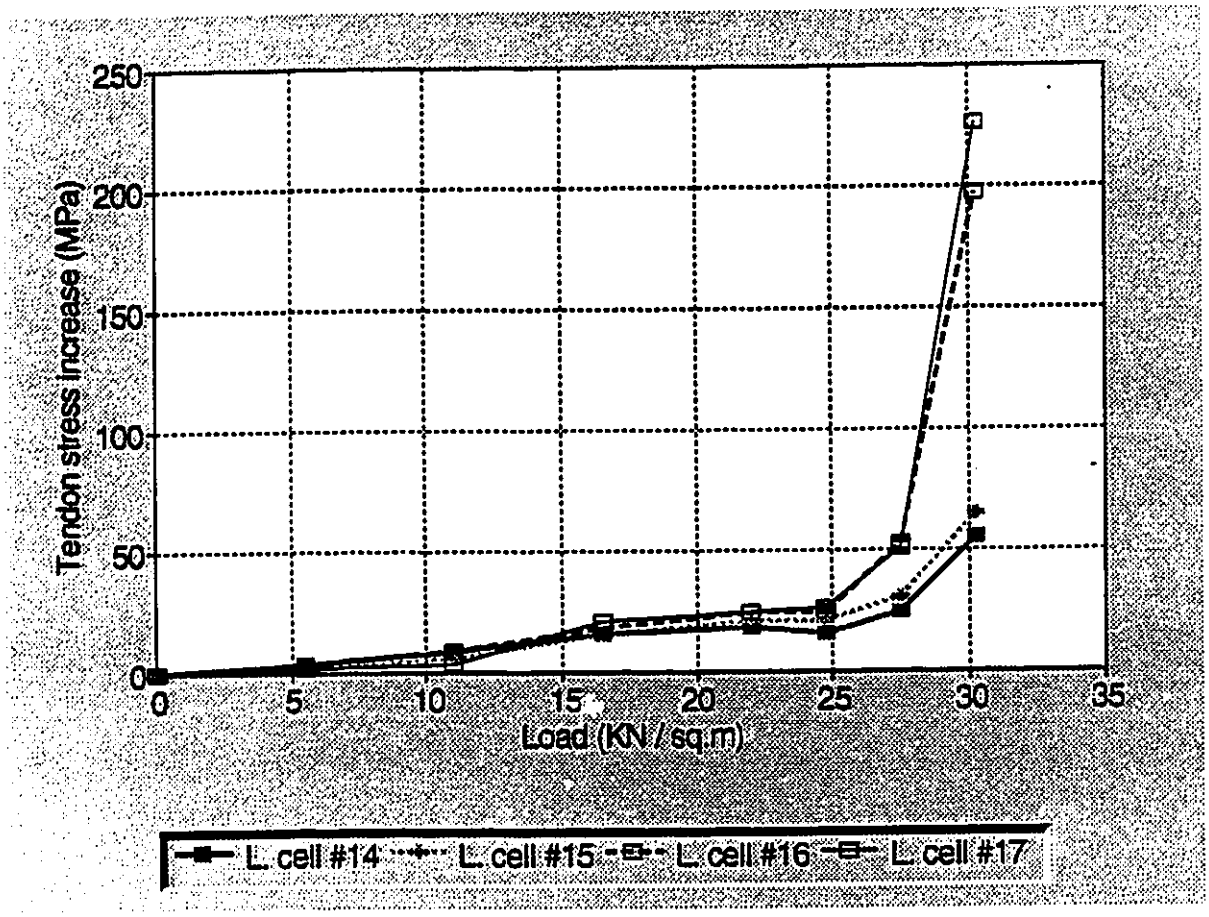

Fig. 3-17b : Variation in tendon force with applied load (test 3)

(uniformly distributed direction)

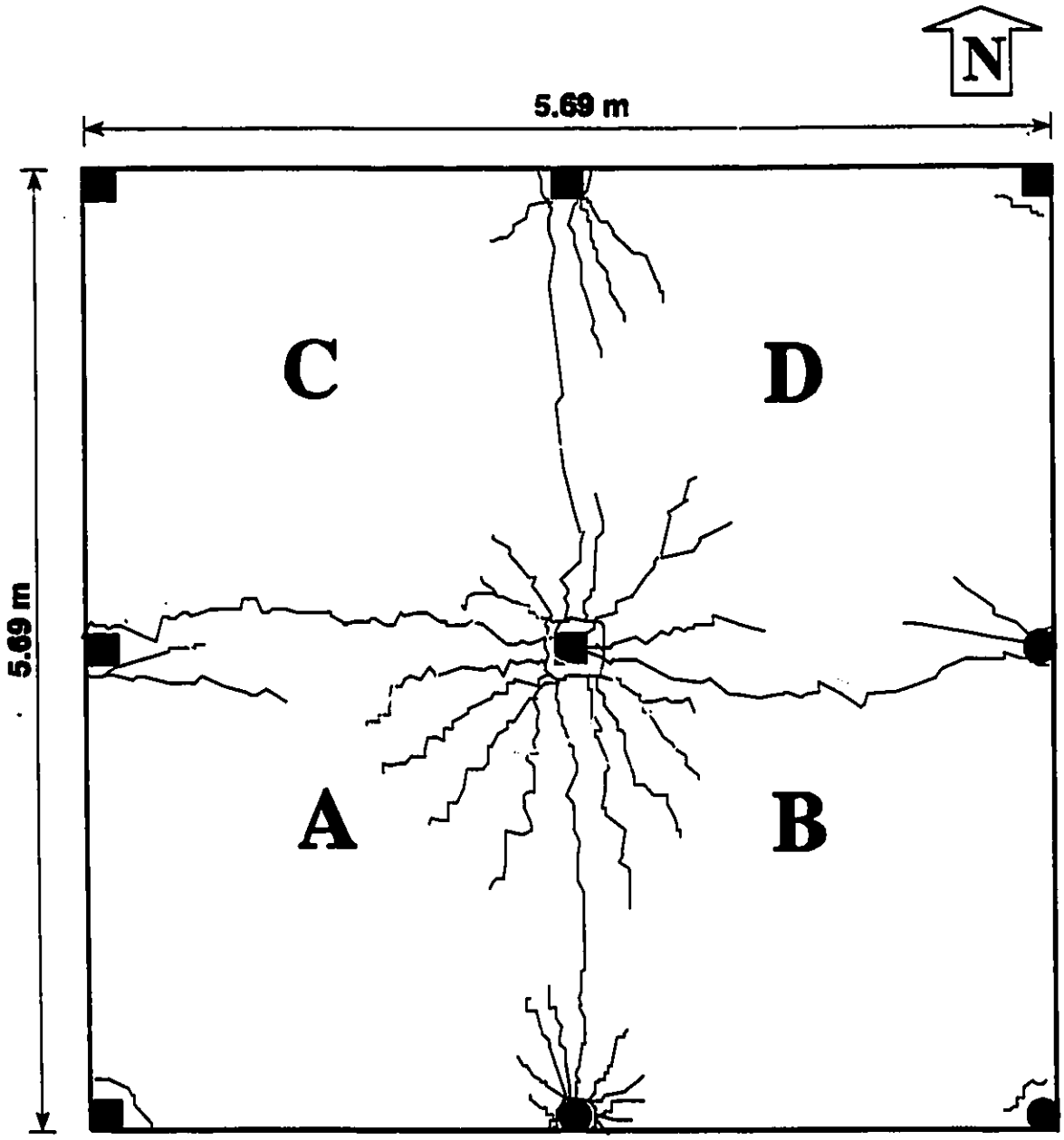

Fig. 3-18 : Crack pattern on the top surface of the slab at the end of test 3

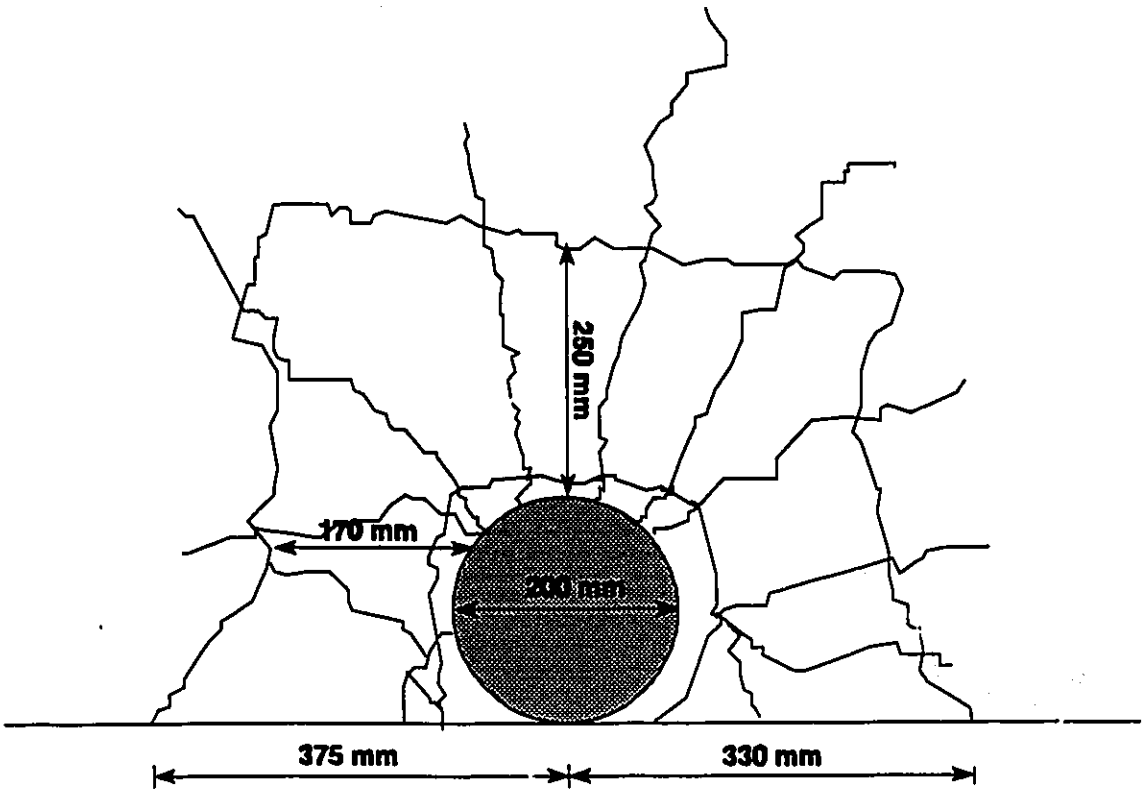

Fig. 3-19 : Punching shear failure at south-edge column

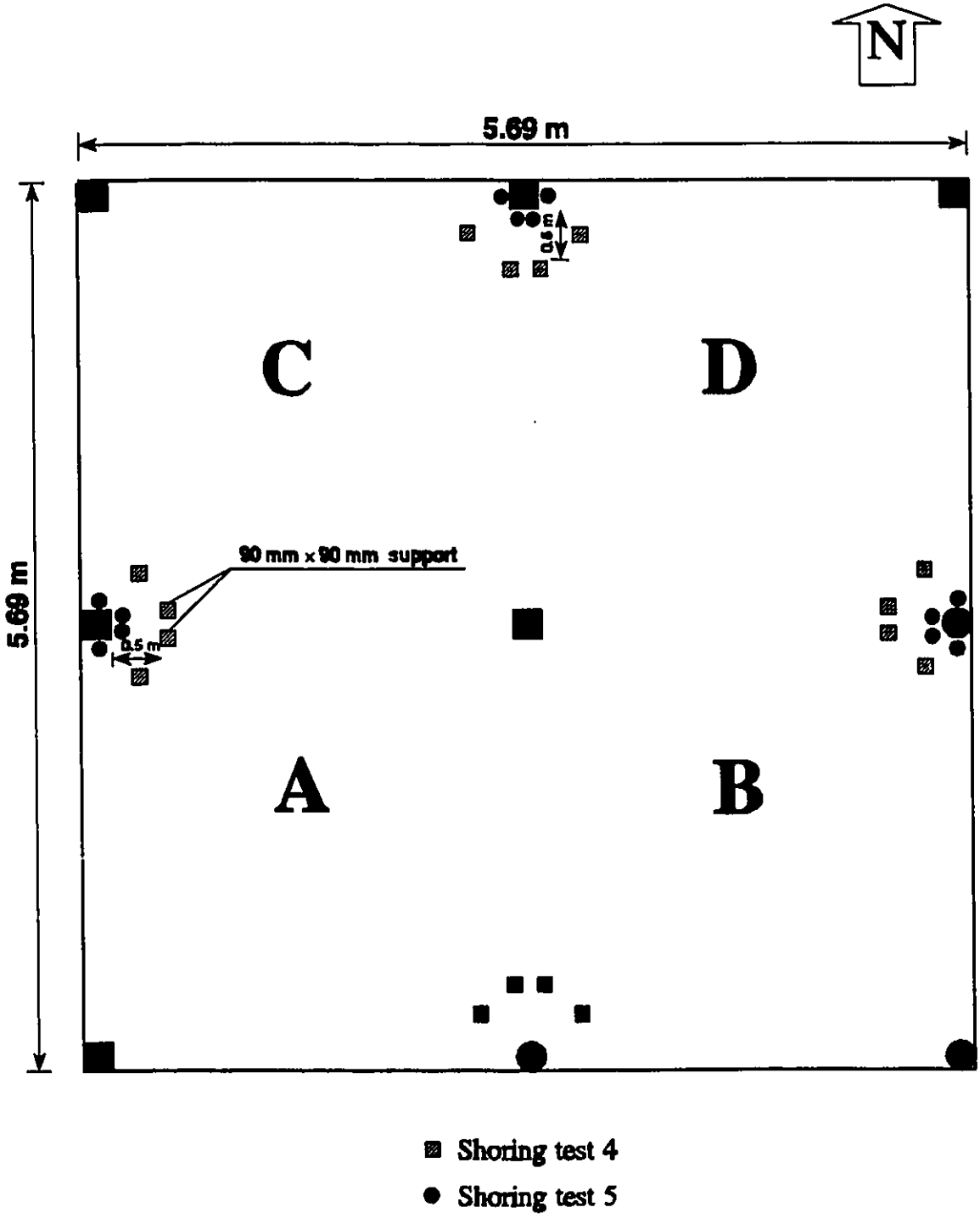

Fig. 3-20 : Typical slab shoring in test 4 and 5

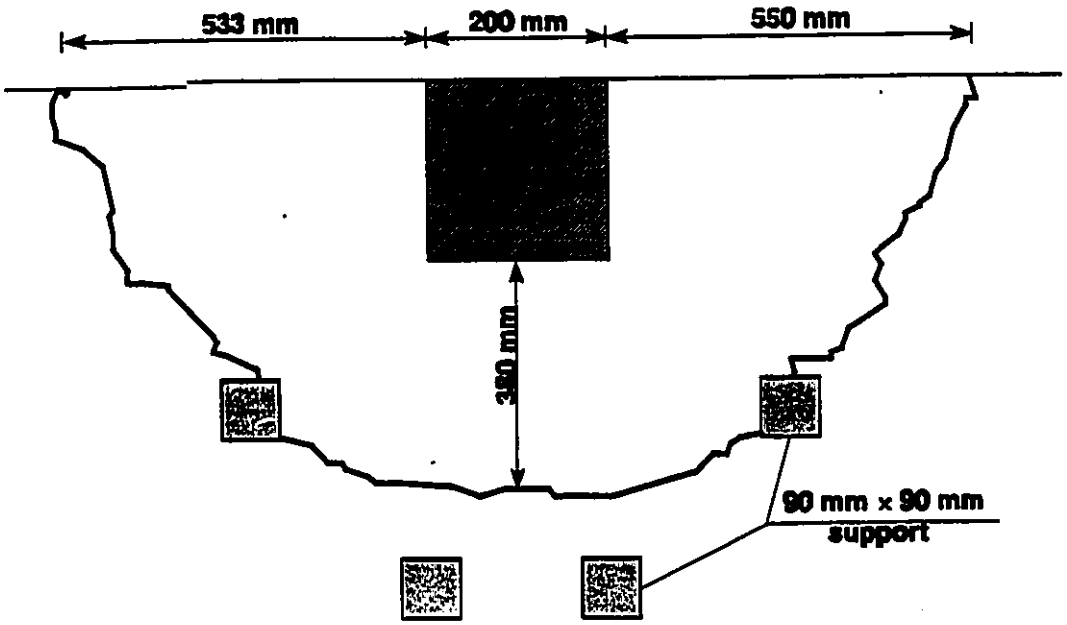

Fig. 3-21 : The flexural crack appeared around the north-edge column in test 4

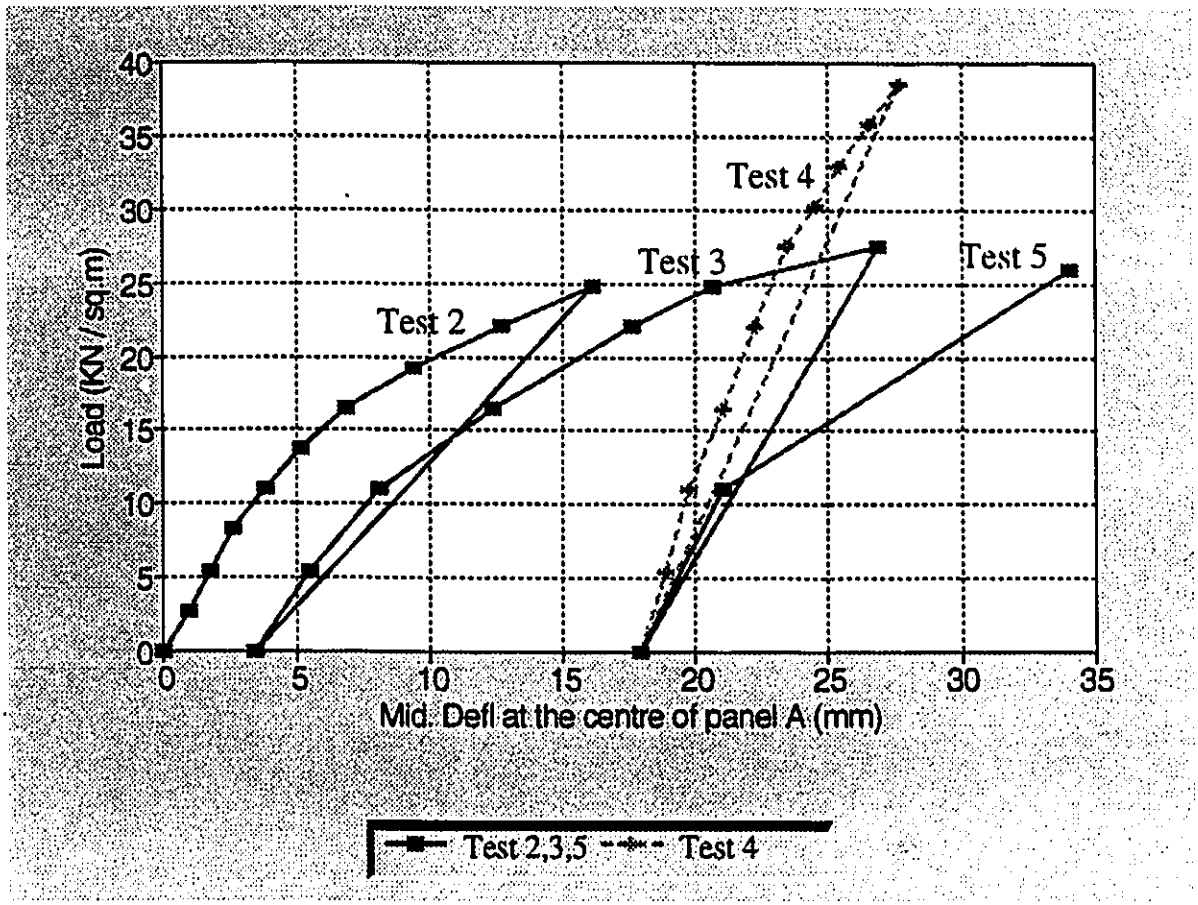

Fig. 3-22 : Load-centre deflection curves (test 2,3,4,5)

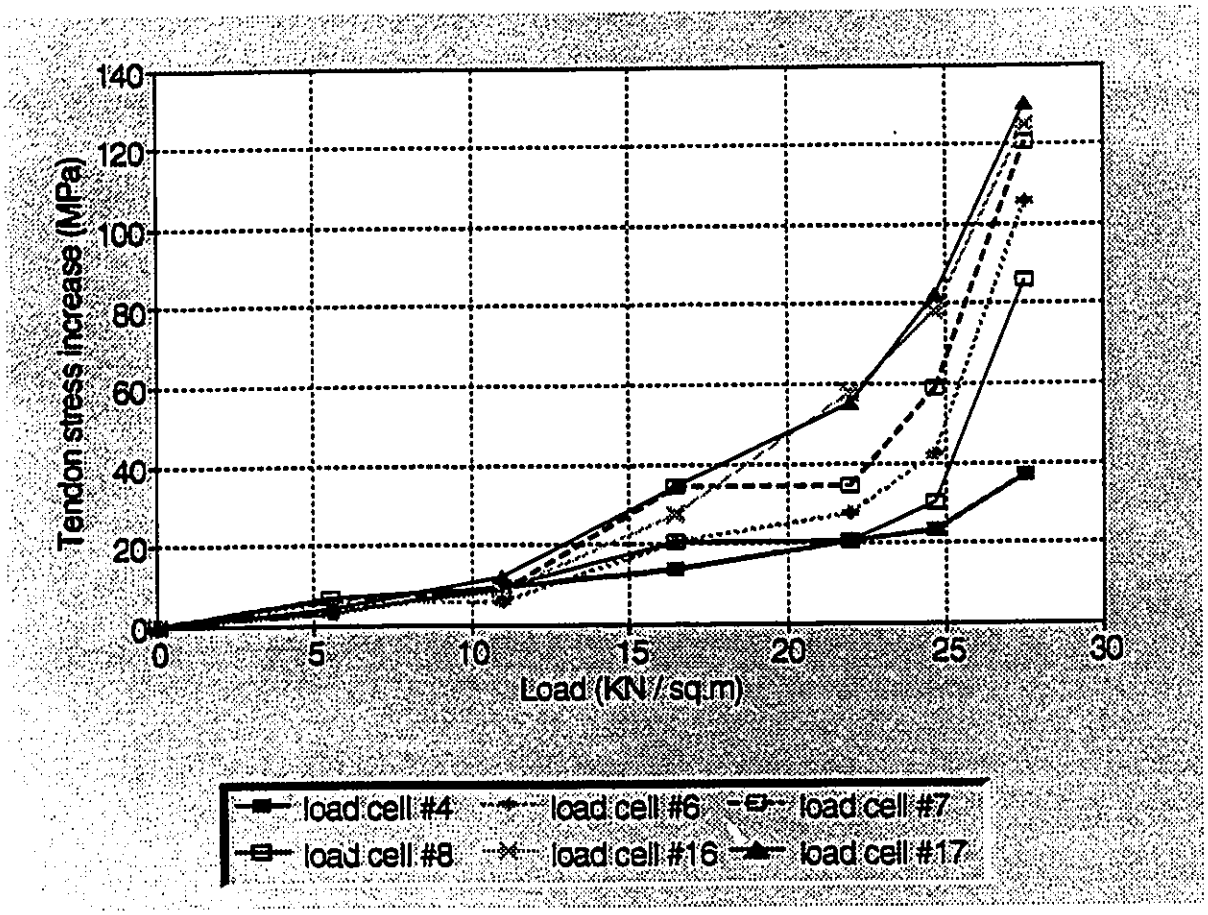

Fig. 3-23 : Tendon stress increase (test 5)

CHAPTER #4

DISCUSSION OF TEST RESULTS

4.1 General Remarks :

Punching shear strength of concrete slabs is affected by several important factors including concrete cylinder strength, ratio of the side length of the loaded area to the slab thickness (c/d) and lateral restraints or the creation of in-plane forces. The presence of axial compressive forces in a flat slab structure reduces the rotational capacity of the slab-column connections and consequently reduces both the ductile behaviour of flexural failures and the warning of collapse load associated with such failures. The magnitude of the in-plane forces generated in a flat slab structure is altered with the loading and support conditions. There is no doubt that the direct application or self-generation of membrane forces significantly increases the capacity of slabs for which flexural characteristics dominate for the unrestrained state. The degree of enhancement in strength is difficult to determine since it depends on both the stiffness of the loaded area and the

rigidity of the slab and the frame against horizontal displacements. If a comparison is made between a prestressed slab and an ordinary reinforced concrete slab, the main difference would be that in a prestressed slab the in-plane forces are directly applied to the slab by prestressing. Therefore, the intensity of effective concrete prestress could be an important factor in the ultimate load capacity of a prestressed slab. Test results have clearly demonstrated that the ultimate shear strength increases with increasing prestress.

It is generally believed that the application of an increasing load to a flat slab produces a tangential flexural crack at the periphery of the column. Radial cracks then develop, starting at the tangential crack and extending away from the column face. These cracks spread so that the slab is divided into rigid radial segments. As the load increases, the first shear crack running in the tangential direction forms. Unfortunately it is difficult to determine a unique value of the load at which the internal diagonal cracking begins to develop. Experimental research has indicated diagonal cracking starts at about 50-70% of the ultimate punching shear. With increasing load, the shear cracks extend within the slab depth resulting in a decrease of the compression zone thickness. Just before failure, the last shear crack located further away from the column face appears and all existing cracks open wider. Final punching failure occurs, when the shear cone projects along this shear crack around the column. The schematic crack pattern for an axisymmetric loading condition in an internal slab-column connection is shown in Fig. 4-1. The opening of the shear cracks indicates that the slab has failed by splitting of the concrete tension side. There are some other failure criteria such as, the collapse of the compression zone either in the radial or tangential directions and yielding of the tension reinforcement in the whole slab.

For prestressed slabs, cracking is confined to the column region with a few radial cracks extending to a short distance from the column face. Compared to reinforced concrete slabs, the crack pattern in prestressed slabs is less widespread and the capacity for lateral displacements is restricted. When an ordinary reinforced concrete slab is subjected to compressive in-plane forces, both the slab ultimate load capacity in flexure and shear increase, but not at the same rate; the load for flexural cracking is usually increased at a faster rate than the load for shear failure, Fig. 4-2. This condition together with the reduction in the extent of flexural cracking will decrease the ductility of the slab prior to failure and increase the suddenness of the failure.

Most of the tests on shear behaviour of prestressed concrete flat slabs have been carried out on isolated slab-column specimens and the effects of continuity have been ignored. The first reason for this is to simplify the testing facilities and equipment required relative to a complex and expensive multi-panel model. The other reason is that in isolated model specimens, the structure is statically determinate, therefore all internal forces produced by external loading and resisted by the connections may be measured directly. However, isolated slab-column specimens impose some limitations, as discussed in Chapter # 3, which makes the reliability of the results questionable. The investigation undertaken at the University of Ottawa was designed to provide additional information and data on the punching shear strength of continuous panels prestressed in both directions. The effects of concrete strength, the average effective prestress in the slab and distribution of tendons on the behaviour of post-tensioned unbonded concrete flat slabs were the major concerns in the experimental program. There were two punching shear tests in this investigation.

4.2 Overall Behaviour :

The test slab behaved elastically up to the appearance of first flexural cracks. Although there was no ordinary bonded reinforcement anywhere in the slab, the load at which the first flexural crack formed was about 8.4 kN/m². The ACI factored load (1.4DL + 1.7LL) for the slab was calculated as 8.35 kN/m². As anticipated, it was found that the distribution of tendons in a narrow band over the column line, and slight difference in the shape of the columns did not affect the performance of the slab for loading within the elastic range. It was intended to increase the strength of the slab in one direction by arranging the tendons closely as a band in the vicinity of the columns. It was believed this would cause the banded area to act as a shallow beam. The behaviour of the two-way prestressed concrete slab after initiation of the cracks in the positive moment regions would then change to a one-way prestressed slab spanning between the shallow beams. This type of arrangement would also cause positive yield line cracks to be formed crossing the tendons in the uniformly distributed direction and parallel to the banded direction, which has a greater strength. In the present test program, it was observed that the portions of slab in the direction of banded tendon arrangement were stiffer than the companion regions in the uniformly distributed tendon direction. Flexural crack lines ran across the slab width in the direction of uniformly spaced tendons. As can be observed from the load-deflection curves, Fig. 4-3, the deflections recorded from gauges No. 12 and 25 in the uniformly distributed direction are larger than gauge No. 23 in the banded direction. Fig. 4-3 indicates that the effect of the banded tendon arrangement was more pronounced as load approached the ultimate.

4.3 Crack Distribution Pattern :

The photographs of the crack pattern around the shear failure areas are presented in Figs. 4-4 and 4-5. The failure of the south-edge column occurred first. Punching shear failure was complete and sudden. The failed south-edge column was shored to permit resuming the application of the load on the slab for shear failure test of the interior column. For the interior column, punching failure occurred suddenly, accompanied by a significant release of energy and loud noise.

The details of the cracks produced around the individual columns at the end of the experiment are illustrated in Figs. 4-6 to 4-9. As it is indicated in the figures, the extent of the cracks is rather small. The interior column suffered from the formation of tangential and radial cracks the most. The two edge columns in the north-south (uniformly distributed tendons) direction exhibited moderate cracks. The edge columns in the banded direction demonstrated minor cracks, a few radial cracks extending from the edges of the slab along the lines of prestressing tendons and heading toward the middle column. The corner columns practically did not develop any circumferential or radial cracks. At loads close to the ultimate, a torsional crack initiated from the inner corners of the columns to the edges at an angle of about 45° was formed, Fig. 4-8.

The two edge columns in the banded direction exhibited a few longitudinal cracks extending from the edges of the slab with a close distance to the columns sides, Fig. 4-6. No tangential cracks were observed around the column periphery in the banded direction. This can be attributed to the effect of high localized prestressing force at the edges. The results from the concrete strain

gauges indicate that banding of tendons has a marked effect on the effective concrete prestress at the exterior columns. The ratio of the local prestress level to the average value was around 2.7. The concentration of prestress is only high in the vicinity of slab edge-column connections, and diminishes rapidly with distance from the column. Therefore, the exterior columns in the banded direction have the advantage of increased prestress compared with the average value of the panel, which in turn enhances the flexural cracking resistance and consequently increases the shear strength.

The south edge column was a circular column with a diameter equal to the side length of the square columns. The column perimeter area for the south-edge column was roughly 27% less than the north-edge column which was similar to the south-edge column except for the column shape. This causes the column to be more susceptible to the development of serious cracks and weaker ultimate shear strength, all because of the lower critical section perimeter resisting shear. According to the previous researchers' results, the shape of the column will affect the shear capacity of slabs. Vanderbilt observed that for the same area of the column, slabs loaded through circular columns are stronger that those loaded through square columns. That was explained by the fact that for square columns there is a concentration of strain towards the corners which increases by increasing the size of the column. For circular columns the concentration of strain is almost absent. In this experiment the south-edge column (circular shape) demonstrated a uniform crack pattern, Fig. 3-19. After the formation of a circumferential crack around the column, the radial cracks appeared in a fairly uniform manner spreading outward from the column with relatively more extensions in the north-south direction. The cracks formed and

extended at an almost similar distance from the column periphery in the banded direction. The failure surface exhibited an almost uniform distance from the face of the column to the edges of the punching shear cone in the banded direction as shown in Figs. 3-16 and 3-19. The punching shear cone in the uniformly spaced tendon direction was slightly larger for this column. This is contrary to what Burns observed in his four-panel half-scale experiment. He reported that the shear cone was larger in the banded direction. The main difference between his slab and the present test was in the effective prestressing force on the slab. The average prestressing stress in Burns's model was 1.24 MPa, which was rather low, so that the primary failure of the slab occurred as flexure, followed by the secondary mode of failure in punching shear. In the present test, the prestress level was 3.5 MPa. As the prestress is increased, the load for flexural cracking is usually increased. Increasing the flexural cracking load will directly affect the rotational demand and consequently the formation of shear cracks in a manner that they will be localized close to the column. Significant increases in load are needed for additional shear cracking to develop further from the face of the column. This will result in a more compact failure zone in the direction in which the effect of the prestressing is more pronounced.

The crack pattern for the north-edge column, immediately before failure occurred in the south-edge column is illustrated in Fig. 4-7. A few radial cracks were observed spreading mostly from the column corners. The propagation of radial cracks toward the corner columns was very limited. The radial cracks showed a tendency to move along the line of prestressing tendons toward the middle column. The torsional cracks initiated close to the column. These cracks opened wider and propagated deeper as the applied load was increased.

For the interior column, the propagation of cracks was more pronounced from the corners than the sides. There was no difference observed in the amount, length and depth of the cracks in the banded or uniform tendon direction. That suggests the arrangement of tendons in a narrow band over the column strip does not have a major effect on the test results for the inner columns. Therefore, the value of prestress level for an interior column can be averaged over the full-panel width. However, the same conclusion can not be drawn for the edge-columns. The angle of inclination that the side of the failure pyramid made with the top surface of the slab varied from the maximum of 14° at the north and east faces of the column to a minimum of approximately 11° at the west and south faces of the column, Fig. 4-10.

4.4 Column Rotation :

In test 3, the top portion of the west edge column exhibited a large rotation as the slab was loaded close to collapse. The base of the column was fixed in position and rotated as a rigid body above the threaded anchor rod. This rotation was measured as 2.84° at the end of the test. Rotation of the column as the load increased was accompanied by a relatively wide bottom crack at a distance 0.7 m from the face of the west-edge column and parallel to the free edge. The bottom crack was so severe that a thin layer of concrete on the top surface of the slab crushed. At the end of the test, the thickness of the slab was measured at this region by drilling a small hole through the slab. The measured thickness was 75 mm or approximately 20% smaller than the designed thickness. This could well be the reason why the behaviour of the slab around this area was not the same as similar areas in the slab. Close to the ultimate, the middle deflection

of the slab between panels A and C was 90 percent higher than the same point deflection between panels B and D, Fig. 4-11. Strain gauge No. 45 indicated a large increase over strain gauge No. 39 as the load approached the ultimate, as shown in Fig. 4-12. The rotation of the west-edge column due to the smaller thickness of the slab induced some extra moment to the midspan. But the middle portion of the slab in the banded direction was strong enough to resist the load even in the absence of positive non-prestressed bonded reinforcement. The influence of this problem was only in the deflections measured around this particular area.

4.5 Shoring The Slab :

In test 4, shoring the slab significantly increased the overall stiffness of the structure. Increasing the load to 39.16 kN/m^2 resulted in smaller deflections for all panels compared to test 3, Fig. 4-13. Even though the load was 27% higher than test 3 and 5, the internal column did not fail. Shoring the slab at a distance close to the exterior columns increased the strength of the panels by reducing the span length of the slab. More specifically, each span was divided into two shorter spans as shown in Fig. 4-14. As load was applied through the threaded rods, it can be seen from the Fig. 4-14 that the major part of the concentrated load close to the shoring point will be taken by this support. Because all the edge columns were tied down to the structural laboratory floor, they are considered to be perfectly restrained against vertical displacements. This will produce a strong coupling action between these columns and the supplementary timber struts. With regard to Fig. 4-14 it can be concluded that as the intensity of the load increased, the exterior columns tended to move up, but the vertical restraints (tension in the bars embedded in

the columns) would generate a relatively high downward forces to support the columns. This action reduced the positive moment between the middle column and supplementary shores. A computer analysis modelling the slab together with the timber strut supports clearly showed why the middle column did not develop punching shear failure in test 4. As it can be seen from the results, Appendix B, the column reaction is less than what was expected to be for punching shear failure. On the other hand, a large amount of negative moment produced over the supplementary struts would have caused the failure of the slab around this region if the load had been increased. There was no reinforcement on the top surface of the slab to resist the tension force generated by negative moment. Unloading the slab left no residual deflection at any point in the slab, indicating that the behaviour of the slab with the presence of timber struts was entirely elastic.

4.6 Interior Column Failure Load :

It is interesting to note that the failure load of the interior column, test 5, was about 10% lower than final load in test 3. Test 5 was a test in which it was intended to fail the middle column while the south-edge and west-edge columns were shored. Test 3 and 5 were identical in load arrangement. The crack patterns developed around the negative regions of the slab were similar. All cracks formed in the previous tests lengthened slightly and widened, and a few new cracks around the interior column initiated. Yet, the ultimate failure loads of the two tests were different. The difference could be because punching shear is preceded by internal diagonal cracking at loads of the order of 1/2 and 2/3 of the ultimate. As the slab was loaded and unloaded in tests 2 and 3, the applied load exceeded the load at which the internal diagonal cracking had occurred

within the slab thickness. The condition after the initiation of inclined cracking, even though the slab underwent relatively large rotations, appeared to be stable. But as the slab was unloaded in the previous tests the internal diagonal cracking remained inside the slab. In an experimental program undertaken by Grira (1990) at the University of Ottawa, two similar specimens were tested, one under monotic loading and the other cyclic loading. The punching shear resistance after four cycles of loading decreased by 19%, Fig. 4-15. Therefore loading and unloading could impose strength degradation on the shear resistance of flat slabs, and this would reduce the total shear capacity of slab-column connections.

The final failure load of the internal column was determined by the sum of shear applied through the external loading and the vertical component of the prestressing force crossing the critical section ($\frac{d}{2}$ from the face of the column). Many researchers have suggested that the effect of tendon inclination over the support may be conservatively neglected as it contributes only a small portion to the shear strength. Depending on the curvature of the tendons, the intensity of the downward forces acting near the column lines changes. The concentration of tendons over the support together with a highly localized concave downward portion of the tendon profile toward the column perimeter will affect the amount of the transverse load imposed over the support. In the model slab tested, the magnitude of the vertical component of prestressing was found, by summing the contributions of the tendons passing through the critical section in the two directions, to be roughly 20% (45 kN) of the collapse load on the slab due to the applied load. As discussed in Chapter 5, increasing the ultimate shear strength of slab-column connections by considering the fact that the tendons near the support carry some load is

recognized by the North American codes. However, the idea of computing the vertical component of prestressing tendons crossing the shear perimeter involves some ambiguities such as : What happens if the location of the control shear perimeter is assumed to change (different countries propose different areas for shear perimeter), what would be the effect of tendons crossing nearby the critical section; should their effect be disregarded or what are the effects of the overall drape of the tendons through the slab width on the creation of transverse forces acting over the support. In order to achieve a reasonable explanation on this subject, it is recommended to consider the entire structure instead of the shear perimeter, and then using the concept of the load balancing method together with the equivalent frame method or any other analytical procedure to determine the final forces and moments resisted by the columns due to the prestressing. The shear stresses acting on the control perimeters can be computed by the summation of the axial loads calculated based on the external loading and those determined due to the prestressing. According to this theory there would be no beneficial effect of the banded tendon arrangement with regard to the vertical loads transmitted to the columns due to the prestressing. For the interior column of the experimental slab tested the vertical beneficial effect of prestress was calculated to be 53.4 kN. The calculation of vertical component of prestress for the edge and corner columns are more complicated as the effect of the edge forces, due to the prestressing, should also be considered in support reactions. The drape of tendons near the edges is a key factor for the calculation of support reactions due to prestressing.

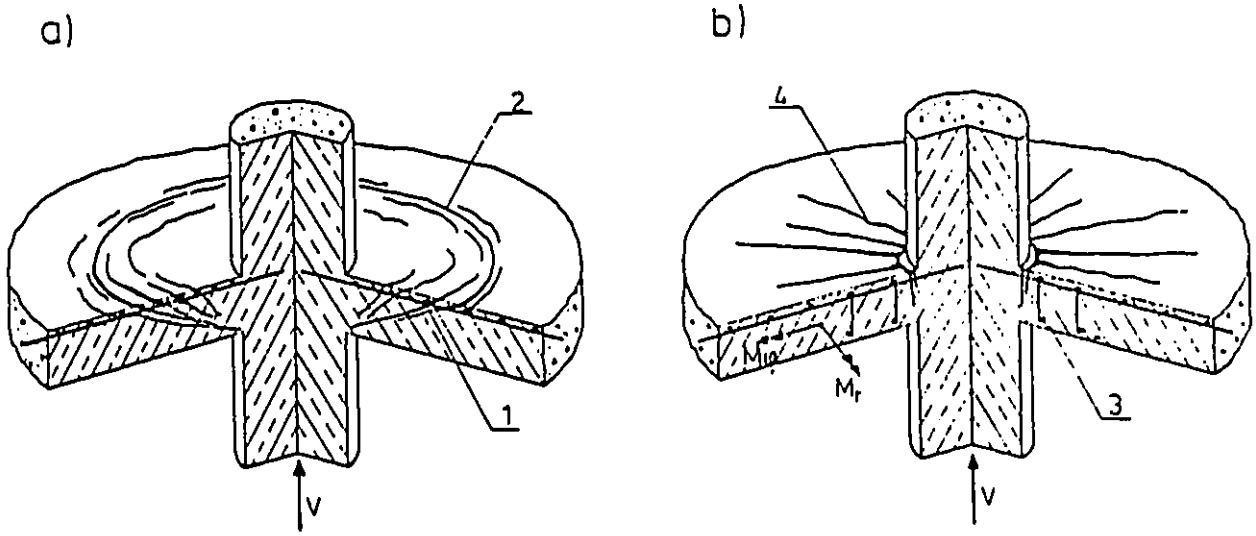

Fig. 4-1 : Crack distribution around an internal loaded support a) shear cracks b) flexural cracks 1) inclined cracks 2) peripheral cracks on the top surface 3) peripheral crack around column, arising from M_r 4) radial cracks (Ajdukiewicz 1990)

Fig. 4-2 : Comparison of the rate of change in moment and shear capacities calculated based on the ACI 318-89 recommendations versus f_{pc} (Hemakom 1975)

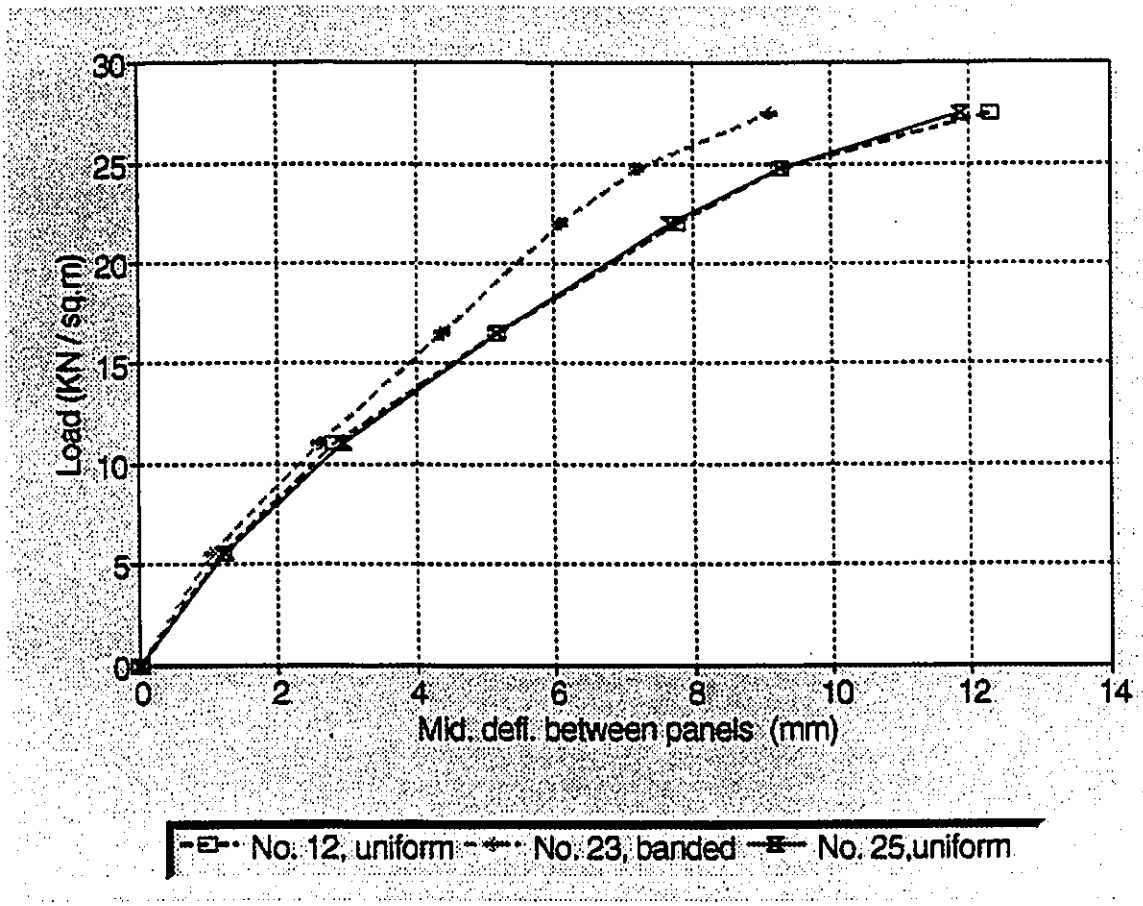

Fig. 4-3 : Comparison of the deflections recorded in the banded and uniformly distributed directions

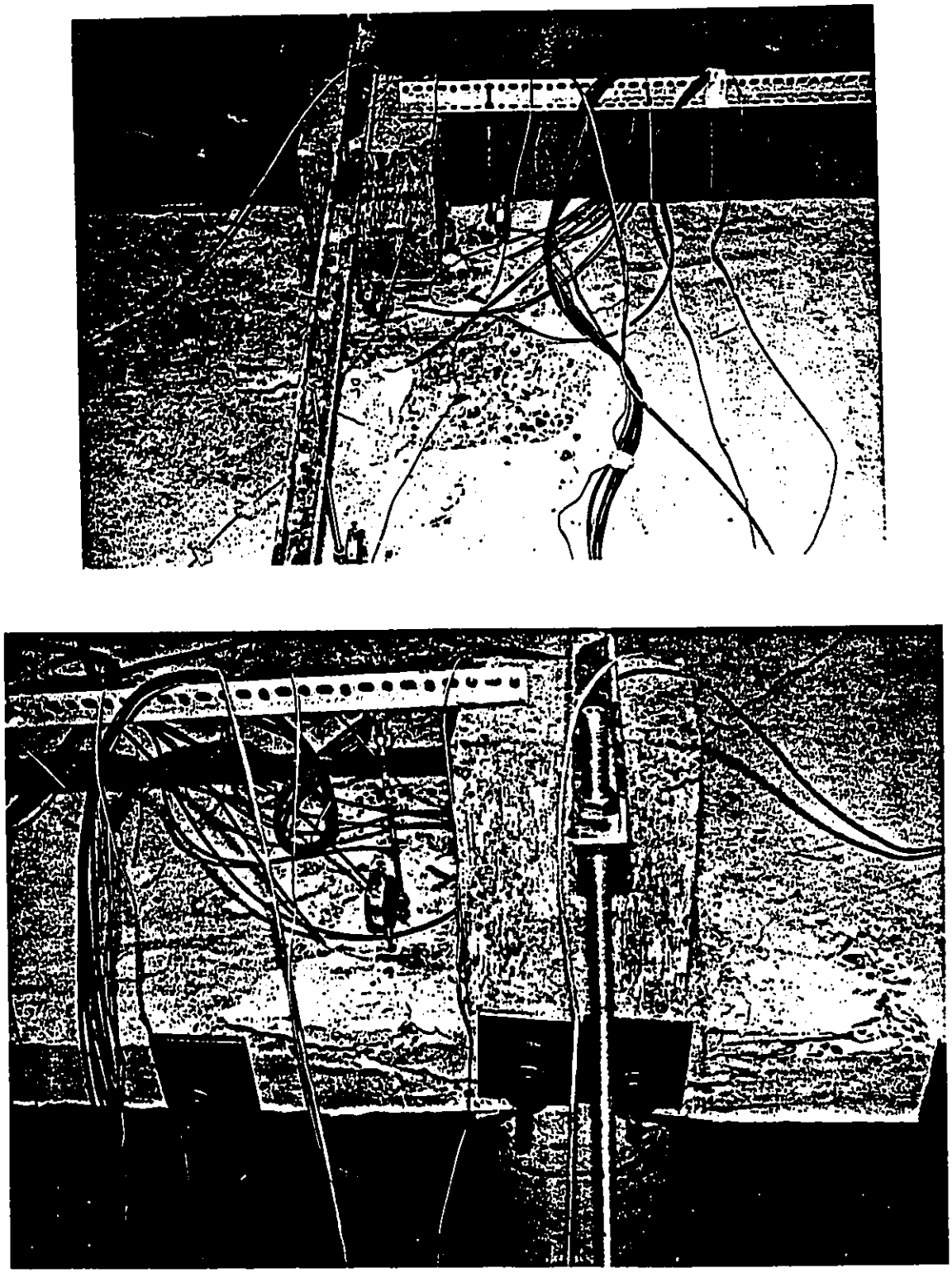

Fig. 4-4 : Photographs of cracking after punching shear failure of south-edge column

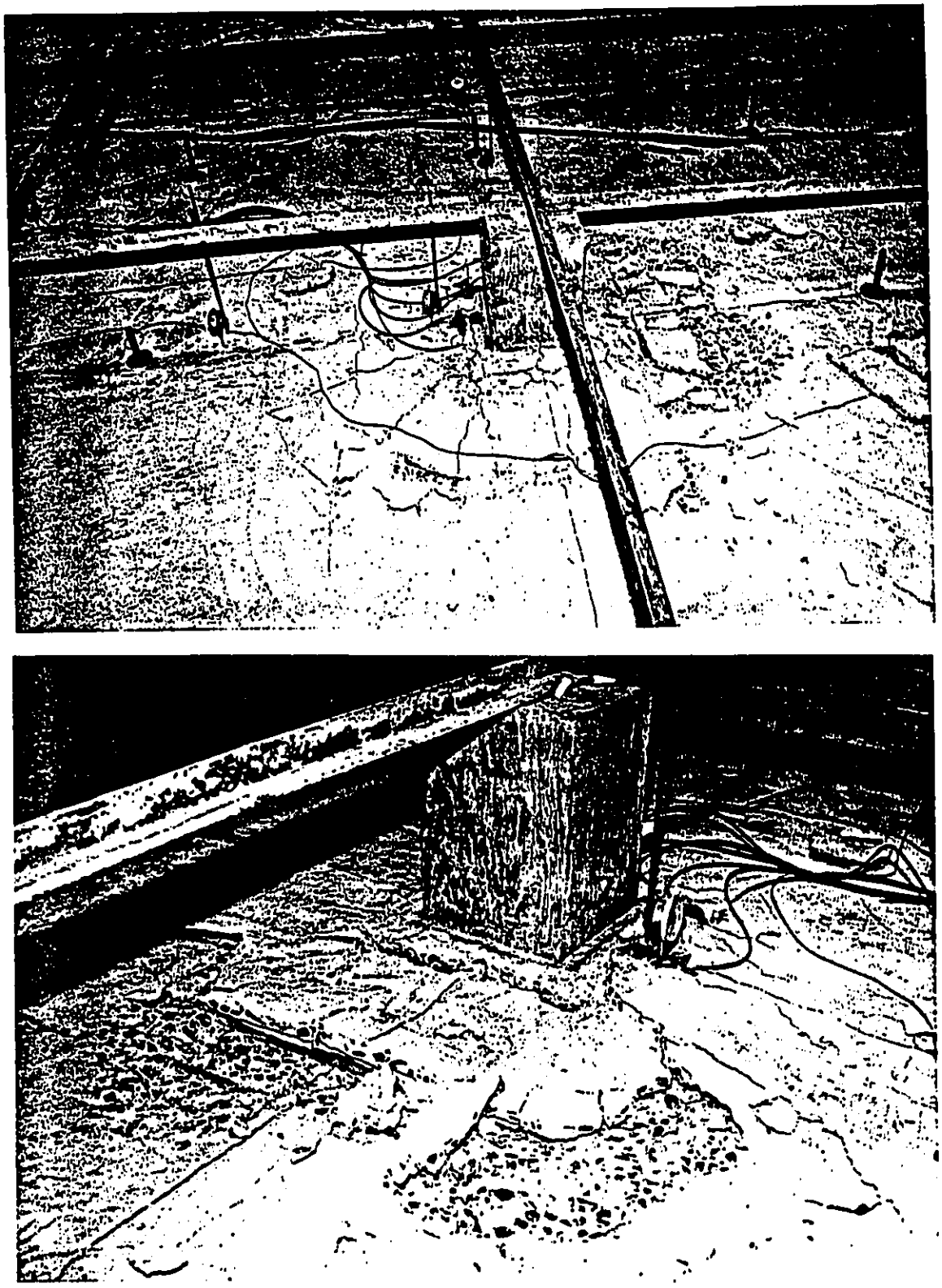

Fig. 4-5 : Photographs of cracking around internal column after punching shear failure

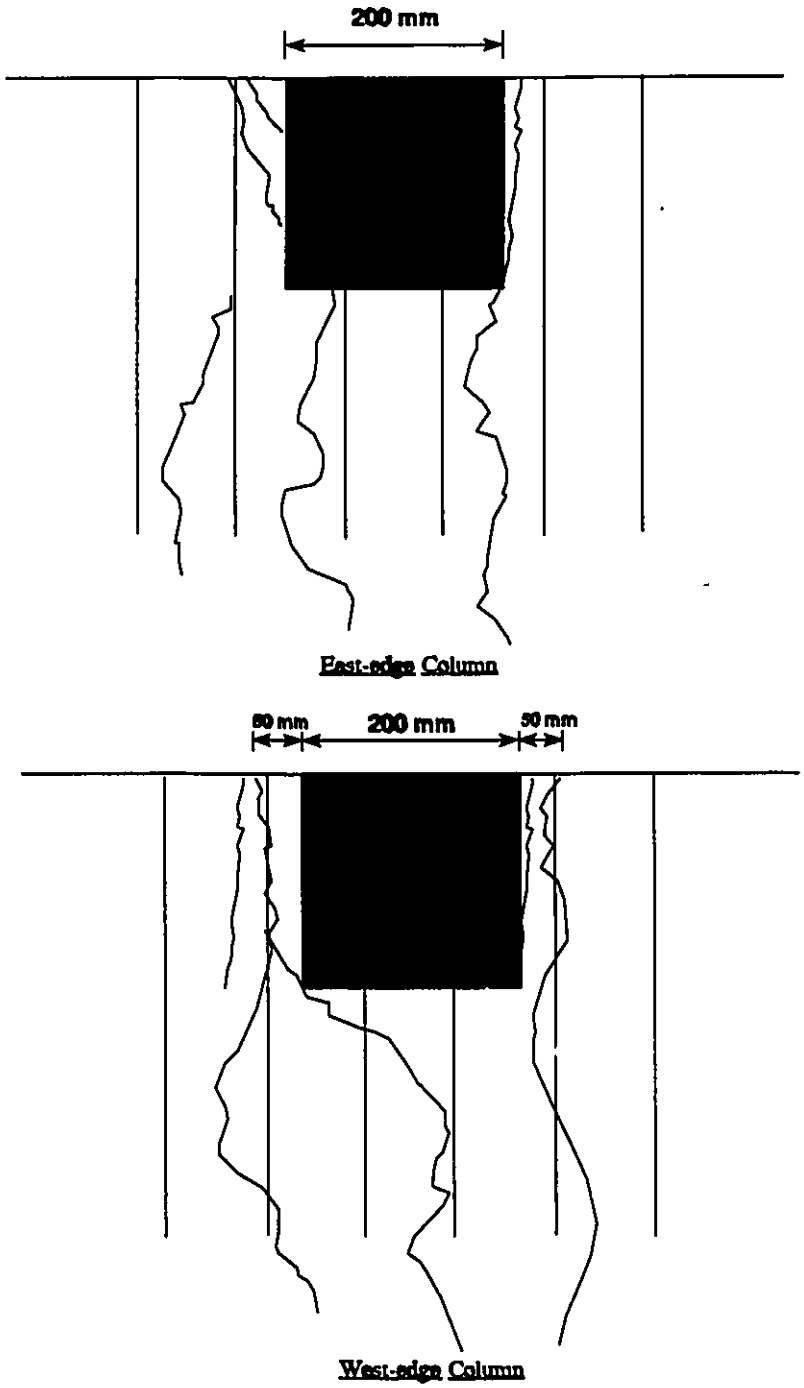

Fig. 4-6 : Crack pattern at failure around the edge columns located in the banded-tendon direction

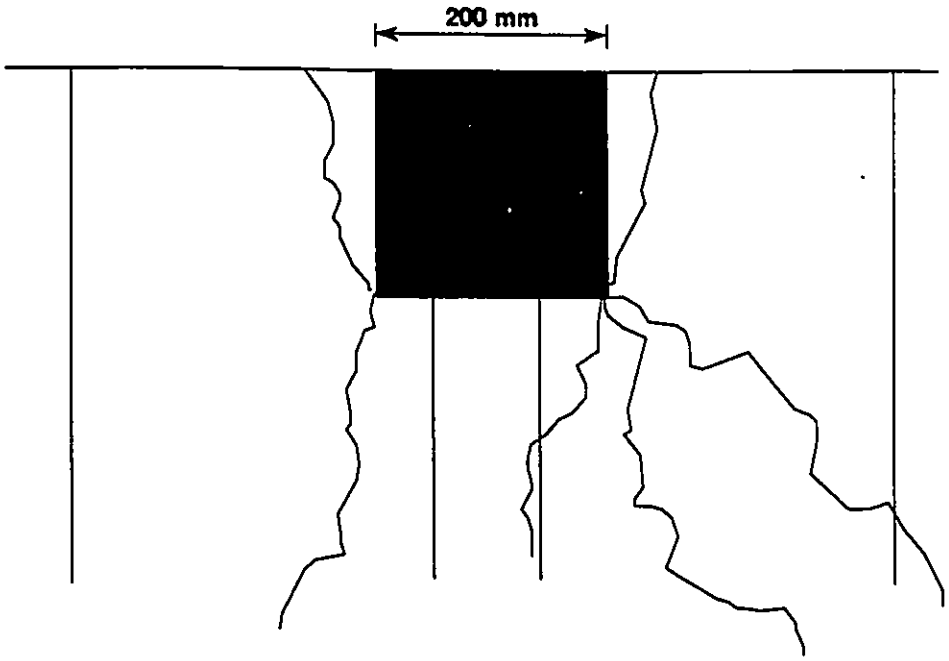

Fig. 4-7 : Crack pattern around north-edge column immediately before the failure in south-edge column

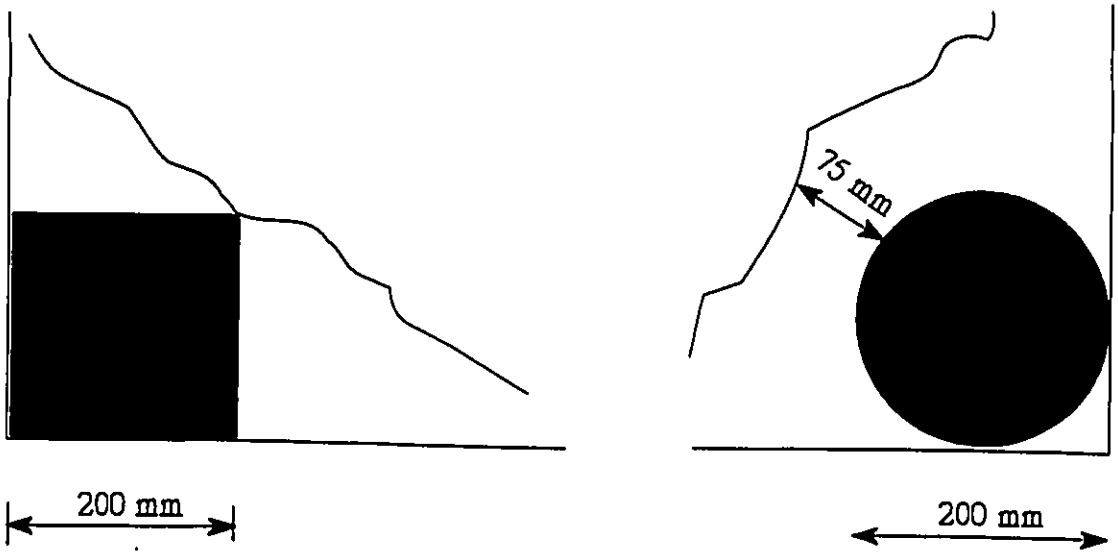

Fig. 4-8 : Typical crack pattern around corner column

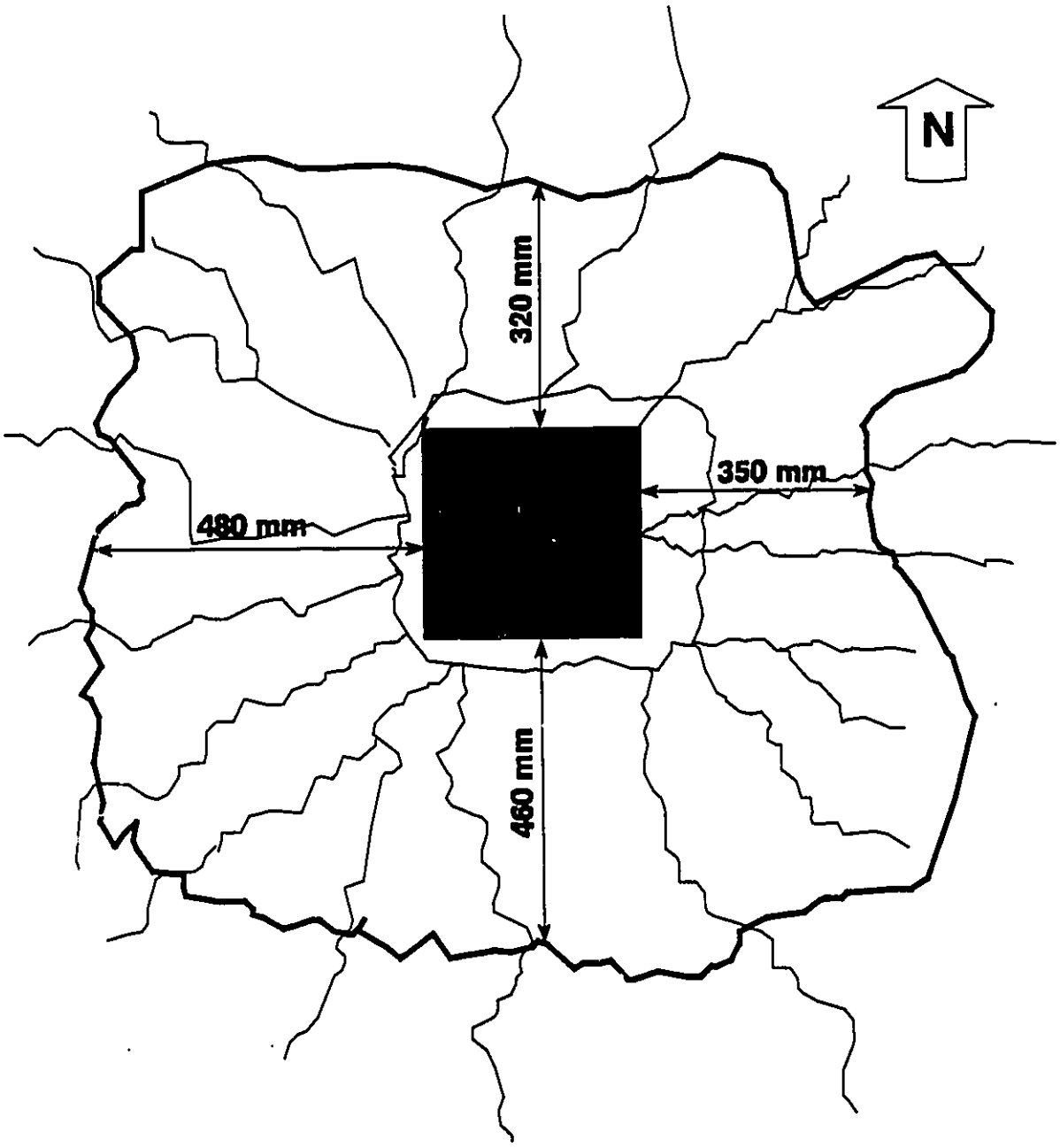

Fig. 4-9 : Crack pattern after failure around the interior column

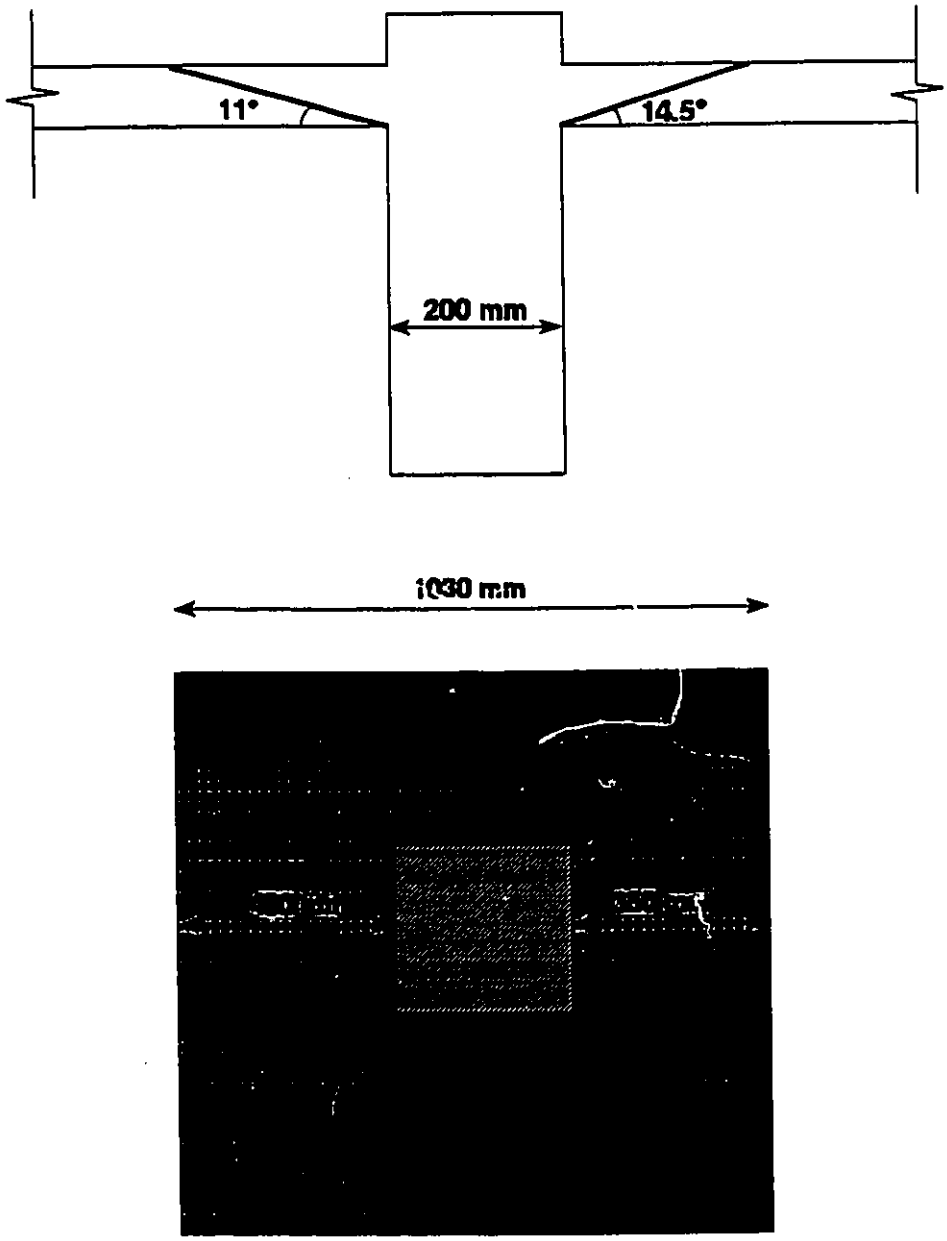

Fig. 4-10 : Size of shear cone at punching shear failure for the internal column (test 5)

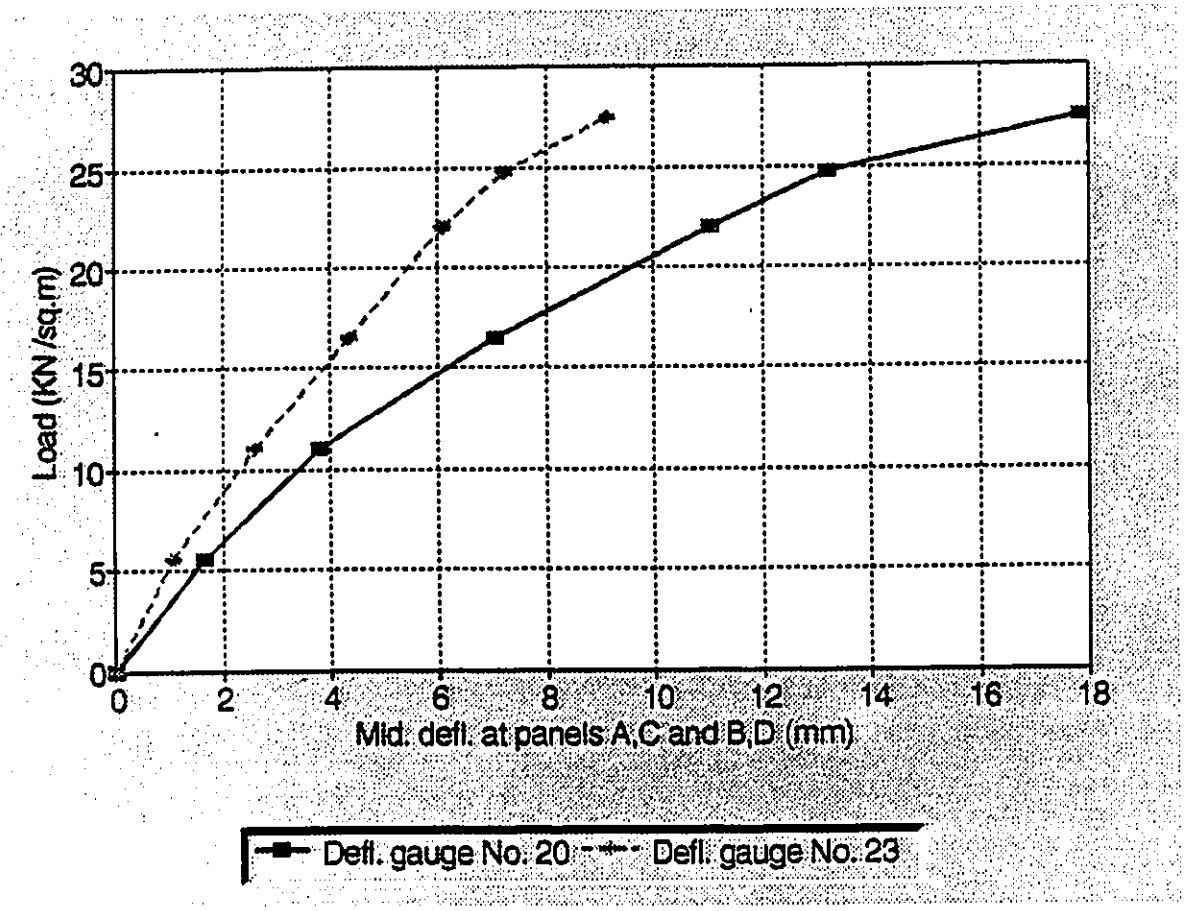

Fig. 4-11 : Comparison of load-deflection curves at the interface of panels A and C as well as panels B and D

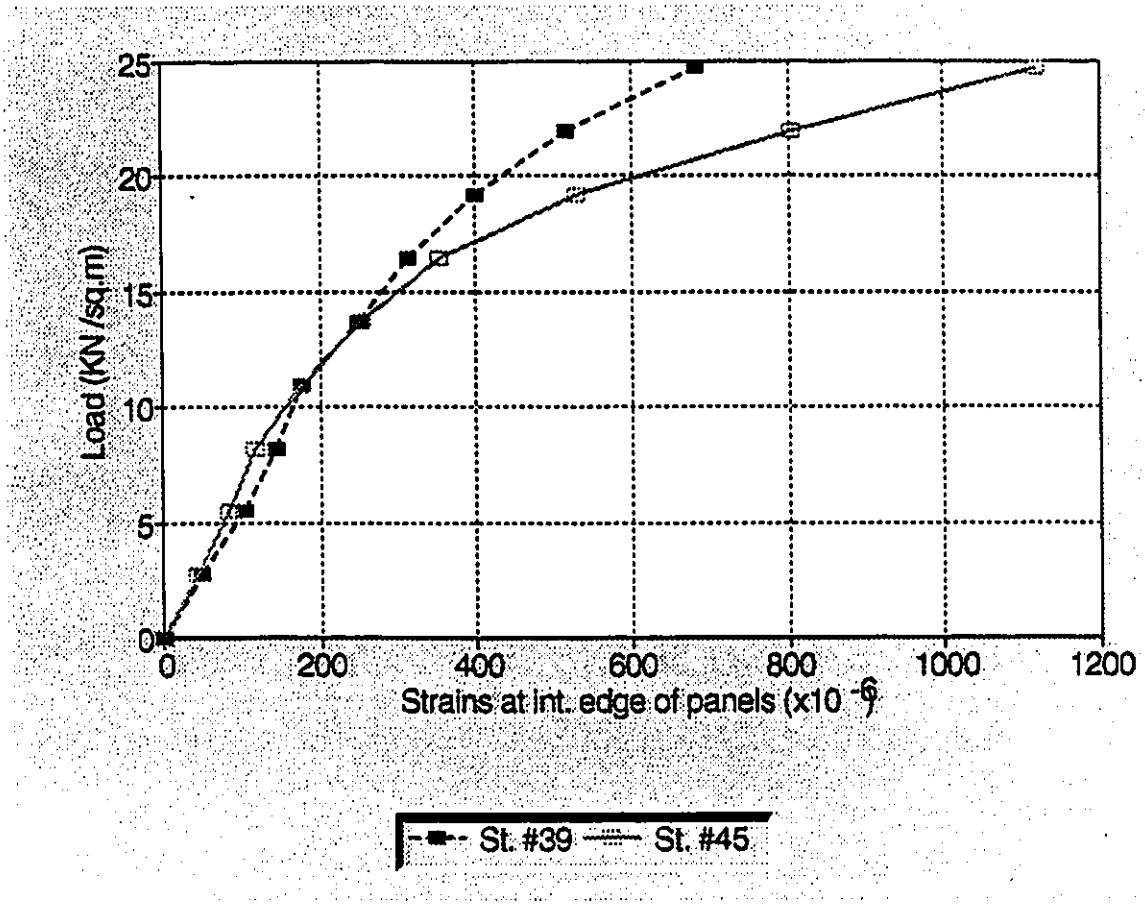

Fig. 4-12 : Comparison of load-strain curves at the interface of panels A and C as well as panels B and D

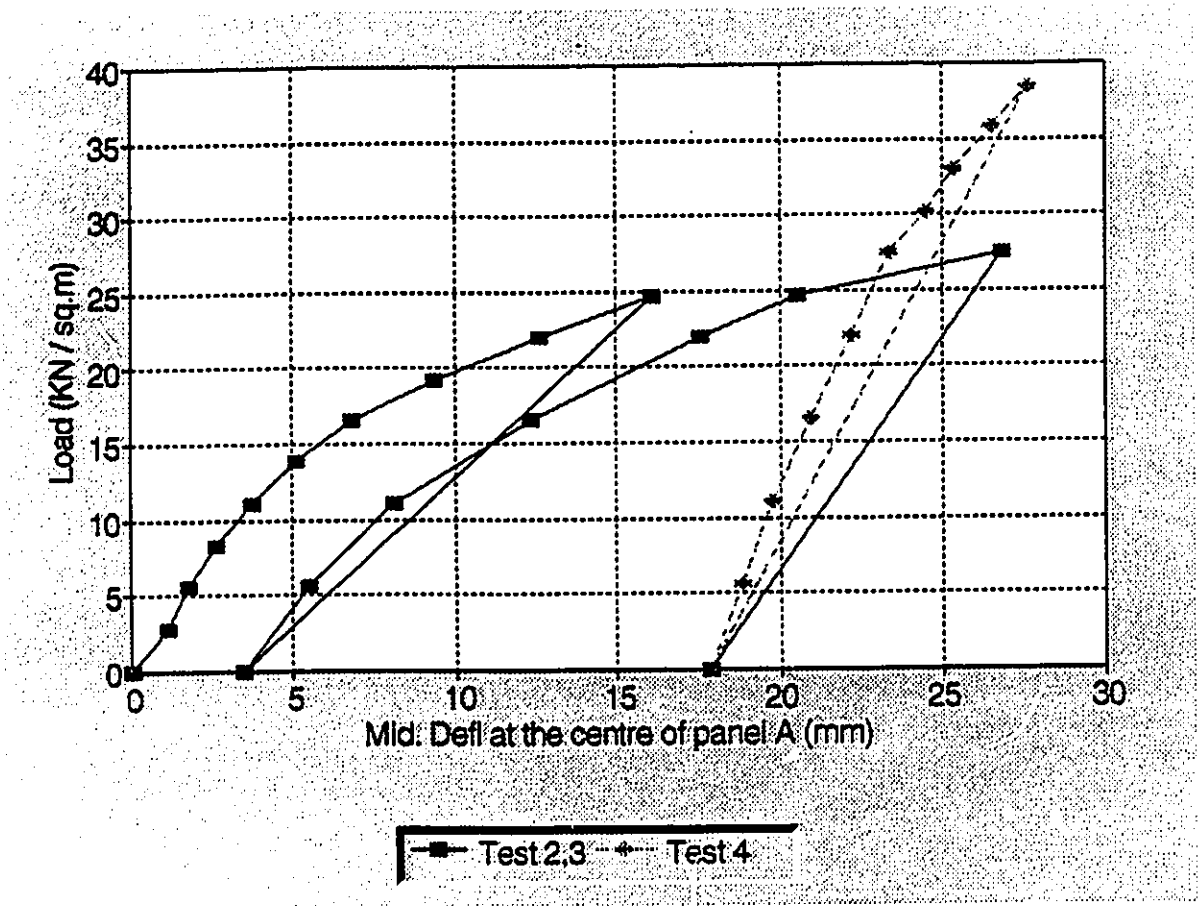

Fig. 4-13 : Comparison of load-deflection curves at the centre of panel A with and without shoring

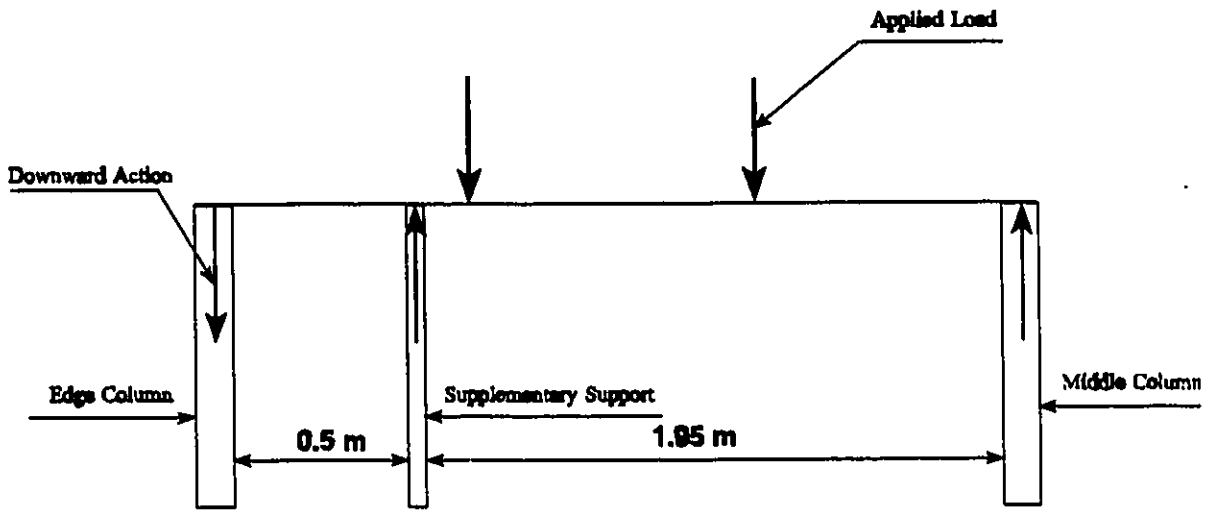

Fig. 4-14 : The elastic frame model of the slab with shoring

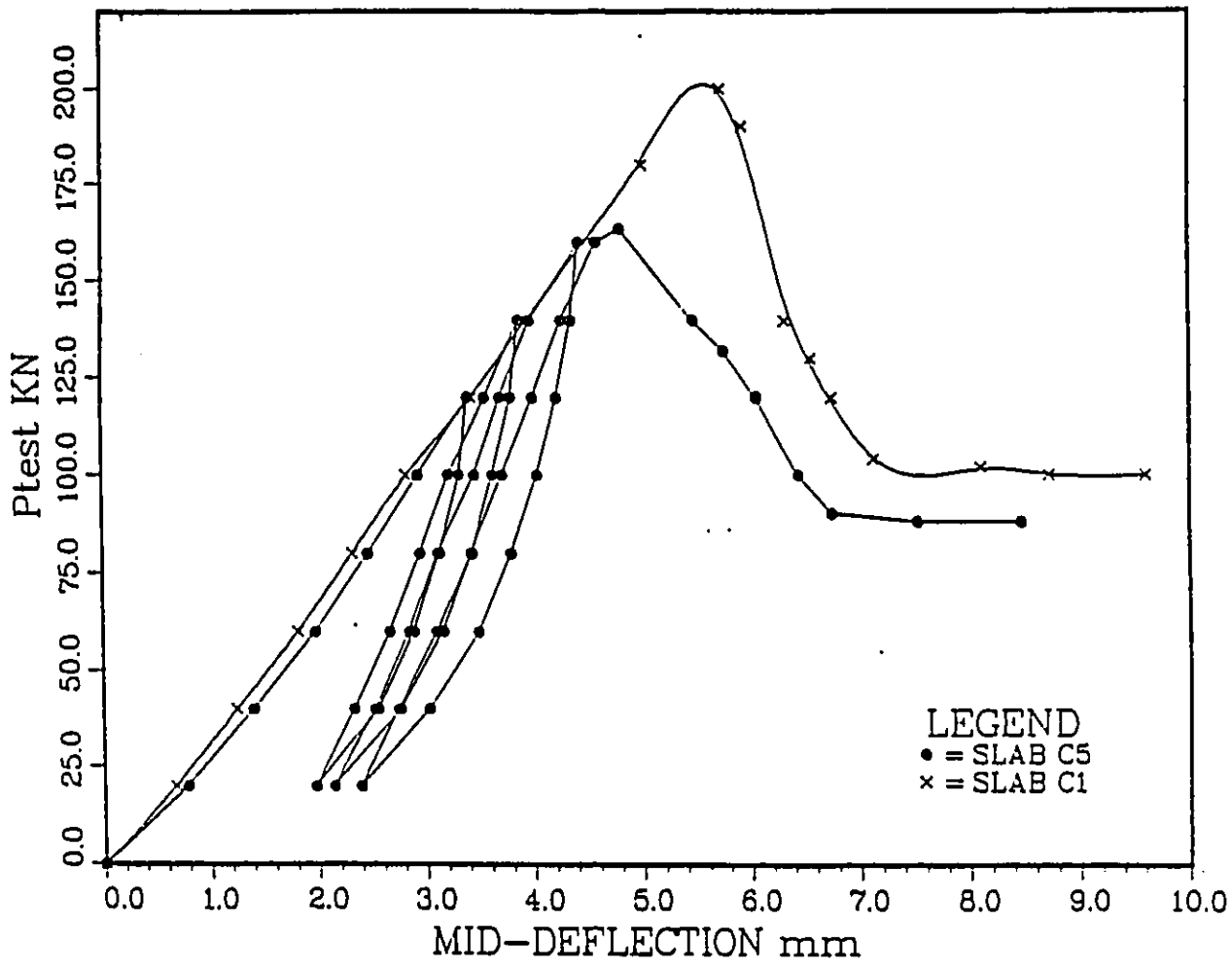

Fig. 4-15 : Effect of cyclic loading on punching shear capacity (Grira 1990)

CHAPTER #5

COMPARISON WITH CODE METHODS

5.1 Introduction :

With the increasing use of flat-slab construction during the past decades, many research programs have been undertaken to investigate the overall performances and ultimate strengths of flat slab structures. With regard to the ability of slab systems to redistribute bending moments and behave in a ductile manner, attention has been given to the strength of concrete flat slabs in punching shear. As discussed in Chapter # 2 the slab-column junction is a location of peak bending moment as well as peak shear force, and a weakness in resisting shear may result to a complete and sudden collapse of the connection. Even though a great number of small-scale or full scale tests performed on flat slab structures have been reported, the available data on punching shear behaviour of the concrete slabs is still meagre. Some researchers have tried to develop physical models, based on observations from the tests, to provide a realistic conceptual

picture of the mechanism of failure. However, all proposed methods are based on certain assumptions which makes their general application difficult.

The code provisions of ACI-ASCE 423, BS 8110, CSA or CEB-FIP (Comité Euro-International du Béton and Federation International de la Precontrainte) codes are similar in that the punching shear strength of a concrete slab is checked by considering a control surface around the loaded area (column section) at a distance equal to a multiple of the effective slab depth, or a fraction of it, as the critical punching section. The mean shear stress acting over this control surface is usually related to the strength of the concrete in tension. However, the value assigned as a limit for the shear stress has little physical meaning as the distribution of shear stress in the vicinity of a slab-column connection is a complex phenomenon. The existing design procedures and code provisions are based primarily on the empirically derived equations. These equations do not necessarily model the mechanism of failure or the general principles governing the true behaviour of flat slabs. They have been chosen primarily for their simplicity in use and the wide range of conditions over which they produce acceptable results.

In the first part of this Chapter, the shear provisions for prestressed concrete slabs proposed by North American and European codes are critically reviewed. The remainder deals with the comparison of different code procedures with respect to previous experimental results and those measured in the present test program.

5.2 Review of Design Specifications

5.2.1 General :

The shear failure of slabs around a concentrated load or reaction can occur either by a failure plane across the entire slab width (this is so-called wide beam shear failure) or by a diagonal cracking along the surface of a truncated cone or pyramid around the concentrated load or reaction, Fig. 5-1. Such localized failures are typical punching shear failures around interior, edge and corner columns in which the ultimate load capacity of the slab is reached after the formation and propagation of diagonal tension cracks around the periphery of the loaded area. Formation of diagonal cracks in slabs takes place in approximately the same manner as in beams. The inclined cracks develop at approximately 60 percent of the ultimate strength and extend rapidly to near the neutral axis. With increasing load, the cracks penetrate gradually and at a slower rate into the compression zone. In many cases the ends of the internal diagonal cracks are very close to the compression surface of the slab near the section of maximum moment. Close to ultimate, the cracks progress to the tension surface of the slab and along the tensile reinforcement. Final failure occurs when the loaded area punches through the slab, pushing up a plug of concrete having the shape of a cut-off cone or pyramid. If a slab is capable of resisting loads in excess of those causing the formation of the internal diagonal tension crack, then the final collapse may be caused by crushing of concrete in compression which is called shear-compression failure. It is accepted by nearly all countries that punching shear failure of a slab without shear reinforcement occurs when the tension in the concrete reaches its limit.

Existing proposals provided by the various code recommendations are similar in treating the shear behaviour of post-tensioned flat slabs as a series of wide beam strips spanning in two directions. In principle, nominal shear stresses are expressed with regard to slab depths and lengths of critical perimeters around column heads in that an equation of the form :

$$v_u = \frac{V_u}{b_o d} \tag{5-1}$$

Where b_o is a critical perimeter and d is a function of the slab thickness.

The basis for the equation is the assumption that there is a direct shear stress, in terms of force/area. It should be noted that Eq. (5-1) is originally an expression of shear stress intended as a measure of diagonal cracking in beams. It was introduced by Mörsch in Germany in 1906 who believed that, if a concrete section is subjected to a pure shear, then a tensile stress of equivalent magnitude must occur on a 45-degree plane. Design specifications for calculating the ultimate punching shear stress of flat slabs have related the measure of diagonal tension to the parameters that differ from one code to another. A comparison of experimental and analytical results, which have been reported during the past decades enables the parameters affecting the load capacity of a flat slab at punching shear to be identified. These parameters, based on their order of importance, are as follows : mean value of the compressive strength of concrete, axial compressive force (due to prestressing or self-generation), ratio of the column cross-section (loaded area) to the effective depth of the slab $\frac{c}{d}$ and distribution and amount of the flexural bonded reinforcement. In general, empirical methods proposed by the various codes are based on experiments which took into account the effects of the previously mentioned parameters. The results obtained from experiments are considered as sufficient supporting evidence for the

derivation of a design equation. However, the equations are limited by the parameters investigated experimentally, and extensions of the proposed equations to all practical purposes could be of limited validity.

5.2.2 Codes Provisions For Prestressed Slabs :

The ACI standard of 1989, ACI 318-89, allows the calculation of nominal shear capacity in a flat slab for a wide-beam shear failure, beam action, using the shear provisions recommended for one-way beam :

$$V_c = \left(0.05\sqrt{f_c'} + 4.8\frac{V_u d}{M_u}\right) b_w d \qquad SI \qquad (5\text{-}2)$$

Where b_w is the length of the shear failure plane and d is the distance from extreme compression fibre to the centroid of prestressed reinforcement or $0.8d$, whichever is greater. It is emphasised by the ACI code that V_c need not be taken less than $0.17\sqrt{f_c'} b_w d$ nor greater than $0.41\sqrt{f_c'} b_w d$ or $(0.29\sqrt{f_c'} + 0.3 f_{pc}) b_w d$.

The ACI code recommends that the punching shear strength around interior columns in two-way prestressed concrete slabs, to be conservatively predicted by :

$$V_c=(\beta_p\sqrt{f_c'}+0.3f_{pc})b_o d+V_p \qquad SI \tag{5-3}$$

Where β_p is the smaller of **0.29** or $\frac{\alpha_s d}{b_o}+0.13$

α_s is **3.33** for interior columns, **2.50** for edge columns and **1.67** for corner columns

b_o is the perimeter of pseudo-critical section located at a distance $\frac{d}{2}$ from the periphery of the concentrated load.

f_{pc} is the average value of prestress, $\frac{P}{A}$, for the two directions. f_{pc} in each direction shall not be less than **0.86** ***MPa*** , nor be taken greater than **3.45** ***MPa*** . If f_{pc} is less than **0.86** ***MPa*** the effect of the prestress on the nominal shear capacity of the slab is conservatively ignored and Eqs. (5-5) through (5-7) derived for ordinary reinforced concrete slabs should be applied.

f_c' should not be taken greater than **34.5** ***MPa***

Design values for f_c' and f_{pc} are limited due to limited test data for higher values. When computing f_{pc} ; loss of prestress due to the restraint of the slab by frames, shearwalls or other structural elements must be taken into account. V_p is the vertical component of all effective prestress forces crossing the critical section. V_p can be calculated from the concave downward portion of the tendon profile, near the column lines. It can be seen from Fig. 5-2 that the radial forces, r , acting on the tendon can be determined from the parabolic geometry of the tendon.

Hence, the contribution of one tendon to V_p is :

$$V_p = \frac{2Ph_2}{(\beta L)^2}(c_1 + d) \qquad (5\text{-}4)$$

The term V_p is very sensitive to the actual tendon profile, and small changes in tendon profile considerably affect the value of V_p .

The ACI code suggests that for exterior columns where the distance of the outside face of the column to the edges of the slab is less than four times the slab thickness, the prestressing force is not fully effective around the perimeter of the critical section, and therefore the nominal shear capacity should conservatively be taken the same as for a non-prestressed slab. For ordinary slabs, V_c shall be the smallest of :

$$V_c = 0.33\sqrt{f_c'}\, b_o d \qquad SI \qquad (5\text{-}5)$$

$$V_c = \left(0.17 + \frac{4}{\beta_c}\right)\sqrt{f_c'}\, b_o d \qquad SI \qquad (5\text{-}6)$$

$$V_c = \left(\frac{\alpha_s d}{b_o} + 0.17\right)\sqrt{f_c'}\, b_o d \qquad SI \qquad (5\text{-}7)$$

The latter two equations were developed to account for the effects of ratio of the largest overall dimension of the loaded area to the largest overall dimension of the loaded area measured perpendicular thereto, β_c , as well as ratio of the column size to slab thickness, $\frac{c}{d}$. It has been demonstrated by experimental research that nominal shear stress provided by concrete decreases

as the ratio of column size to slab thickness increases. Eq. (5-7) is related to a diagonal tension failure of the concrete initiating at the critical section. Eq. (5-6) corresponds to a punching shear failure of the concrete compression zone around the perimeter of loaded area.

Unbalanced moment in slab-column connections, such as edge columns or corner columns contributes to the shear stresses experienced by the slab. It has been found that punching is more critical when a slab-column connection is subjected to a transfer of moment as well as a shear loading. The following briefly describes the methods proposed by each code.

The ACI code assumes that part of the unbalanced moment, $\gamma_f M_{ul}$, is transferred by flexural stresses in a slab within an effective slab width between lines that are $1.5h$ outside opposite faces of the column, Fig. 5-3. The remaining part of the unbalanced moment, $\gamma_v M_{ul}$, shall be considered to be transferred by eccentricity of axial force about the centroid of the critical section. As it can be seen from the equation derived for γ_v , the portion of the moment transferred by shear decreases as the width of the face of the critical section resisting the moment increases. Approximate values of 40% transferred by eccentricity of the shear about the centroid of critical section and 60% transferred by flexure across the perimeter of the critical section have been proposed by ACI code. The resulting shear stress is assumed to vary linearly about the centroid of the critical section. The final shear stress can be written by summing the uniform shear stress due to the axial force, V_u , and the linearly varying shear stress due to the moment. Therefore :

$$v_u = \frac{V_u}{A} + \frac{\gamma_{v1} M_{u1} e_1}{J_1} + \frac{\gamma_{v2} M_{u2} e_2}{J_2} \qquad (5\text{-}8)$$

Where : J = Polar moment of inertia of the critical section about its centroidal axis

The terms in this equation are defined for rectangular columns as follows :

(a) Interior Column :

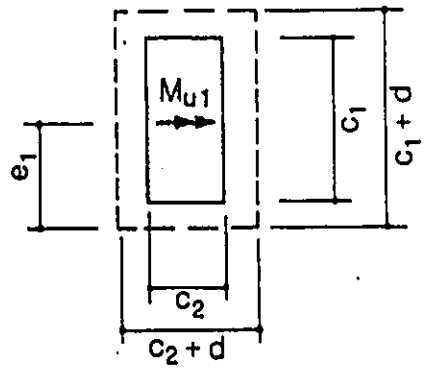

$$A = 2d(c_1 + c_2 + 2d) \quad , \quad e_1 = \frac{c_1 + d}{2}$$

$$J_1 = \frac{(c_1 + d)d^3}{6} + \frac{(c_1 + d)^3 d}{6} + \frac{d(c_2 + d)(c_1 + d)^2}{2}$$

$$\gamma_v = 1 - \frac{1}{1 + \frac{2}{3}\sqrt{\frac{c_1 + d}{c_2 + d}}}$$

(b) Edge Column :

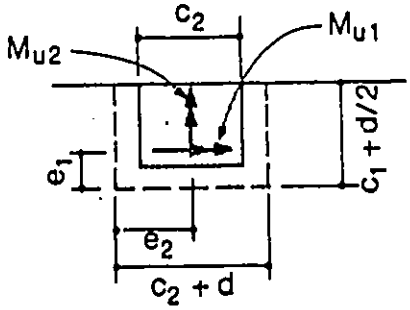

$$A = d(2c_1 + c_2 + 2d) \quad , \quad e_1 = \frac{(c_1 + \frac{d}{2})^2}{(2c_1 + c_2 + 2d)} \quad , \quad e_2 = \frac{c_2 + d}{2}$$

$$J_1 = \frac{[(c_1 + \frac{d}{2})d^3 + (c_1 + \frac{d}{2})^3 d]}{6} + (c_2 + d)de_1^2 + 2(c_1 + \frac{d}{2})d[(\frac{c_1 + \frac{d}{2}}{2}) - e_1]^2$$

$$J_2 = \frac{[(c_2 + d)d^3 + (c_2 + d)^3 d]}{12} + 2(c_1 + \frac{d}{2})de_2^2$$

$$\gamma_{v1}=1-\frac{1}{1+\frac{2}{3}\sqrt{\frac{c_1+\frac{d}{2}}{c_2+d}}} \quad , \quad \gamma_{v2}=1-\frac{1}{1+\frac{2}{3}\sqrt{\frac{c_2+d}{c_1+\frac{d}{2}}}}$$

The shear resistance of a concrete flat slab in the vicinity of concentrated loads or reactions in CSA A23.3-84 is treated in a similar procedure to the ACI code. The effects of both beam action and two-way action are considered separately. For beam action the following equation derived for prestressed members, with an effective prestress force not less than 40% of the tensile strength of the flexural reinforcement, is recommended :

$$V_c=\left(0.06\lambda\sqrt{f'_c}+6\frac{V_u d_{ps}}{M_u}\right)b_w d \qquad SI \tag{5-9}$$

Two-way action of prestressed slabs with a critical section perpendicular to the plane of the slab and located at a distance $\frac{d}{2}$ from the concentrated load or reaction area should be designed according to :

$$V_c=0.4\lambda\sqrt{f'_c}\left(\sqrt{1+\frac{f_{pc}}{0.4\lambda\sqrt{f'_c}}}\right)b_o d+V_p \qquad SI \tag{5-10}$$

The derivation of Eq. (5-10) is based on constructing the Mohr's circle for an element located at the level of neutral axis and subjected to shear forces together with a compressive force resulted from prestressing. The limitations applied for the ACI code equations are also applicable for the CSA recommendations. Transfer of moment in slab-column connections is exactly the same as the ACI code procedures.

In England a completely different approach to the design problem of shear in slabs has been practiced. The punching shear resistance of a prestressed concrete slab is treated by two different methods. In the first method the cross-sectional area of the tendons can be replaced by an equivalent area of ordinary reinforcing steel.

$$A_s = A_{ps}\frac{f_{pu}}{410} \tag{5-11}$$

Then the equivalent reinforcement area is substituted into the relevant expression for the shear strength of an ordinary reinforced concrete slab. In BS 8110-85, design concrete shear stress derived based on experimental observations, is defined as :

$$v_c = 0.79\left(\frac{100A_s}{b_o d}\right)^{\frac{1}{3}}\left(\frac{400}{d}\right)^{\frac{1}{4}}\left(\frac{f_{cu}}{25}\right)^{\frac{1}{3}} \qquad SI \tag{5-12}$$

$\frac{100A_s}{b_o d}$ is the reinforcement ratio and should not be taken as greater than 3.0 .

d is the distance from the extreme compression fibre to the centroid of the steel area $(A_{ps}+A_s)$ in the tension zone.

$\frac{400}{d}$ takes into account of size effect and should not be taken as less than 1.0

f_{cu} should not be taken as greater than 40.0 *MPa*

The maximum design shear stress at the column face calculated from the above equation is limited to maximum $0.8\sqrt{f_c'}$ or 5.0 *MPa* . This is because where large shears are carried, it is possible for the diagonal compressive stresses to cause crushing of the concrete. The second method which is based on more logic is to calculate the punching resistance of a prestressed slab as for an ordinary reinforced concrete slab, Eq. (5-12), using the actual area of tendons, and to

add the load required to compensate the effect of the prestress in terms of the stress at the extreme fibres set into zero by the applied loading. This method was first introduced by Regan for one-way bonded prestressed slabs, and extended to two-way slabs. For the case of unbonded tendons, the BS 8110-85 code recommends that the calculated punching resistance be reduced by about 10%.

The nominal shear stress computed from Eq. (5-12) is applied to the control perimeter taken as rectangular in shape, $1.5d$ from the column or loaded area. Where it is desired to check perimeters closer to the loaded area than $1.5d$, v_c can be increased by a factor $\frac{1.5d}{a_v}$, where a_v is the distance from the edge of the loaded area to the perimeter considered.

In BS 8110-85, the allowance for moment transfer is defined by the following equations for internal column connections and for edge columns where bending is about an axis perpendicular to the free edge :

For an Internal Column : $$V_{eff} = V_t\left(1 + \frac{1.5M_t}{V_t \cdot x}\right) \qquad (5\text{-}13)$$

For an Edge Column : $$V_{eff} = V_t\left(1.25 + \frac{1.5M_t}{V_t \cdot x}\right) \qquad (5\text{-}14)$$

For simplicity, the recommended approximate values of the design effective shear forces when moments are transmitted by the connections are : $V_{eff} = 1.15\,V_t$ for internal columns; $V_{eff} = 1.4\,V_t$ for the edge columns where bending axis is perpendicular to the free edge and $V_{eff} = 1.25\,V_t$ for corner columns and edge columns where bending axis is parallel to the free edge. Fig. 5-4 and

5-5 show the application of the above recommendations.

The CEB-FIP-90 code defines the effect of prestress on the shear behaviour of slabs as an external action-effect. The shear resistance of prestressed slabs is taken as the superposition of the load corresponding to decompression of the tension face of the slab in the vicinity of the connection and the load resisted as an ordinary reinforced concrete slab. The shear resistance of a reinforced concrete slab, expressed as a shear on a control perimeter of a distance $2d$ from the periphery of a column or concentrated load is recommended by CEB-FIP-90 code in a form of :

$$v_c = 0.12\,\xi(100\rho . f_{ck})^{\frac{1}{3}} \quad SI \quad Where \quad \xi = 1 + \sqrt{\frac{200}{d}} \qquad (5\text{-}15)$$

The reinforcement ratio may be calculated as the average for two orthogonal directions. In each direction the effective width in the calculation of ρ is equal to the side dimension of the column plus $3d$ to the either side of it. Bonded prestressing tendons can be included in the calculation of ρ but unbonded tendons should be excluded. The effective depth of the slab is assumed constant and may normally be taken as that to the mean plane of an orthogonal arrangement of tension reinforcement, but f_{ck} should be limited to less than $50.0\ MPa$.

If the distribution of the load is non-symmetrical due to the transfer of an unbalanced moment from the slab to a column, the maximum shear produced at the control perimeter is :

$$v_u = \frac{P_u}{b_o d} + \frac{0.6 M_u}{W d} \qquad (5\text{-}16)$$

W is a property of the control perimeter defined as : $W = \int e_1 dl$. dl is an infinitesimal length of the control perimeter. For a rectangular column with regard to Fig. 5-6, the property W corresponding to a distribution of shear around an internal column can be calculated as :

$$W = \left[\frac{c_1^2}{2} + c_1 c_2 + 4 c_2 d + 16 d^2 + 2 \pi d c_1 \right] \qquad (5\text{-}17)$$

For edge column connections the applied shear stress at the control perimeter follows the same procedure, except W is calculated for the critical section shown in Fig. 5-7a. To avoid unnecessary and time consuming calculations, the CEB code recommends that for any eccentricity of the load perpendicular to the slab edge while there is no eccentricity parallel to the edge, the applied shear stress may be computed on the reduced control perimeter shown in Fig. 5-7b, therefore : $v_u = \frac{P_u}{b_o^* d}$. b_o^* is the reduced control perimeter. Where there is a moment acting in the direction parallel to the slab-edge, it should be taken to produce an additional shear stress. Therefore, the total shear stress applied on the control perimeter would be :

$$v_u = \frac{P_u}{b_o^* d} + \frac{0.6 M_u}{W d}$$

5.3 Discussion of Code Provisions

5.3.1 Concrete Strength :

Regardless of the derivation of each equation, it should be observed that all the proposed equations are closely connected with the compressive strength of concrete while the other important parameters are treated rather differently in each code. The experimental results on the

variation of the behaviour of flat slabs with concrete strength have demonstrated. Fig. 5-8, that the trends of data are reasonably well presented by :

$$v_u \propto \sqrt[3]{f_c'} \quad or \quad v_u \propto \sqrt{f_c'} \tag{5-18}$$

A cube root relationship of shear stress to concrete strength has been adopted by European codes while the North American codes prefer the square root of the concrete strength. The current ACI 318-89 and CSA A23.3-84 code equations are basically based on the principle of limiting tensile stress. The shear capacity is predicted when the principal tensile stress at a distance $\frac{d}{2}$ from the column is limited to a value, which is a function of square root of the cylinder crushing concrete strength, $\sqrt{f_c'}$.

5.3.2 Control Perimeter :

There are strong arguments over for the location of the critical section among researchers. The limiting shear stress is particularly sensitive to the location assumed for the critical section. In the ACI and CSA codes the critical section of punching shear is assumed to be at a distance of $\frac{d}{2}$ from a column face, and then the perimeter of critical section, b_o is equal to the average perimeter of the bases of punching truncated cone or pyramid which has height d and sides sloping at 45°, as shown in Fig. 5-9. The critical section is assumed to have a rectangular shape. If the supporting column has a circular cross-section, the equivalent square section should be used in the design, as illustrated in Fig. 5-10. CSA assumes a circular shear perimeter when the cross-section of the loaded area is a circle. ACI code emphasises that the critical section for shear in slabs subjected to bending in both directions would be best to be taken at the junction of the slab

and the column. Based on experimental research, the code concludes that the shear stress acting on this section is a function of the ratio of column size to slab depth. The ACI code recommends that by assuming the critical section located at a distance $\frac{d}{2}$ from the periphery of the column, the shear strength can be considered independent of the ratio of column size to slab depth.

The assumption of the British Standard, BS 8110-85, and CEB-FIP-90 differs considerably with respect to the definition of the control perimeter. The BS code recommends an area of slab bounded by two parallel lines $1.5d$ apart as the definition of the shear perimeter around a column. The shape of the column has no effect on the shear perimeter. Whether the column is rectangular, circular or regular polygon shaped, the shear perimeter is always taken by straight lines drawn parallel to and at a distance $1.5d$ from the edges of the loaded area, Fig. 5-11. The control perimeter adopted by CEB code is taken further away from the loaded area. The code defines the critical perimeter at a distance $2d$ from the periphery of loaded area or reaction force. In this code the shape of the control perimeter is a circle for circular loaded areas and a rectangle with round corners for square loaded areas, Fig. 5-12.

Considering the critical section to be in the immediate vicinity of the column was first introduced by Moe in 1961, and supported by other researchers. They believed that the mechanism initiating failure takes place at the junction of the slab and the column which experiences maximum shear and significant flexural stresses due to the moments produced at the slab-column connection. Other researchers believe that it doesn't make any difference where the critical section is taken, provided the allowable strength is adjusted accordingly. They consider

punching shear failure as local flexural failures which begins by local yielding of reinforcement. But the fact is that in many experimental programs it has been demonstrated that the perimeter of failure is formed relatively far away from the column. The projected length of shear cracks sometimes appears at distances even greater than $5d$ from the column face. Assuming the location of critical section at a distance $\frac{d}{2}$ from the column adopted by the North American codes seems to be too close to the column and may cause an overestimation of the slab-column connection strength for large loaded areas. The location of shear perimeter, as far as the real failure is concerned, would be best taken between $1.5d$ and $2.5d$ from the periphery of the column.

It is noteworthy that the control perimeter in BS 8110-85 is defined as a rectangle regardless of the shape of the column. For a circular column this is a square of side equal to the diameter of the column plus $3d$. Thus, the critical sections of a square column with side length equal to the diameter of a circular column are identical. It means the shear resistances of the two columns computed based on the code expression would be similar. This conclusion has not been confirmed by researchers. It is believed that for the same area, slabs loaded through circular areas are capable to carry more load than those loaded through square areas. But in this case, it is hard to believe that while the control perimeter area of circular columns are 27% less than square columns, they have similar shear failure loads. In the present test program the north-edge and south-edge columns were identical in all respects except the shape of the column. The circular one , south-edge, failed first indicating that the BS code approach does not apply in this case of a prestressed concrete slab.

5.3.3 Flexural Reinforcement :

It has long been recognized that the shear strength of a slab-column connection is influenced by the flexural characteristic of the connection. Tests by Burns *et al* have been clearly shown that shear strength of prestressed slabs is controlled by total tendon force and the amount and location of non-prestressed reinforcement. The ACI code strongly recommends the use of bonded reinforcement in the top of the slab directly over and adjacent to the column. The requirement is that the bonded reinforcement should be placed within a distance of 1.5 times the slab thickness from faces of the column. This helps ensure flexural continuity and ductility of the slab and controls cracking, temperature and shrinkage. Even though the ACI code necessitates the placement of minimum amount of bonded reinforcement in the negative moment regions of the slab no attempt is made to take into consideration its direct effect in the punching shear equation. The ACI code relies mostly on the tests performed by Elstner and Hognestad and by Moe. Their tests indicated no increase in shear strength due to the concentration of tensile reinforcement over the shear area. They believed that concentration of steel through the column increases the stiffness of a slab, decreases the centre-deflections, raises the load at which first yielding takes place and finally reduces the violence of failure. But these advantages of concentrating tension reinforcement in the vicinity of the column only affect the flexural behaviour of the slabs, and have little influence on the shear behaviour of flat slabs. ACI-ASCE committee 423 (1974) suggested that if non-prestressed ordinary reinforcement is not provided in accordance with ACI code recommendations, shear capacities should be limited to 0.9 of those predicted by Eq. (5-3).

The British code's first method in treating prestressed slabs is uncertain for two reasons. Firstly

the equivalent ratio of reinforcement is determined not by the intensity of prestressing force but by the ultimate strength of the tendons. Ignoring the real value of prestressing force on the slab, f_{pc} , is a great disadvantage for the BS code. Secondly the value of ρ is calculated for the width of the control perimeter very close to the column vicinity. This implies a great advantage to banded arrangement of tendons which is unlikely to be justified. Tests have shown that banded tendons do not have a significant influence on the punching shear strength of internal slab-column connections. The decompression approach appears to work well, but a difficulty arises in estimating P_o for a prototype continuous structures. Regan suggested equating m_o to the average elastic moment within $0.2L$ to $0.25L$ from the column of a flat slab (the relationship between P_o and m_o is defined in Chapter # 2). Another restriction for this method is that the effects of tendon inclination are not considered. Tendons very close to the support carry some transverse load which could be significant especially where cables are heavily concentrated towards column lines. Another limitation is that the influence of bond of the tendons is not clear. It is evident that the absence of bond results in some loss of strength, and the extent of this loss might be greater for the prototype structure which tendon anchorages are far apart, but the percentage of the loss has not been studied thoroughly. The 10% reduction of the ultimate strength for unbonded cables in BS 8110-85 is just based on one single specimen tested by Regan.

The CEB-FIP-90 code recommendation to disregard the effect of unbonded tendons in the calculation of ρ is unrealistic. There have been a number of specimens tested by Scordelis, Vanderbilt and Burns in which none of the specimens contained any form of bonded

reinforcement. All of them carried the shear load without flexural distress with final failures in punching shear. According to the CEB code none of them were capable of resisting any external load, except the load corresponding to the decompression load. In the present test program, no bonded reinforcement was provided anywhere in the slab. The slab carried a load about 10 times the design live load before the occurrence of punching shear failure in the south-edge column.

The distribution of tendons between the column strips and middle strips could be very important, since it may affect the strength and behaviour of the flat plate structures, especially for the edge and corner columns. There is no recommendation in the current ACI and CSA codes regarding tendon distribution. The neglect of the effect of prestressing force for edge and corner columns in the ACI and CSA codes gives very conservative predictions of the punching strength at these connections. It has been shown, by Gamble and Long, that there is a significant benefit in the predicted strength if the effect of the prestress, f_{pc}, can be taken into account, especially if a banded-tendon arrangement is selected for the design of prototype structure. The use of a banded-tendon arrangement to simplify construction has become popular, even though it is not acknowledged in the codes. In the European codes the definition of ρ is affected by the arrangement of tendons, as placing the tendons in a narrow band over the column line increases the value of ρ and consequently the calculated shear strength of the connection.

5.3.4 Size Effect :

It has been shown by the tests of geometrically similar slabs with different thicknesses that the relative punching strength reduces with increasing effective depth of the slab, Fig. 5-13. The

relative strength is the ratio of the ultimate shear stress of the slab calculated as $\frac{P_u}{d(\Sigma b+\pi d)}$ to the ultimate stress for a slab of the same series with d=200 mm . The introduction of size effect has been totally ignored by the North American codes. However, the experimental evidence of a size effect is strong, and European countries strongly recommend that the effect of the slab thickness on the punching shear strength should be taken into account in design. The logic of fracture mechanics, Bazant 1990, gives a strong theoretical justification of the importance of size effect.

5.4 Experimental Results

This section provides a comparison of the predicted capacities by ACI 318-89, CSA A23.3-84, BS 8110-85 and CEB-FIP-90 with the actual failure loads obtained from the present experimental programme and those from various tests in the past. The comparison is made in three different categories :

1) Internal columns without any supplementary bonded reinforcement

2) Internal columns with the addition of bonded reinforcing steel

3) Edge columns

5.4.1 Calculation of failure loads in the tested slab :

The column loads at failure were measured by the load cells placed underneath the columns. Another estimation for the reactions at the columns was made from the hydraulic pressure,

recorded from the pressure gauges attached to the pumps, times the tributary areas of the columns at the failure. The theoretical moments and reaction forces were also determined by using finite element method.

The internal slab-column connection was the main concern in this investigation. It was intended to first fail the middle column in punching shear, but failure occurred in the south-edge column. When after the failed connection had been shored the slab was reloaded to failure, the internal column failed unexpectedly at a load 10% lower than the previous test in which the column had survived the load. However, the load corresponding to the punching shear failure of the internal column would be certainly, if not slightly higher, at least the same as the load that caused punching failure in the south-edge column. Exhibiting extensive cracks together with the widened and lengthened tangential and radial cracks around the middle column accompanied by very large deflections in the slab just prior to failure in the south-edge column could be interpreted as a sign of warning before failure for the interior column. Therefore, it can be assumed that the punching shear load of internal column to be taken similar to that for the south-edge column. The following tables (Table 5-1 through 5-6) and figures (Fig. 5-15 through 5-28) demonstrate the ultimate shear load capacities predicted by the ACI, CSA, BS and CEB codes of practice.

5.5 Discussion of Codes Results

The code provisions selected for this study employ different approaches to predict the shear strength of prestressed slabs. In the following subsections, the shear strengths obtained from the test results of previous investigations and present work are discussed with the nominal allowable shear strengths predicted by using the North American and the two major European standard codes, BS 8110-85 and CEB-FIP-90.

5.5.1 Internal Columns Without Additional Bonded Reinforcement :

Tables 5-1 and 5-2 are the summary comparison of the measured and calculated shear resistance values of internal slab-column connections without providing additional non-prestressed bonded reinforcement in the vicinity of column regions. The two-way slab specimens tested by Scordelis simulated lift slab constructions. The nominal shear capacities predicted according to the ACI and CSA codes using the minimum value for d as $0.8h$ resulted in relatively higher capacities than the observed values. The fairly unconservative estimations for some of the specimens are probably due to the very low effective depth of the prestressing tendons which is untypical of most lift slab structures. The load-deflection curves for these slabs indicated that the failure was influenced by the flexural cracking that took place prior to failure in each case. In the meantime, using the actual values of the effective depths, d , in the ACI equation gave a more consistent results, indicating that in the cases which the real value of d is low, assuming $0.8h$ as an effective depth for the critical section would result to the over-prediction of shear capacities. The CSA code has the same disadvantage together with overall higher prediction of

shear strength of prestressed concrete slabs. Calculating the shear values using the resistance factor, φ_c , equal to 0.6 would result, of course, in smaller values of shear strengths. The predictions of the BS code are not excellent but reasonable and consistent. The CEB code underestimates the shear strengths. That's because the CEB code uses the same equation derived for the shear capacity of ordinary reinforced concrete slabs as for prestressed slabs, and increases this by adding the load corresponding to decompression of the tension face of the slab. But there is no clear definition for the calculation of load required to produce decompression of the slab in the code. The specimens tested by Burns in 1971 are safely predicted by all the codes. Vanderbilt's tests results are in good agreement with the ACI code predictions. The CSA code overestimates the shear strength of lightweight concrete by about 15 percent, while the CEB code underestimates by about 20 percent. The variations of the predicted capacities by the BS code for all the specimens are quite minor. Vanderbilt's slabs may have had the disadvantage of being small scale models, but, they are the only group in which the level of prestress was the main variable, while the geometric ratio and strength of the reinforcement were constant and concrete strength altered slightly. The results showed an increase in strength with increasing prestress. The BS code has no sense of increasing or decreasing the level of prestress in the specimens. According to the BS code all of them are treated similarly. The one specimen tested by Burns in 1974 is overestimated by all the codes, except the CEB code. This is because the specimen failed in a combination of flexure and shear with a primary failure in flexure. The result obtained in the present investigation was well-predicted by the ACI and the BS codes. The CSA code overestimated the shear strength by about 25 percent. Unfortunately, the CEB code predictions are very conservative with regard to the test results.

5.5.2 Internal Columns With Additional Bonded Reinforcement :

The ACI, CSA and BS predictions of the Scordelis's continuous slab were considerably higher than the experimental result, but the CEB showed perfect agreement with the test result. The ACI and the CSA codes have trouble predicting the punching resistance of prestressed slabs with bonded flexural reinforcement or when the flexural behaviour of the slab becomes more important in the overall behaviour of slab-column connections. In these two codes the shear behaviour of slabs is treated separately from the flexural behaviour, and this is the main reason why they fail to predict the ultimate shear resistance of slabs in which there exist extensive flexural cracking or distress prior to failure. The BS code approach seems to be unfortunate in calculating the reinforcement ratio over the width of control perimeter only. In fact, the equivalent ratio of reinforcement should be computed over a larger area in the vicinity of the column or loaded area. As mentioned earlier, the effect of the prestressing stress in tendons should also be considered in determination of equivalent reinforcement ratio. All four codes are unable to reasonably predict Burns's slab models tested in 1971. The slabs were 7 in. thick and the shear capacity was reached before the flexural capacity in all cases. The specimens exhibited cracks of relatively great width prior to failure. The use of supplementary reinforcing steel increased the specimens' ductility as well as the ability of post-tensioned flat slabs to transmit loads to the columns and consequently increased the shear capacities of the connections. In contradiction, the strength of the specimens tested by Burns in 1974 were overestimated by all codes. The specimens failed by the formation of yield line mechanisms, indicating the primary mode of failure was in flexural mode. The CEB code showed the most consistent results demonstrating the capability of code's equation to bring into account the effects of flexural

cracking and distress in the calculation of ultimate punching shear capacity of slab-column connections. The two continuous slabs tested by Hemakom in 1975 also exhibited extensive cracking around the columns followed by large rotations associated with flexural failure, which consequently resulted in lower shear strengths for the slab-column connections. Shehata's specimens were underestimated by all codes. The geometries and behaviour of specimens were closely identical to the Burns 's specimens tested in 1971. Rahman's slabs are relatively well-predicted by the ACI and the CEB codes, but are over-predicted by the CSA and BS codes. Long's specimen is reasonably predicted by all codes. Roschke's specimen is in good correlation with the ACI prediction, but is overestimated by the European codes. Roschke concentrated relatively a great amount of bonded reinforcement in the vicinity of the column.

It is believed that the increase in flexural reinforcement effectively increases the ultimate punching strength, but there is a limit for this. Tests of slabs with reinforcement concentrated toward the column lines have been made by Elstner, Hognestad, Moe and Regan. Fig. 5-14 shows ultimate shear stress with the steel ratio calculated for the full slab width, the column side plus $3d$ to either side and the column width plus $1.5d$ to either side. It is best achieved when ρ is determined for the full slab width. As it is shown by Fig. 5-14 the arrangement of reinforcement to a band concentrated over the column is not always beneficial. In fact, Moe's and Elstner's results showed a decrease in shear strength due to concentration of tensile reinforcement through the shear area.

5.5.3 Edge Columns :

Slab shear stress in the vicinity of column consists of the shear due to column axial load combined with shear due to moment transfer between slab and column. Tests have shown that the shear stress can be substantially increased by the effect of moment transfer especially at the exterior columns. The analysis of data from failures at exterior columns is more difficult than that for interior columns, because of the influence of flexural effects. The ACI and the CSA codes consider the effect of eccentricity as an important factor in the shear capacity of slab-column connections. On the other hand, the BS and the CEB codes's expressions are simple and independent of the eccentricity of the load. Their predictions of the Gamble's four test specimens are significantly high. This is due to the considerable effect of moment transfer in reducing the shear strengths of the connections, which is neglected by the European codes. In the specimens tested by Long, the predictions of the ACI and CSA codes were below the measured values by a factor between 1.5 and 2.0. The models tested by Long had the advantage of carefully controlled boundary conditions over the isolated slab-column models. As a result, the slab deformations were simulated to be similar to those in a prototype structure; redistribution of moments due to cracking and yielding would occur in a similar manner that takes place in a real structure; the generation of compressive membrane action was allowed within the test models, which in turn could have a great influence on the enhancement of the shear capacities of the model slabs. The failure load obtained in the present investigation for the south-edge column is closely predicted by all codes except CSA, which as usual overestimated the results.

5.5.4 Corner Columns :

The load required to fail a corner column in a multipanel continuous structure is normally very high. The smaller tributary area associated with such columns together with the column size similar to an edge or even an internal column is the main reason. In the present test program, all four corner columns, even after the application of severe external loading, showed only minor fine cracks running in a direction that made an angle of approximately 45° with the slab edges. The ultimate shear capacities predicted by each code is presented in the following table :

P-test (KN)	P-ACI (KN)	P-CSA (KN)	P-BS (KN)	P-CEB (KN)
55.70	57.90	79.79	54.18	57.37

Table 5-7 : Ultimate load predictions of the tested slab corner column

As it is indicated by the table, according to all four codes the corner columns were close to failure. However no severe cracking or flexural distress was observed around the corner columns. Although no attempt was made to fail any of corner columns, but it was evident that they can sustain a load beyond the load caused failure in the interior or edge column. Therefore, it is believed that the codes predictions for the corner columns in the present experimental program are conservative.

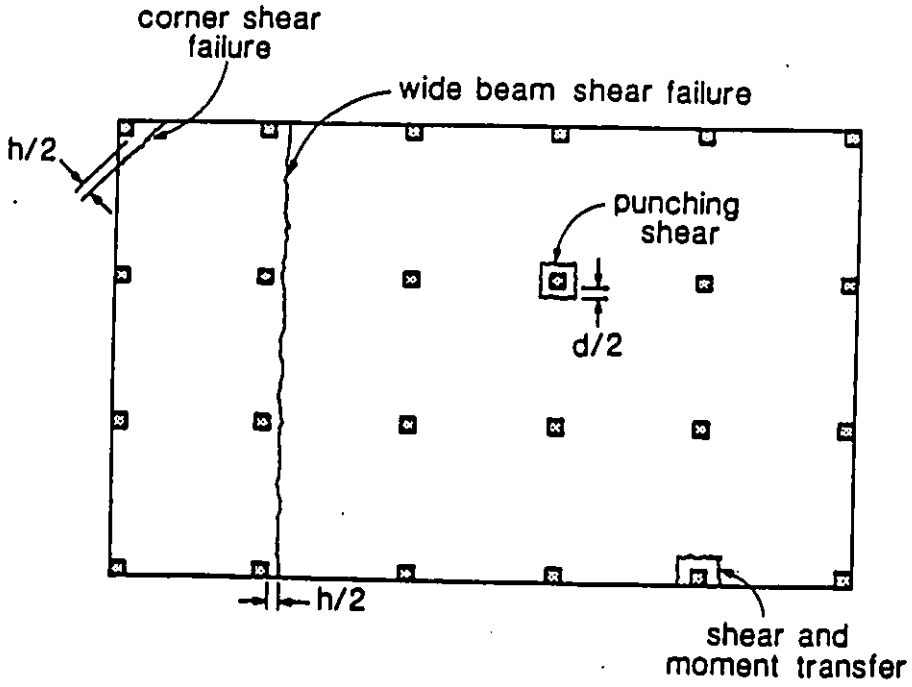

Fig. 5-1 : Types of shear failures

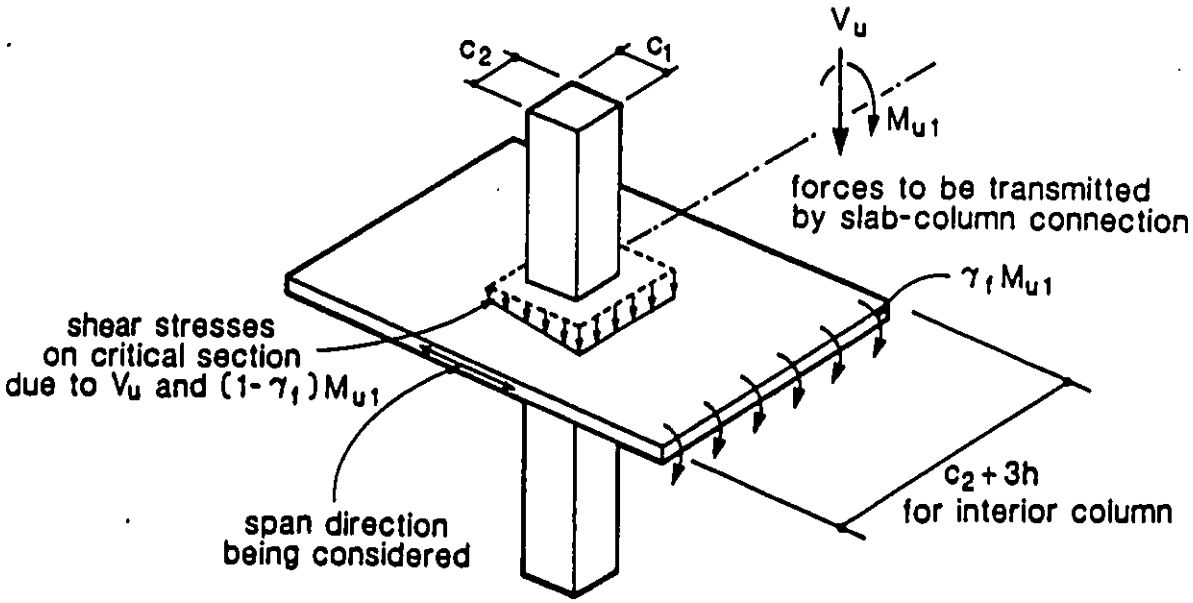

Fig. 5-3 : Shear and moment transfer in slab-column connections

(According to the ACI and CSA codes)

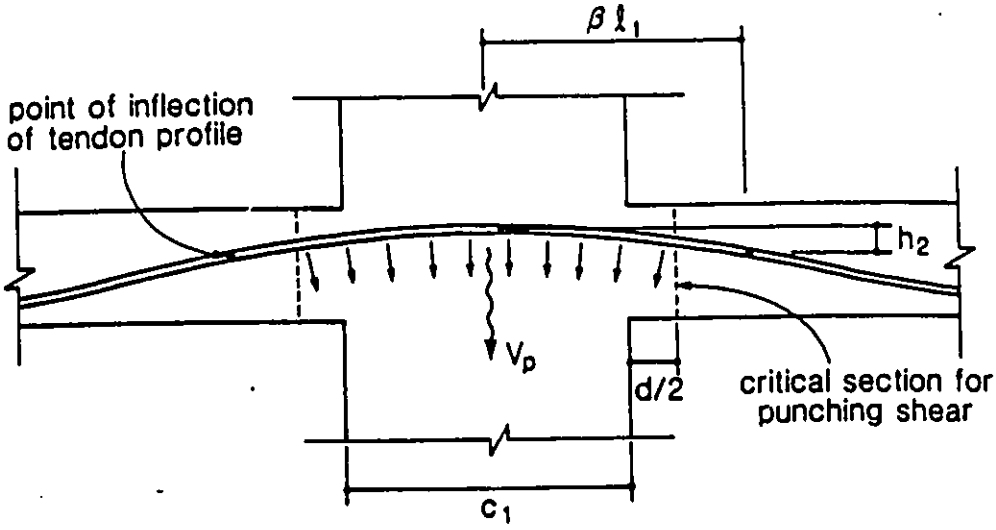

(a) Tendon profile through column region

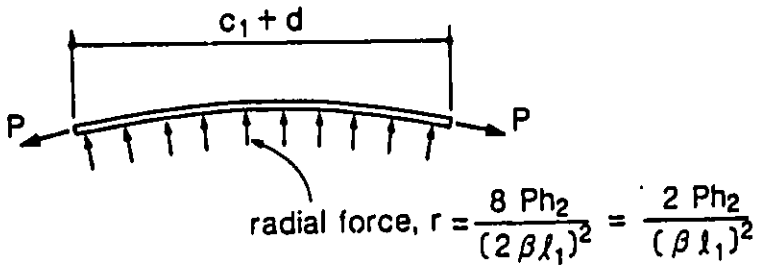

Fig. 5-2 : Calculation of vertical component of prestressing force crossing the critical section

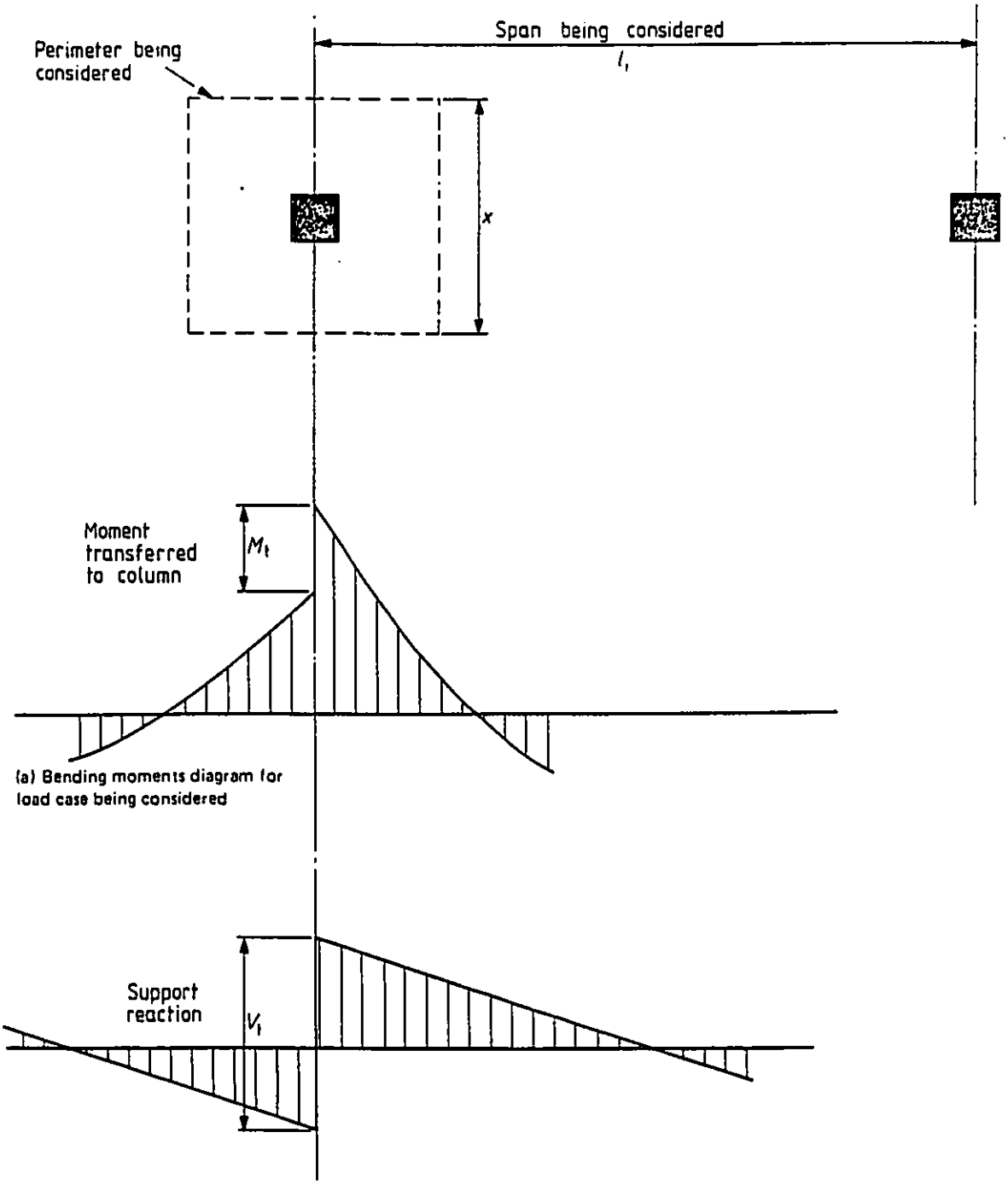

Fig. 5-4 : Shear at slab-column connections (BS 8110-85)

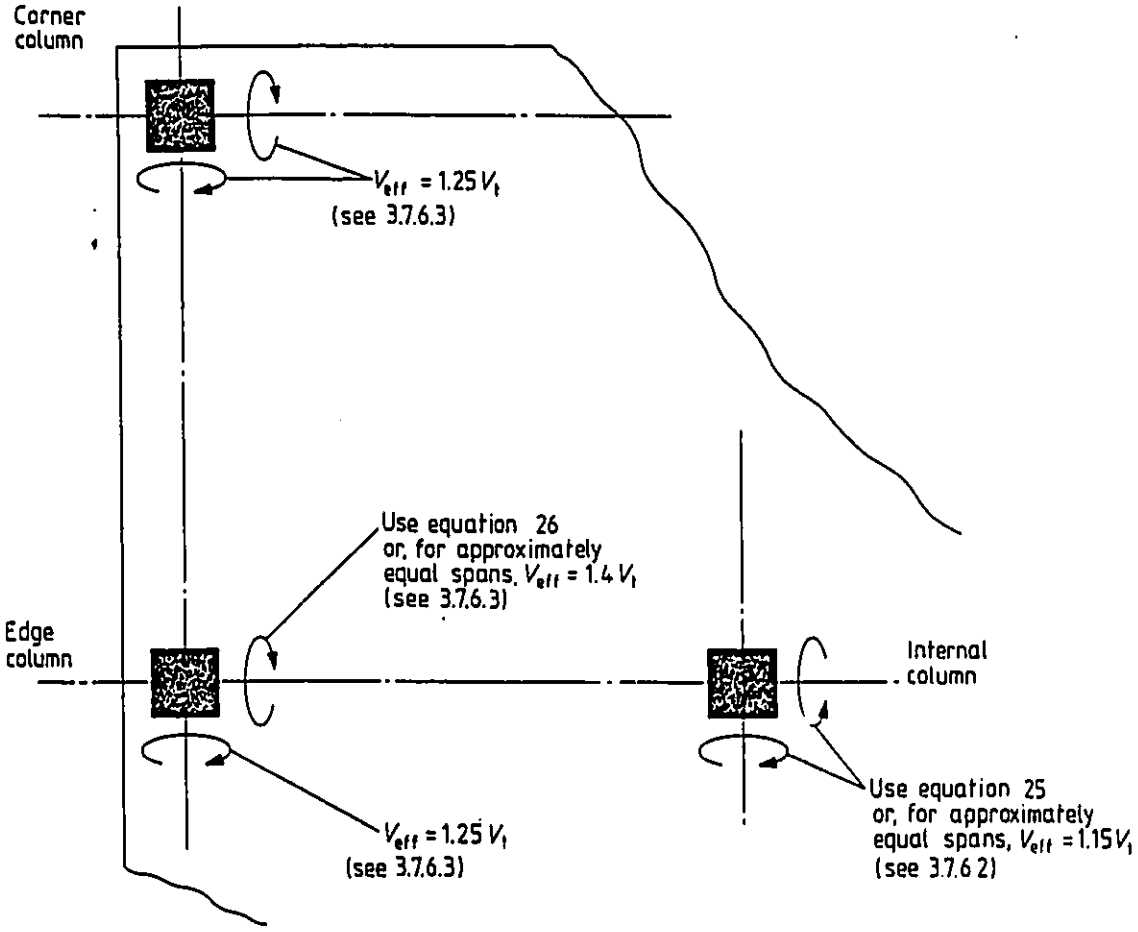

Fig. 5-5 : Shear at slab-column connections (BS 8110-85)

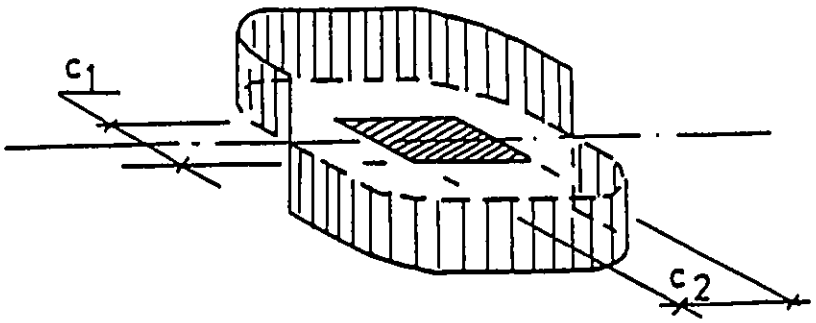

Fig. 5-6 : Shear distribution with moment transfer around an internal column (CEB-FIP-90)

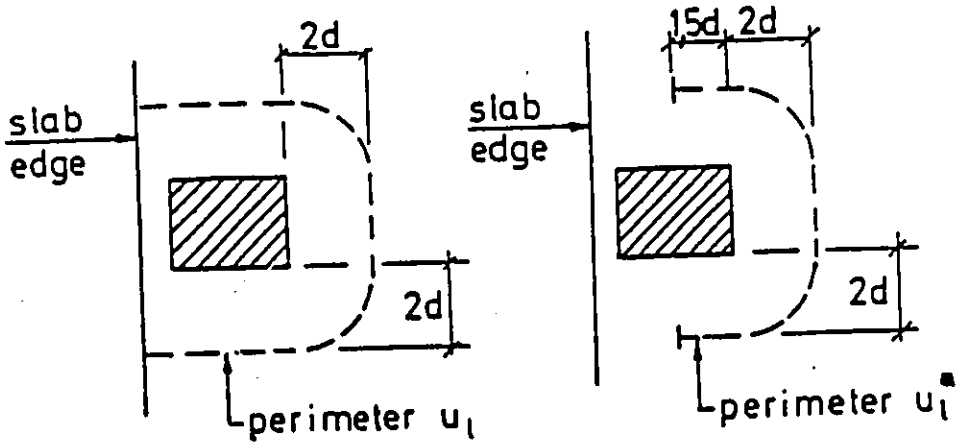

Fig. 5-7 : Control perimeters at edge columns with and without moment transfer (CEB-FIP-90)

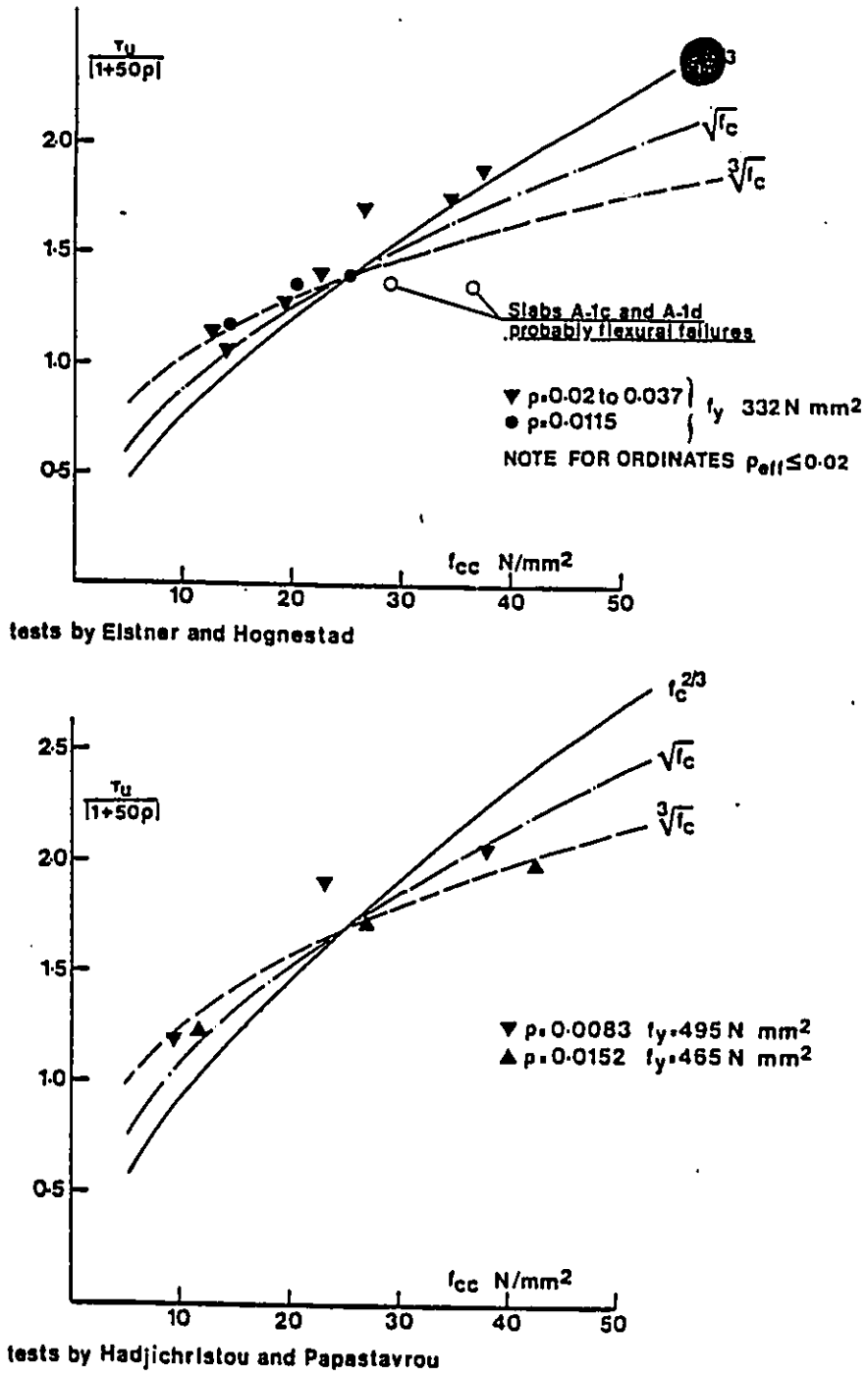

Fig. 5-8 : Variation of punching shear resistance with concrete strength (Regan 1985)

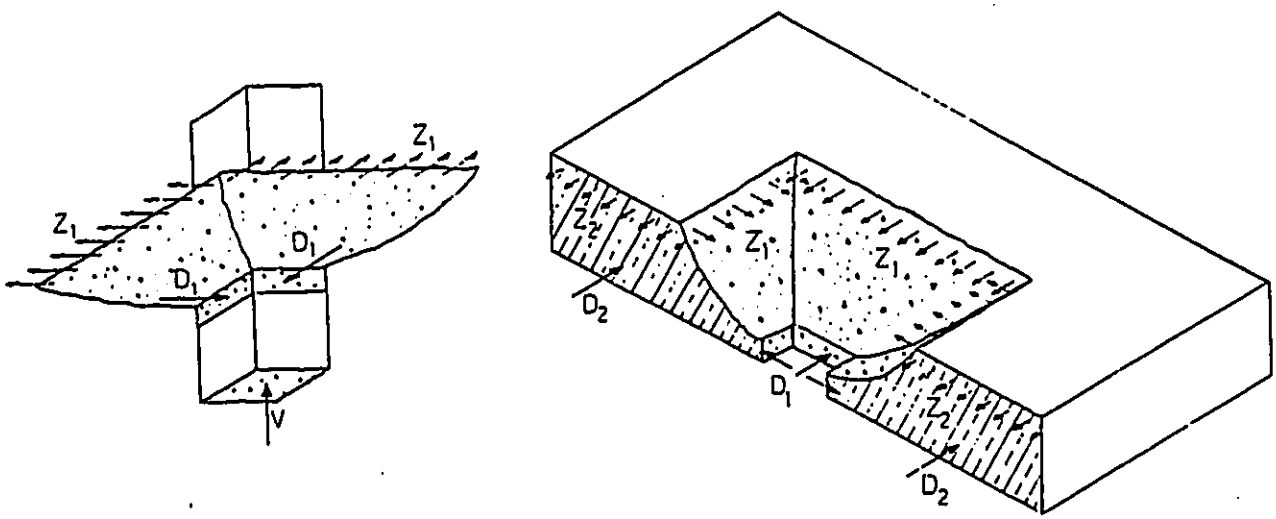

Fig. 5-9 : Schematic of punching shear cone

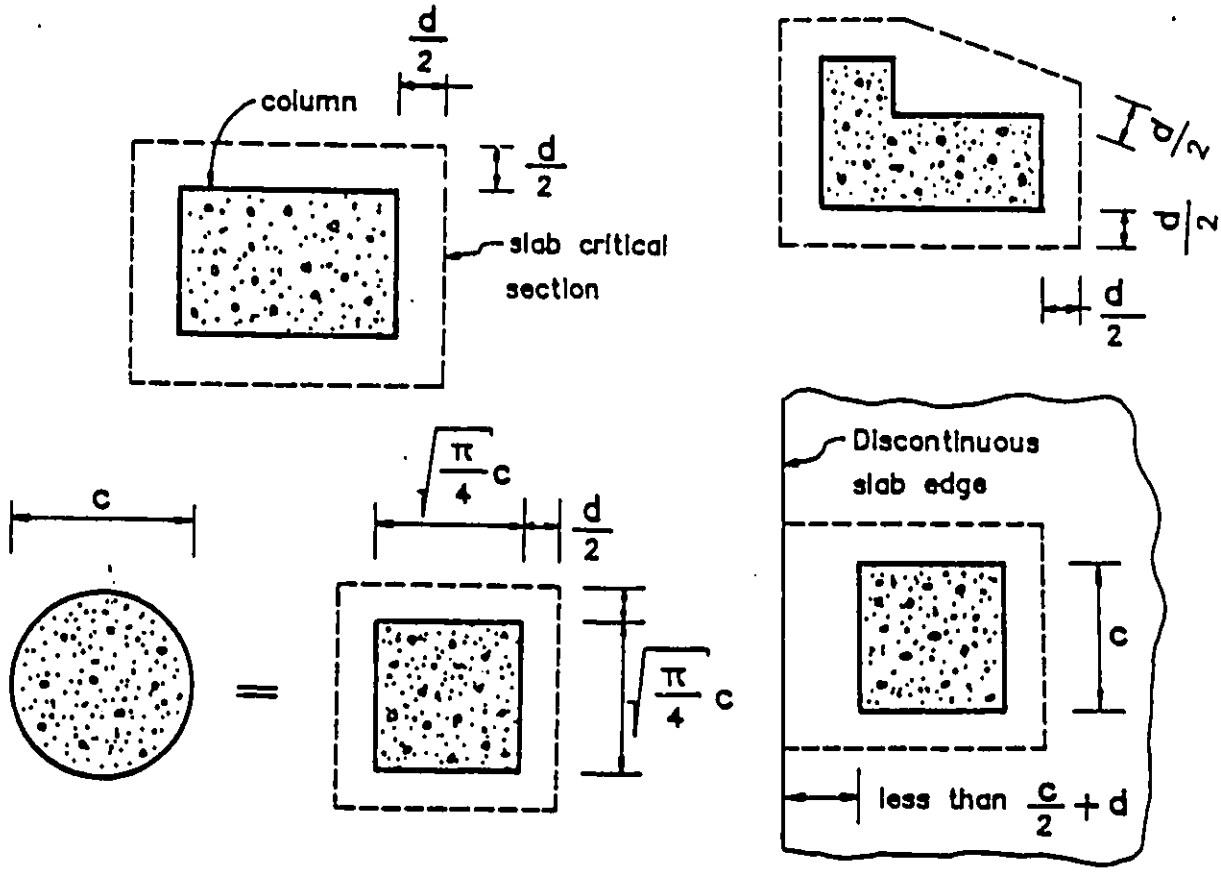

Fig. 5-10 : Examples of slab critical sections (ACI 318-89)

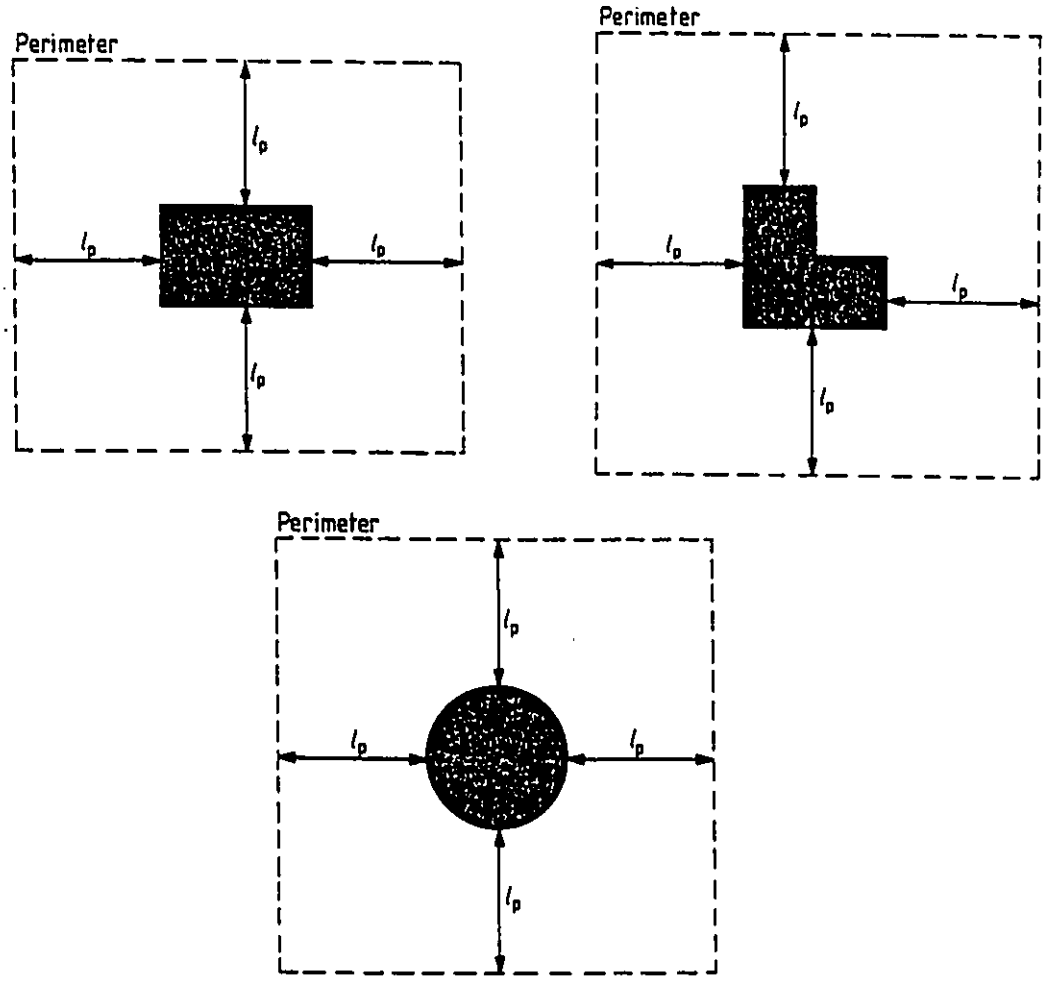

Fig. 5-11 : Definition of a shear perimeter for typical cases (BS 8110-85)

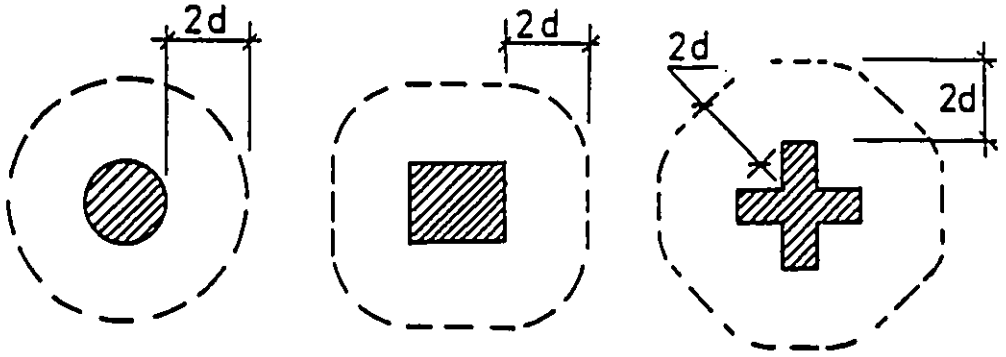

Fig. 5-12 : Control perimeters at interior columns (CEB-FIP-90)

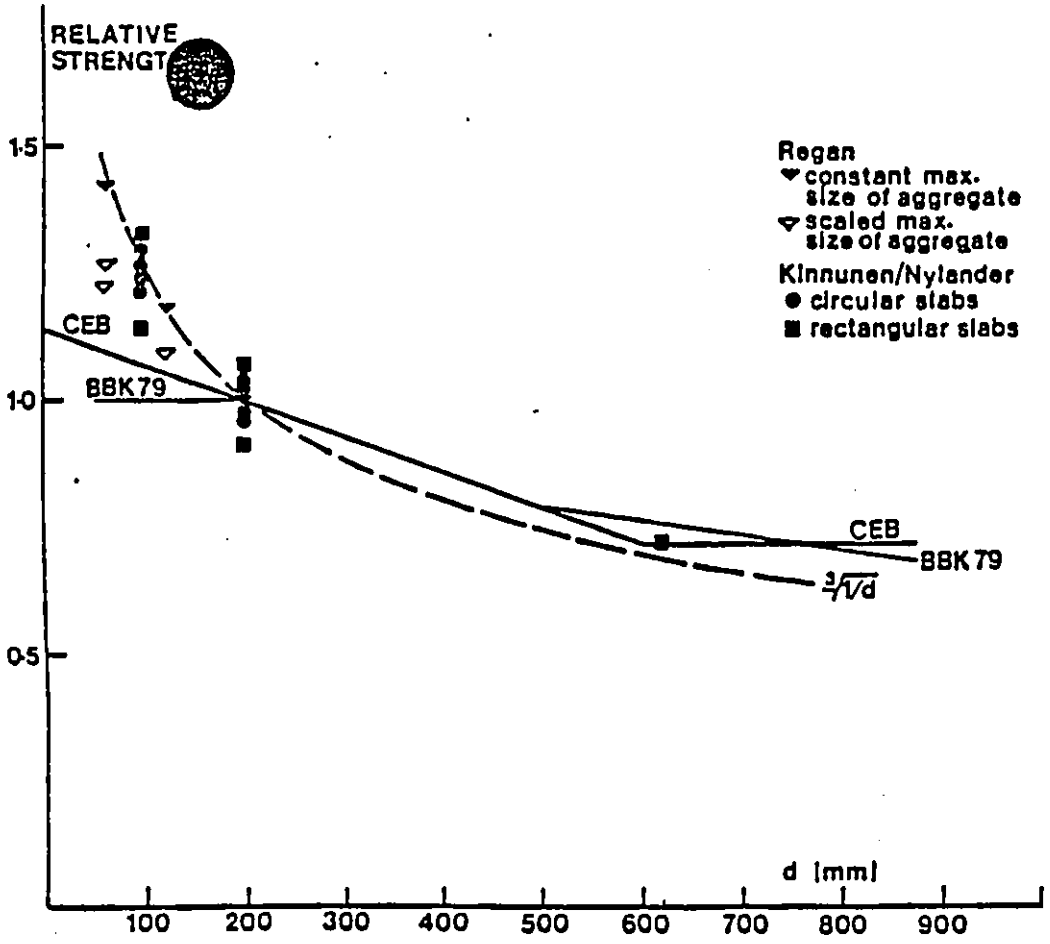

Fig. 5-13 : Influence of slab depth on unit punching strength (Regan 1985)

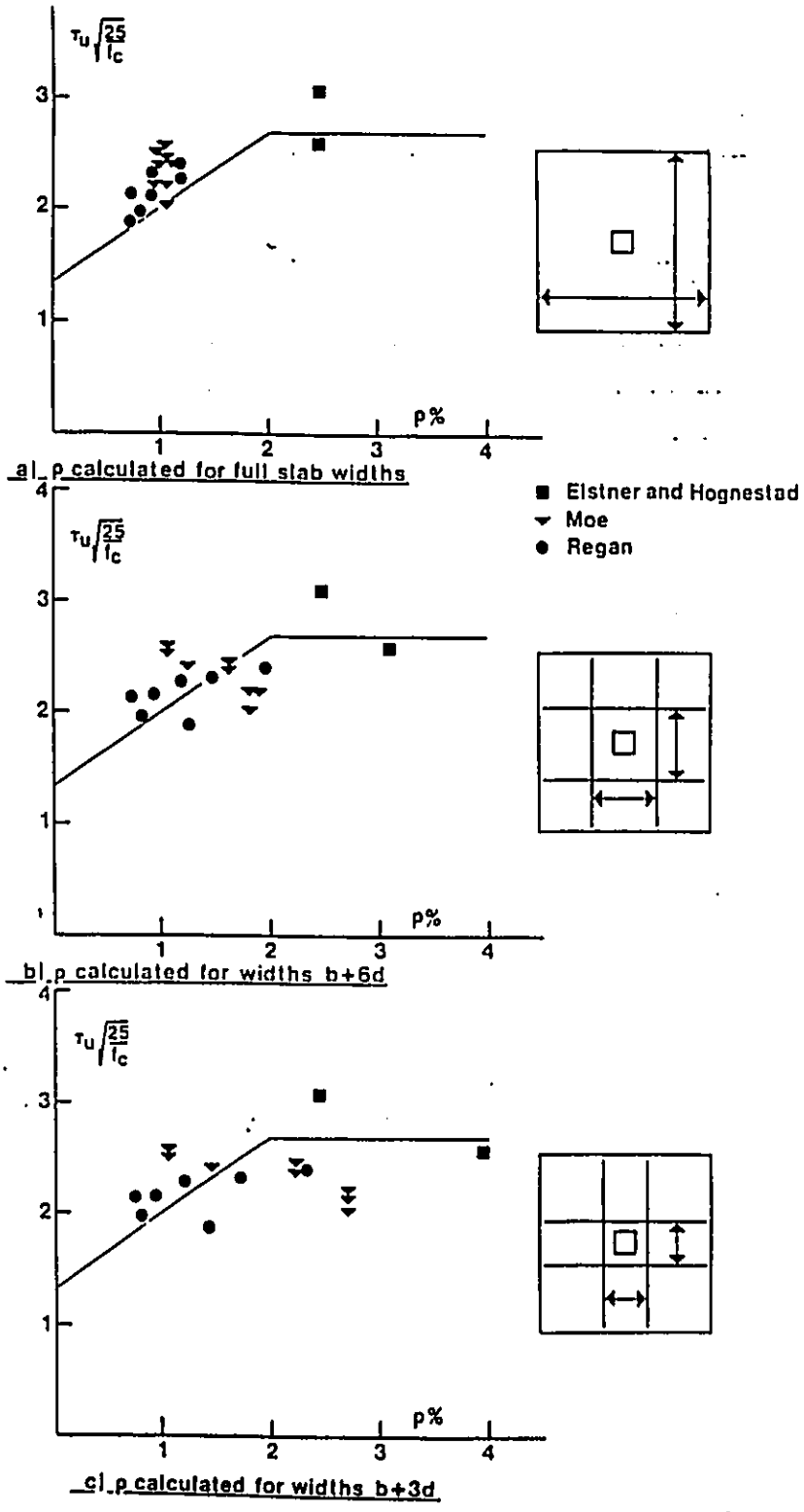

Fig. 5-14 : Influence of arrangement of reinforcement on punching strength (Regan 1985)

description / Researcher	slab No.	h (mm)	fpc (MPa)	f'c (MPa)	St. ratio P-BS	St. ratio P-CEB	stub col. (mm)	d (mm)	P-test (KN)	P-ACI (KN)	P-CSA (KN)	P-BS (KN)	P-CEB (KN)
Scordelis (1958)	s-5	152.4	1.72	20.24	3.705	0.632	330.2	76.2	266.88	225.66	311.89	316.39	169.58
	s-6	152.4	1.72	32.41	2.820	0.466	330.2	92.2	349.17	337.73	470.19	423.41	209.60
	s-7	152.4	3.45	19.93	2.135	0.685	330.2	111.3	540.43	457.74	600.83	413.59	287.01
	s-8	152.4	3.45	29.98	2.820	0.466	330.2	92.2	442.58	408.47	547.39	412.57	247.23
	s-9	152.4	1.72	30.17	2.505	0.43	406.4	92.2	467.04	388.01	539.72	447.32	220.92
	s-10	152.4	3.44	32.19	2.505	0.43	406.4	92.2	524.86	492.32	661.91	457.07	266.56
	s-11	254	2.07	35.34	0.893	0.132	330.2	193.8	1000.80	952.33	1320.78	779.01	433.97
	s-14	203.2	2.59	33.10	1.454	0.223	330.2	143.0	747.26	661.53	907.67	594.49	339.15
Burns (1971)	c-1	177.8	1.72	36.54	1.664	0.252	304.8	135.0	788.19	577.42	804.92	575.55	437.48
	L-1	177.8	1.72	36.54	1.664	0.252	304.8	135.0	877.15	577.42	804.92	575.55	437.48
	L-7	177.8	1.72	36.54	1.664	0.252	304.8	135.0	892.27	577.42	804.92	575.55	437.48
Vanderbilt (1967)	G-0	76.2	0.04	27.58	2.585	0.836	203.2	50.8	103.64	74.37	102.81	116.85	75.39
	G-2	76.2	0.79	29.37	2.585	0.836	203.2	50.8	118.76	91.25	127.74	119.33	81.55
	G-3	76.2	1.16	28.55	2.585	0.836	203.2	50.8	113.87	97.24	135.51	118.20	83.05
	G-4	76.2	1.90	24.89	2.585	0.836	203.2	50.8	118.76	106.67	145.30	112.92	84.18
	G-5	76.2	1.93	31.58	2.585	0.836	203.2	50.8	125.43	116.03	159.05	122.25	90.35
	G-6	76.2	2.31	29.30	2.585	0.836	203.2	50.8	115.20	120.47	162.81	119.24	90.72
	G-7	76.2	2.69	30.54	2.585	0.836	203.2	50.8	125.43	129.39	172.93	120.90	94.09
	G-8	76.2	3.06	32.20	2.585	0.836	203.2	50.8	141.89	138.66	183.43	123.04	97.73
	G-10	76.2	3.70	30.34	2.585	0.836	203.2	50.8	145.00	148.58	191.48	120.62	100.03
	G-12	76.2	4.52	28.20	2.585	0.836	203.2	50.8	154.79	161.80	201.07	117.72	103.20
Burns (74)	s-1	69.9	2.24	29.99	2.669	0.659	203.2	54.4	112.31	130.90	180.43	164.67	109.90
Rahman (91)	sp-12	165	0.88	29.00	0.986	0.133	300.0	130.0	453.00	416.43	583.11	422.92	187.25
Pre. Work		95.25	3.50	44.00	3.970	0.906	203.2	69.9	280.00	280.68	365.25	290.24	146.94

Table 5-1 : Ultimate load predictions of the internal slab-column connections without additional bonded reinforcement with the ACI, CSA,BS and CEB codes

Analysis / Researcher	No. of Samples	P-test / P-ACI			P-test / P-CSA			P-test / P-BS			P-test / P-CEB		
		Mean	Standard Dev.	Coef. of Var.	Mean	Standard Dev.	Coef. of Var.	Mean	Standard Dev.	Coef. of Var.	Mean	Standard Dev.	Coef. of Var.
Scordelis	8	1.116	0.067	0.060	0.818	0.054	0.066	1.098	0.189	0.172	1.938	0.259	0.134
Burns (71)	3	1.476	0.097	0.066	1.059	0.070	0.066	1.481	0.098	0.066	1.949	0.129	0.066
Vanderbilt	10	1.094	0.153	0.140	0.812	0.093	0.115	1.060	0.128	0.121	1.401	0.068	0.048
Burns (74)	1	0.858	-	-	0.622	-	-	0.682	-	-	1.022	-	-
Rahman	1	1.088	-	-	0.777	-	-	1.071	-	-	2.419	-	-
Pre. work	1	0.998	-	-	0.767	-	-	0.965	-	-	1.905	-	-
Total Average		**1.135**	**0.178**	**0.157**	**0.834**	**0.118**	**0.142**	**1.106**	**0.215**	**0.194**	**1.696**	**0.367**	**0.216**

Table 5-2 : Statistical analysis of the predicted values for the internal slab-column connections without additional bonded reinforcement

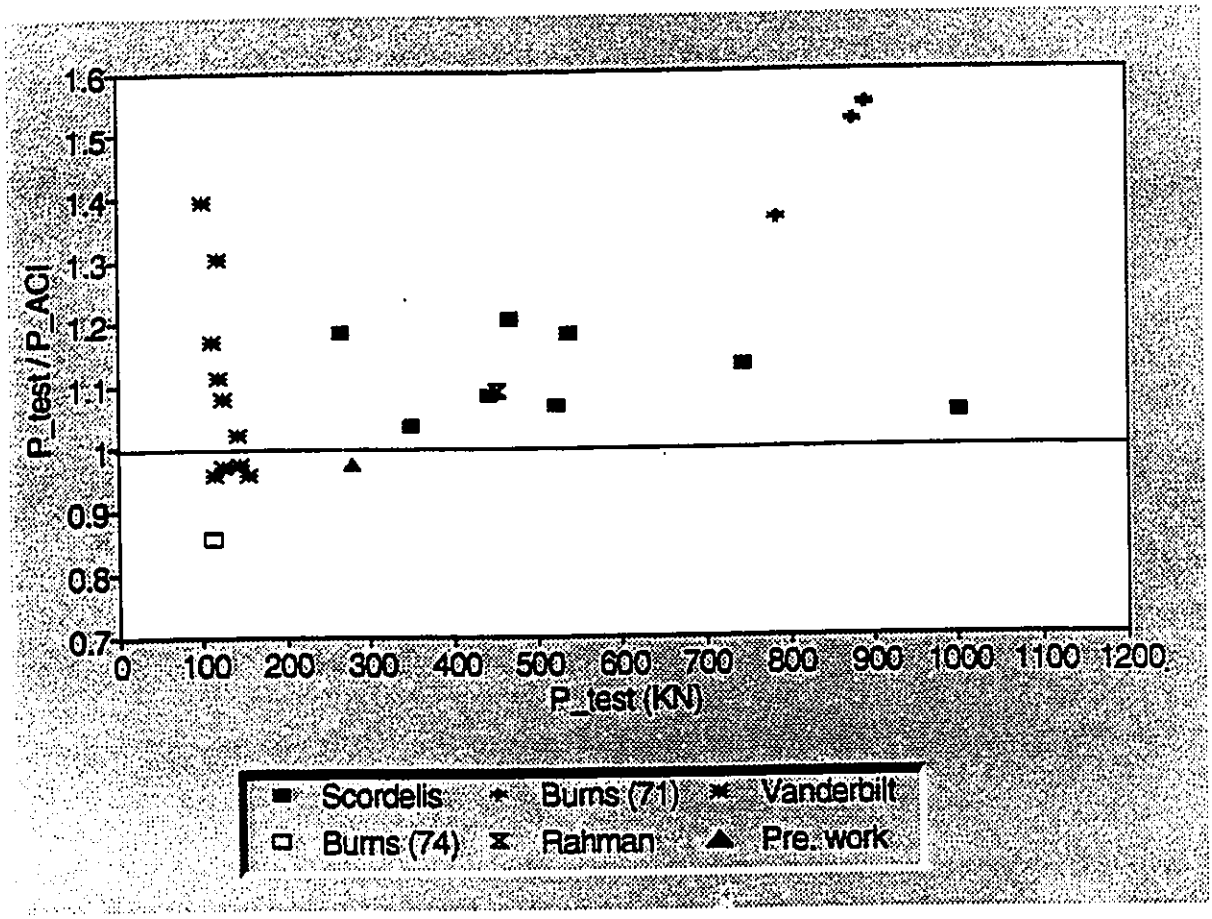

Fig. 5-15 : ACI code predictions of internal slab-column connections without additional bonded reinforcement

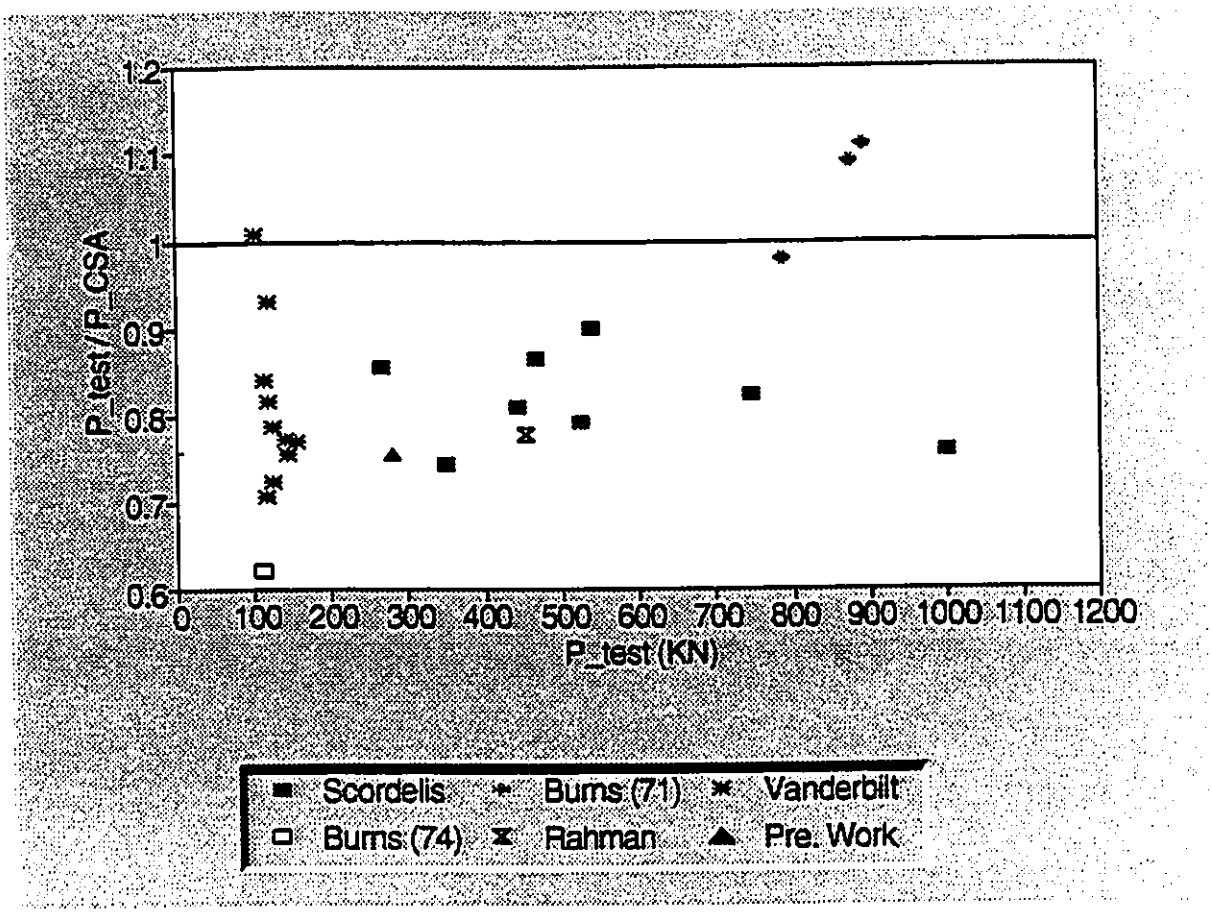

Fig. 5-16 : CSA code predictions of internal slab-column connections without additional bonded reinforcement (without resistance factor for concrete, φ_c)

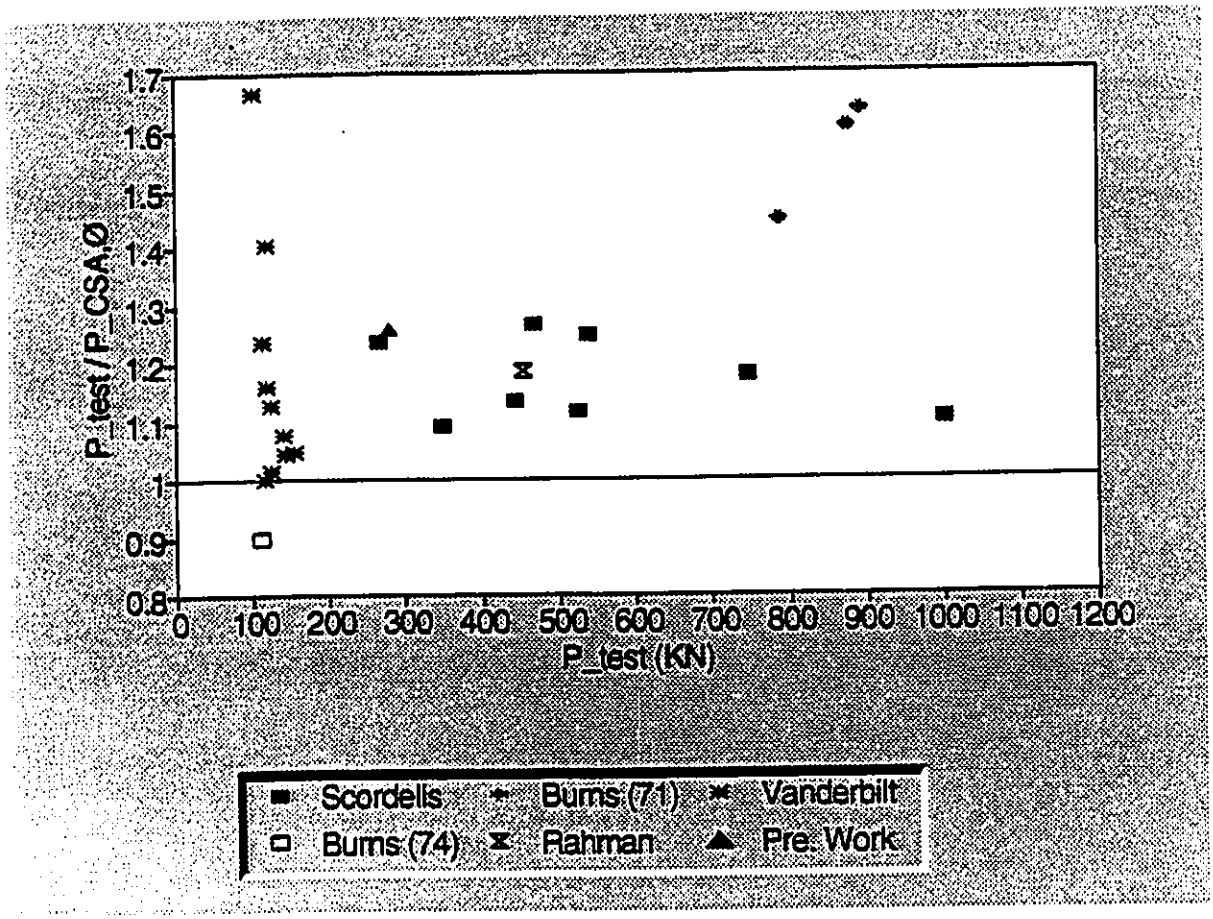

Fig. 5-17 : CSA code predictions of internal slab-column connections without additional bonded reinforcement (with resistance factor for concrete, φ_c=0.6)

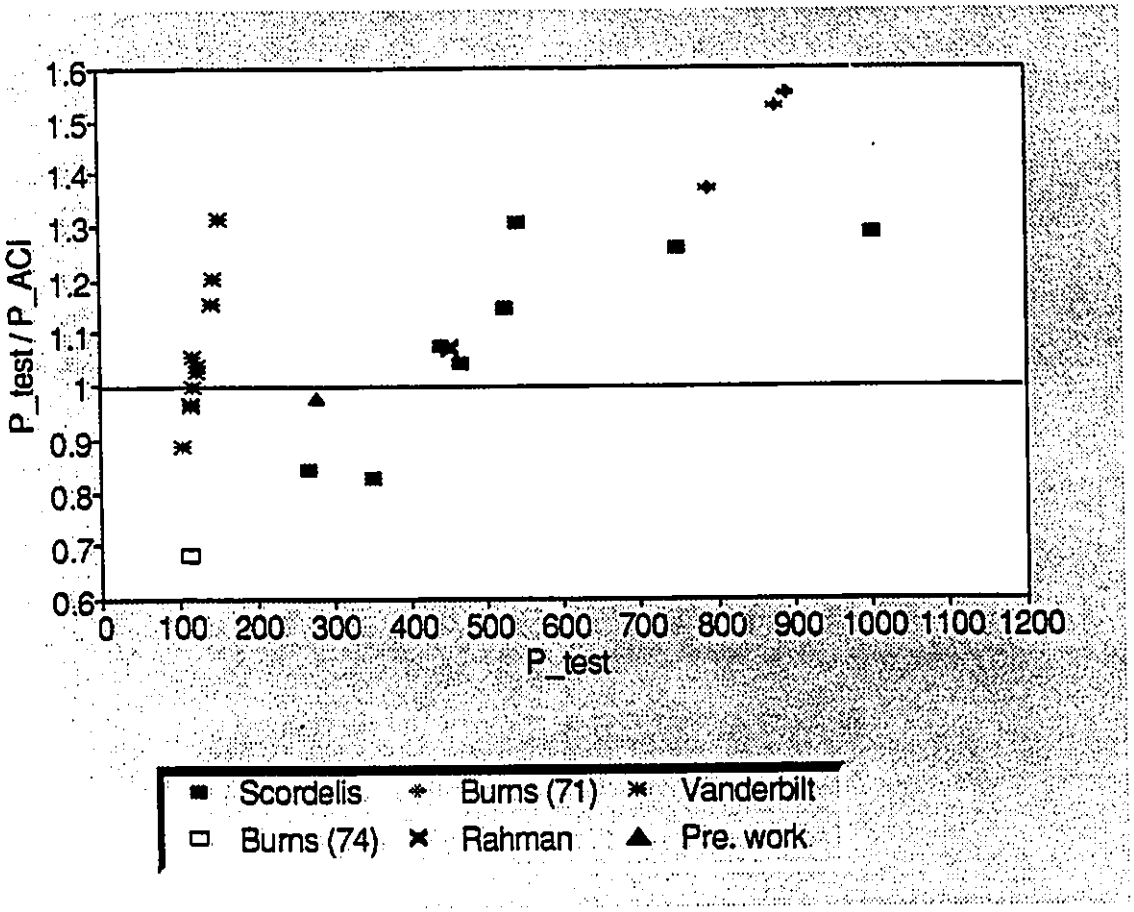

Fig. 5-18 : BS code predictions of internal slab-column connections without additional bonded reinforcement

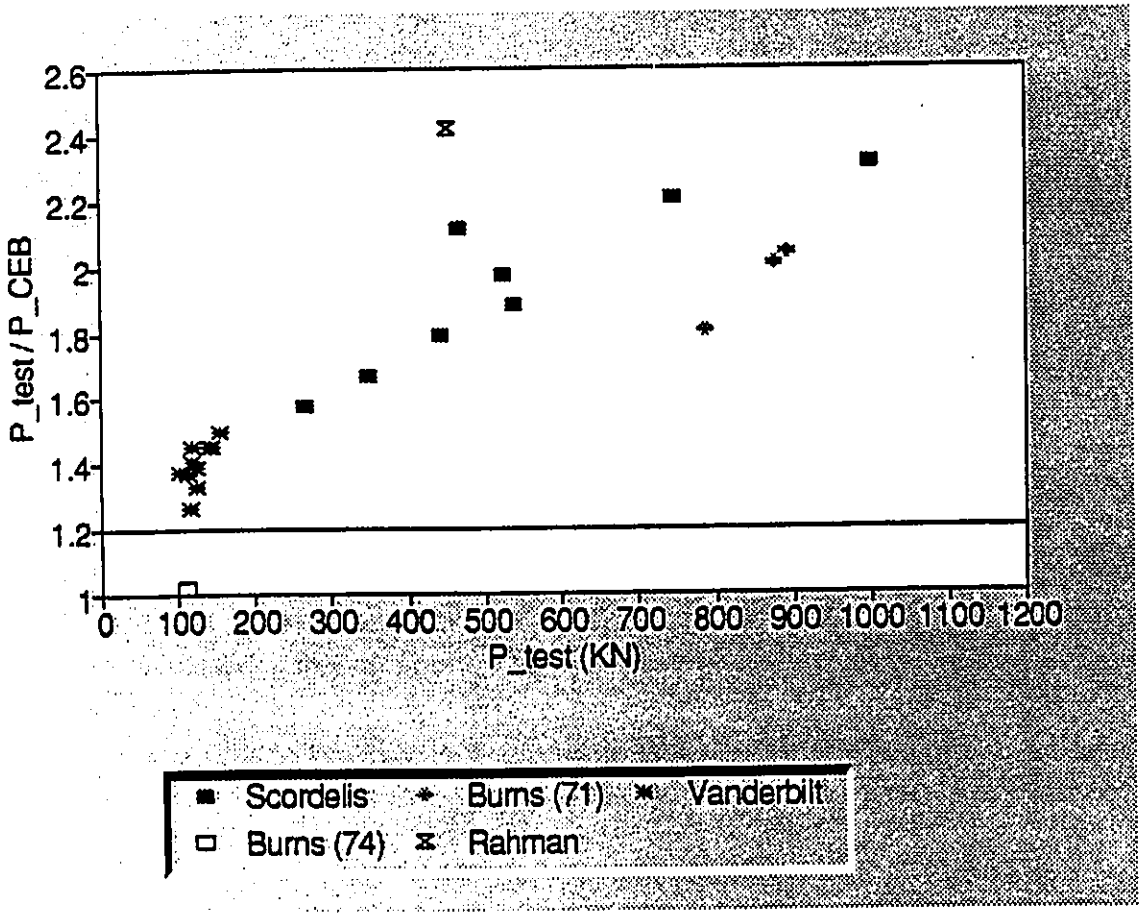

Fig. 5-19 : CEB code predictions of internal slab-column connections without additional bonded reinforcement

description / Researcher	slab No.	h (mm)	fpc (MPa)	f'c (MPa)	St. ratio P-BS	St. ratio P-CEB	stub col. (mm)	d (mm)	P-test (KN)	P-ACI (KN)	P-CSA (KN)	P-BS (KN)	P-CEB (KN)
Scordelis (1959)		76.2	1.15	37.60	0.885	0.247	228.6	63.5	90.80	149.91	209.89	157.87	83.51
Burns (1971)	c-2	177.8	1.72	31.72	2.225	0.641	304.8	139.7	857.07	546.88	761.18	632.86	516.83
	c-3	177.8	1.72	33.89	2.225	0.641	304.8	139.7	901.57	560.86	781.23	646.98	523.50
	c-4	177.8	1.72	33.99	2.642	0.899	304.8	139.7	812.57	561.52	782.17	685.81	560.33
	I-2	177.8	1.72	31.03	2.225	0.641	304.8	139.7	890.89	542.33	754.66	628.24	514.65
	I-3	177.8	1.72	31.79	2.225	0.641	304.8	139.7	935.39	547.32	761.82	633.31	517.05
	I-4	177.8	1.72	33.23	2.642	0.899	304.8	139.7	857.07	556.69	775.26	680.67	557.76
Burns (1974)	s-2	69.9	2.24	29.99	3.080	1.124	203.2	54.4	121.50	130.90	180.43	172.56	124.78
	s-3	69.9	2.24	29.99	3.491	1.403	203.2	54.4	135.30	130.90	180.43	179.92	131.84
Hemakom (1975) slab I	col.5	69.9	2.24	33.79	3.318	1.144	203.2	46.1	128.61	108.31	149.66	151.55	91.76
	col.6	73.7	2.24	33.78	2.388	0.885	203.2	59.3	152.60	146.84	202.90	183.24	110.46
	col.7	73.7	2.24	33.78	2.388	0.885	203.2	59.3	157.10	146.84	202.90	183.24	110.46
	col.10	73.7	2.24	33.78	2.388	0.885	203.2	59.3	162.40	146.84	202.90	183.24	110.46
	col.11	73.7	2.24	33.78	2.388	0.885	203.2	59.3	125.00	146.84	202.90	183.24	110.46
slab II	col.10	73.0	0.93	32.75	2.810	0.885	203.2	59.3	99.20	120.75	169.08	191.46	102.11
Shehata (1982)	sp-1	180.0	2.51	37.80	2.941	0.670	190.0	135.0	988.00	488.02	672.71	589.94	367.65
	sp-4	180.0	3.19	43.20	3.732	0.850	190.0	135.0	884.00	550.67	752.32	667.71	430.96
	sp-5	180.0	2.34	42.40	3.732	0.850	190.0	135.0	780.00	498.20	690.23	663.57	392.42
	sp-6	180.0	2.18	44.00	2.546	0.580	190.0	135.0	728.00	495.61	688.59	591.45	353.73
Long (1982)	7b	60.0	2.43	38.00	2.420	1.102	160.0	48.0	127.90	100.51	138.76	130.28	101.11
Rahman (1991)	sp-9	165.0	1.59	29.00	3.966	0.947	300.0	130.0	564.00	464.78	647.47	672.59	356.38
	sp-10	165.0	0.88	29.00	2.515	0.743	300.0	130.0	416.00	416.43	583.11	577.84	307.52
Roschke (1991)		235.0	5.38	33.10	4.187	0.882	254.0	188.0	920.00	818.14	1047.99	1118.94	1204.10

Table 5-3 : Ultimate load predictions of the internal slab-column connections with additional bonded reinforcement with the ACI, CSA,BS and CEB codes

Analysis / Researcher	No. of Samples	P-test / P-ACI			P-test / P-CSA			P-test / P-BS			P-test / P-CEB		
		Mean	Standard Dev.	Coef. of Var.	Mean	Standard Dev.	Coef. of Var.	Mean	Standard Dev.	Coef. of Var.	Mean	Standard Dev.	Coef. of Var.
Scordelis	1	0.606	-	-	0.433	-	-	0.575	-	-	1.087	-	-
Burns (71)	6	1.586	0.090	0.057	1.139	0.065	0.057	1.348	0.108	0.080	1.651	0.134	0.081
Burns (74)	2	0.981	0.075	0.076	0.712	0.054	0.076	0.728	0.034	0.047	1.000	0.037	0.037
Hemakom	6	1.013	0.145	0.144	0.731	0.107	0.147	0.771	0.143	0.186	1.296	0.199	0.153
Shehata	4	1.666	0.246	0.147	1.208	0.181	0.150	1.351	0.224	0.166	2.196	0.329	0.150
Long	1	1.273	-	-	0.922	-	-	0.982	-	-	1.265	-	-
Rahman	2	1.106	0.152	0.137	0.792	0.111	0.141	0.779	0.084	0.108	1.468	0.162	0.111
Roschke	1	1.125	-	-	0.878	-	-	0.822	-	-	0.764	-	-
Average		**1.280**	**0.348**	**0.272**	**0.926**	**0.251**	**0.271**	**1.022**	**0.323**	**0.316**	**1.501**	**0.439**	**0.292**

Table 5-4 : Statistical analysis of the predicted values for the internal slab-column connections with additional bonded reinforcement

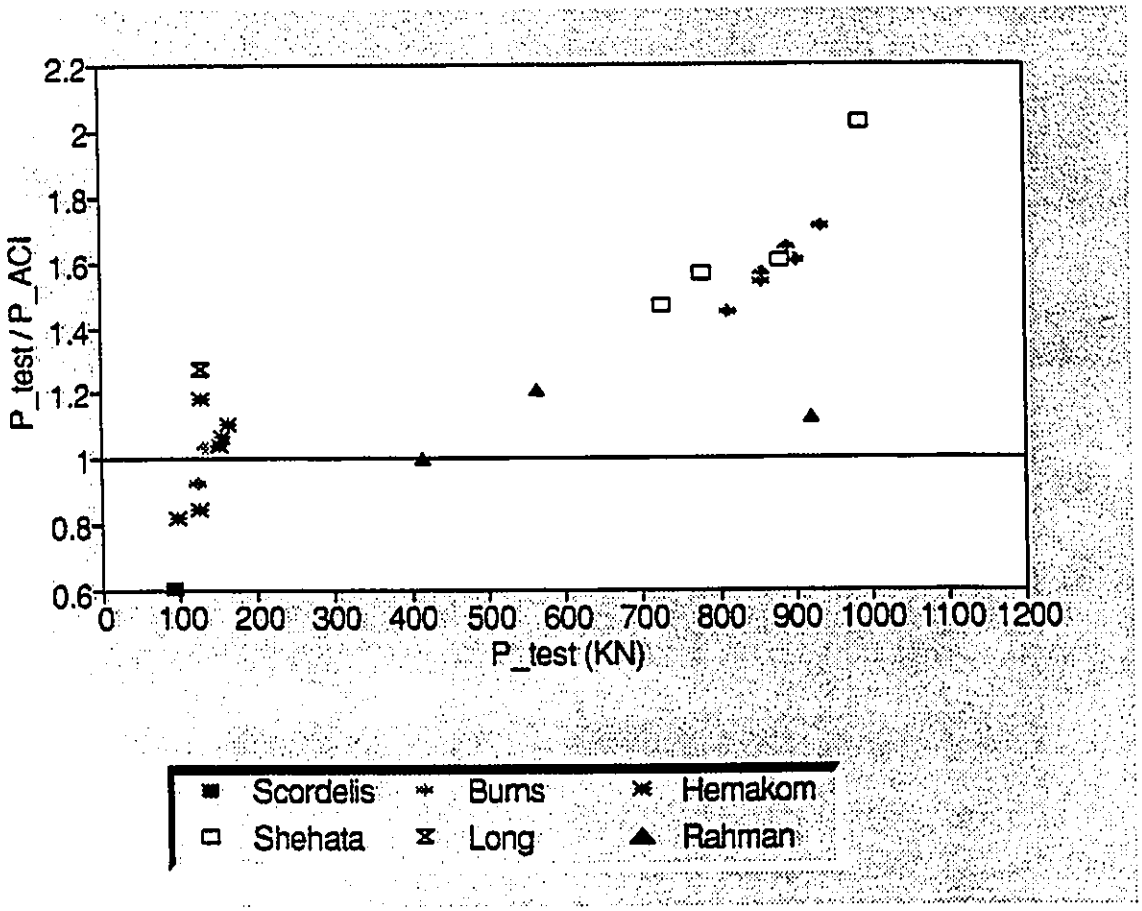

Fig. 5-20 : ACI code predictions of internal slab-column connections with additional bonded reinforcement

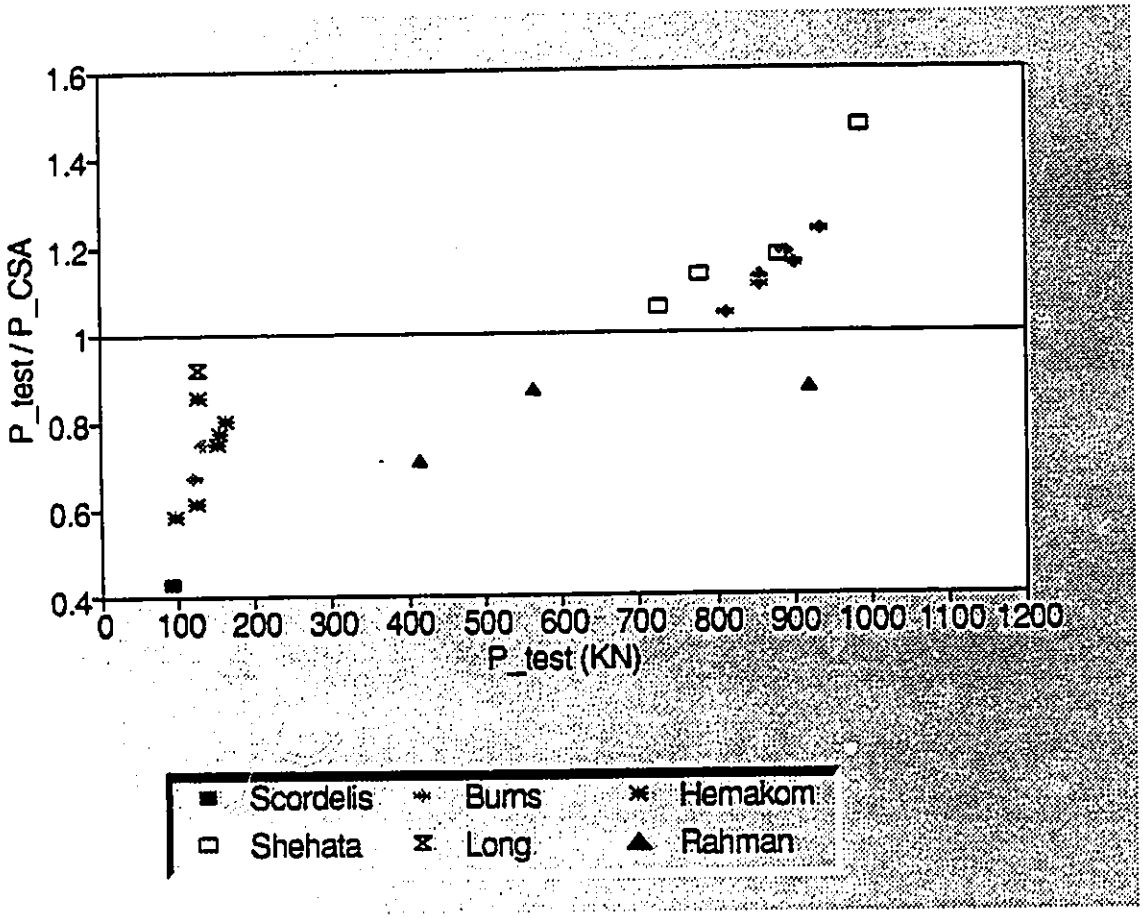

Fig. 5-21 : CSA code predictions of internal slab-column connections with additional bonded reinforcement (without resistance factor for concrete, φ_c)

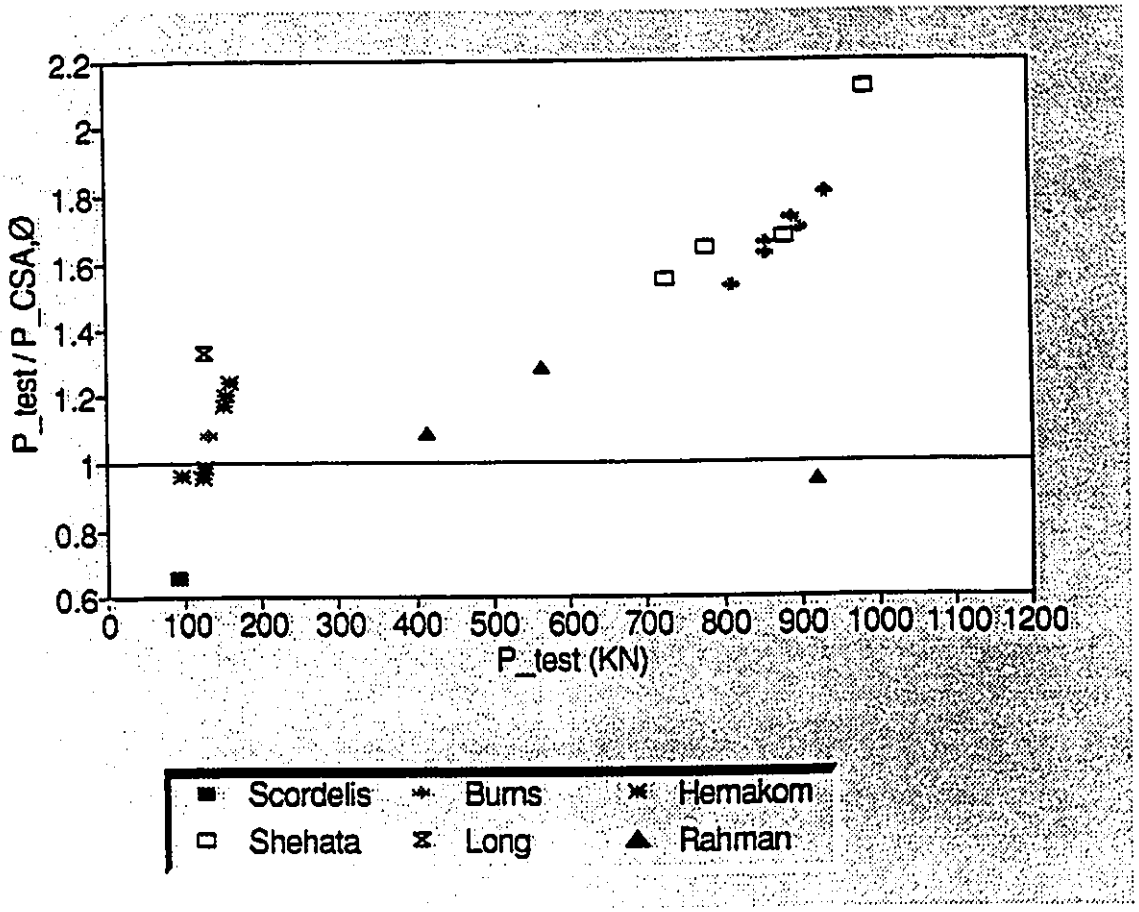

Fig. 5-22 : CSA code predictions of internal slab-column connections with additional bonded reinforcement (with resistance factor for concrete, φ_c=0.6)

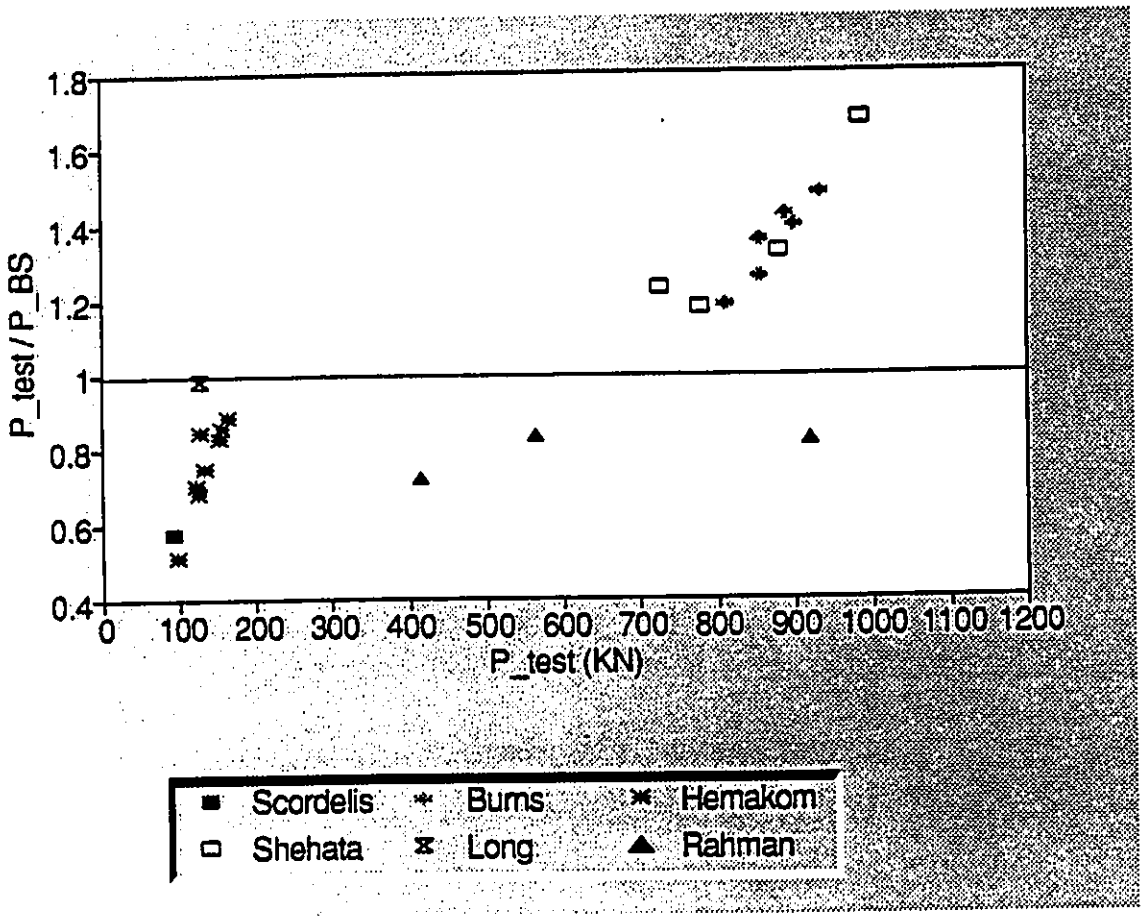

Fig. 5-23 : BS code predictions of internal slab-column connections with additional bonded reinforcement

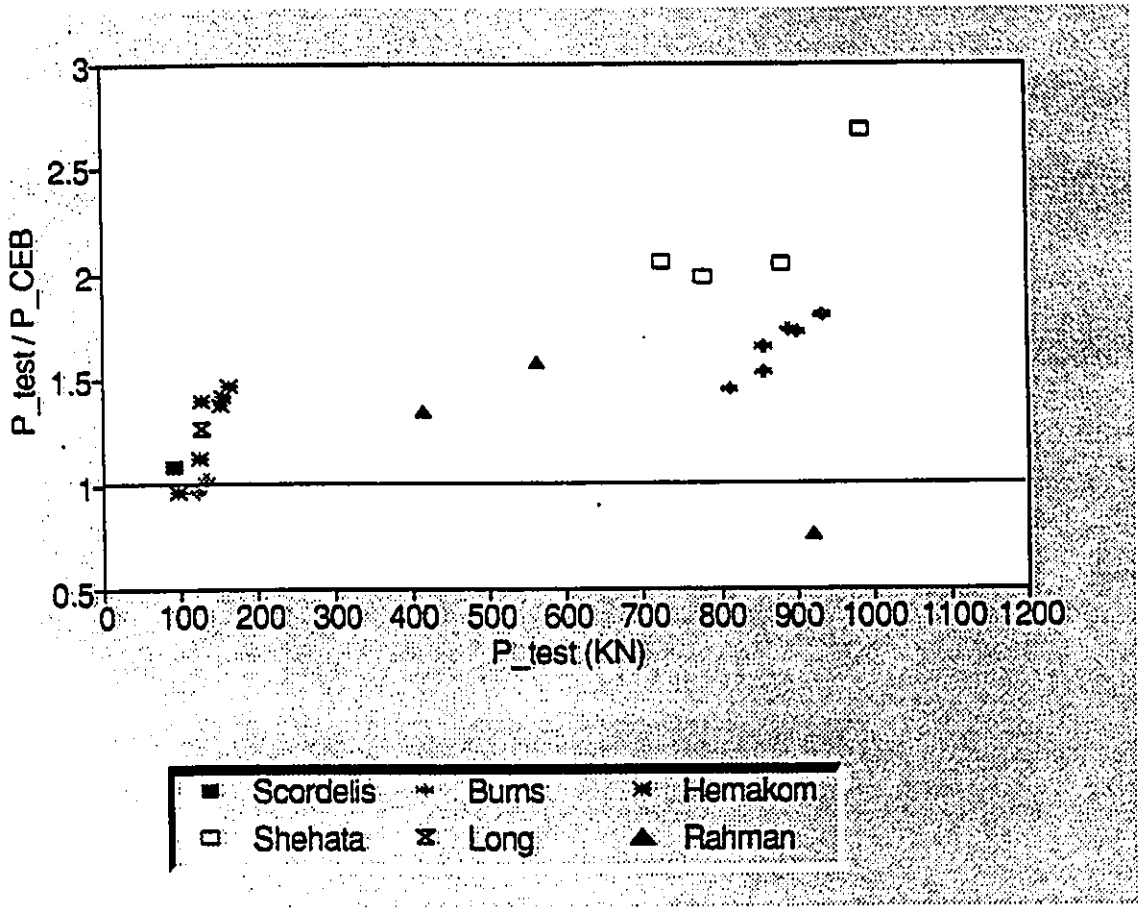

Fig. 5-24 : CEB code predictions of internal slab-column connections with additional bonded reinforcement

description / Researcher	slab No.	h (mm)	fpc (MPa)	f'c (MPa)	St. ratio P-BS	St. ratio P-CEB	stub col. (mm)	d (mm)	P-test (KN)	P-ACI (KN)	P-CSA (KN)	P-BS (KN)	P-CEB (KN)
Gamble (1989)	s1	101.6	3.09	50.33	4.12	2.62	304.8	50.8	57.76	59.18	73.35	142.98	116.99
	s2	101.6	3.50	42.75	4.12	2.62	304.8	50.8	83.39	82.86	97.43	135.41	117.03
	s3	101.6	2.22	42.06	4.85	1.65	304.8	50.8	67.20	71.71	86.19	142.20	107.18
	s4	101.6	2.18	48.26	4.85	1.65	304.8	50.8	113.87	105.77	120.84	148.87	110.59
Dilger (1989)	s1	150	2.74	35.81	4.92	1.315	250	120	180.00	126.44	173.32	311.11	316.81
	s5	150	2.50	41.31	4.94	1.315	250	120	180.00	109.13	178.50	326.73	323.75
Long (1993)	E1	50.8	2.34	35.79	2.92	2.01	162.5	25.4	46.73	23.35	32.24	35.51	28.10
	E2	50.8	2.34	37.85	3.1	1.85	162.5	33.02	49.84	24.38	33.70	48.14	37.83
	E3	50.8	3.52	40.82	3.1	1.85	162.5	33.02	56.07	27.88	37.77	49.37	41.80
	E4	50.8	1.17	38.21	3.1	1.85	162.5	33.02	40.94	22.40	31.35	48.29	34.76
	E5	50.8	2.34	36.21	3.1	1.85	162.5	33.02	52.96	23.12	31.93	47.44	37.36
Pre. Work		88.9	3.45	44.01	5.2	1.55	203.2	50.8	122.80	101.22	139.86	110.82	82.22

Table 5-5 : Ultimate load predictions of the edge slab-column connections with the ACI, CSA,BS and CEB codes

Analysis / Researcher	No. of Samples	P-test / P-ACI			P-test / P-CSA			P-test / P-BS			P-test / P-CEB		
		Mean	Standard Dev.	Coef. of Var.	Mean	Standard Dev.	Coef. of Var.	Mean	Standard Dev.	Coef. of Var.	Mean	Standard Dev.	Coef. of Var.
Gamble	4	0.999	0.059	0.059	0.841	0.076	0.090	0.564	0.160	0.284	0.799	0.228	0.285
Diger	2	1.537	0.160	0.104	1.023	0.021	0.021	0.565	0.020	0.035	0.562	0.009	0.015
Long	5	2.035	0.166	0.081	1.475	0.125	0.085	1.090	0.170	0.156	1.383	0.179	0.129
Pre. work	1	1.213	-	-	0.878	-	-	1.108	-	-	1.494	-	-
Total Average		**1.538**	**0.491**	**0.319**	**1.139**	**0.316**	**0.277**	**0.829**	**0.306**	**0.370**	**1.033**	**0.422**	**0.408**

Table 5-6 : Statistical analysis of the predicted values for the edge slab-column connections

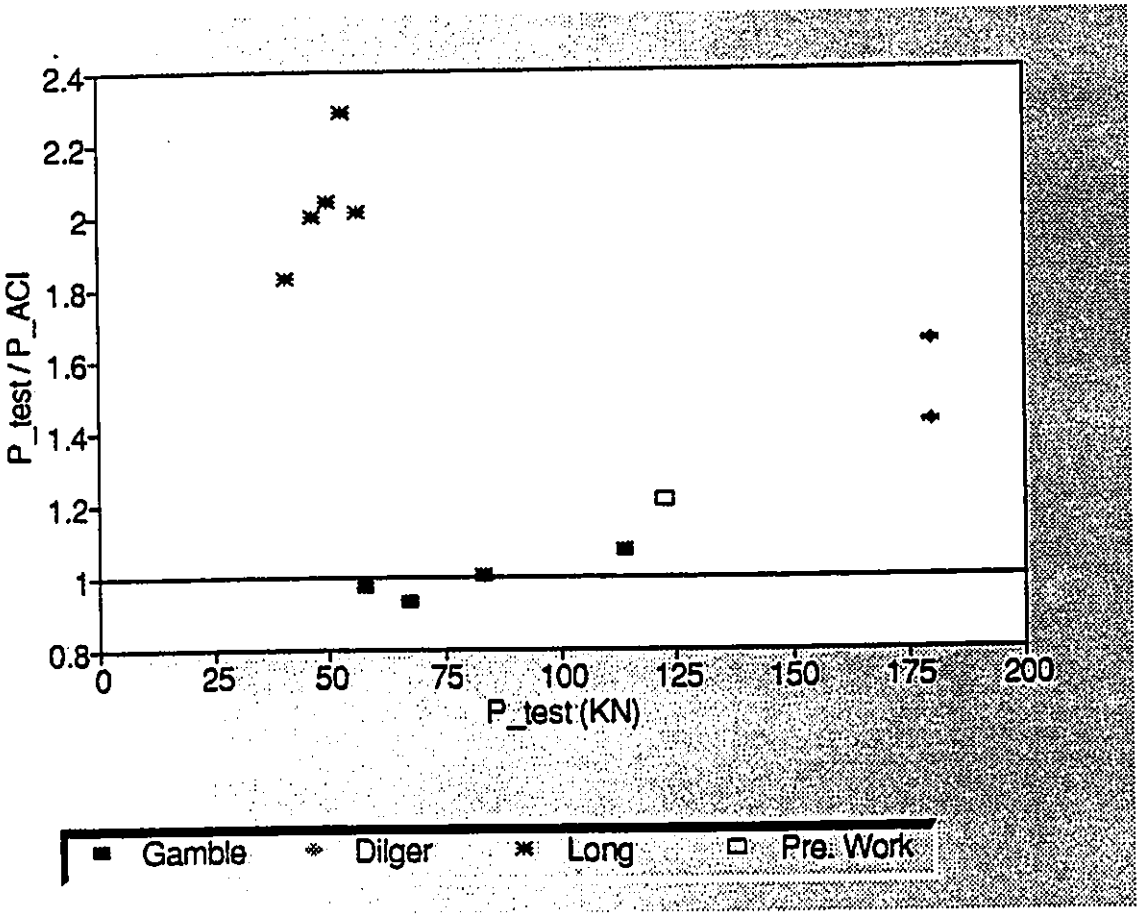

Fig. 5-25 : ACI code predictions of edge slab-column connections

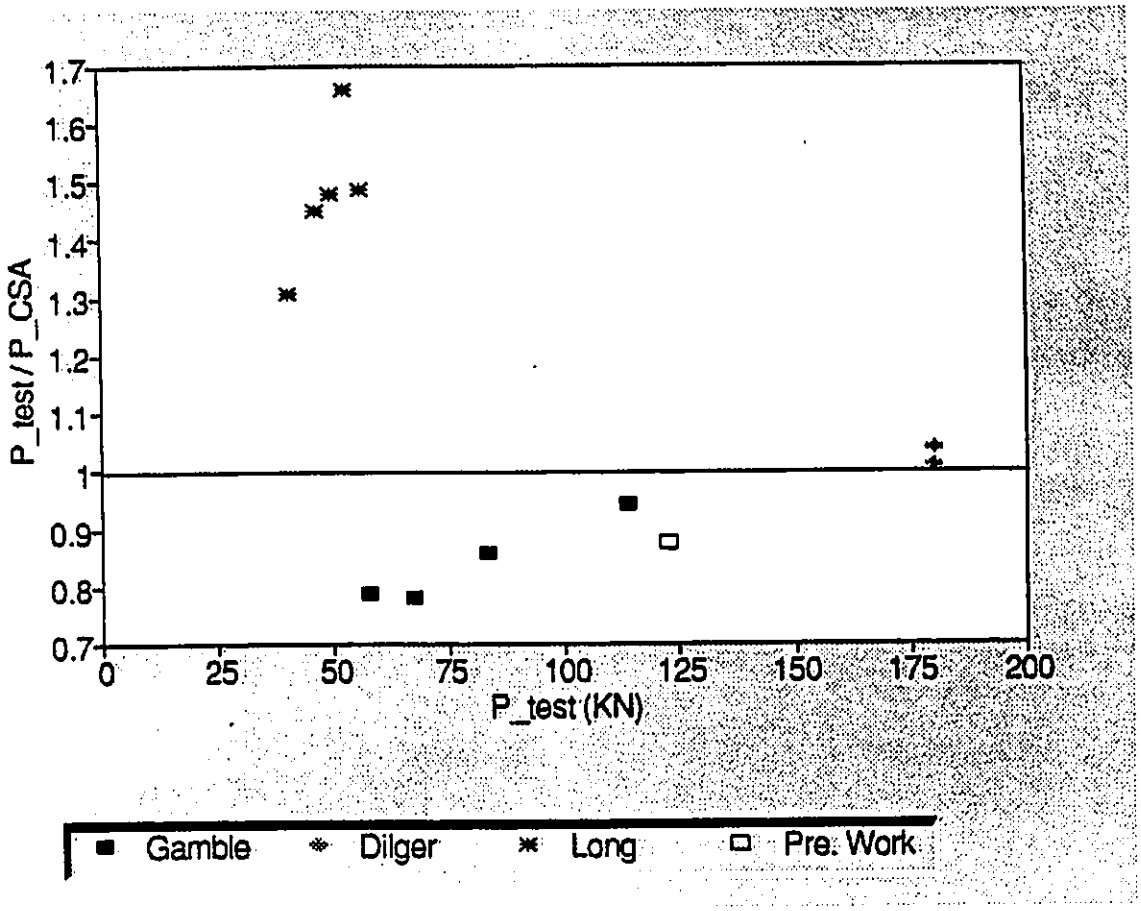

Fig. 5-26 : CSA code predictions of edge slab-column connections

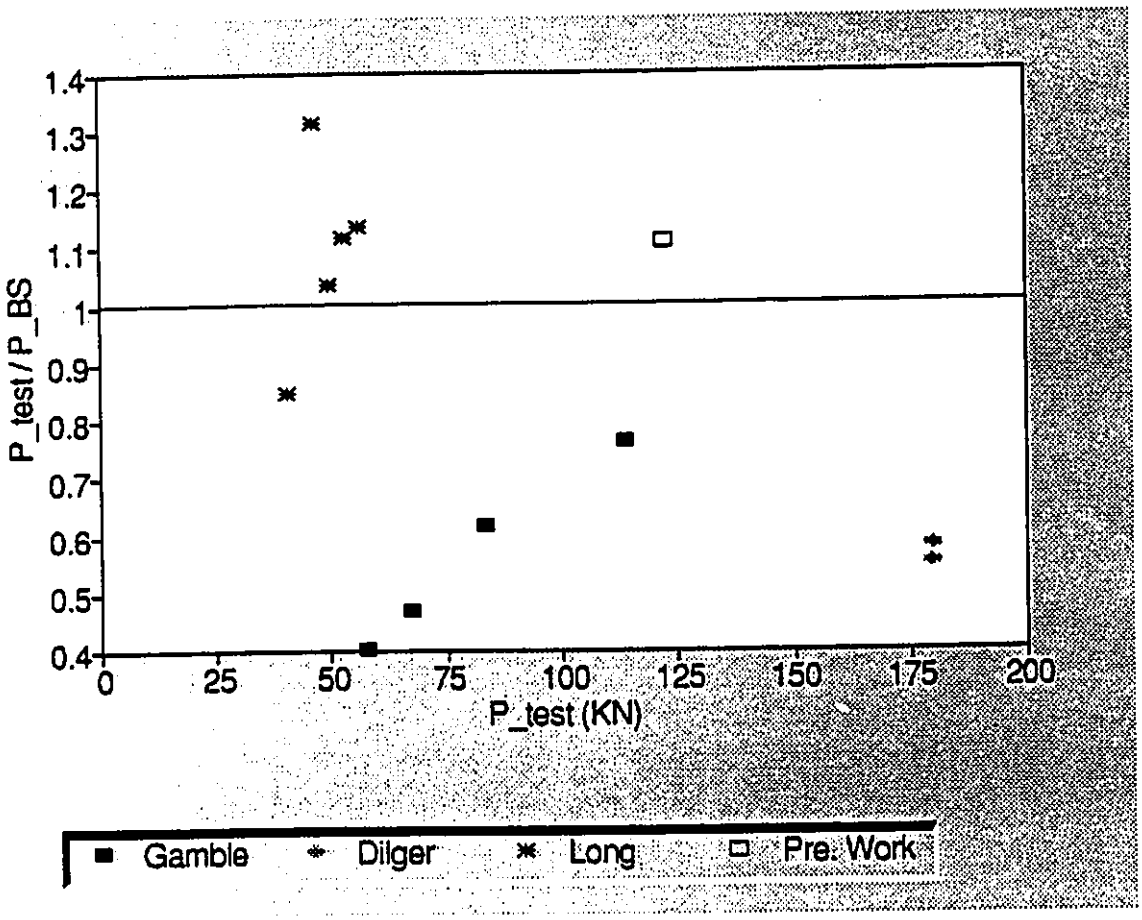

Fig. 5-27 : BS code predictions of edge slab-column connections

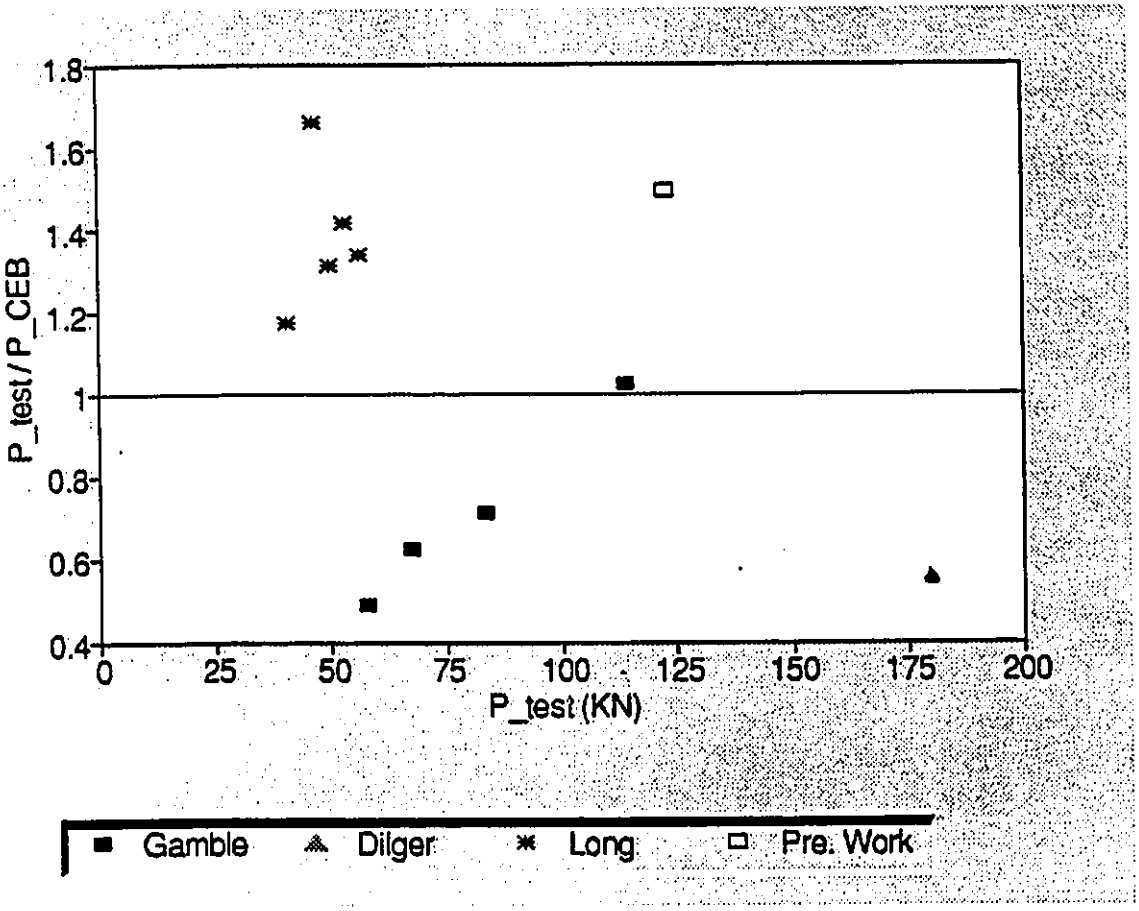

Fig. 5-28 : CEB code predictions of edge slab-column connections

CHAPTER #6

CONCLUSIONS AND RECOMMENDATIONS

On the basis of the reported experimental results and those of other previous researchers the following conclusions may be reached :

★ The overall behaviour of the unbonded post-tensioned test slab was very good. Even without bonded positive or negative reinforcement anywhere in the slab, the slab sustained large increases in load before widespread cracking took place. Cracks were localized to areas of high moments.

★ Banded arrangement of tendons could have a great influence on the strength of exterior columns as it gives the advantage of increased localized prestress compared with the average value of the panel. As a result, the flexural cracking resistance is enhanced and consequently the shear strength of the connection increases. Banding of the tendons

together with a relatively large prestressing force also helps to limit the extent of the punching failure zone.

★ The increase in tendon stress at failure varied between 15 and 25 percent of the applied stress. The maximum increase was recorded for the two tendons passing over the column centreline and running in the uniformly distributed direction. The recorded tendon stress was in a similar range to that reported by previous investigators using either isolated slab-column connections or scaled continuous slab models.

★ Contrary to the BS 8110-85 code, when the south-edge column (circular one) failed the companion square section column (north-edge column) did not appear to be even close to failure. The assumption of similar shear resistance for a square column and a circular column having a diameter equal to the side length of the square column is not confirmed in this case of a prestressed concrete slab.

★ The shear strength of both reinforced and prestressed concrete flat plates reduces under repeated load application if the previous load was larger than the load required to cause internal diagonal cracking.

★ The ACI 318-89 code recommendation that the shear stress equations derived for conventionally reinforced concrete slabs be used for the edge columns of prestressed slabs is believed to be to conservative. All the edge-column specimens tested by previous researchers and the one failed in this experimental program resisted even larger stresses than the predicted values on the basis of the limiting shear stress recommended by the ACI 318-89 equation derived for internal columns. Ignoring the effect of prestress, especially when banded tendon arrangement is used, would be too restrictive.

★ The ACI 318-89, CSA A23.3-84, BS 8110-85 and the CEB-FIP-90 building codes limitations on maximum values of characteristic concrete strength, f_c', do not appear to be necessary on the basis of the present work or the information gathered from the previous investigations. In the present work the mean concrete strength was considerably higher than the f_c'=34.5 ***MPa*** limit of the ACI and CSA; the f_c'=32 ***MPa*** limit of BS 8110-85 code and f_c'=40 ***MPa*** limited by the CEB code.

★ Converting the prestressing steel area to the equivalent reinforcement percentage proposed by BS 8110-85 using the ultimate strength of prestressing steel gives inconsistent results and in some cases even results an overestimation of the shear capacity of the connection. It is clear that unbonded tendons never reach stresses near their ultimate value in a real slab structure. A more logical approach would be to utilize the tensile stress in tendons at slab failure instead of the ultimate characteristic strength of prestressing tendons for the calculation of equivalent reinforcement ratio. The limit of 3% for the equivalent steel ratio does not seem to be necessary, as in the present experiment the value of ρ was computed as 5.1 percent while the agreement between the code equation and experimental load was quite good.

★ The definition of ρ specified by BS 8110-85 is applied for the width of the control perimeter very close to the column vicinity. It would be more realistic if ρ calculated for the full width of the effective slab strip, slab breadth, for isolated slab-column specimens and column strip for continuous structures.

★ The single magnification factor of 1.25 for edge columns according to the BS code irrespective of column or slab dimensions can be quite unconservative, for example, in

models tested by Gamble as the moment-shear ratio changed the behaviour of the specimens also changed from a completely ductile manner to a brittle punching shear fashion. By changing the location of loading points, the ultimate moment and shear capacities of the connections differed considerably while according to BS 8110-85 all the specimens would be predicted to carry similar loads. The same comment is also valid for the CEB code.

★ Excluding unbonded tendons in the calculation of ρ in the CEB code is inappropriate, as omitting the effect of the unbonded tendons gives a very conservative predictions for shear strength.

★ The experimental evidence of a size effect indicates that the nominal shear strength decreases with increasing effective depth of the slab if the other parameters are kept constant. The ACI 318-89 and CSA A23.3-84 should bring into account the effect of the slab thickness on the punching shear strength, as for thin slabs this effect might be very important.

★ The definition of effective depth for prestressed slabs especially when there are also ordinary reinforcing steel in the slab is not clear in the European codes. The North American codes' constant value of $0.8h$ is not appropriate if the tendons are placed in the mid-surface of the slab cross-section.

★ The effect of transverse load carried by the inclination of tendons over the support becomes very important as the initial prestress and the concentration of tendons towards the column line increase. The importance of this factor has been noticed by the North American codes while the European codes prefer to ignore it. The definition of V_p is

recommended to be calculated over the entire length of the tendon instead of the shear perimeter.

★ The CSA code overpredicts the nominal ultimate shear strength values by about 20 to 30 percent over the ACI code predictions. This is due to the way the material understrength factor is incorporated in the CSA code.

REFERENCES

ACI Committee 318, "Building Code Requirements for Reinforced Concrete (ACI 318-89) and Commentary - ACI 318 R-89," American Concrete Institute, Detroit, 1989, 353 pp.

ACI-ASCE Committee 326, "Shear and Diagonal Tension," *ACI Journal*, Proceedings Vol. 59, No. 1, January, 1962, pp. 1-30, No. 2, February, 1962, pp. 277-334, No. 3, March, 1962, pp. 352-396

ACI-ASCE Committee 423, "Tentative Recommendations for Prestressed Concrete Flat Plates," *ACI Journal*, Vol. 71, No. 2, February, 1974, pp. 61-71

ACI-ASCE Task Committee 426, "The Shear Strength of Reinforced Concrete Members - Slabs," *Journal of Structural Engineering, ASCE*, Vol. 100, No. ST8, August, 1974, pp. 1543-1591

ACI-ASCE Committee 426, "Recommendations for Concrete Members Prestressed With Unbonded Tendons," *ACI Structural Journal*, Vol. 86, No. 3, May-June, 1989, pp. 301-318

Ajdukiewicz A., Starosolski W., *Reinforced Concrete Slab-Column Structures*, Elsevier Science Publishing Co., Inc., New york, 1990, 372 pp.

Brotchie J.F. and Beresford F.D., "Experimental Study of a Prestressed Concrete Flat Plate Structure," *Civ. Eng. Trans. Inst. Eng. (Australia)*, Vol. CE9, No. 2, October, 1967, pp. 276-282

Brotchie J.F., "On The Design of Prestressed Flat Plates," *Commonwealth Scientific and Industrial Research Organization, Australia*, No. 3, 1974, 39 pp.

British Standard Institution, "Structural Use of Concrete, Part 1 and Part 2, Code of Practice for Design and Construction, BS 8110 : 1985," London

Burns N.H. and Hemakom R., "Test of Scale Model Post-Tensioned Flat Plate," *Journal of Structural Engineering, ASCE*, Vol. 103, No. ST6, June, 1977, pp. 1237-1255

Burns N.H. and Hemakom R., "Test of Post-Tensioned Flat Plate With Banded Tendons," *Journal of Structural Engineering, ASCE*, Vol. 111, No. 9, September, 1985, pp. 1899-1915

CEB-FIP Model Code for Concrete, Comite Euro-International du Beton / Federation International de la Precontrainte, Paris, 1990

Clark B.E., "The Shear Strength of Post-Tensioned Flat Slab Floors," *Proc. Instn. Civ. Engrs*, Part 2, 65, March, 1978, pp. 175-178

Cleland D.J., Franklin Y., Long A.E, "The Punching Strength of Unbonded Post-Tensioned Slabs at Columns," *Proceedings of the International Conference on Concrete Slabs Held at Dundee University*, 3-6 April 1979, pp. 197-207

Collins M.P., Mitchel D., *Prestressed Concrete Structures*, Prentice-Hall International, Inc., New Jersy, 1991, 766 pp.

CSA Standard CAN3-A23.3-M84, "Design of Concrete Structures for Buildings," Canadian Portland Cement Association, Ottawa, 1985, 485 pp.

Dilger W.H. and Shatila M., "Shear Strength of Prestressed Concrete Edge Slab-Column Connections With and Without Shear Stud Reinforcement," *Canadian Journal for Civil Engineering*, Vol. 16, 1989, pp. 807-819

Elstner R.C. and Hognestad E., "Shearing strength of reinforced concrete Slabs," *ACI Journal*, Proceedings Vol. 53, July, 1956, pp. 29-58

Foutch D.A., Gamble W.L., Sunidja H., "Tests of Post-Tensioned Concrete Slab-Edge Column Connections," *ACI Structural Journal*, Vol. 87, No. 2, March-April, 1990, pp. 167-179

Franklin S.O., Cleland D.J., Long A.E., "A Flexural Method for the Prediction of the Punching Capacity of Unbonded Post-Tensioned Flat Slabs at Internal Columns," *Proc. Instn Civ. Engrs*, Part 2, 73, June, 1982, pp. 277-298

Franklin S.O. and Long A.E., "The Punching Behaviour of Unbonded Post-Tensioned Flat Plates," *Proc. Instn Civ. Engrs*, Part 2, 73, September, 1982, pp. 609-631

Gerber L.L. and Burns N.H., "Ultimate Strength Tests of Post-Tensioned Flat Plates," *PCI Journal*, Vol. 16, No. 6, November-December, 1971, pp. 40-58

Grira M., "A Critical Review of The Symmetric Punching Shear of Reinforced Concrete Flat Slabs," Thesis presented to the University of Ottawa, at Ottawa, in 1990, in partial fulfilment of the requirements for the degree of Master of Applied Science

Grow J.B. and Vanderbilt M.D., "Shear Strength of Prestressed Lightweight Aggregate Concrete Flat Plates," *PCI Journal*, Vol. 12, No. 4, August, 1967, pp. 18-28

Hemakom R., "Strength and Behaviour of Post-Tensioned Flat Plates With Unbonded Tendons," Thesis presented to the University of Texas, at Austin, Tex., in 1975, in partial fulfilment of the requirements for the degree of Doctor of Philosophy

Kinnunen S., Nylander H., Tolf P., "Plattjocklekens Inverkan På Betongplattors Hållfasthet Vid Genomstansning. Försök Med Rektangulära Plattor," Institutionen För Byggnadssfaik Kungl Tekniska Högskolan, Sí, TRITA - BST - 0137, No. 137, 1980, 72 pp.

Kosut M., Burns N.H., Victor Winter C., "Test of Post-Tensioned Flat Plate," *Journal of Structural Engineering, ASCE*, Vol. 111, No. 9, September, 1985, pp. 1916-1929

Lin T.Y., "Load-Balancing Method for Design and Analysis of Prestressed Concrete Structures," *ACI Journal*, Proceedings Vol. 60, No. 6, June, 1963, pp. 719-742

Long A.E. and Cleland D.J., "Post-Tensioned Concrete Flat Slabs at Edge Columns," *ACI Materials Journal*, Vol. 90, No. 3, May-June, 1993, pp. 207-213

Marti P., Ritz P., Thürlimann B., "Prestressed Concrete Flat Slabs," *International Association for Bridge and Structural Engineering*, S-1/77, September, 1977, 17 pp.

Muspratt M.A., "Behaviour of a Prestressed Concrete Waffle Slab with Unbonded Tendons," *ACI Journal*, Vol. 66, December, 1969, pp. 1001-1004

Post-Tensioning Institute, *Design of Post-Tensioned Slabs*, Post-Tensioning Institute, Glenview, Illinois, 1977, 52 pp.

Post-Tensioning Institute, *Post-Tensioning Manual, Fifth Edition*, Post-Tensioning Institute, Glenview, Illinois, 1990, 406 pp.

Rahman, A.H., "Effect of Steel Corrosion on the Strength of Slab-Column Connections," *National Research Council Canada*, March, 1992, 20 pp.

Ravindra, K.D. and Munday, G.L.J, *Advances in Concrete Slab Technology*, Proceedings of the International Conference on Concrete Slabs Held at Dundee University, 3-6 April 1979

Regan P.E. and Breastrup M.W., "Punching Shear in Reinforced Concrete, A State of Art Report," *Bulletin d'Information*, No. 168, Comite Euro International du Beton, Lausanne, January, 1985, 232 pp.

Regan P.E., "The Punching Resistance of Prestressed Concrete Slabs," *Proc. Instn Civ. Engrs*, Part 2, 79, December, 1985, pp. 657-680

Roschke P.N. and Masamichi Inoue, "Effects of Banded Post-Tensioning in Prestressed Concrete Flat Slab," *Journal of Structural Engineering, ASCE*, Vol. 117, No. 2, February, 1991, pp. 563-583

Scordelis A.C., Pister K.S., Lin T.Y, "Strength of a Concrete Slab Prestressed in Two Directions," *ACI Journal*, Proceedings Vol. 53, No. 3, September, 1956, pp. 241-256

Scordelis A.S., Lin T.Y., May H.R., "Shearing Strength of Prestressed Lift Slabs," *ACI Journal*, Proceedings Vol. 55, No. 4, October, 1958, pp. 485-506

Scordelis A.C., Lin T.Y., Itaya R., "Behaviour of a Continuous Slab Prestressed in Two Directions," Proceedings Vol. 56, No. 6, December, 1959, pp. 441-459

Shehata Ibrahim A.E.M. and Regan Paul E., "Punching in R.C. Slabs," *Journal of Structural Engineering, ASCE*, Vol. 115, No. 7, July, 1989, pp. 1726-1740

Shehata Ibrahim A.E.M., "Simplified Model for Estimating the Punching Resistance of Reinforced Concrete Slabs," *Materials and Structures/Matériaux et Constructions*, 23, 1990, pp. 364-371

Smith S.W. and Burns N.H., "Post-Tensioned Flat Plate to Column Connection Behaviour," *PCI Journal*, Vol. 19, No. 5, May, 1974, pp. 74-91

Whitney C.S., "Ultimate shear Strength of Reinforced Concrete Flat Slabs, Footings, Beams, and Frame members Without Shear Reinforcement," *ACI Journal*, Proceedings Vol. 54, October, 1957, pp. 265-298

A P E N D I X A

****

DESIGN OF PRESTRESSED CONCRETE FLAT SLAB :

The model slab was designed according to the ACI 318-89 procedures. Design was done based on the equivalent frame method together with the load balancing technique. The interior strip of the slab was selected as a design element. The exterior strip was treated as a half-strip in providing tendons.

compressive strength of the concrete: $f'c := 6500 \cdot psi$

weight-density of the concrete: $\rho_c := \frac{0.15}{12 \cdot 12 \cdot 12} \cdot \frac{Kips}{in^3}$

average value of prestressing stress (P/A) in two direction $f_{pc} := 500 \cdot psi$

column dimension & length of the column: $c := 8 \cdot in \quad l := 24 \cdot in$

eccentricity of tendons (edge & middle & interior) :

$e_1 := 0.25 \cdot in \quad e_2 := 1 \cdot in \quad e_3 := 1 \cdot in \quad h := 3.5 \cdot in$

length of the span: $L_s := 108 \cdot in \quad \beta := \frac{1}{18} \quad \lambda := 0.5 \quad L := L_s + \frac{c}{2}$

force & area of tendons: $F_{ps} := \frac{f_{pc} \cdot h \cdot (2 \cdot L + c)}{20} \quad A_{ps} := .153 \cdot in^2$

$d_1 := \frac{h}{2} + e_1 \qquad d_2 := \frac{h}{2} - e_2 \qquad d_3 := \frac{h}{2} + e_3$

$h_1 := \frac{\beta}{\lambda} \cdot [e_2 + e_3] \qquad d_f := d_3 - h_1$

Plotting the Parabolic Drape of Tendon Layout with Points of Inflection:

$$L_1 := L - \beta \cdot L \qquad L_2 := 2 \cdot \beta \cdot L \qquad t := 0 \cdot in, 1 \cdot in \,..\, L_1$$

$$r := L_1, L_1 + 1 \cdot in \,..\, L_1 + L_2 \qquad s := L_1 + L_2, L_1 + L_2 + 1 \cdot in \,..\, 2 \cdot L$$

$$f(t) := 2 \cdot \frac{d_f + d_1 - 2 \cdot d_2}{L_1^2} \cdot t^2 + \frac{4 \cdot d_2 - 3 \cdot d_1 - d_f}{L_1} \cdot t + d_1$$

$$g(r) := \frac{-h_1}{(\beta \cdot L)^2} \cdot r^2 + \frac{2 \cdot h_1 \cdot L_1}{(\beta \cdot L)^2} \cdot r + d_f + \frac{h_1 \cdot L_1^2}{(\beta \cdot L)^2} - \frac{2 \cdot h_1 \cdot L_1 \cdot L}{(\beta \cdot L)^2}$$

$$Z := \left\lceil \frac{3 \cdot L_1}{2} + 2 \cdot \beta \cdot L \right\rceil \qquad AA := Z^2 - 4 \cdot L^2 \qquad BB := Z - 2 \cdot L$$

$$A' := \left\lceil d_f - d_1 - \frac{d_2 - d_1}{BB} \cdot (\beta \cdot L - L) \right\rceil$$

$$B' := \left\lceil (L + \beta \cdot L)^2 - \frac{AA}{BB} \cdot (\beta \cdot L - L)^2 - 4 \cdot L^2 \right\rceil \qquad A := \frac{A'}{B'}$$

$$B := \frac{d_2 - d_1 - A \cdot AA}{BB} \qquad C := d_1^2 - 2 \cdot B \cdot L - 4 \cdot A \cdot L^2$$

$$u(s) := A \cdot s^2 + B \cdot s + C$$

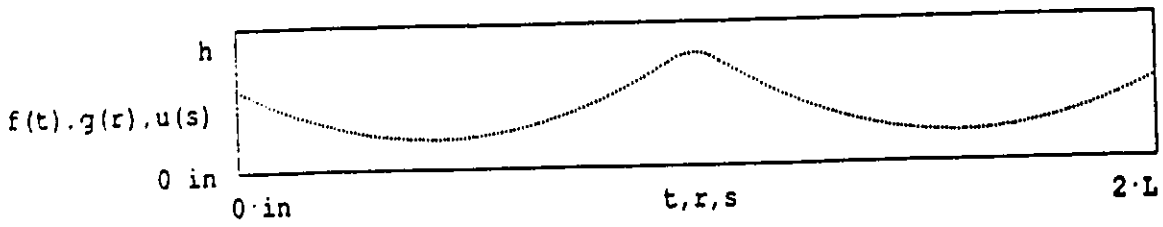

Calculating The Shear Capacity of the Interior Column :

$$\beta_{1p} := 40 \cdot \left[\frac{\frac{d}{3}}{c + d} + 1.5 \right] \qquad \beta_p := if\left[\beta_{1p} < 3.5, \beta_{1p}, 3.5 \right]$$

$$V_c := \left[\beta_p \cdot \sqrt{f'c \cdot psi} + 0.3 \cdot f_{pc} \right] \cdot 4 \cdot \left[c + \frac{d}{3} \right] \cdot d \qquad V_c = 51.105 \cdot Kips$$

No. of tendons passing through the interior column: $n := 4$

$$V_p := \frac{2 \cdot F_{ps} \cdot h_1 \cdot \left[c + \frac{d}{3} \right]}{(\beta \cdot L)^2} \cdot n \qquad V_p = 10.021 \cdot Kips$$

The total nominal shear strength is :

$$V_{tot} := V_c + V_p$$

****
* *
* $V_{tot} = 61.126 \cdot Kips$ *
* *
****

The direct shear capacity of the column is calculated over the tributary area of the column with 20% increase to account for the increase in tributary area and moment transfer :

$$W_{live} := \frac{V_c}{L_s \cdot L_s \cdot 1.2} - \rho_c \cdot h$$

$$W_{live} = 482.023 \cdot psf$$

Equivalent Frame Properties:

$$I_{col} := \frac{c \cdot c^3}{12} \qquad I_{slab} := \frac{L_s \cdot h^3}{12} \qquad K_c := \frac{4 \cdot I_{col}}{l - 2 \cdot h} \qquad K_s := \frac{4 \cdot I_{slab}}{L_s - \frac{c}{2}}$$

K_t = torsional stiffness of slab in column line

K_{ec} = equivalent column stiffness

$$C := \left[1 - 0.63 \cdot \frac{h}{c}\right] \cdot \frac{h^3 \cdot c}{3} \qquad K_t := \frac{2 \cdot 9 \cdot C}{L_s \cdot \left[1 - \frac{c}{L_s}\right]} \qquad K_{ec} := \frac{1}{\frac{1}{K_c} + \frac{1}{K_t}}$$

- distribution factors:

at exterior joint : $DF_e := \frac{K_s}{K_s + K_{ec}}$ $DF_e = 0.541$

at interior joint : $DF_i := \frac{K_s}{2 \cdot K_s + K_{ec}}$ $DF_i = 0.351$

Moment distribution due to unbalanced load :

$$W_{dead} := \rho_c \cdot h \cdot L_s \qquad W_{dead} = 0.394 \cdot \frac{Kips}{ft}$$

$$Wbal_{cen} := W_{dead} - \frac{8 \cdot 10 \cdot F_{ps} \cdot \left[e_1 + e_2 + \frac{d_f - d_1}{2} \right]}{\left[L_s - \beta \cdot L_s \right]^2}$$

$$Wbal_{cen} = -2.442 \cdot \frac{Kips}{ft}$$

$$Wbal_{col} := \frac{8 \cdot 10 \cdot F_{ps} \cdot h_1}{\left[2 \cdot \beta \cdot L_s \right]^2} + W_{dead}$$

$$Wbal_{col} = 30.468 \cdot \frac{Kips}{ft}$$

Fixed End Moments Due to Unbalanced Loads :

$$LL1 := L_s^4 - \left[\beta \cdot L_s \right]^3 \cdot \left[4 \cdot L_s - 3 \cdot \beta \cdot L_s \right]$$

$$LL2 := \left[\beta \cdot L_s \right]^3 \cdot \left[4 \cdot L_s - 3 \cdot \beta \cdot L_s \right]$$

$$FEM_{edge} := \frac{\frac{Wbal_{cen}}{2}}{12 \cdot L_s} \cdot LL1 + \frac{\frac{Wbal_{col}}{2}}{12 \cdot L_s} \cdot LL2$$

$$KK1 := \left[L_s - \beta \cdot L_s\right]^3 \cdot \left[L_s + 3 \cdot \beta \cdot L_s\right]$$

$$KK2 := \left[L_s^4 - \left[L_s - \beta \cdot L_s\right]^3 \cdot \left[L_s + 3 \cdot \beta \cdot L_s\right]\right]$$

$$FEM_{middle} := \frac{Wbal_{cen}}{12 \cdot L_s^2} \cdot KK1 + \frac{Wbal_{col}}{12 \cdot L_s^2} \cdot KK2$$

$FEM_{edge} = -16.337 \cdot Kips \cdot ft$ $FEM_{middle} = -12.668 \cdot Kips \cdot ft$

M O M E N T D I S T R I B U T I O N

C.O.F.	0.5			0.5
D.F.	0.541	0.351	0.351	0.541
F.E.M.	-16.337	12.668	-12.668	16.337
	8.838	0	0	-8.838
	0	4.419	-4.419	0
	-7.454	17.087	-17.087	7.454

(Resultants elastic moments are based on unit K-ft)

Shear applied to the internal column :

$$V1 := Wbal_{cen} \cdot \frac{\left[L_s - \beta \cdot L_s\right]^2}{2} + Wbal_{col} \cdot \beta \cdot L_s \cdot \left[L_s - \frac{\beta \cdot L_s}{2}\right]$$

$$V_{int} := \frac{V1 - 17.087 \cdot 1000 \cdot 12 \cdot lb \cdot in + 7.454 \cdot 12000 \cdot lb \cdot in}{L_s}$$

$$V_{int} = 3.939 \cdot Kips$$

75 percent of the total moment is resisted by the column strip :

$$M_{int} := 17.087 \cdot 12000 \cdot lb \cdot in - \frac{V_{int} \cdot c}{3}$$

Moment per unit width :

$$M_{int1} := \frac{M_{int} \cdot 0.75}{4.5 \cdot 12 \cdot in}$$

$$M_{int1} = 2.702 \cdot \frac{Kips}{ft} \cdot ft$$

Concrete stress in top fibre :

$$f_{top} := f_{pc} \cdot (-1) - \frac{M_{int1} \cdot 6}{(h)^2} \qquad f_{top} = -1.823 \cdot 10^3 \cdot psi < 0.45\ fc$$

$$f_{bot} := f_{pc} \cdot (-1) + \frac{M_{int1} \cdot 6}{h^2} \qquad f_{bot} = 823.407 \cdot psi$$